Fancy skulls and simple minds: (neuro)anatomical implications for palaeobiology of non-avian dinosaurs

I n a u g u r a l d i s s e r t a t i o n

zur
Erlangung des akademischen Grades
Dr. rer. nat. (Doctor rerum naturalium)
der
Mathematisch-Naturwissenschaftlichen Fakultät
der
Universität Greifswald

vorgelegt von
Marco Schade
Greifswald, Dezember 2022

Dekan: Prof. Dr. Gerald Kerth
1. Gutachter: Prof. Dr. Ingelore Hinz-Schallreuter
2. Gutachter: Prof. Dr. Steffen Harzsch
3. Gutachter: Prof. Dr. Eberhard Frey
4. Gutachter: Prof. Dr. Lawrence Witmer

Tag der Promotion: 25.05.2023

Das Gehirn ist der Parasit, oder Pensionär, des ganzen Organismus.

Arthur Schopenhauer

Meiner Frau und meinen Kindern…

Content

1. Abstract

The skull is an extremely informative part of the vertebrate body. Skulls are involved to hunt, feed and drink, to nurse, fight, dig, and to many other activities. Also, main sensory organs are situated on the head in order to enable a given animal to see, smell, taste, feel, listen, equilibrate and think; hence, the head is the main connection to the external world. It follows that a skull, with and without soft tissue, can tell a lot about its owner. Each skull consists of many individual bones constituting regions (e.g., snout and braincase) that represent different aspects of an anatomical mosaic, which in turn allows deeper (palaeo)biological insights.

In the past three centuries, palaeontologists dug out countless fossils from all over the world and from many preserved periods and groups, including dinosaurs. Hence, public and private collections house numerous fossil skull specimens. To further enlighten our understanding of palaeoecological, physiological and phylogenetic affinities of dinosaurian representatives belonging to different groups, and in order to reveal new aspects on their (neuro)anatomy, behaviour, ontogeny and evolution, a thoroughly examination with modern techniques is the aim of this thesis.

In order to get a phylogenetically broad understanding, fossil remains from at least four extinct species, including *Irritator challengeri* (a theropod: mostly bipedal carnivores) from the Early Cretaceous of northeastern Brazil, *Europasaurus holgeri* (a sauropod: long-necked, quadrupedal herbivores) from the Late Jurassic of Lower Saxony, *Emausaurus ernsti* together with an unnamed taxon from the Early Jurassic of Mecklenburg-Western Pomerania, and *Struthiosaurus austriacus*, Late Cretaceous of eastern Austria (the latter three are thyreophorans: armoured, mostly quadrupedal herbivores), were in closer focus. To document and digitally reconstruct cranial bones and cavities therein, the material was examined with micro computed tomography (microCT). On this basis, the full morphology of the preserved anatomy was revealed, described and contextualized, for example, in conjunction with comparative anatomy and biomechanical considerations. During this process, further methods were used to investigate and depict individual fossils: macro- and micro-photography, photogrammetry and phylogenetic analyses, each encompassing multiple sub-tasks and being supported by 3D prints.

As part of the result, it was possible to formulate reasoned assumptions about the lifestyle of the taxa in focus. For instance, the neuroanatomy and the osteological characteristics of the spinosaurid *Irritator challengeri* implicate that this taxon was an agile hunter with a habitually inclined snout that was specialized in catching relatively small prey with a robust dentition and a comparably weak - but fast - bite, with a remarkable jaw mechanism which enabled the animal to kinetically widen the pharynx during lower jaw depression. The (neuro)anatomy of *I. challengeri*, *S. austriacus*, *E. ernsti* and *E. holgeri* presented here, enrich our knowledge about a plethora of (lifestyle-related) aspects of these animals, their closer relatives and the prehistoric world they lived in.

Institutional abbreviations:

BRSMG, Bristol City Museum and Gallery, Bristol, UK; DFMMh/FV, Dinosaurier-Freilichtmuseum Münchehagen/Verein zur Förderung der Niedersächsischen Paläontologie e.V., Rehburg-Loccum, Germany; GG, Greifswalder Geologische Sammlungen, University of Greifswald, Germany; IPUW, Institut für Paläontologie Wien, Austria; SMNS, Staatliches Museum für Naturkunde Stuttgart, Germany; YPM, Peabody Museum of Natural History, Yale University, New Haven, USA.

2. Introduction

The braincase is a central cranial complex of this thesis because it potentially holds plenty information about (neuro)anatomy that - under actualistic considerations - bear lifestyle-related interpretability about different aspects, such as foraging and self-defense methods, niche partitioning, intraspecific communication, physiology and ontogeny.

2.1. Brief historical consideration of braincase endocasts

One of the first descriptive works on neurocranial material of a dinosaur was published about a braincase assigned to the genus *Iguanodon* by Hulke in 1871 (however, the specimen is nowadays considered as *Mantellisaurus*; see Knoll et al., 2021). Also, famous palaeontologists Marsh (1880) and Osborn (1912) worked on braincase endocasts. In this context, an endocast represents the cavities within a bony braincase; above all, the cavity which once housed the brain. Later, authors such as Nopcsa (1917) and Edinger (e.g., 1929; 1942) drew bigger pictures on brain evolution in extinct and extant taxa. Jerison (e.g., 1969) and Hopson (e.g., 1977; 1980) provided the bases on which braincase endocasts could be compared and contextualized. Today, numerous braincase endocasts from different fossil taxa are known to science (see e.g., Buchholtz, 2012; Balanoff & Bever, 2017). Whereas such endocasts were produced physically in former times (which often had a detrimental effect on the fossil), it was the advent - around the turn of the last millennium - of non-destructive methods, with computer tomographs (CT), that allowed accelerated production of digital endocasts. This kind of endocast is readily available for further investigations (e.g., statistics and morphometrics; see e.g., Watanabe et al., 2019), more complete (because they can well encompass the cranial nerves and endosseous labyrinths), printable, easily shareable, and computer tomographs (CT) do usually not affect fossils.

2.2. Structure of the brain

The primary embryonic vesicles of the amniote (reptiles, birds and mammals) brain are the forebrain (prosencephalon), the midbrain (mesencephalon) and the hindbrain (rhombencephalon; Liem et al., 2001; Hildebrand & Goslow, 2004; Kardong, 2015; Lessner & Holliday, 2022). Further differentiation takes place during ontogeny into telencephalon and diencephalon (both parts of the forebrain), the midbrain with the cephalic flexure, and the metencephalon with the pontine flexure and the myelencephalon (both parts of the hindbrain) which terminates with the cervical flexure (**Fig. 1** of this dissertation; Liem et al., 2001; Hildebrand & Goslow, 2004; Kardong, 2015; Lessner & Holliday, 2022). In the (topologically) adult brain, the telencephalon encompasses the olfactory bulbs and tracts, cerebral hemispheres, corpus striatum and hippocampus, whereas the diencephalon comprises the thalamus, pituitary (or hypophysis) and the pineal gland (Hildebrand & Goslow, 2004). The midbrain comprises optic and auditory lobes. The metencephalon forms the cerebellum and the pons. The myelencephalon forms the

medulla oblongata; the spinal cord follows outside the foramen magnum (Hildebrand & Goslow, 2004; Lessner & Holliday, 2022).

The cranial nerves (CN) originate on different sections of the brain, tendentially from anterior to posterior position: CN 0, nervus terminalis (possibly associated with the perception of pheromones); CN I, n. olfactorius (smell); CN II, n. opticus (vision); the nerves involved in eye movements CN III, IV and VI, n. oculomotorius, trochlearis and abducens (e.g., Lautenschlager et al., 2014; Jones et al., 2019; Kuzmin et al., 2021; Lessner & Holliday, 2022). Additionally, there are CN V, n. trigeminus with the three branches ophthalmic, maxillary and mandibular (sensation of facial skin and chewing); CN VII, n. facialis (facial expressions, taste, cephalic glands, muscles of the inner ear); CN VIII, n. vestibulocochlearis (equilibrium and audition); CN IX, n. glossopharyngeus (taste, muscles of the throat, parotid); CN X, n. vagus (visceral nervous system); CN XI, n. accessorius (muscles of neck and upper back); CN XII, n. hypoglossus (tongue movement; Liem et al., 2001; Hildebrand & Goslow, 2004; Kardong, 2015).

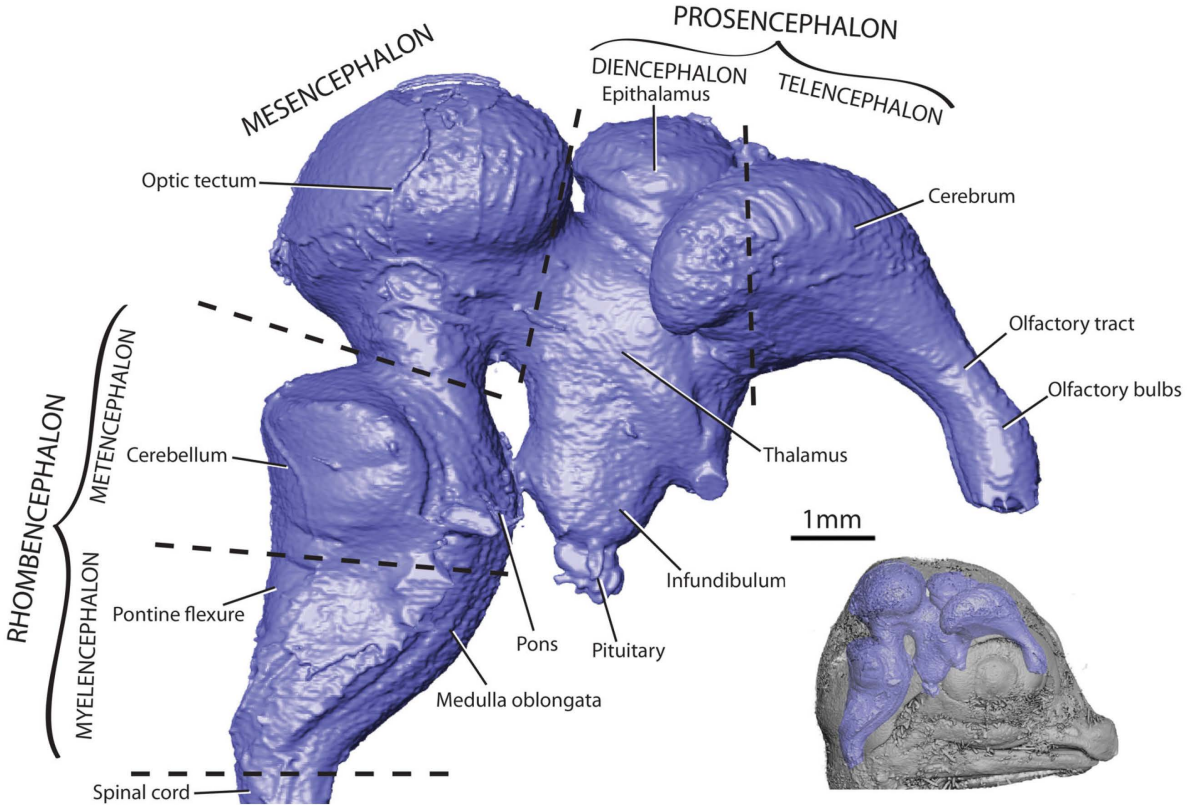

Fig. 1 Renderings of a 27-28 days old embryo skull (lower right) of *Alligator mississippiensis* with brain reconstruction and labeled brain features (upper left) in right lateral view; from Lessner & Holliday, 2022. Scale does only refer to the labeled brain depiction.

2.3. Approaching endocasts and their bearing

Braincase endocasts prompted manifold significant (palaeo)biological implications with increasingly large scales of considered taxa and backgrounds (see e.g., Billet et al., 2012; Balanoff et al., 2013; Cerio & Witmer, 2019; Watanabe et al, 2021; Dembitzer et al., 2022; Araújo et al., 2022). In the following, non-exhaustive endocast-related approaches are exemplified in order to further contextualize the articles of this thesis.

Prominently stated in Jerison (1973), the “principle of proper mass”, advocates for a close association of the size of a given neural structure and the respective capacity to process neural information. For example, it is generally accepted that the relative size of the olfactory bulbs correlates with the acuteness of olfaction in birds (Zelenitsky et al., 2011; Corfield et al., 2015) and non-avian dinosaurs (e.g., Zelenitsky et al., 2009; Müller, 2021; see also Bird et al., 2018 for osteological and molecular evidence for olfactory acuteness in mammals). As such, the morphology of the brain (and the endocast) can tell a lot about behavioural capacities, since complex behavior is also a question of relative size of brain compartments. While the brain of most birds and mammals occupies a large volume of the braincase (e.g., Rowe et al., 2011; Balanoff et al., 2015; Early et al., 2020), this is different in other groups, such as turtles and crocodiles (Evers et al., 2019; Hu et al., 2020). Also, the endosseous labyrinth (containing the inner ear) may differ in size and morphology from its soft tissue content (Evers et al., 2019). Still, different compartments of the brain can reach the internal wall of the braincase, with meningeal membranes, accompanied by blood supply and fatty tissue in between, and as a result, the respective endocast can show more or less detailed features of the soft tissue morphology in different groups (e.g., Balanoff et al., 2015).

Extinct, non-avian dinosaurs are phylogenetically placed within Archosauria, the group that also encompasses extant crocodiles and birds (e.g., Witmer, 1995). Since the actual soft tissue (such as the brain) does usually not fossilize (however, see e.g., Trinajstic et al., 2022), phylogenetic bracketing allows reasoned inferences of brain anatomy in extinct species when associated osteological correlates deliver indirect hints to such features if these are known in extant related taxa (e.g., Witmer, 1995). Traditionally, dinosaur brains are expected for having filled approx. 50%-60% of the respective cavities which was occasionally considered an oversimplification, ignoring factors such as phylogeny (see e.g., Buchholtz, 2012). The attempts to estimate the relation of endocast and actual brain volume are diverse (e.g., Marsh, 1880; Hopson, 1977; Hurlburt et al., 2013; Balanoff & Bever, 2017; Jirak & Janacek, 2017; Knoll et al., 2021). Furthermore, ontogeny can influence the amount of volume a brain occupies its braincase (Jirak & Janacek, 2017). More specifically, in young chickens (1 day), the brain can fill around 60% of the respective endocranial space; this increases in age up to 93% in individuals older than 8 weeks (Watanabe et al., 2019). On the other hand, there seems to be a conversed trend in crocodiles: 52% are filled in 2-3 year old individuals, but 99% in individuals younger than a year (these values vary between individuals; Watanabe et al., 2019). Consequently, Knoll et al. (2021) advocated for the use of 73% (52+93/2=72.5) in non-avian dinosaurs. Tendentially, the larger an animal, the larger its brain becomes in order to solve the

growing need of somatosensory processing; however, there is an allometric relation between brain and body size (e.g., Jerison, 1973; Northcutt, 2002). The definition of intelligence is still an open issue, may encompassing certain sensory capabilities, diverse (solution-focused) behavioural facets, abstract thinking and a self-awareness (see e.g., Kirsch et al., 2008). Furthermore, from investigations of recent mammals and birds, it is known that parrot and songbird brains can contain twice as many neurons per brain mass as same-sized primates do; thereby, many neurons located in the telencephalon (part of the forebrain) in parrots and corvids (Olkowicz et al., 2016). This may be part of the explanation why some birds solve problems of considerable cognitive demand (Kirsch et al., 2008; see also Fischer et al., 2022 for considerations of genetically driven neocortex growth in primate organoids, likely associated with increased cognitive abilities in human evolutionary history). The Encephalization Quotient (Jerison, 1973) is a measure involving the relation of brain to body size (weight or volume) and, in a following step, the relation of measured brain size and empirically expected brain size. Hopson (1977) used this approach to access the brain-body mass relation among fossil dinosaurs. However, Hopson inferred 100% infilling of the braincase for sauropods and 50% for other dinosaurs, which is nowadays considered problematic; see above. Leaving aside the issue of infilling, whereas the crocodile or reptile norm was considered value 1, Sauropoda (approx. 0.2-0.3), Ankylosauria (approx. 0.5), Stegosauria (approx. 0.6) and Ceratopsia (approx. 0.7-0.9) plot below this norm (Hopson, 1977). The only non-avian dinosaur groups that cross the crocodilian line of 1 are Ornithopoda (approx. 0.85-1.5; however, see also Knoll et al., 2021 for considerably higher values) and Theropoda (approx. 1-2) with some coelurosaurs plotting approx. at 5.8 (Hopson, 1977). Deducing a clear-cut statement from this is not admissive, but it might give a hint towards the distribution of cognitive capacities in non-avian dinosaurs.

2.4. Objectives and taxa in focus

It is widely accepted that oseological features of cranial material can be very informative in a wide array of different aspects (“Show me your teeth and I will tell you who you are.” - Georges Cuvier). Yet, what level of detail and information that can be withdrawn from more or less fragmentary cranial remains has to be established and can build upon a broad base of previous studies. Whereas detailed anatomical descriptions were delivered in the articles included in this thesis to contribute to the comparative literature base, it was a main objective to get a more complete and deeper understanding of lifestyle-related palaeobiological facets of non-avian dinosaurs in general. Hence, the taxa in focus here were chosen because they are phylogenetically (a theropod, a sauropod and several thyreophorans) and spatio-temporally (Early Jurassic - Late Cretaceous from Brazil, Austria and Germany) dispersed (**Fig. 2, 3**). Additionally, there was a great amount of references based on closely related taxa that provided a good ground for comparison and interpretation.

The braincases, endocranial cavities and the resulting palaeobiological implications for *Irritator challengeri*, *Struthiosaurus austriacus* and *Europasaurus holgeri* were the scope of three separate scientific articles (Schade et al., 2020; Schade et al., 2022a; b). Whereas the holotype of *I. challengeri* (SMNS 58022) consists of a largely complete skull only missing its anteriormost portions, the holotype of *S. austriacus* (IPUW 2349/6) represents an incomplete braincase. For detailed examination of the *E. holgeri* braincase material, belonging to different ontogenetic stages, eleven different specimens were under consideration: the almost complete braincase with two separate parietals DFMMh/FV 581.1, 2 & 3, the fragmentary braincase DFMMh/FV 1077, the three prootics DFMMh/FV 466, 561 and 964, and the four otoccipitals DFMMh/FV 205, 249, 898 and 981.2.

Two additional articles (Schade & Ansorge, 2022; Schade et al., in review) with a stronger emphasis on osteology (rather than endocranial cavities), are included in this thesis; one of which completes the picture of *I*. *challengeri* (SMNS 58022) in respect to palaeoecological and evolutionary tendencies: all preserved skull bones and teeth were described and contextualized. The second article is focused on osteoderms of thyreophorans (=representatives of Thyreophora; GG 85/1 23, assigned to the holotype of *Emausaurus ernsti* and GG 504, assigned to an unknown thyreophoran taxon) in which, among others, potential ontogenetic implications for *E*. *ernsti* are considered.

The mentioned articles mainly base on (micro)CT data, encompass cranial material of non-avian dinosaurs of the Mesozoic and are briefly outlined directly below (Roman numerals indicate the chronological order of articles):

I + V - Schade et al., 2020; in review: *I. challengeri*, SMNS 58022 (near-complete skull) - Aptian Romualdo Formation, Early Cretaceous of northeastern Brazil

II - Schade et al., 2022a: *S. austriacus*, IPUW 2349/6 (incomplete braincase) - Campanian Grünbach Formation, Late Cretaceous of eastern Austria

III - Schade & Ansorge, 2022: *E. ernsti*, GG 85/1 23 (osteoderm); GG 504 (osteoderm) - Pliensbachian/Toarcian dislocated clay deposit, Early Jurassic of northeastern Germany

IV - Schade et al., 2022b: *E. holgeri*, DFMMh/FV 581.1, 2 & 3 (near-complete braincase with parietals); DFMMh/FV 1077 (fragmentary braincase); DFMMh/FV 466, 561 and 964 (near-complete prootics); DFMMh/FV 205, 249, 898 and 981.2 (near-complete otoccipitals) - Kimmeridgian Süntel Formation, Late Jurassic of northern Germany

Considering the discussions about working with fossils from Brazil (including the holotype of *I. challengeri*; e.g., Cisneros et al., 2022), it may be refered to the ethics statement in the manuscript of Schade et al. (in review) included here. The raw data and the respective digitally reconstructed models of *I. challengeri*, *S. austriacus* and *E. holgeri* have been uploaded for a free download on morphosource.org (Duke University, USA); see individual articles for further details. It is worth noting that, herein, in order to facilitate a discussion and to follow conventions, structures on the digital endocasts were often referred to as if they represent the actual soft tissue, although the digital models actually represent abstractions of cavities that once housed the respective soft tissue (see also Witmer et al., 2008). The raw data that (micro)computed tomographs produce, which is the basis for digital reconstructions or segmentations, consist of thousands of single slices. These slices visualize differences in material density and other properties (e.g., bone, sedimentary matrix, metal) through many grey nuances between black (mostly air) and white (mostly metal). Eventually, the person working with these data has to decide which pixel (or voxel) belongs to a certain anatomical structure. It follows that every single reconstructed model is an individual interpretation of the underlying data.

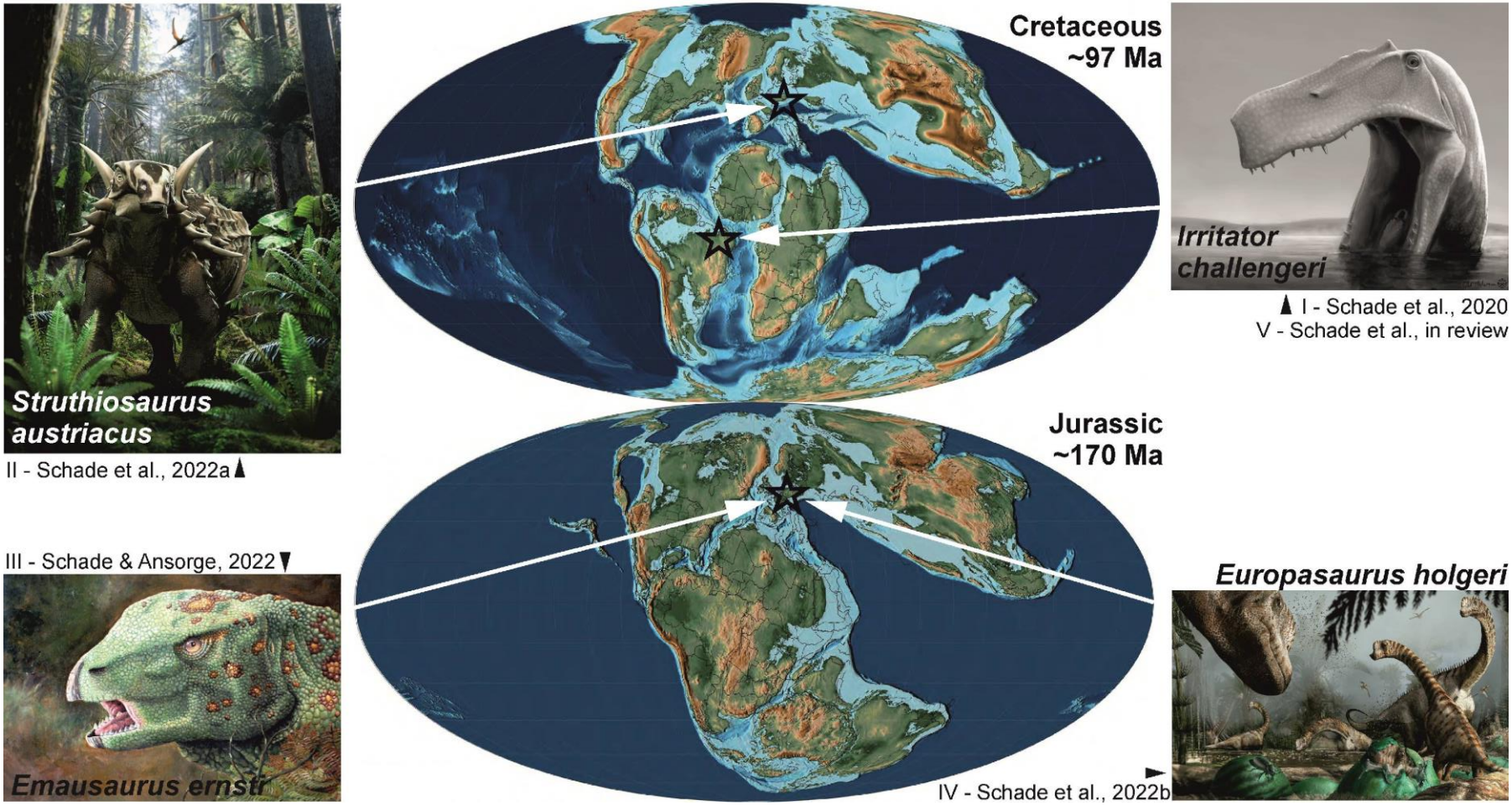

Fig. 2 Palaeogeographical maps of the Middle Jurassic (Bajocian/Bathonian) and Late Cretaceous (Cenomanian) indicating the provenance of fossil taxa in focus of this thesis. Roman numerals indicate the chronological order of articles. Life reconstructions by Fabrizio De Rossi (*Struthiosaurus austriacus*), Cornelia Haubold (*Emausaurus ernsti*), Olof Moleman (*Irritator challengeri*) and Davide Bonadonna (*Europasaurus holgeri*); maps altered from Scotese, 2014a; b.

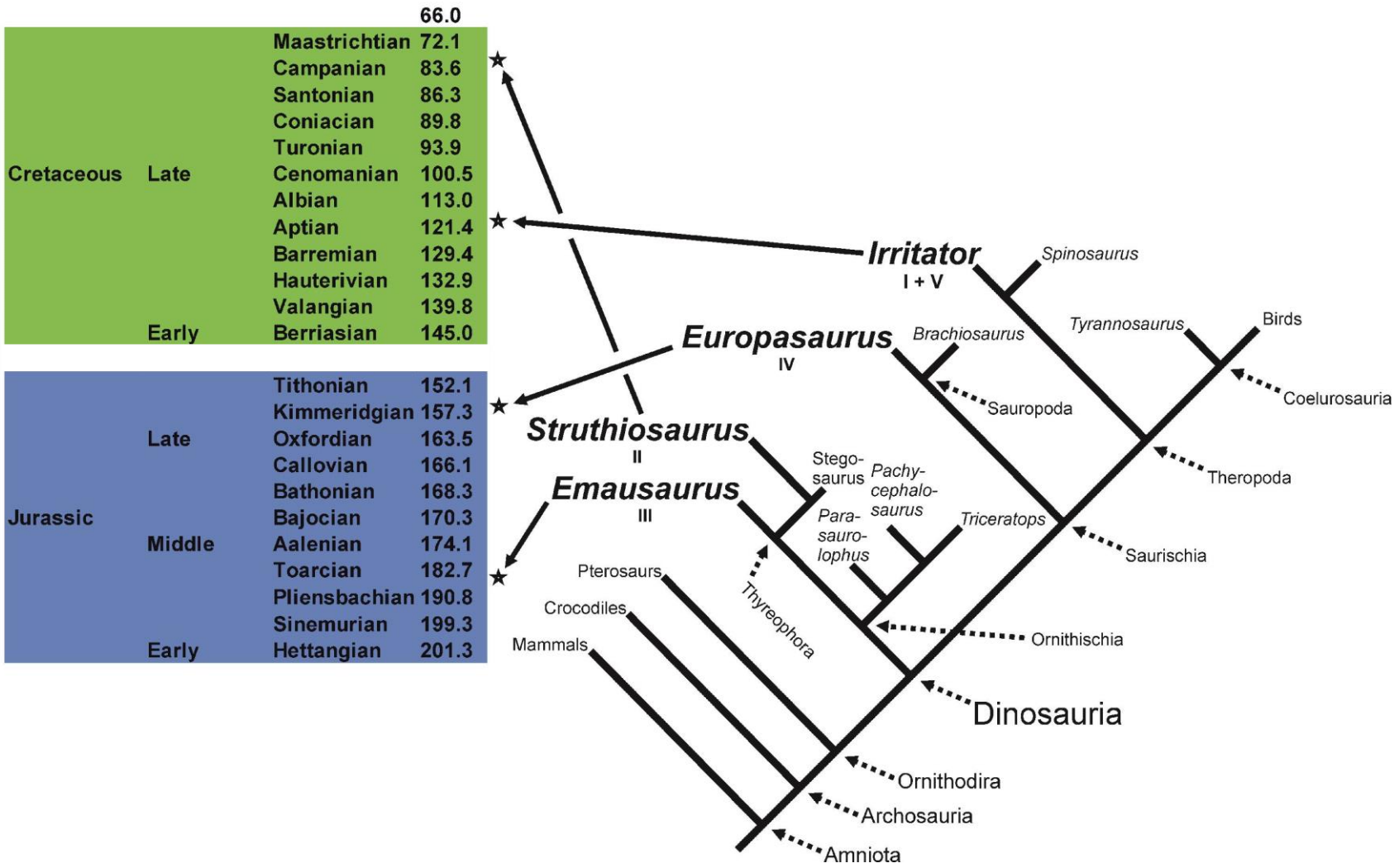

Fig. 3 Phylogenetic relationships and chronostratigraphic distribution of fossil taxa in focus of this thesis. Ages indicate the basis of the respective stage (from Cohen et al., 2022). Roman numerals: I - Schade et al., 2020; II - Schade et al., 2022a; III - Schade & Ansorge, 2022; IV - Schade et al., 2022b; V - Schade et al., in review.

3. Results and discussion

3.1. Part I - Implications of neurocranial endocasts

Reasoned assumptions about association of neurocranial anatomy and lifestyle-related issues are further considered below with brief mentions of underlying concepts and hypotheses, together with their significance for the studies of this thesis.

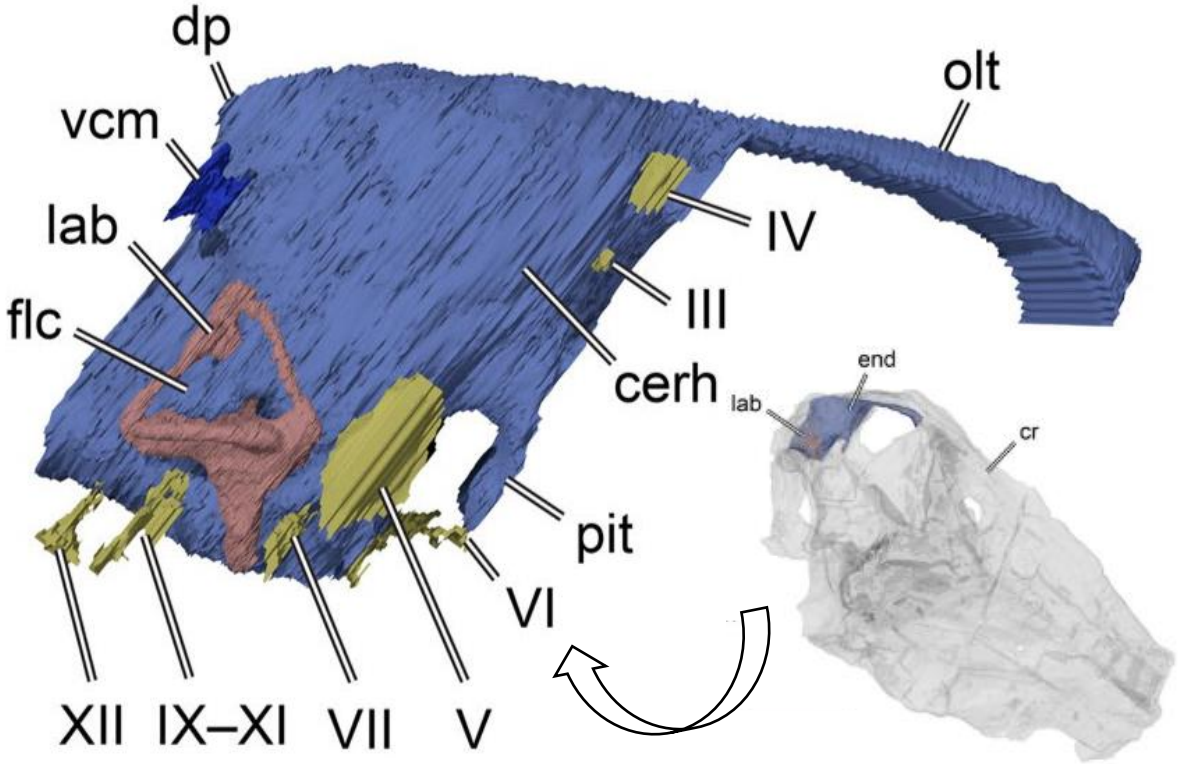

Fig. 4 Renderings of the holotype (lower right) and digital braincase endocast (upper left) of *Irritator challengeri* (SMNS 58022) in right lateral view; altered from Schade et al., 2020. Abbreviations: cerh, cerebral hemisphere; cr, cranium; dp, dural peak; end, endocast; flc, floccular recess; lab, endosseous labyrinth; olt, olfactory tract; pit, pituitary; vcm, dorsal middle cerebral vein; Roman numerals indicate cranial nerves. Length of the preserved cranium: ~ 550 mm.

3.1.1. Olfactory system

A “good” sense of (chemosensory) smell is thought to having been important for predatory dinosaurs (e.g., Zelenitzky et al., 2009; 2011) and long olfactory tracts are considered a plesiomorphic (ancestral) condition in theropods (Witmer & Ridgely, 2008). The olfactory nerve, represented by the olfactory bulbs and trunks, often leave impressions on the ventral surface of the frontal and/or parietal (parts of the skull roof) in reptiles and birds (Fabbri et al., 2017). In the course of debates surrounding (semi)aquatic affinities of spinosaurids (=representatives of Spinosauridae), Arden et al. (2019) reported on supposedly small olfactory bulb impressions on isolated frontoparietal material assigned to spinosaurids. When

judging about spinosaurids, the authors suggested that “Olfactory cues would have been of little use to an animal that primarily hunted underwater…” (Arden et al., 2019). Firstly, crocodiles as predators with a semiaquatic lifestyle are not known for a reduction of olfaction of any kind (see e.g., Zelenitzky et al., 2009 and references therein, as well as Ngwenya et al., 2018 for evidence of neurogenesis mainly in the telencephalon of adult crocodiles), and secondly, a semiaquatic lifestyle was found to be strongly associated with the evolution of large olfactory bulbs in birds (Corfield et al., 2015). In 2020, the first spinosaurid braincase endocast reconstruction has been published, from *Irritator challengeri* (**Fig. 4**); the endocast exhibits long olfactory tracts and proximal olfactory bulb portions that show no indication for a reduction in comparison to other theropods (Schade et al., 2020: **Figure 2**). Hence, the plesiomorphic condition for theropods is present and an ancestral “good” sense of smell seems likely, at least for this particular spinosaurid taxon (see Witmer & Ridgely, 2008; Schade et al., 2020).

3.1.2. Pituitary

In extant vertebrates, the pituitary is - among others - responsible for the production of hormones for growth (Liem et al., 2001, Hildebrand & Goslow, 2004, Kardong, 2015). Very early in the scientific history of fossil braincase endocasts, authors assumed that relatively large pituitary recesses could be a proxy for large body sizes in fossil taxa (Nopcsa, 1917; Edinger, 1942). Since then, early-diverging sauropodomorphs (=representatives of Sauropodomorpha; between the Late Triassic and Early Jurassic) are known to possess pituitary fossae of modest size (Müller et al., 2021). Indeed, when colossal sauropods evolved, their seemed to be a tendency in relative growth of the pituitary fossa (see e.g., Sues et al., 2015). Now, the secondarily dwarfed island dweller *Europasaurus holgeri* is phylogenetically placed within a group of sauropods that encompasses the largest known taxa that ever walked on earth (Sander et al., 2006). However, *E. holgeri* itself is one of the smallest representatives of the group (being an island dwarf; see Foster, 1965; Van Valen, 1973; however, see also Lokatis & Jeschke, 2018 for a critical synopsis of the island rule). The braincase endocast of *E. holgeri* indeed possesses a relatively small pituitary (in comparison to the remaining endocast compartments; Schade et al., 2022b: **Figure 1A**). This gives further support to the idea of the pituitary size being a proxy for body size (Nopsca, 1917; Edinger, 1942; Müller et al., 2021).

3.1.3. Flocculus

The flocculus is a part of the cerebellum, in many taxa laterally protruding towards the intercanal space of the endosseous labyrinth (**Fig. 4**). The flocculus is involved in processing of the vestibulo-occular reflex (VOR, e.g., compensatory eye movements during head rotation) and the vestibulo-collic reflex (VCR, e.g., stabilizing the head and neck during body movements), and hence, critical for gaze stabilisation (e.g., Voogd & Wylie, 2004; Walsh et al., 2013). However, the floccular recess does not necessarily reflect the size of the actual flocculus, also containing vascular tissue in extant birds and mammals which hinders direct ecological

implications (Walsh et al., 2013; Ferreira-Cardoso et al., 2017). On the other hand, the floccular recess can be prone to underestimation because of ontogeny (Witmer & Ridgely, 2009). Still, the expression on endocasts has often been used as a hint towards a certain agility of fossil taxa (e.g., Witmer et al., 2003; King et al., 2020; Ezcurra et al., 2020).

The flocculus of *I. challengeri* is especially long and wide for a large-bodied theropod (however, several other taxa also possess a large flocculus; see e.g., Rogers, 1998; Franzosa & Rowe, 2005; Cerroni and Paulina-Carabajal, 2019) which has been interpreted as part of the anatomical mosaic that supports an active (likely bipedal) lifestyle, specialized for hunting small prey items (in relation to its own body size; see also Sampson & Witmer, 2007; Schade et al., 2020; in review).

The flocculus of *E. holgeri* is only represented by a very subtle eminence (Schade et al., 2022b: **Figure 1A**). However, this is one of the few sauropod taxa that shows this feature on the endocast (see also Paulina-Carabajal, 2012; Witmer et al., 2008; Knoll & Schwarz-Wings, 2009) which may tentatively hint towards a more flexible use of its neck and generally more flexible movement abilities associated with a comparably small body size (Sander et al., 2006).

On the other hand, also the lack of a structure like the flocculus can bear some information: a floccular recess is not present on the endocast of *Struthiosaurus austriacus* (Schade et al., 2022a: **Figure 2A**). The absence of a flocculus on the endocast seems to be a usual feature in nodosaurids (=representatives of Nodosauridae; see e.g, Ősi et al., 2014; Paulina-Carabajal et al., 2016); the genus *Struthiosaurus* is phylogenetically placed within this group of heavily armoured dinosaurs that possess large spikes in their neck and shoulder region (see e.g., Thompson et al., 2012; Brown, 2017). In contrast, some representatives of the sister group, the ankylosaurids (=representatives of Ankylosauridae), possess large bony knobs on the distal end of their tails (Thompson et al., 2012; Arbour & Currie, 2015). Another group of thyreophorans is known to possess beweaponed terminal tails: stegosaurs (Carpenter et al., 2005; Mallison, 2010). Now, the only thyreophoran genera (*Stegosaurus*, *Kentrosaurus*, *Euoplocephalus* and *Tarchia*) with a braincase endocast also exhibiting a (small) flocculus (Galton, 1988; 2001; Miyashita et al., 2011; Paulina-Carabajal et al., 2018), display a spiked or knobbed tail as formidable means for self-defence too (Carpenter et al., 2005; Arbour, 2009; Mallison, 2010; Arbour et al., 2013; Arbour & Currie, 2015); both features may indicate increased coordination and targeting capabilities (potentially involving a more flexible use of the neck) for these taxa. The lack of a floccular recess is part of the mosaic feature that supports a comparably inert lifestyle with rather passive defensive strategies for *S. austriacus* and, possibly, nodosaurids in general.

3.1.4. Inner ear and endosseous labyrinth

Another important cavity complex of the braincase, that is potentially informative, is the inner ear, or - when speaking about endocasts - the endosseous labyrinth (Witmer et al., 2008). It consists of two main parts: the more dorsally situated one, the vestibular apparatus consists of three discrete so-called semicircular canals; an anterior, posterior and lateral one for (mechano)sensory

coverage of the three dimensions of space (e.g., Liem et al., 2001; Hildebrand & Goslow, 2004; Kardong, 2015). In life, endolymphatic fluid moves within those canals during head, neck and body movements and extremely small hair-like structures (cilia) pass on electric impulses of the resulting information to processing brain compartments that make the living entity realize head inclination, for example (Liem et al., 2001; Hildebrand & Goslow, 2004; Hullar, 2006; Kardong, 2015). The geometry and size of the semicircular canals is known to influence the inherent endolymphatic flow and seems associated with locomotion at least in mammals (Spoor et al., 2007; Cox & Jeffery, 2010; Pfaff et al., 2015; 2017). It follows that, as the closely associated flocculus, the morphology, geometry and size of the semicircular canals were suspected to be informative for agility and lifestyle aspects in fossil taxa; with a tendency to thin and long canals advocating for a certain agility (e.g., bipedality, because the endolymphatic fluid inertia is thought to be lower in long canals making them more sensitive; Sobral & Müller, 2016), whereas dorsoventrally relatively low endosseous labyrinths with thick and short semicircular canals rather suggest (semi)aquatic habits and/or inertia (e.g., Witmer et al., 2003; Sampson & Witmer, 2007; Spoor et al., 2007; David et al., 2010; Neenan et al., 2017; Schwab et al., 2020; Ezcurra et al., 2020). However, there is still an ongoing debate about the question to what extent the morphological information of the endosseous labyrinth - which is potentially also influenced by factors such as spatial constraints in the braincase, phylogeny, allometry and neck mobility - can be used to approach lifestyle-related aspects (e.g., Georgi & Sipla, 2008; Spoor & Thewissen, 2008; Neenan et al., 2017; Benson et al., 2017; Evers et al., 2019; Dudgeon et al., 2020; Bronzati et al., 2021; Hanson et al., 2021; David et al., 2022; Hanson et al., 2022; Evers et al., 2022). Thus, because of their potential use to approximate and add to such intriguing palaeobiological aspects, the endosseous labyrinths in focus here were considered as hints and object to tentative interpretations (Schade et al., 2020; 2022a; b).

I. challengeri bears relatively elaborated and slender vertical semicircular canals which may further support an active lifestyle, enabling rapid head and neck movements, which appears not too surprising in respect to the phylogenetic position of this taxon (Sampson & Witmer, 2007; Schade et al., 2020: **Figure 3**; Schade et al., in review: **Figure 37**).

Whereas cranial material of *E. holgeri* has been described by Marpmann et al. (2014), a detailed examination of the endocranial cavities was still pending. Marpmann et al. (2014) considered different specimens as belonging to different ontogenetic stages (morphological ontogenetic stages 1-3). This was done on the basis of size, build, rugosity of articular facets and bone surface smoothness (see also Benton et al., 2010). Two braincase specimens were considered stage 3 (adult), three prootics (a thin anterolaterally situated bone on the braincase, housing the anterior part of the endosseous labyrinth) were considered stage 2-3, and four otoccipitals (a posterior element of the braincase, housing the posterior part of the endosseous labyrinth) were considered substages of stage 1 (juvenile; Marpmann et al., 2014). Indeed, the otoccipitals are very small, while the prootics display size and general appearance of those belonging to the more complete and adult braincase material (Schade et al., 2022b: **Figure 7–figure supplement 1, Figure 8–**

figure supplement 1). However, one prootic and one otoccipital were originally found in close vicinity to each other and seem to belong to the same individual, since both bones articulate very well; this has not been noticed in former studies (see Marpmann et al., 2014; Schade et al., 2022b: **Figure 5, Figure 5–figure supplement 1**). It follows that both together contain an almost complete endosseous labyrinth of near-adult size and morphology (missing the dorsalmost parts of the common crus and the vertical semicircular canals, as well as the ventralmost part of the cochlear duct). Among other implications, this was considered as evidence that very young individuals of *E. holgeri* already developed adult-like inner ears, which in turn suggests some form of precociality with adult-like capacities for the (mechanosensory) sense of equilibrium and the capability of being "light on their feed" very early in life (Schade et al., 2022b; see also Iwaniuk & Nelson, 2003 and Dial, 2003 for nuances of precociality in birds). Furthermore, the great difference in body mass of newly hatched sauropods (attaining enormous growth rates; Hallett & Wedel, 2016; Curry Rogers et al., 2016) and their parents would have been life-threatening for the former, suggesting a rather loose relationship with limited nursing habits but a precocial lifestyle with the ability to move independently shortly after hatching (see e.g., Sander et al, 2010; Curry Rogers et al., 2016). Additionally, similar interpretations were stated on the endosseous labyrinth of the dinosaurs *Dysalotosaurus lettowvorbecki* (together with other hints; Lautenschlager & Hübner, 2013; Hübner & Rauhut, 2010), *Triceratops* (Morhardt et al., 2018) and the recent ostrich (for which the precocial lifestyle is known: Romick, 2013; see also Brigande et al., 2000 for embryonic developmental stages of chicken inner ears and Jeffery & Spoor, 2004 for - potentially phylogenetically induced - adult-sized inner ears in human foeti). In conclusion, while some sort of precociality has been previously suggested for sauropods by other means (such as nests and ichnofossils; see e.g., Sander et al., 2011; Schade et al., 2022b and references therein), endosseous labyrinths have been used so for other dinosaurian taxa (see e.g., Lautenschlager & Hübner, 2013).

The endosseous labyrinth of *S. austriacus* bears very low and thick canals, tentatively hinting towards a relatively inert lifestyle (Schade et al., 2022a: **Figure 4**). Furthermore, whereas semicircular canals are usually smoothly rounded, the lateral canal of *S. austriacus* has a unique acute angle distally (Schade et al., 2022a). Bearing in mind that also the endosseous labyrinth morphology does not necessarily reflect the morphology of the soft tissue it once housed (Evers et al., 2019), an acute angle is still likely for having hindered a smooth endolymphatic flow, potentially resulting in a reduced sensitivity in this taxon.

Together with other features, the lateral semicircular canal of tetrapods can give an idea of how an animal habitually held its skull; the horizontal orientation of the lateral semicircular canal serves as a hint of how a taxon orients its skull (or snout) in order to optimize the acuity of its senses, including maximization of the field of binocular view (e.g., Dujim, 1951; Wilson & Melville-Jones, 1979; Spoor & Zonneveld, 1998; Hullar, 2006; Sampson & Witmer, 2007, Sereno et al., 2007; Witmer et al., 2008; however, see also Marugán-Lobón et al., 2013; Benoit et al., 2020).

In many non-avian dinosaurs, this is an almost horizontal or only slightly inclined skull orientation (e.g., Witmer et al., 2008; Witmer & Ridgely, 2009). However, if the lateral semicircular canal of *I. challengeri* is horizontally oriented, it becomes obvious that this taxon held its snout approx. 45° ventrally inclined which is more than in any other known non-avian theropod (Schade et al., 2020: **Figure 1**). Together with other osteological correlates (orientation of the occipital condyle and a notch, produced by the dorsal pre-orbital skull bone arrangement, both features seem also to be present in other spinosaurids; see Barker et al., 2021; Sereno et al., 2022; Schade et al., in review: **Figure 2A, 3A, 4A**), this may support a certain specialization for small prey items, since such a skull orientation maximized the field of binocular vision in this taxon (see also Stevens, 2006). If the lateral semicircular canal of *S. austriacus* is oriented horizontally, the basisphenoid (posteroventrally positioned bone of the braincase) is strongly anteroventrally inclined (Schade et al., 2022a: **Figure 2A, B**). Thus, the findings support an earlier study on the bony braincase of *S. austriacus*, in which outer osteological features were compared to the relative *Panoplosaurus mirus* (Pereda-Suberbiola & Galton, 1994). These authors concluded a very similar orientation of the braincase of *S. austriacus* which may have resulted in a very slightly inclined snout region for this taxon.

The horizontal orientation of the lateral semicircular canal of *E. holgeri* also supports an earlier study on an articulated braincase, resulting in a slightly inclined snout (Marpmann et al., 2014, Schade et al., 2022b: **Figure 1A, B**). Hence, the hypothesized head postures in *I. challengeri*, *E. holgeri* and *S. austriacus* may strengthen the case for the horizontal orientation of the lateral semicircular canal being a proxy for habitual head posture in fossil taxa, since they appear consistent with additional, independent clues.

The ventrally situated part of the vertebrate inner ear is the cochlear or lagena (e.g., Liem et al., 2001; Hildebrand & Goslow, 2004; Kardong, 2015). Here, mainly (mechanosensory) hearing takes place. Again, endolymphatic fluid and cilia take up physically induced movements (from the tympanic membrane and auditory ossicles) and pass on the information to processing centres of the brain (e.g., Liem et al., 2001; Hildebrand & Goslow, 2004; Kardong, 2015). The size of the lagena in relation to the basicranium (measured between the dorsal margin of the pituitary fossa and the distalmost portion of the occipital condyle) can be used to broadly estimate auditory capabilities in extinct and extant taxa (see e.g., Walsh et al., 2009; Ballell et al., 2021). In numerous recent reptile and bird taxa, this proved to be usefully associated with aspects of (social) behaviour, such as vocal complexity and aggregation (Walsh et al., 2009). In addition, other methodological approaches have

been used to access auditory capabilities involving body mass estimations and braincase height, respectively (Gleich et al., 2005; Choiniere et al., 2021). However, estimating body mass would have produced much speculation in the taxa in focus here, since postcranial elements (on which body mass estimations are usually based; see e.g., Sander et al., 2011) are not responsibly referable to the respective braincase material or not preserved at all. Furthermore, the unusual braincase morphology of *I. challengeri* and *S. austriacus* (mainly because of the dorsoventrally elongated basisphenoid; see Schade et al., 2022a; in review) could hinder direct comparison with other taxa. The mentioned methods are considered as approximation of the auditory complex issue. Additionally, the cochlear duct is thought to be only incompletely filled with auditory neural tissue; it is worth being mentioned, although not considered by most studies investigating fossil endosseous labyrinths, that Gleich et al. (2005), Witmer et al. (2008) and Paulina-Carabajal et al. (2016) advocate for a dorsoventrally incomplete measurement of what is often considered the cochlear duct. The reason is functional: following Witmer et al. (2008) and Paulina-Carabajal et al. (2016), the fenestra ovalis (=fenestra vestibuli; in life, spanning a membrane that receives the vibration from the auditory ossicles) marks the dorsal junction of the cochlear duct and the ventral junction of the vestibule; as a result, measuring the whole dorsoventral length (as demonstrated in Walsh et al., 2009) of the alleged cochlear duct could result in overestimated auditory capacities. Following Gleich et al., (2005), only two thirds of the cochlear duct length is associated with auditive tissue, the ventralmost part being the lagenar macula and possibly rather associated with the sense of equilibrium (see also Khorevin, 2008). Despite these uncertainties, the auditory capabilities of the taxa in focus were calculated in order to compare them with each other and to relatives, and to integrate the resulting information into the ensemble of additional cues (Schade et al., 2020; 2022a; b).

Following the measurements and equations outlined by Walsh et al. (2009), *I. challengeri* and *E. holgeri* were potentially enabled to receive a wide range of frequencies (3196 Hz and 3702 Hz, respectively; probably with a sound perceiving ability inferior to most birds but superior to most crocodiles and turtles; see Walsh et al, 2009) with mean hearing frequencies of 1950 Hz and 2225 Hz, respectively (Schade et al., 2020; 2022b). In contrast, *S. austriacus* bears the shortest cochlear duct known in a dinosaur so far (Schade et al., 2022a). Hence, while a pronounced reliability on hearing seems clearly critical for a predator such as *I. challengeri*, as well as for a taxon with potential gregarious habits (as inferred for sauropodomorphs; see e.g., Lockley et al., 2002; Sander et al., 2008; Myers & Fiorillo, 2009; Pol et al., 2021) like *E. holgeri*, the narrow band width of 1868 Hz with a mean hearing frequency of 1230 Hz in *S. austriacus* suggests the lack of superior audition, and possibly limited sound-based social interactions in the latter taxon (Schade et al., 2020; 2022a; b).

3.1.5. Vascular tissue

Like mentioned above, the braincase is not only filled with the brain itself and meninges, it also contains vascular tissue (e.g., Liem et al., 2001; Hildebrand & Goslow, 2004; Witmer et al, 2008; Kardong, 2015). *S. austriacus* has several discrete vascular canals dorsal to its endocranial cavity (Schade et al., 2022a: **Figure 2, 3**). In this taxon, anteroposteriorly long and mediolaterally thick canals assigned to the transverso-occipital vein, are situated laterally or dorsolaterally to the endosseous labyrinth, the posterior branching plexus is characterized by more difficile canals on the dorsal aspect of the skull roof. Other ankylosaurs show different patterns of vascularization (e.g., Kuzmin et al., 2020). Together with large, long and elaborated nasal passages, this led to the assumption that ankylosaurs possessed an efficient mechanism which cooled their brains and reduced moisture loss through respiration (Bourke et al., 2018; Porter & Witmer, 2019; Kuzmin et al., 2020). The heavily armoured (and hence likely heat-keeping) skulls, the large body sizes and partly arid habitats of ankylosaurs render such an associated function reasonable (Bourke et al., 2018; Porter & Witmer, 2019); the pattern of vascular structures found in the braincase of *S. austriacus* adds to the known diversity of those and may suggest the presence of the above-described physiological mechanisms in this taxon. The vascular structures being most extensive in the smallest, and allegedly youngest, specimens of *E. holgeri* independently support the respective interpretations of earlier investigations on their build and surface (Marpmann et al., 2014; Schade et al., 2022b).

3.1.6. Summarizing the endocasts (Schade et al., 2020; 2022a; b)

Evidently, braincase endocasts can reveal many palaeobiological insights through comparative (neuro)anatomical approaches. These include palaeoecological aspects like behaviour, as well as ontogeny, physiology and evolution. In addition to numerous, thoroughly described and depicted anatomical details that provide documented basis for comparison in future studies, the most concrete implications of the neuroanatomical articles are briefly summarized below.

Struthiosaurus austriacus – The endocast of *S. austriacus* shows features like poorly marked brain regions, the lack of a flocculus and a short and thick anterior semicircular canal. The shortest known cochlear duct of a non-avian dinosaur suggests a narrow range of frequency perception and rather limited need for airborne social interactions and acoustic predator perception for this species (**Fig. 5**). A so far unknown pattern of vascular canals in *S. austriacus* adds to the diversity of such structures (Kuzmin et al., 2020) and suggests the need for excess heat release of the brain region (Bourke et al., 2018; Porter & Witmer, 2019). The findings of Schade et al. (2022a) are consistent and add to previous works that render ankylosaurs as slow-moving (Coombs, 1978; Maidment & Barrett, 2014), heavily armoured (Scheyer & Sander, 2004; Hayashi et al., 2010) herbivores, specialized on low vegetation (Brown et al., 2020), which was potentially digested via large guts (Carpenter, 2012). Nodosaurids may tend to bear less elaborated nasal passages (Bourke et al., 2018), delivered stronger bites (Mallon & Anderson, 2014; Ősi et al., 2017), may preferred coastal or fluvial habitats (Butler & Barrett, 2008) and adopted a more selective feeding style (Brown et al., 2020), in contrast to its sister group, the ankylosaurids, and hence, realized different ecological niches. Possibly, the general absence of tail clubs (Arbour & Currie, 2015) and flocculi (e.g, Ősi et al., 2014; Paulina-Carabajal et al., 2016), as well as the thickened osteoderms (Scheyer & Sander, 2004; Hayashi et al., 2010) hint towards an ecological differentiation that made nodosaurids adopt a rather passive style to defend themselves. On the other hand, the seeming presence of small floccular recesses (Galton, 1988; 2001; Miyashita et al., 2011; Paulina-Carabajal et al., 2018) in thyreophoran taxa that also possessed suitable tail weapons (Carpenter et al., 2005; Arbour, 2009; Mallison, 2010; Arbour et al., 2013; Arbour & Currie, 2015), both possibly being useful for active targeting, may be challenged by future studies (Schade et al., 2022a).

Fig. 5 Life reconstruction of a heavily armoured, lonesome individual of *Struthiosaurus austriacus* in a Late Cretaceous forest of modern-day Austria; a sluggish lifestyle and limited need for airborne perception of conspecifics or predators is suggested by its neuroanatomy (estimated body length of *Struthiosaurus*: ~ 3 m; see Schade et al., 2022a) - commissioned artwork by Fabrizio De Rossi.

Europasaurus holgeri – Whereas the group of sauropods *E. holgeri* is phylogenetically placed in, the Macronaria, encompasses the largest terrestrial vertebrates known, also the smallest sauropods belong to this group (e.g., Janensch, 1935; Sander et al., 2006). So far unknown and uniform vascular structures within very young individuals have been described (Schade et al., 2022b: **Figure 7, 8, Figure 7–figure supplement 2, Figure 8–figure supplement 2**). Additionally, the large and morphologically adult-like endosseous labyrinth in a very small individual of *E. holgeri* suggests precociality in this taxon, further supports earlier appraisals of sauropods (see also Sander et al, 2010; Lautenschlager & Hübner, 2013; Romick 2013; Curry Rogers et al., 2016; Morhardt et al., 2018) and sets a good example for ontogenetic tendencies of neuroanatomy (**Fig. 6**). Following the possible association of calculated auditory capacities, vocal complexity and aggregating (social) behaviour, the results further support such affinities for *E. holgeri* and sauropodomorphs in general (Walsh et al., 2009; Myers & Fiorillo, 2009; Pol et al., 2021). Furthermore, the braincase endocast of *E. holgeri* seems to endorse its status as an - for a sauropod - exceptionally small taxon (probably an island dwarf; Sander et al., 2006) due to the relatively small pituitary (Nopcsa, 1917; Edinger, 1942; Müller et al., 2021). Hence, Schade et al. (2022b) could independently support different assessments from earlier studies with other approaches.

Fig. 6 Life reconstruction of a flock of the dwarfed island dweller *Europasaurus holgeri* in the Late Jurassic of what is now Germany with very young individuals leaving their nest short after hatching; indicated by neuroanatomy (the estimated body height of *Europasaurus*: ~ 3 m; see Schade et al., 2022b) - commissioned artwork by Davide Bonadonna.

Irritator challengeri – The reconstruction of the braincase endocast of *I. challengeri* represents the first published of a spinosaurid (Schade et al., 2020). *I. challengeri* was potentially the apex predator of its ecosystem in the Early Cretaceous Romualdo Formation of Brazil (Aureliano et al., 2018; Arai & Assine, 2020). Like most other large-bodied theropods, *I. challengeri* possessed a brain that did not completely fill the respective cavity (e.g., Sampson & Witmer, 2007). The hunter had long olfactory tracts with no sign for a reduction of olfaction in comparison to other large-bodied theropods (Zelenitsky et al., 2009; Witmer & Ridgely, 2009). The endocast of *I. challengeri* bears a large flocculus and a long anterior semicircular canal, both tentatively hinting towards enabling *I. challengeri* for fast and coordinated movements of its snout (Schade et al., 2020 and references therein). Thereby, the horizontal orientation of the lateral semicircular canal suggests a habitually ventrally inclined snout, which is also the pose that likely maximized the field of binocular vision in front of the skull, allowing perception of distance (see also Stevens, 2006). The cochlear duct suggests "proper" hearing abilities in comparison to other fossil theropods (e.g., Lautenschlager et al., 2012; however, without being an auditive specialist; Choiniere et al., 2021). The braincase endocast potentially renders *I. challengeri* an agile hunter of relatively small prey items and - independently from other studies - may hints towards a piscivore specialization of spinosaurids (e.g., Charig & Milner, 1997; Buffetaut et al., 2004). For a more complete picture of *I. challengeri* and spinosaurids as a whole, see the summary of the article on the cranial osteology of this taxon below.

3.2. Part II - Implications of skull bones, teeth and osteoderms

3.2.1. Cranial osteology of *Irritator challengeri* and implications for spinosaurids (Schade et al., in review)

Spinosaurids are a group of large-bodied, mostly bipedal and carnivorous dinosaurs (phylogenetically placed in Theropoda; Carrano et al., 2012). To date, indubitable taxa are only known from the Cretaceous; substantial material comes from Europe, Asia, South America and Africa (e.g., Stromer, 1915; Charig & Milner, 1986; Sereno et al., 1998; Allain et al., 2012; Ibrahim et al., 2014; 2020a; b; Malafaia et al., 2020; Barker et al., 2021; Mateus & Estraviz-López, 2022; Sereno et al., 2022). Since the description of the name-giving taxon, *Spinosaurus aegyptiacus*, over a century ago (Stromer, 1915), the general perception of spinosaurids changed from "usual" terrestrial predators, but with some remarkable features (conical teeth, elongated skull and neural spines) hinting towards ichthyophagous habits, to a taxonomically diverse clade that may include taxa having been able to effectively forage aquatically (e.g., Charig & Milner, 1997; Sereno et al., 1998; Buffetaut et al., 2004; Ibrahim et al., 2020a; Barker et al., 2021; Fabbri et al., 2022). Spinosaurids encompass some of the largest terrestrial predators known to science (Dal Sasso et al., 2005; Therrien & Henderson, 2007; Hone & Holtz, 2017). In contrast to other gigantic theropodan hunters that are considered top predators with a hypercarnivorous diet including large prey (e.g., Molnar & Farlow, 1992; Chin et al., 1998; Carpenter et al., 2005; DePalma et al., 2013), spinosaurids are thought to

having been specialized on rather small prey (in relation to their own body size), including fish; the respective evidence comes from skull and tooth morphology (e.g., Stromer, 1915; Taquet, 1984; Charig & Milner, 1986; 1997; Therrien et al., 2005; Sales & Schultz, 2017; Heckberg & Rauhut, 2020), biomechanical considerations (Rauhut, 2001; Rayfield et al., 2007; 2011; Schade et al., in review: **Figure 39**), isotope investigations of teeth (Amiot et al., 2009; 2010a; b; Hassler et al., 2018), gut content and other direct evidence (Charig & Milner, 1997; Buffetaut et al., 2004), and (neuro)anatomical hints (Schade et al., 2020; in review). Additionally, spinosaurids, and possibly even other megalosauroids (=representatives of Megalosauroidea in which spinosaurids are phylogenetically placed), preferred habitats with a relatively strong aquatic influence (Sales et al., 2016; Rauhut et al., 2016; Beevor et al., 2021). Also, the spinosaurid co-occurrence together with other multi-ton carnivorous dinosaurs, in the Late Cretaceous of northern Africa, early prompted the inference of niche partitioning in respect to food preferences (Stromer, 1936). Whereas large-bodied terrestrial herbivores seem rare (at least in the fossil record), the heterogeneous palaeoenvironment, seemingly strongly influenced by deltas and other large water bodies, with a great aquatic biodiversity, maybe served as potential food source (see Stromer, 1936; Russell, 1996; Russell & Paesler, 2003; Cavin et al., 2010; Läng et al., 2013; Benyoucef et al., 2015; Ibrahim et al., 2020b).

I. challengeri was initially described as a crested maniraptoran theropod (=representatives of Maniraptora, which also include birds; Martill et al., 1996). Despite numerous new fossils assigned to spinosaurids (e.g., Kellner & Campos, 1996; Taquet & Russell, 1998; Kellner et al., 2011; Barrett et al., 2011; Richter et al., 2012; Evers et al., 2015; Aureliano et al., 2018; Arden et al., 2018; Lakin & Longrich, 2018; Maganuco & Dal Sasso, 2018; Barker et al., 2021; 2022; Heckeberg & Rauhut, 2020; Ibrahim et al., 2014; 2020a; b; Smyth et al., 2020; Samathi et al., 2021; Sereno et al., 2022), the most complete spinosaurid skull known to science is still represented by the holotype of *I. challengeri* (Martill et al., 1996; Sues et al., 2002; Sales & Schultz, 2017; Schade et al., 2020; in review: **Figure 1-4**). However, while already described by Sues et al. (2002) in some detail, many aspects of the preserved bones could not be described until recently (Schade et al., in review). With the aid of (micro)CT it was possible to reveal the morphology of preserved skull bones that are completely or partly hidden within the sedimentary matrix, such as the palatal and braincase complexes. With a detailed investigation and description of the digitally reconstructed skull bones, Schade et al. (in review) were able to unravel the complete holotype specimen and re-arrange the skull of *I. challengeri*. This resulted in new insights into the anatomy of this predator, such as a special morphology of the retroarticular process (muscle attachment site on the rear of the lower jaw), a large and ventrally inclined surangular shelf (muscle attachment site on the lateral aspect of lower jaw) and tooth replacement. Such anatomical revelations allowed for a better understanding of lifestyle-related aspects, for example, a strong and deeply implemented dentition with up to three generations of teeth per tooth position (Schade et al., in review: **Figure 5, 6**), and a comparably weak but fast bite (in contrast to other large-bodied carnivorous dinosaurs; see e.g., Therrien et al., 2005). Additionally, support was found for an optimized field of binocular view when the skull was held strongly ventrally inclined, and a unique kinetic mode of jaw-opening

movement; the latter producing laterally spreading and rotating lower jaw rami (see Hendrickx et al., 2016; Schade et al., 2020; in review: **Figure 2A, 3A, 4A, 40**). Further examinations included the phylogenetic coding of newly uncovered cranial features of *I. challengeri* (first hand with own data) and other tetanurans (=representatives of Tetanurae; first hand and literature-sourced), based on a previously published matrix (Rauhut & Pol, 2019). Subsequently, the codings were analyzed using parsimony methods to approach the special spinosaurid cranial anatomy and the underlying evolutionary history. Although spinosaurids are endowed with an aberrant cranial morphology, the group does not show especially high evolutionary rates which might be explained by a long ghost lineage on its base (Early Cretaceous or before; Schade et al., in review: **Figure 36-38**). Based on the findings of Schade et al. (in review), thoroughly descriptions of all preserved skull bones are presented, adding to our knowledge of palaeobiological aspects of *I. challengeri*, and by reasoned inference, other spinosaurids.

The morphology of the endosseous labyrinth and the large flocculus of the braincase endocast suggest an active predator (see remarks above; Schade et al., 2020; in review). In situations demanding the optimization of sensory capabilities (see also Sampson & Witmer, 2007), *I. challengeri* likely held its skull strongly inclined which is indicated by the horizontal orientation of the lateral semicircular canal of the endosseous labyrinth, the inclination of the occipital condyle, and the maximization of the field of binocular view in front of the skull (see also Stevens, 2006); the latter being enabled by the composition of the preorbital region (seemingly also present in other spinosaurids; see Barker et al., 2021; Sereno et al., 2022; Schade et al., in review: **Figure 2A, 3A, 4A**).

Biomechanically, the vertebrate mandibles can be understood as third-order levers, with the jaw-closing muscles (adductors) inserting on the lower jaw in between a hypothetical weight or prey on the anteriormost jaw portion and the posterior jaw joint, representing the fulcrum (see Barel, 1983; Westneat, 1994; 2003; Schade et al., in review: **Figure 39**). Hence, the arrangement of jaw articulation, muscle attachment sites and the morphology of bony protagonists are crucial in understanding the ensemble of such interrelationships resulting in functional anatomy. Physically, rapid jaw movements with a comparably weak bite force in *I. challengeri* (in contrast to other large-bodied theropods; see e.g., Holliday, 2009) are induced by the arrangement and morphology of the muscle attachment sites, for example, in respect to the relatively far-posteriorly placed coronoid eminence (musculus adductor mandibulae externus profundus, jaw closer; Holliday & Witmer, 2007; Sellers et al., 2017; Cost et al., 2022; Schade et al., in review: **Figure 2, 3, 34, 35, 39**), the large and ventrally oriented surangular shelf (dorsally: musculus adductor mandibulae externus superficialis and ventrally: musculus pterygoideus ventralis, both jaw closer) and the large retroarticular process (musculus depressor mandibulae, jaw opener); all three features are situated on the lower jaw. Furthermore, the quadrate is anteroventrally inclined in *I. challengeri*; the quadrate is posteroventrally inclined or vertically oriented in most other non-avian theropods, potentially creating enormous bite forces with relative ease (e.g., Therrien et al., 2005; Sampson & Witmer, 2007; Holliday, 2009; Schade et al., in review; however, see also Mazzetta et al., 2009 and references therein). Additional insight into jaw

biomechanics come from the slight lateromedial orientation of the intercondylar sulcus, as well as the lateromedially wide ectocondyle (Schade et al., in review: **Figure 19E**; present in spinosaurids, but different in other non-avian theropods; Hendrickx et al., 2016) of the quadrate, and the likely unfused mandibular symphysis of most non-avian theropods (Stromer, 1915; Charig & Milner, 1997; Holliday & Nesbitt, 2013; Hendrickx et al., 2016). Whereas the quadrate features forced the lower jaw rami slightly outwards during depression, the unfused symphysis produced a flexible connection with soft tissue in life which may allowed a certain lateral stretching on the symphysis. Because the posterior edge of the glenoid fossa would cut into the posterior aspect of the quadrate in greater opening angles (ignoring the effect of the formerly present cartilaginous caps), *I. challengeri* was able to open its mouth about 40° (considerable greater angles might have been possible in other large theropods; Lautenschlager, 2015); during this movement, the lower jaw rami slightly rotated and spread laterally, widening the pharynx about 30 mm per side (Schade et al., in review: **Figure 40**).

Together, these and other anatomical features prompt the assumption of fast, and hence, powerful jaw movements (also because of the relatively long muzzle and the tension produced by the stretched soft tissue on the mandidular symphysis, which in turn may explain the large retroarticular facet for jaw opening as antagonist; see also Henderson, 2002; Therrien et al., 2005), accompanied by laterally rotating and spreading jaws, widening the pharynx and enabling gravitational-lead gulping of small and fatally injured prey items with ease (**Fig. 7**). Strong, deeply implemented and fast-replaced dentition (e.g., Heckberg & Rauhut, 2020; Schade et al., in review), and precise and powerful skull movements (potentially indicated by the endosseous labyrinth morphology and long neck vertebrae with ventral rugosities of other spinosaurids; Evers et al., 2015 and references therein; Schade et al., 2020) complete the concept of an - in comparison to the ecology of other large-bodied theropods - unusual hunter that possibly thrived in the vicinity of exploitable water bodies (with the snout partially submerged; indicated by posteriorly placed external nares; Sues et al., 2002; Schade et al., in review: **Figure 2**) in Early Cretaceous ecosystems of modern-day Brazil (Martill et al., 1996; Sues et al., 2002; Selden & Nudds, 2012; Aureliano et al., 2018). Like most, if not all present-day predators, *I. challengeri* choose to feed on carcasses too, but was probably very well adapted to an active hunting mode (Hone & Holtz, 2017; 2019; 2021), equipped with grappling hands (like other spinosaurids; Charig & Milner, 1997; Sereno et al., 1998; 2022) and spreading jaws (Hendrickx et al., 2016; Schade et al., in review: **Figure 40**). In summary, the comprehensive investigation of the (neuro)anatomy of the holotype of *I. challengeri* produced a plethora of previously unknown anatomical details, providing a well-documented basis for comparison of future studies. Furthermore, it enlightens our perception of spinosaurid palaeobiology with ecological aspects such as (sensorial-led) behavior, feeding style and biomechanics (with implications for niche partitioning), in turn providing a direct basis for further studies such as finite-element analyses and morphometrics. Finally, the findings of Schade et al. (in review) add to the phylogenetical framework and understanding of the evolutionary history of spinosaurids.

Fig. 7 Life reconstruction of *Irritator challengeri* foraging in a shallow water body of Early Cretaceous Brazil with an inclined skull revealing the remarkable pharyngeal widening; induced by (neuro)anatomy (estimated skull length of *Irritator*: ~ 650 mm; see Schade et al., 2020; in review) - commissioned artwork by Olof Moleman.

3.2.2. Osteoderms of thyreophoran dinosaurs from the Early Jurassic of Mecklenburg-Western Pomerania (Schade & Ansorge, 2022)

Two thyreophoran (armoured, herbivorous dinosaurs, ranging from the Early Jurassic to the Late Cretaceous with a worldwide distribution, encompassing taxa like *Stegosaurus* and *Ankylosaurus*; Thompson et al., 2012) osteoderms from the Lower Jurassic of Mecklenburg-Western Pomerania were the objects of closer examination (one of them with the aid of microCT) in another study included in this thesis (Schade & Ansorge, 2022: **Figure 2A, 3A, 5A**).

Since its discovery in the 1960s and the formal description in 1990, *Emausaurus ernsti* represents the only dinosaur known to science in the state of Mecklenburg-Western Pomerania from substantial material (see also Stumpf et al., 2015). The holotype of *E. ernsti* consists of over 50 individual bones, many belonging to a largely complete skull (mainly missing the palate and braincase complexes), but also vertebrae, ribs, phalanges and osteoderms are known (Haubold, 1990). Because of the unproblematic separation of some skull elements from each other and the minor degree of ossification of, for example, vertebral centra and neural arches, *E. ernsti* was considered to represent a juvenile or subadult (Haubold, 1990); the author estimated a body length of the holotype individual of around 2 m. Since the description of *E. ernsti*, the more complete material of a closely related and slightly older (Sinemurian) basal thyreophoran from England has been described: *Scelidosaurus harrisonii* (BRSMG LEGL 0004; Norman, 2020a; b). Recently, Schade & Ansorge (2022) re-examined the specimen GG 85/1 23, representing the largest and most complete osteoderm of *E. ernsti* which was thought to having originally been situated on a parasagittal position on the postcranium (Haubold, 1990). However, the occipital osteoderms of the *S. harrisonii* specimen BRSMG LEGL 0004 seem morphologically very similar to the osteoderm GG 85/1 23 (Haubold, 1990; Norman 2020a; b). In case GG 85/1 23 also represents an occipital osteoderm of *E. ernsti*, it would have occupied approx. 70% of the skull width on the posterodorsal aspect; in contrast to the suspected subadult *S. harrisonii* individual BRSMG LEGL 0004, in which this is 65% (Haubold, 1990; Norman, 2020a; b). Hence, the likely socio-sexual component of the keratinized osteoderms of thyreophorans may render the holotype of *E. ernsti* rather a subadult than a juvenile (see also Main et al., 2005; Farlow et al., 2010; Brown et al., 2017; Brown, 2017; Norman, 2020a; b; Schade & Ansorge, 2022).

Furthermore, the microCT data allowed to reconstruct vascular canals inside the osteoderm GG 85/1 23. The canals on the base reach not far to the apex which is similar in the *Stegosaurus* plate YPM 57716 (Farlow et al., 2010). However, whereas there is a main canal in *Stegosaurus* from which different other canals diverge (Farlow et al., 2010), the pattern in *Emausaurus* rather consists of numerous discrete canals on both sides and edges of the osteoderm (Schade & Ansorge, 2022: **Figure 5**).

In addition to the re-examination of the *Emausaurs* osteoderm, a new fossil assigned to an unknown thyreophoran dinosaur (similar to *E. ernsti* and *S. harrisonii*) was thoroughly described and, after consideration of other alternatives, interpreted to represent an osteoderm as well (Schade & Ansorge, 2022: **Figure 2-4**). The new

osteoderm was potentially situated in the lateral shoulder region of an individual larger than the holotype of *E. ernsti* and BRSMG LEGL 0004, because of the large size of the incomplete plate (155 mm proximodistally; see also Norman, 2020a; b; Schade & Ansorge, 2022).

4. Final remarks

From what we know so far, non-avian dinosaurs inhabited this planet approx. 165 million years, between the Late Triassic (or earlier) and the Late Cretaceous. In this time, the group diversified, evolved astonishing anatomical adaptations and realized ecological niches without a proper extant equivalent. The thorough (neuro)anatomical descriptions delivered here will provide bases of comparison for future examinations of skulls and braincase endocasts. Given the fragmentary nature of the investigated material, it has still proven to be source of an extremly wide variety of information regarding palaeobiological aspects of the respective taxa. The fossil material being the main subject of this thesis belongs to animals that would have never encountered each other because they roamed their respective ecosystems in different times and places. However, the investigation of their (neuro)crania has exposed to be exceedingly insightful and comparable; partly with each other and with their respective relatives. Among others, previously unknown internal vascular structures in *Emausaurus ernsti* add to our knowledge about such patterns in osteoderms, support previous assessments of ontogenetic stages in braincase material of *Europasaurus holgeri*, and suggest the presence of special physiological adaptations involved in thermoregulation in *Struthiosaurus austriacus*. The delivered appraisals and implications of neuroanatomy of *Irritator challengeri*, *S. austriacus* and *E. holgeri* greatly enhance our understanding of their palaeoecology, for example in respect to foraging and self-defense methods, niche partitioning, audition and intraspecific communication; they give insights into a long-gone life when planet earth and many organisms upon were very different from what we know.

As is usually the case in science, more data is needed to validate, tame or falsify the mentioned affinities. Extending sampling of braincase endocasts of future studies promises anew revelations about extinct and extant taxa, and clarifies the reasonableness of certain interpretations. The data emerged from the studies of this thesis is freely available for anybody to implement in further considerations like statistics, phylogenetic or morphometric approaches; the digitally re-arranged skull of *I. challengeri* may be used for closer examination of bite forces and jaw biomechanics, for example.

The author considers science a means to roughly describe nature; aspects mentioned in this thesis conveying the impression of emerging hybris were not intended. The five scientific articles of this thesis were produced during a pandemic situation and a time of increased consequences and awareness of drastic global climate changes associated with human action; extensive collection visits and conferences overseas were avoided.

5. References

Allain, R., Xaisanavong, T., Richir, P. & Khentavong, B. The first definitive Asian spinosaurid (Dinosauria: Theropoda) from the Early Cretaceous of Laos. *Sci. Nat.* 99, 369–377. https://doi.org/10.1007/s00114-012-0911-7 (2012).

Amiot, R. *et al*. Oxygen isotope composition of continental vertebrate apatites from Mesozoic formations of Thailand; environmental and ecological significance. *Geol. Soc. Spec. Publ.* 315(1), 271–283. https://doi.org/10.1144/SP315.19 (2009).

Amiot, R. *et al*. Oxygen isotope evidence for semi-aquatic habits among spinosaurid theropods. *Geology* 38, 139–142. https://doi.org/10.1130/G30402.1 (2010a).

Amiot, R. *et al*. Oxygen and carbon isotope compositions of middle Cretaceous vertebrates from North Africa and Brazil: Ecological and environmental significance. *Palaeogeogr. Palaeoclimatol. Palaeoecol.* 297, 439–451. https://doi.org/10.1016/j.palaeo.2010.08.027 (2010b).

Araújo, R. *et al.* Inner ear biomechanics reveals a Late Triassic origin for mammalian endothermy. *Nature* 607, 726–731. https://doi.org/10.1038/s41586-022-04963-z (2022).

Arbour, V. M. Estimating impact forces of tail club strikes by ankylosaurid dinosaurs. *PLoS ONE* 4(8), e6738. https://doi.org/10.1371/ journal.pone.0006738 (2009).

Arbour, V. M., Lech-Hernes, N. L., Guldberg, T. E., Hurum, J. H. & Currie, P. J. An ankylosaurid dinosaur from Mongolia with in situ armour and keratinous scale impressions. *Acta Palaeontol. Pol.* 58(1), 55–64. https://doi.org/10.4202/app.2011.0081 (2013).

Arbour, V. M. & Currie, P. J. Ankylosaurid dinosaur tail clubs evolved through stepwise acquisition of key features. *J. Anat.* 227, 514–523. https://doi.org/10.1111/joa.12363 (2015).

Arai, M. & Assine, M. L. Chronostratigraphic constraints and paleoenvironmental interpretation of the Romualdo Formation (Santana Group, Araripe Basin, Northeastern Brazil) based on palynology. *Cretac. Res.* 116, 104610. https://doi.org/10.1016/j.cretres.2020.104610 (2020).

Arden, T. M. S., Klein, C. G., Zouhri, S. & Longrich, N. R. Aquatic adaptation in the skull of carnivorous dinosaurs (Theropoda: Spinosauridae) and the evolution of aquatic habits in spinosaurids. *Cretac. Res.* 93, 275–284. https://doi.org/10.1016/j.cretres.2018.06.013 (2019).

Aureliano, T. *et al*. Semi-aquatic adaptations in a spinosaur from the Lower Cretaceous of Brazil. *Cretac*. *Res*. 90, 283–295 (2018).

Balanoff, A. M., Bever, G. S., Rowe, T. B. & Norell, M. A. Evolutionary origins of the avian brain. *Nature* 501, 93–96. https://doi.org/10.1038/nature12424 (2013).

Balanoff, A. M. *et al*. Best practices for digitally constructing endocranial casts: examples from birds and their dinosaurian relatives. *J. Anat*. 229 (2). https://doi.org/10.1111/joa.12378 (2015).

Balanoff, A. M. & Bever, G. S. The role of endocasts in the study of brain evolution in *Evolution of nervous systems* (ed. Kaas, J.) 223–241. https://doi.org/10.1016/B978-0-12-804042-3.00023-3 (2017).

Ballell, A., King, L., Neenan, J., Rayfield, E. & Benton, M. The braincase, brain and palaeobiology of the basal sauropodomorph dinosaur *Thecodontosaurus antiquus*. *Zool. J. Linn. Soc.* 193. https://doi.org/10.1093/zoolinnean/zlaa157 (2021).

Barel, C. D. N. Toward a constructional morphology of cichlid fishes (Teleostei, Perciformes). *Neth. J. Zool*. 33, 357–424 (1983).

Barker, C. T. *et al*. New spinosaurids from the Wessex formation (Early Cretaceous, UK) and the European origins of Spinosauridae. *Sci. Rep*. 11, 19340. https://doi.org/10.1038/s41598-021-97870-8 (2021).

Barrett, P. M., Benson, R. B. J., Rich, T. H. & Vickers-Rich, P. First spinosaurid dinosaur from Australia and the cosmopolitanism of Cretaceous dinosaur faunas. *Biol. Lett.* 7, 933–936. https://doi.org/10.1098/rsbl.2011.0466 (2011).

Beevor, T. *et al*. Taphonomic evidence supports an aquatic lifestyle for *Spinosaurus*. *Cretac. Res.* https://doi.org/10.1016/j.cretres.2020.104627 (2021).

Benoit, J. *et al.* A test of the lateral semicircular canal correlation to head posture, diet and other biological traits in “ungulate” mammals. *Sci. Rep.* 10, 19602. https://doi.org/10.1038/s41598-020-76757-0 (2020).

Benson, R. B. J., Starmer-Jones, E., Close, R. A. & Walsh, S. A. Comparative analysis of vestibular ecomorphology in birds. *J. Anat.* 231, 990–1018. https://doi.org/10.1111/joa.12726 (2017).

Benton, M. J. *et al*. Dinosaurs and the island rule: the dwarfed dinosaurs from Hateg Island. *Palaeogeogr. Palaeoclimatol. Palaeoecol.* 293, 438–454 (2010).

Benyoucef, M. *et al*. Overabundance of piscivorous dinosaurs (Theropoda: Spinosauridae) in the mid-Cretaceous of North Africa: The Algerian dilemma. *Cretac. Res*. 55. https://doi.org/10.1016/j.cretres.2015.02.002 (2015).

Billet, G. *et al.* High morphological variation of vestibular system accompanies slow and infrequent locomotion in three-toed sloths. *Proc. R. Soc. B: Biol. Sci*. 279, 3932-9. https://doi.org/10.1098/rspb.2012.1212 (2012).

Bird, D. J. *et al.* Olfaction written in bone: cribriform plate size parallels olfactory receptor gene repertoires in Mammalia. *Proc. R. Soc. B* 285. https://doi.org/10.1098/rspb.2018.0100 (2018).

Bourke, J. M., Porter, W. R. & Witmer, L. M. Convoluted nasal passages function as efficient heat exchangers in ankylosaurs (Dinosauria: Ornithischia: Thyreophora). *PLoS ONE* 13(12), e0207381. https://doi.org/10.1371/journal.pone.0207381 (2018).

Brigande, J. V., Kiernan, A. E., Gao, X., Iten, L. E. & Fekete, D. M. Molecular genetics of pattern formation in the inner ear: Do compartment boundaries play a role? *PNAS* 97(22), 11700–11706. https://doi.org/10.1073/pnas.97.22.11700 (2000).

Bronzati, M. *et al.* Deep evolutionary diversification of semicircular canals in archosaurs. *Curr. Biol.* 31(12), 2520–2529.e6. https://doi.org/10.1016/j.cub.2021.03.086 (2021).

Brown, C. M. An exceptionally preserved armored dinosaur reveals the morphology and allometry of osteoderms and their horny epidermal coverings. *PeerJ* 5, e4066. https://doi.org/10.7717/peerj.4066 (2017).

Brown, C. M. *et al.* An exceptionally preserved three-dimensional armored dinosaur reveals insights into coloration and Cretaceous predator-prey dynamics. *Curr. Bio.* https://doi.org/10.1016/j.cub.2017.06.071 (2017).

Brown, C. M. *et al.* Dietary palaeoecology of an Early Cretaceous armoured dinosaur (Ornithischia; Nodosauridae) based on floral analysis of stomach contents. *R. Soc. Open Sci.* 7, 200305. https://doi.org/10.1098/rsos.200305 (2020).

Buchholtz, E. Dinosaur paleoneurology in *The Complete Dinosaur* (ed. Brett-Surmann, M. K., Holtz, T. R. Jr. & Farlow, J. O.) 191–208 (Indiana University Press, 2012).

Buffetaut, E., Martill, D. M. & Escuillié, F. Pterosaurs as part of a spinosaur diet. *Nature* 430, 33 (2004).

Butler, R. J. & Barrett, P. M. Palaeoenvironmental controls on the distribution of Cretaceous herbivorous dinosaurs. *Sci. Nat.* 95, 1027–1032 (2008).

Carpenter, K., Sanders, F., McWhinney, L. A. & Wood, L. Evidence for predator–prey relationships: examples for *Allosaurus* and *Stegosaurus* in *The Carnivorous Dinosaurs* (ed. Carpenter, K.) 325–350 (Indiana University Press, 2005).

Carrano, M. T., Benson, R. B. J. & Sampson, S. D. The phylogeny of Tetanurae (Dinosauria: Theropoda). *J. Syst. Palaeontol.* 10, 211–300. https://doi.org/10.1080/14772019.2011.630927 (2012).

Cavin L. *et al.* Vertebrate assemblages from the early Late Cretaceous of southeastern Morocco: An overview. *J. Afr. Earth Sci*. 57, 391–412. https://doi.org/10.1016/j.jafrearsci.2009.12.007 (2010).

Cerio D. G. & Witmer L. M. Intraspecific variation and symmetry of the inner-ear labyrinth in a population of wild turkeys: implications for paleontological reconstructions. *PeerJ* 7:e7355. https://doi.org/10.7717/peerj.7355 (2019).

Cerroni, M. A. & Paulina-Carabajal, A. Novel information on the endocranial morphology of the abelisaurid theropod *Carnotaurus sastrei*. *C. R. Palevol.* 18, 985–995. https://doi.org/10.1016/j.crpv.2019.09.005 (2019).

Charig, A.J. & Milner, A.C. *Baryonyx*, a remarkable new theropod dinosaur. *Nature* 324, 359–361 (1986).

Charig, A. J. & Milner, A. C. *Baryonyx walkeri*, a fish-eating dinosaur from the Wealden of Surrey. *J. Syst. Palaeontol.* 53, 11–70 (1997).

Chin, K. *et al.* A king-sized theropod coprolite. *Nature* 393, 680–682. https://doi.org/10.1038/31461 (1998).

Choiniere, J. *et al.* Evolution of vision and hearing modalities in theropod dinosaurs. *Science* 372, 610–613. https://doi.org/10.1126/science.abe7941 (2021).

Cisneros, J. C., Ghilardi, A. M., Raja, N. B. & Stewens, P. P. The moral and legal imperative to return illegally exported fossils. *Nat. Ecol. Evol.* 6, 2–3. https://doi.org/10.1038/s41559-021-01588-9 (2022).

Cohen, K. M., Finney, S. C., Gibbard, P. L. & Fan, J.-X. (2013; updated) The ICS International Chronostratigraphic Chart. Episodes 36: 199–204 (2022).

Corfield, J. R. *et al.* Diversity in olfactory bulb size in birds reflects allometry, ecology, and phylogeny. *Front. Neuroanat.* 9, 102. https://doi.org/10.3389/fnana.2015.00102 (2015).

Coombs, W. P. Jr. Forelimb muscles of the Ankylosauria (Reptilia, Ornithischia). *J. Paleontol.* 52, 642–657 (1978).

Cost, I. N. *et al.* 2D and 3D visualizations of archosaur jaw muscle mechanics, ontogeny and phylogeny using ternary diagrams and 3D modeling. *J. Exp. Biol.* 225. https://doi.org/10.1242/jeb.243216 (2022).

Cox, P. G. & Jeffery, N. Semicircular canals and agility: the influence of size and shape measures. *J. Anat.* 216, 37–47. https://doi.org/10.1111/j.1469-7580.2009.01172.x (2010).

Curry Rogers, K., Whitney, M., D'Emic, M. & Bagley, B. Precocity in a tiny titanosaur from the Cretaceous of Madagascar. *Science* 352, 450–453. https://doi.org/10.1126/science.aaf1509 (2016).

Dal Sasso, C., Maganuco, S., Buffetaut, E. & Mendez, M. A. New information on the skull of the enigmatic theropod *Spinosaurus*, with remarks on its size and affinities. *J. Vertebr. Paleontol*. 25, 888–896. https://doi.org/10.1671/0272-4634(2005)025[0888:NIOTSO]2.0.CO;2 (2005).

David, R. *et al*. Motion from the past. A new method to infer vestibular capacities of extinct species. C. R. Palevol 9, 397–410. https://doi.org/10.1016/j.crpv.2010.07.012 (2010).

David, R., Bronzati, M. & Benson, R. B. J. Comment on "The early origin of a birdlike inner ear and the evolution of dinosaurian movement and vocalization". *Science* 376, eabl6710. https://doi.org/10.1126/science.abl6710 (2022).

Dembitzer, J. *et al.* Small brains predisposed Late Quaternary mammals to extinction. *Sci. Rep.* 12, 3453. https://doi.org/10.1038/s41598-022-07327-9 (2022).

DePalma, R. A., Burnham, D. A., Martin, L. D., Rothschild, B. M. & Larson, P. L. Physical evidence of predatory behavior in *Tyrannosaurus rex*. *PNAS* 110(31), 12560–12564. https://doi.org/10.1073/pnas.1216534110 (2013).

Dial, K. P. Evolution of avian locomotion: correlates of flight style, locomotor modules, nesting biology, body size, development, and the origin of flapping flight. *J. Ornithol.* 120(4), 941–952 (2003).

Dudgeon, T. W., Maddin, H. C., Evans, D. C. & Mallon, J. C. The internal cranial anatomy of *Champsosaurus* (Choristodera: Champsosauridae): Implications for neurosensory function. *Sci. Rep.* 10, 7122 (2020).

Dujim, M. On the head posture in birds and its relation to some anatomical features. *Proceedings of the Koninklijke Nederlandse Akademie Van Wetenschappen, Series C. Biological and Medical Sciences* 54, 260–271 (1951).

Early, C. M., Iwaniuk, A. N., Ridgely, R. C. & Witmer, L. M. Endocast structures are reliable proxies for the sizes of corresponding regions of the brain in extant birds. *J. Anat.* 237, 1162–1176. https://doi.org/10.1111/joa.13285 (2020).

Edinger, T. Die fossilen Gehirne. *Ergebnisse der Anatomie und Entwicklungsgeschichte* 28, 1–249 (1929).

Edinger, T. The pituitary body in giant animals fossil and living: a survey and a suggestion. *Q. Rev. Biol.* 17, 31–45 (1942).

Evers, S. W., Rauhut, O. W. M., Milner, A. C., McFeeters, B. & Allain, R. A reappraisal of the morphology and systematic position of the theropod dinosaur *Sigilmassasaurus* from the “middle” Cretaceous of Morocco. *PeerJ* 3, e1323. https://doi.org/10.7717/peerj.1323 (2015).

Evers, S. W. *et al*. Neurovascular anatomy of the protostegid turtle *Rhinochelys pulchriceps* and comparisons of membranous and endosseous labyrinth shape in an extant turtle. *Zool*. *J. Linnean. Soc.* 187, 800–828. https://doi.org/10.1093/zoolinnean/zlz063 (2019).

Evers, S. W. *et al.* Independent origin of large labyrinth size in turtles. *Nat. Commun.* 13, 5807. https://doi.org/10.1038/s41467-022-33091-5 (2022).

Ezcurra, M. D. *et al.* Enigmatic dinosaur precursors bridge the gap to the origin of Pterosauria. *Nature* 588(7838), 445–449. https://doi.org/10.1038/s41586-020-3011-4 (2020).

Fabbri, M. *et al*. The skull roof tracks the brain during the evolution and development of reptiles including birds. *Nat. Ecol. Evol*. 1(10), 1543–1550. https://doi.org/10.1038/s41559-017-0288-2 (2017).

Fabbri, M. *et al.* Subaqueous foraging among carnivorous dinosaurs. *Nature* 603, 852–857. https://doi.org/10.1038/s41586-022-04528-0 (2022).

Farlow, J. O., Hayashi, S. & Tattersall, G. J. Internal vascularity of the dermal plates of *Stegosaurus* (Ornithischia, Thyreophora). *Swiss J. Geosci.* 103, 173–185. https://doi.org/10.1007/s00015-010-0021-5 (2010).

Ferreira-Cardoso, S. *et al.* Floccular fossa size is not a reliable proxy of ecology and behaviour in vertebrates. *Sci. Rep.* 7(1), 2017. https://doi.org/10.1038/s41598-017-01981-0 (2005).

Fischer, J. *et al*. Human-specific ARHGAP11B ensures human-like basal progenitor levels in hominid cerebral organoids. *EMBO Rep*. 13, e54728. https://doi.org/10.15252/embr.202254728 (2022).

Foster, J. B. The evolution of mammals on islands. *Nature* 202(4929), 234–235. https://doi.org/10.1038/202234a0 (1964).

Franzosa, J. & Rowe, T. Cranial endocast of the Cretaceous theropod dinosaur *Acrocanthosaurus atokensis*. *J. Vertebr. Paleontol.* 25, 859–864 (2005).

Galton, P. M. Skull bones and endocranial casts of stegosaurian dinosaur *Kentrosaurus* Hennig, 1915 from Upper Jurassic of Tanzania, East Africa. *Geol. Palaeontol.* 22, 123–143 (1988).

Galton, P. M. Endocranial casts of the plated dinosaur *Stegosaurus* (Upper Jurassic, Western USA): A complete undistorted cast and the original specimens of Othniel Charles Marsh in *The Armored Dinosaurs* (ed. Carpenter, K.) 103–129 (Indiana University Press, 2001).

Georgi, J. A. & Sipla, J. S. Comparative and functional anatomy of balance in aquatic reptiles and birds in *Sensory evolution on the threshold: adaptations in secondarily aquatic vertebrates* (ed. Thewissen, J. G. M. & Nummela, S.) 233–256 (University of California Press, 2008).

Gleich, O., Dooling, R. J. & Manley, G. A. Audiogram, body mass, and basilar papilla length: correlations in birds and predictions for extinct archosaurs. *Naturwissenschaften* 92, 595–589. https://doi.org/10.1007/s00114-005-0050-5 (2005).

Hallett, M. & Wedel, M. J. *The sauropod dinosaurs. Life in the age of giants.* 320p (Johns Hopkins University Press, 2016).

Hanson, M., Hoffman, E. A., Norell, M. A. & Bhullar, B. S. The early origin of a birdlike inner ear and the evolution of dinosaurian movement and vocalization. *Science* 372(6542), 601–609. https://doi.org/10.1126/science.abb4305 (2021).

Hanson, M., Hoffman, E. A., Norell, M. A. & Bhullar, B. S. Response to Comment on "The early origin of a birdlike inner ear and the evolution of dinosaurian movement and vocalization". *Science* 376, eabl8181. https://doi.org/10.1126/science.abl8181 (2022).

Hassler, A. *et al.* Calcium isotopes offer clues on resource partitioning among Cretaceous predatory dinosaurs. *Proc. Biol. Sci.* 285. https://doi.org/10.1098/rspb.2018.0197 (2018).

Haubold, H. Ein neuer Dinosaurier (Ornithischia, Thyreophora) aus dem unteren Jura des Nordlichen Mitteleuropa. *Rev. Paléobiol.* 9, 149–177 (1990).

Hayashi, S., Carpenter, K., Scheyer, T. M., Watanabe, M. & Suzuki, D. Function and evolution of ankylosaur dermal armor. *Acta Palaeontol. Pol.* 55(2), 213–228 (2010).

Heckeberg, N. & Rauhut, O. W. M. Histology of spinosaurid dinosaur teeth from the Albian-Cenomanian of Morocco: Implications for tooth replacement and ecology. *Palaeontol. Electron.* https://doi.org/10.26879/1041 (2020).

Henderson, D. M. The eyes have it: the sizes, shapes, and orientations of theropod orbits as indicators of skull strength and bite force. *J. Vertebr. Paleontol.* 22, 766–778. https://doi.org/10.1671/0272-4634(2002)022[0766:TEHITS]2.0.CO;2 (2002).

Hendrickx, C., Mateus, O., & Buffetaut, E. Morphofunctional analysis of the quadrate of Spinosauridae (Dinosauria: Theropoda) and the presence of *Spinosaurus* and a second spinosaurine taxon in the Cenomanian of North Africa. *PLoS ONE* 11(1), e0144695. https://doi.org/10.1371/journal.pone.0144695 (2016).

Hildebrand, M. & Goslow, G. *Vergleichende und funktionelle Anatomie der Wirbeltiere*. 709p. https://doi.org/10.1007/978-3-642-18951-7 (Springer, 2004).

Holliday, C. M. & Witmer, L. M. Archosaur adductor chamber evolution: integration of musculoskeletal and topological criteria in jaw muscle homology. *J. Morphol*. 268(6), 457–484. https://doi.org/10.1002/jmor.10524 (2007).

Holliday, C.M. New insights into dinosaur jaw muscle anatomy. *Anat. Rec*. 292, 1246–1265. https://doi.org/10.1002/ar.20982 (2009).

Holliday, C. & Nesbitt, S. Morphology and diversity of the mandibular symphysis of archosauriforms. *Geol. Soc. Spec. Publ*. 379, 555-571. https://doi.org/10.1144/SP379.2 (2013).

Hone, D. W. E. & Holtz, T. R. Jr. A century of spinosaurs - a review and revision of the Spinosauridae with comments on their ecology. *Acta Geol. Sin-Engl.* 91, 1120–1132. https://doi.org/10.1111/1755-6724.13328 (2017).

Hone, D. W. E. & Holtz, T. R. Jr. Comment on: Aquatic adaptation in the skull of carnivorous dinosaurs (Theropoda: Spinosauridae) and the evolution of aquatic habits in spinosaurids. 93, 275e284. *Cretac. Res*. https://doi.org/10.1016/ j.cretres.2019.05.010 (2019).

Hone, D. W. E. & Holtz, T. R., Jr. Evaluating the ecology of *Spinosaurus*: Shoreline generalist or aquatic pursuit specialist? *Palaeontol. Electron*. 24, a03. https://doi.org/10.26879/1110 (2021).

Hopson, J. A. Relative brain size and behavior in archosaurian reptiles. *Annu. Rev. Ecol. Syst.* 8, 429–448. http://www.jstor.org/stable/2096736 (1977).

Hopson, J. A. Relative brain size in dinosaurs: Implications for dinosaurian endothermy in *A cold look at the warm-blooded dinosaurs* (ed. Thomas, R. D. K. & Olson, E. C.) 287– 310 (American Association for the Advancement of Science, 1980).

Hu, K. *et al.* Ontogenetic endocranial shape change in alligators and ostriches and implications for the development of the non-avian dinosaur endocranium. *Anat. Rec.* 304, 1759–1775. https://doi.org/10.1002/ar.24579 (2021).

Hübner, T. & Rauhut, O. W. M. A juvenile skull of *Dysalotosaurus lettowvorbecki* (Ornithischia: Iguanodontia), and implications for cranial ontogeny, phylogeny, and taxonomy in ornithopod dinosaurs. *Zool. J. Linn. Soc.* 160, 366–396. https://doi.org/10.1111/j.1096-3642.2010.00620.x (2010).

Hullar, T. E. Semicircular canal geometry, afferent sensitivity, and animal behavior. *Anat. Rec.* 288A, 466–472. https://doi.org/10.1002/ar.a.20304 (2006).

Hurlburt, G. R., Ridgely, R. C., & Witmer, L. M. Relative size of brain and cerebrum in tyrannosaurid dinosaurs: An analysis using brain-endocast quantitative relationships in extant alligators in *Tyrannosaurid paleobiology* (ed. Parrish, J. M., Molnar, R. E., Currie, P. J. & Koppelhus, E. B.) 134– 154 (Indiana University Press, 2013).

Hulke, J. W. Note on a large reptilian skull from Brooke, Isle of Wight, probably dinosaurian, and referable to the genus *Iguanodon*. *Quart. J. Geol. Soc. London* 27, 199– 206 (1871).

Ibrahim, N. *et al*. Semiaquatic adaptations in a giant predatory dinosaur. *Science* 345, 1613–1616. https://doi.org/10.1126/science.1258750 (2014).

Ibrahim, N. *et al*. Tail-propelled aquatic locomotion in a theropod dinosaur. *Nature* 581, 67–70 (2020a).

Ibrahim N. *et al*. Geology and paleontology of the Upper Cretaceous Kem Kem Group of eastern Morocco. *ZooKeys* 928, 1–216. https://doi.org/10.3897/zookeys.928.47517 (2020b).

Iwaniuk, A. N. & Nelson, J. E. Developmental differences are correlated with relative brain size in birds: a comparative analysis. *Can. J. Zool.* 81, 1913–1928. https://doi.org/10.1139/z03-190 (2003).

Janensch, W. Die Schädel der Sauropoden *Brachiosaurus*, *Barosaurus* und *Dicraeosaurus* aus den Tendaguru-Schichten Deutsch-Ostafrikas. *Palaeontographica*, Suppl. 7, 1(2), 147–298 (1935).

Jeffery, N. & Spoor, F. Prenatal growth and development of the modern human labyrinth. *J. Anat*. 204, 71–92 (2004).

Jerison, H. J. Fossil brains and the evolution of behavior. *Proc. Ann. Conven.Am. Psychol. Ass.* 4(Pt. 1), 7–8 (1969).

Jerison, H. J. *Evolution of the brain and intelligence*. 482p (Academic Press, 1973).

Jirak, D., & Janacek, J. Volume of the crocodilian brain and endocast during ontogeny. *PLoS ONE* 12(6), e0178491. https://doi.org/10.1371/journal.pone.0178491 (2017).

Jones, M. E. H. *et al.* Digital dissection of the head of the rock dove (*Columba livia*) using contrast-enhanced computed tomography. *Zool. Lett.* 5, 17. https://doi.org/10.1186/s40851-019-0129-z (2019).

Kardong, K. V. Vertebrates: comparative anatomy, function, evolution. 795p (McGraw-Hill Education, 2015).

Kellner, A. W. A. & Campos, D. First Early Cretaceous theropod dinosaur from Brazil with comments on Spinosauridae. *Neues Jahrb. Geol. Paläontol. Abh*. 199, 151–166 (1996).

Kellner, A. W. A., Azevedo, S. A. K., Machado, E. B., Carvalho, L. B. de & Henriques, D. D. R. A new dinosaur (Theropoda, Spinosauridae) from the Cretaceous (Cenomanian) Alcântara Formation, Cajual Island, Brazil. Anais de Academia Brasileira de Ciências. 83, 99–108 (2011).

Khorevin, V. The lagena (the third otolith endorgan in vertebrates). *Neurophysiol*. 40, 142–159. https://doi.org/10.1007/s11062-008-9021-8 (2008).

King, J. L., Sipla, J. S., Georgi, J. A., Balanoff, A. M. & Neenan, J. M. The endocranium and trophic ecology of *Velociraptor mongoliensis*. *J. Anat.* 237, 861–869 (2020).

Kirsch, J. A., Güntürkün, O. & Rose, J. Insight without cortex: Lessons from the avian brain. *Conscious. Cogn.* 17, 475–483 (2008).

Knoll, F. & Schwarz-Wings, D. Palaeoneuroanatomy of *Brachiosaurus*. *Ann. Paléontol.* 95, 165–175. https://doi.org/10.1016/j.annpal.2009.06.001 (2009).

Knoll, F. *et al.* Palaeoneurology of the early cretaceous iguanodont *Proa valdearinnoensis* and its bearing on the parallel developments of cognitive abilities in theropod and ornithopod dinosaurs. *J. Comp. Neurol*. 529(18), 3922–3945. https://doi.org/10.1002/cne.25224 (2021).

Kuzmin, I. T. *et al.* The braincase of *Bissektipelta archibaldi*—new insights into endocranial osteology, vasculature, and paleoneurobiology of ankylosaurian dinosaurs. *Biol. Commun.* 65(2), 85–156. https://doi.org/10.21638/spbu03.2020.201 (2020).

Kuzmin, I. T. *et al.* Braincase anatomy of extant Crocodylia, with new insights into the development and evolution of the neurocranium in crocodylomorphs. *J. Anat.* 239, 983–1038. https://doi.org/10.1111/joa.13490 (2021).

Läng, E. *et al*. Unbalanced food web in a Late Cretaceo us dinosaur assemblage. *Palaeogeogr. Palaeoclimatol. Palaeoecol.* 381-382, 26–32. https://doi.org/10.1016/j.palaeo.2013.04.011 (2013).

Lakin, R. & Longrich, N. Juvenile spinosaurs (Theropoda: Spinosauridae) from the middle Cretaceous of Morocco and implications for spinosaur ecology. *Cretac. Res*. 93, 129–142. https://doi.org/10.1016/j.cretres.2018.09.012 (2018).

Lautenschlager, S., Rayfield, E. J., Altangerel, P., Zanno, L. E. & Witmer, L. M. The endocranial anatomy of therizinosauria and its implications for sensory and cognitive function. *PLoS ONE* 7(12), e52289. https://doi.org/10.1371/journal.pone.0052289 (2012).

Lautenschlager, S. & Hübner, T. Ontogenetic trajectories in the ornithischian endocranium. *J. Evol. Biol.* 26, 2044–2050. https://doi.org/10.1111/jeb.12181 (2013).

Lautenschlager, S., Bright, J. A. & Rayfield, E. J. Digital dissection - using contrast-enhanced computed tomography scanning to elucidate hard- and soft-tissue anatomy in the common Buzzard *Buteo buteo*. *J. Anat.* 224, 412–431. https://doi.org/10.1111/joa.12153 (2014).

Lautenschlager, S. Estimating cranial musculoskeletal constraints in theropod dinosaurs. *R. Soc. Open Sci.* 2, 150495150495. http://doi.org/10.1098/rsos.150495 (2015).

Lessner, E. J. & Holliday, C. M. A 3D ontogenetic atlas of *Alligator mississippiensis* cranial nerves and their significance for comparative neurology of reptiles. *Anat. Rec.* 305, 2854–2882. https://doi.org/10.1002/ar.24550 (2022).

Liem, K., Bemis, W., Walker, W. & Grande, L. Functional Anatomy of the Vertebrates. 703p (Thomson Learning ,2001).

Lockley, M. G., Schulp, A. S., Meyer, C. A., Leonardi, G. & Mamani, D. K. Titanosaurid trackways from the Upper Cretaceous of Bolivia: Evidence for large manus, wide-gauge locomotion, and gregarious behaviour. *Cret. Res.* 23, 383–400 (2002).

Lokatis, S. & Jeschke, J. M. The island rule: An assessment of biases and research trends. *J Biogeogr*. 45, 289–303. https://doi.org/10.1111/jbi.13160 (2018).

Maganuco, S. & Dal Sasso, C. The smallest biggest theropod dinosaur: a tiny pedal ungual of a juvenile Spinosaurus from the Cretaceous of Morocco. *PeerJ* 6, e4785. https://doi.org/10.7717/peerj.4785 (2018).

Malafaia, E. *et al.* A new spinosaurid theropod (Dinosauria: Megalosauroidea) from the Upper Barremian of Vallibona, Spain: implications for spinosaurid diversity in the Early Cretaceous of the Iberian peninsula. *Cretac. Res*. 106, 104221. https://doi.org/10.1016/j.cretres.2019.104221 (2020).

Mallison, H. CAD assessment of the posture and range of motion of *Kentrosaurus aethiopicus* Hennig 1915. *Swiss. J. Geosci.* 103, 211–233. https://doi.org/10.1007/s00015-010- 0024-2 (2010).

Mallon, J. C. & Anderson, J. S. The functional and palaeoecological implications of tooth morphology and wear for the megaherbivorous dinosaurs from the dinosaur park formation (Upper Campanian) of Alberta, Canada. *PLoS ONE* 9(6), e98605. https://doi.org/10.1371/journal.pone.0098605 (2014).

Maidment, S. C. R. & Barrett, P. M. Osteological correlates for quadrupedality in ornithischian dinosaurs. *Acta Palaeontol. Pol.* 59(1), 53–70 (2014).

Main, R., A. De Ricqlès, J. Horner & K. Padian. The evolution and function of thyreophoran dinosaur scutes: implications for plate function in stegosaurs. *Paleobiology* 31(2), 291–314. https://doi.org/10.1666/0094-8373(2005)031[0291:TEAFOT]2.0.CO;2 (2005).

Marpmann, J. S., Carballido, J. L., Sander, M. P. & Knötschke, N. Cranial anatomy of the Late Jurassic dwarf sauropod *Europasaurus holgeri* (Dinosauria, Camarasauromorpha): ontogenetic changes and size dimorphism. *J. Syst. Palaeontol.* https://doi.org/10.1080/14772019.2013.875074 (2014).

Marsh, O. C . Odontornithes: a monograph on the extinct toothed birds of North America. 201 p (United States Geological Exploration of the 40th Parallel, 1880).

Marugán-Lobón, J., Chiappe, L. M. & Farke, A. A. The variability of inner ear orientation in saurischian dinosaurs: testing the use of semicircular canals as a reference system for comparative anatomy. *PeerJ* 1, e124. https://doi.org/10.7717/peerj.124 (2013).

Martill, D. M., Cruickshank, A. R. I. & Frey, E. A new crested maniraptoran dinosaur from the Santana Formation (Lower Cretaceous) of Brazil. *J. Geol. Soc.* 153, 5–8 (1996).

Mateus, O. & Estraviz-López, D. A new theropod dinosaur from the early cretaceous (Barremian) of Cabo Espichel, Portugal: Implications for spinosaurid evolution, *PLoS ONE* 17(2), e0262614. https://doi.org/10.1371/journal.pone.0262614 (2022).

Mazzetta, G., Cisilino, A., Blanco, R. E. & Calvo, N. Cranial mechanics and functional interpretation of the horned carnivorous dinosaur *Carnotaurus sastrei*. *J. Vertebr. Paleontol*. 29, 822–830. https://doi.org/10.1671/039.029.0313 (2009).

Miyashita, T., Arbour, V. M., Witmer, L. M. & Currie, P. J. The internal cranial morphology of an armoured dinosaur *Euoplocephalus* corroborated by X-ray computed tomographic reconstruction. *J. Anat.* 219, 661–675. https://doi.org/10.1111/j.1469-7580.2011.01427.x (2011).

Molnar, R. E. & Farlow, J. O. Carnosaur paleobiology in *The Dinosauria* (ed. Weishampel, D. B., Dodson, P. & Osmolska, H.) 210–224 (Berkeley: University of California Press, 1990).

Morhardt, A. C. *et al.* Study of endocranial & ontogeny in the Late Cretaceous non-avian dinosaur genus *Triceratops* using computed tomography & 3D visualization. (Poster, 2018).

Müller, R. Olfactory acuity in early sauropodomorph dinosaurs. *Hist. Biol*. 34. . https://doi.org/10.1080/08912963.2021.1914600 (2021).

Müller R. T., Ferreira, J. D., Pretto, F. A., Bronzati, M., & Kerber, L. The endocranial anatomy of *Buriolestes schultzi* (Dinosauria: Saurischia) and the early evolution of brain tissues in sauropodomorph dinosaurs. *J. Anat.* 238, 809–827. https://doi.org/10.1111/joa.13350 (2021).

Myers, T. & Fiorillo, A. Evidence for gregarious behavior and age segregation in sauropod dinosaurs. *Palaeogeogr. Palaeoclimatol. Palaeoecol*. 274, 96–104. . https://doi.org/10.1016/j.palaeo.2009.01.002 (2009).

Neenan, J. M. *et al*. Evolution of the sauropterygian labyrinth with increasingly pelagic lifestyles. *Curr. Biol.* 27, 3852–3858.e3. https://doi.org/10.1016/j.cub.2017.10.069 (2017).

Ngwenya, A., Patzke, N., Herculano-Houzel, S. & Manger, P. R. Potential Adult Neurogenesis in the Telencephalon and Cerebellar Cortex of the Nile Crocodile Revealed with Doublecortin Immunohistochemistry. *Anat. Rec.* 301, 659–672. https://doi.org/10.1002/ar.23738 (2018).

Nopcsa, F. v. Über Dinosaurier: Die Riesenformen unter den Dinosauriern. *Centralblatt für Mineralogie*. 332–351 (1917).

Norman, D. B. *Scelidosaurus harrisonii* from the Early Jurassic of Dorset, England: Cranial anatomy. *Zool. J. Linn. Soc.* 188(1), 1–81. https://doi.org/10.1093/zoolinnean/zlz074 (2020a).

Norman, D. B. *Scelidosaurus harrisonii* from the Early Jurassic of Dorset, England: the dermal skeleton. *Zool. J. Linn. Soc.* 190(1), 1–53. https://doi.org/10.1093/zoolinnean/zlz085 (2020b).

Northcutt, R. G. Understanding vertebrate brain evolution. *Integr. Comp. Biol.* 42, 743–756 (2002).

Olkowicz, S. *et al.* Birds have primate-like numbers of neurons in the forebrain. *PNAS* 113(26), 7255–7260. https://doi.org/10.1073/pnas.1517131113 (2016).

Osborn, H. F. Crania of *Tyrannosaurus* and *Allosaurus*. *Mem. Am. Mus. Nat. Hist.* 1, 3– 30 (1912).

Ősi, A., Pereda Suberbiola, X. & Földes, T. Partial skull and endocranial cast of the ankylosaurian dinosaur *Hungarosaurus* from the Late Cretaceous of Hungary: Implications for locomotion. *Palaeontol. Electro.* 17(1). https://doi.org/10.26879/405 (2014).

Ősi, A., Prondvai, E., Mallon, J. & Bodor, E. R. Diversity and convergences in the evolution of feeding adaptations in ankylosaurs (Dinosauria: Ornithischia). *Hist. Biol.* 29(4), 539–570. https://doi.org/10.1080/08912963.2016.1208194 (2017).

Paulina-Carabajal, A. Neuroanatomy of titanosaurid dinosaurs from the Upper Cretaceous of Patagonia, with comments on endocranial variability within sauropoda. *Anat. Rec.* 295, 2141–2156. https://doi.org/10.1002/ar.22572 (2012).

Paulina-Carabajal, A., Lee, Y. N. & Jacobs, L. L. Endocranial morphology of the primitive nodosaurid dinosaur *Pawpawsaurus campbelli* from the Early Cretaceous of North America. *PLoS ONE* 11(3), e0150845. https://doi.org/10.1371/journal.pone.0150845 (2016).

Paulina-Carabajal, A., Lee, Y. N., Kobayashi, Y., Lee, H. J. & Currie, P. J. Neuroanatomy of the ankylosaurid dinosaurs *Tarchia teresae* and *Talarurus plicatospineus* from the Upper Cretaceous of Mongolia, with comments on endocranial variability among ankylosaurs. *Palaeogeogr. Palaeoclimatol. Palaeoecol.* 494, 135–146. https://doi.org/10.1016/j.palaeo.2017.11.030 (2018).

Pereda-Suberbiola, X. & Galton, P. M. Revision of the cranial features of the dinosaur *Struthiosaurus austriacus* Bunzel (Ornithischia: Ankylosauria) from the Late Cretaceous of Europe. *Neues Jahrb. Geol. Palaontol. Abh.* 191, 173–200 (1994).

Pfaff, C., Martin, T. & Ruf, I. Bony labyrinth morphometry indicates locomotor adaptations in the squirrel-related clade (Rodentia, Mammalia). *Proc. R. Soc. B.* 282, 20150744. https://doi.org/10.1098/rspb.2015.0744 (2015).

Pfaff, C., Czernym, S., Nagel, D. & Kriwet, J. Functional morphological adaptations of the bony labyrinth in marsupials (Mammalia, Theria). *J. Morphol.* 278, 742–749, https://doi.org/10.1002/jmor.20669 (2017).

Pol, D. *et al.* Earliest evidence of herd-living and age segregation amongst dinosaurs. *Sci. Rep.* 11, 20023. https://doi.org/10.1038/s41598-021-99176-1 (2021).

Porter, W. R. & Witmer, L. M. Vascular patterns in the heads of dinosaurs: Evidence for blood vessels, sites of thermal exchange, and their role in physiological thermoregulatory strategies. *Anat. Rec.* 303, 1075–1103. https://doi.org/10.1002/ar.24234 (2019).

Rauhut, O. W. M. Morphology and mechanics of the jaws of spinosaurid theropods (Dinosauria): implications for predation. *Ameghiana* 38(4) Suplemento-Resumenes (2001).

Rauhut, O. W. M., Hübner, T. R., & Lanser, K.-P. A new megalosaurid theropod dinosaur from the late Middle Jurassic (Callovian) of north-western Germany: Implications for theropod evolution and faunal turnover in the Jurassic. *Palaeontol. Electro.* 19, 26A. https://doi.org/10.26879/654 (2016).

Rauhut, O. W. M. & Pol, D. Probable basal allosauroid from the early Middle Jurassic Cañadón Asfalto Formation of Argentina highlights phylogenetic uncertainty in tetanuran theropod dinosaurs. *Sci. Rep*. 9, 18826. https://doi.org/10.1038/s41598-019-53672-7 (2019).

Rayfield, E. J., Milner, A. C., Xuan, V. B. & Young, P. G. Functional morphology of spinosaur 'crocodile-mimic' dinosaurs. *J. Vertebr. Paleontol*. 27, 892–901. https://doi.org/10.1671/0272-4634(2007)27[892:FMOSCD]2.0.CO;2 (2007).

Rayfield, E. J. Structural performance of tetanuran theropod skulls, with emphasis on the Megalosauridae, Spinosauridae and Carcharodontosauridae. *Spec. Pap. Palaeontol.* 86, 241–253 (2011).

Richter, U., Mudroch, A., & Buckley, L.G. Isolated theropod teeth from the Kem Kem Beds (Early Cenomanian) near Taouz, Morocco. *PalZ*. 87, 291–309. https://doi.org/10.1007/s12542-012-0153-1 (2013).

Rogers, S. W. Exploring dinosaur neuropaleobiology: viewpoint computed tomography scanning and analysis of an *Allosaurus fragilis* endocast. *Neuron* 21, 673–679 (1998).

Romick, C. A. Ontogeny of the brain endocasts of Ostriches (Aves: *Struthio camelus*) with implications for interpreting extinct dinosaur endocasts [Undergraduate thesis, Ohio University]. OhioLINK Electronic Theses and Dissertations Center. http://rave.ohiolink.edu/etdc/view?acc_num=ouashonors1368018907 (2013).

Rowe, T. B., Macrini, T. E. & Luo, Z.-X. Fossil evidence on the origin of the mammalian brain. *Science* 332, 955–957. https://doi.org/10.1126/science.1203117 (2011).

Russell, D. A. Isolated dinosaur bones from the Middle Cretaceous of the Tafilalt, Morocco. *Bull. Mus. Hist. Nat. Paris* 19, 349–402 (1996).

Russell, D. A, & Paesler, M. A. Environments of Mid-Cretaceous Saharan dinosaurs. *Cretac. Res*. 24, 569–588. https://doi.org/10.1016/S0195-6671(03)00072-7 (2003).

Sales, M. A. F., Lacerda, M. B., Horn, B. L. D., Oliveira, I. A. P. de & Schultz, C. L. The "χ" of the matter: testing the relationship between paleoenvironments and three theropod clades. *PLoS ONE* 11(2), e0147031. https://doi.org/10.1371/journal.pone.0147031 (2016).

Sales, M. A. F. & Schultz, C. L. Spinosaur taxonomy and evolution of craniodental features: evidence from Brazil. *PLoS ONE* 12(11), e0187070. https://doi.org/10.1371/journal.pone.0187070 (2017).

Samathi, A., Sander, P. M. & Chanthasit, P. A spinosaurid from Thailand (Sao Khua Formation, Early Cretaceous) and a reassessment of Camarillasaurus cirugedae from the Early Cretaceous of Spain. *Hist. Biol.* 33, 3480–3494. https://doi.org/10.1080/08912963.2021.1874372 (2021).

Sampson, S. D. & Witmer, L. M. Craniofacial anatomy of *Majungasaurus crenatissimus* (Theropoda: Abelisauridae) from the Late Cretaceous of Madagascar. *J. Vertebr. Paleontol*. 27, 32–104. https://doi.org/10.1671/0272-4634(2007)27[32:CAOMCT]2.0.CO;2 (2007).

Sander, P. M., Mateus, O., Laven, T. & Knötschke, N. Bone histology indicates insular dwarfism in a new Late Jurassic sauropod dinosaur. *Nature* 441, 739–741 (2006).

Sander, P. M., Peitz, C., Jackson, F. D. & Chiappe, L. M. Upper Cretaceous titanosaur nesting sites and their implications for sauropod dinosaur reproductive biology. *Palaeontogr. A* 284, 69–107 (2008).

Sander, P. M. *et al*. Biology of the sauropod dinosaurs: the evolution of gigantism. *Biol. Rev.* 86, 117–155. https://doi.org/10.1111/j.1469-185X.2010.00137.x (2011).

Schade, M., Rauhut, O. W. M. & Evers, S. W. Neuroanatomy of the spinosaurid *Irritator challengeri* (Dinosauria: Theropoda) indicates potential adaptations for piscivory. *Sci. Rep.* 10, 9259. https://doi.org/10.1038/s41598-020-66261-w (2020).

Schade, M., Stumpf, S., Kriwet, J., Kettler, C. & Pfaff, C. Neuroanatomy of the nodosaurid *Struthiosaurus austriacus* (Dinosauria: Thyreophora) supports potential ecological differentiations within Ankylosauria. *Sci. Rep. 12, 144.* https://doi.org/10.1038/s41598-021-03599-9 (2022a).

Schade, M. & Ansorge, J. New thyreophoran dinosaur material from the Early Jurassic of northeastern Germany. *PalZ* 96. https://doi.org/10.1007/s12542-022-00605-x (2022).

Schade, M., Knötschke, N., Hörnig, M. K., Paetzel, C. & Stumpf, S. Neurovascular anatomy of dwarf dinosaur implies precociality in sauropods. *eLife* 11, e82190. https://doi.org/10.7554/eLife.82190 (2022b).

Schade, M., Evers, S. W., Foth, C., Moleman, O. & Rauhut, O. W. M. A reappraisal of the cranial osteology of the spinosaurid *Irritator challengeri* (Dinosauria: Theropoda). *Palaeontol. Electron.* (in review).

Scheyer, T. M. & Sander, P. M. Histology of ankylosaur osteoderms: Implications for systematics and function. *J. Vertebr. Paleontol.* 24, 874–893 (2004).

Schwab, J. A. *et al*. Inner ear sensory system changes as extinct crocodylomorphs transitioned from land to water. *PNAS* 117(19), 10422–10428. https://doi.org/10.1073/pnas.200214611 (2020).

Scotese, C. R. Atlas of Jurassic Paleogeographic Maps, PALEOMAP Atlas for ArcGIS, volume 3, The Jurassic and Triassic, Maps 32 – 42, Mollweide Projection, PALEOMAP Project, Evanston, IL. https://doi.org/10.13140/2.1.4850.4321 (2014a).

Scotese, C. R. Atlas of Late Cretaceous Paleogeographic Maps, PALEOMAP Atlas for ArcGIS, volume 2, The Cretaceous, Maps 16 – 22, Mollweide Projection, PALEOMAP Project, Evanston, IL. https://doi.org/10.13140/2.1.4691.3284 (2014b).

Selden, P., & Nudds, J. *Evolution of fossil ecosystems*. 288p (CRC Press, 2012).

Sellers, K. C., Middleton, K. M., Davis, J. L. & Holliday, C. M. Ontogeny of bite force in a validated biomechanical model of the American alligator. *J. Exp. Biol.* 220, 2036–2046. https://doi.org/10.1242/jeb.156281 (2017).

Sereno, P. C. *et al*. A long-snouted predatory dinosaur from Africa and the evolution of spinosaurids. *Science* 282, 1298–1302 (1998).

Sereno, P. C. *et al.* Structural extremes in a Cretaceous dinosaur. *PLoS ONE* 2(11), e1230. https://doi.org/10.1371/journal.pone.0001230 (2007).

Sereno, P. C. *et al. Spinosaurus* is not an aquatic dinosaur. *eLife* 11, e80092. https://doi.org/10.7554/eLife.80092 (2022).

Smyth, R. S. H., Ibrahim, N., & Martill, D. M. *Sigilmassasaurus* is *Spinosaurus*: a reappraisal of African spinosaurines. *Cretac. Res*. 114, 104520. https://doi.org/10.1016/j.cretres.2020.104520 (2020).

Sobral, G. & Müller, J. Archosaurs and their kin: the ruling reptiles in *Evolution of the vertebrate ear* (ed. Clack, J. A., Fay, R. R. & Popper, A. N.) 285–326 (Springer, 2016).

Spoor, F. & Zonneveld, F. Comparative review of the human bony labyrinth. *Yearb. Phys. Anthropol.* 41, 211–251 (1998).

Spoor, F. *et al*. The primate semicircular canal system and locomotion. *PNAS* 104(26), 10808–10812. https://doi.org/10.1073/pnas.0704250104 (2007).

Spoor, F. & Thewissen, J. G. M. Comparative and functional anatomy of balance in aquatic mammals in *Sensory evolution on the threshold, adaptations in secondarily aquatic vertebrates*. (ed. Thewissen, J. G. M. & Nummela, S.) 65-81 (University of California Press, 2008).

Sues, H.-D., Frey, E., Martill, D. M. & Scott, D. M. *Irritator challengeri*, a spinosaurid (Dinosauria: Theropoda) from the Lower Cretaceous of Brazil. *J. Vertebr. Paleontol*. 22, 535–547; https://doi.org/10.1671/0272-4634(2002)022[0535:ICASDT]2.0.CO;2 (2002).

Sues, H.-D., Averianov, A., Ridgely, R. C. & Witmer, L.M. Titanosauria (Dinosauria, Sauropoda) from the Upper Cretaceous (Turonian) Bissekty Formation of Uzbekistan. *J. Vertebr. Paleontol.* doi:10.1080/02724634.2014.889145 (2015).

Stevens, K. A. Binocular vision in theropod dinosaurs. *J. Vertebr. Paleontol*. 26, 321–330. https://doi.org/10.1671/0272-4634(2006)26[321:BVITD]2.0.CO;2 (2006).

Stromer, E. Ergebnisse der Forschungsreisen Prof. Stromers in den Wüsten Ägyptens. II Wirbeltier-Reste der Baharije-Stufe (unterstes Cenoman). 3. Das Original des Theropoden Spinosaurus aegyptiacus nov. gen., nov. spec. *Abh. Math.-Phys. Kl, K. Bayer. Akad. Wiss.* 28, 1–32 (1915).

Stumpf, S., Ansorge, J. & Krempien, W. Gravisaurian sauropod remains from the marine late Early Jurassic (Lower Toarcian) of North-Eastern Germany. *Geobios*. https://doi.org/10.1016/j.geobios.2015.04.001 (2015).

Taquet, P. Une curieuse spécialisation du crâne de certains Dinosaures carnivores du Crétacé: Le museau long et étroit des Spinosauridés. *C. R. Acad. Sci. Paris* 299, 217–222 (1984).

Taquet, P. & Russel, D. A. New data on spinosaurid dinosaurs from the Early Cretaceous of the Sahara. *C. R. Acad. Sci. Paris* 327, 347–353 (1998).

Therrien, F., Henderson, D. M., & Ruff, C. B. Bite me: biomechanical models of theropod mandibles and implications for feeding behavior in *The Carnivorous Dinosaurs* (ed. Carpenter, K.) 179–237 (Indiana University Press, Bloomington and Indianapolis, 2005).

Therrien, F. & Henderson, D. M. My theropod is bigger than yours … or not: estimating body size from skull length in theropods. *J. Vertebr. Paleontol.* 27, 108–115. https://doi.org/10.1671/0272-4634(2007)27[108:MTIBTY]2.0.CO;2 (2007).

Thompson, R. S., Parish, J. C., Maidment, S. C. R. & Barrett, P. M. Phylogeny of the ankylosaurian dinosaurs (Ornithischia: Thyreophora). *J. Syst. Palaeontol.* 10(2), 301–312 (2012).

Trinajstic, K. *et al*. Exceptional preservation of organs in Devonian placoderms from the Gogo lagerstätte. *Science* 377, 1311–1314. https://doi.org/10.1126/science.abf3289 (2022).

Walsh, S. A., Barrett, P. M., Milner, A. C., Manley, G. & Witmer, L. M. Inner ear anatomy is a proxy for deducing auditory capability and behaviour in reptiles and birds. *Proc. R. Soc. B* 276, 1355–1360 (2009).

Walsh, S. A. *et al*. Avian cerebellar floccular fossa size is not a proxy for flying ability in birds. *PLoS ONE* 8(6), e67176. https://doi.org/10.1371/journal.pone.0067176 (2013).

Watanabe, A. *et al.* Are endocasts good proxies for brain size and shape in archosaurs throughout ontogeny? *J. Anat.* 234, 291–305. https://doi.org/10.1111/joa.12918 (2019).

Watanabe, A. *et al.* Novel neuroanatomical integration and scaling define avian brain shape evolution and development. *eLife* 10, e68809. https://doi.org/10.7554/eLife.68809 (2021).

Westneat, M. W. Transmission of force and velocity in the feeding mechanisms of labrid fishes (Teleostei, Perciformes). *Zoomorphology* 114, 103-118 (1994).

Weastneat, M. W. A biomechanical model for analysis of muscle force, power output and lower jaw motion in fishes. *J. Theor. Biol*. 223, 269–281 (2003).

Wilson, V. J. & Melville-Jones, G. *Mammalian vestibular physiology*. 365p (Springer, 1979).

Witmer, L. M. The extant phylogenetic bracket and the importance of reconstructing soft tissues in fossils in *Functional morphology in vertebrate paleontology* (ed. Thomason, J. J.) 19–33 (Cambridge University Press, 1995).

Witmer, L. M., Chatterjee, S., Franzosa, J. & Rowe, T. Neuroanatomy of flying reptiles and implications for flight, posture and behaviour. *Nature* 425, 950–953. https://doi.org/10.1038/nature02048 (2003).

Witmer, L. M. & Ridgley, R. C. The paranasal air sinuses of predatory and armored dinosaurs (Archosauria: Theropoda and Ankylosauria) and their contribution to cephalic structure. *Anat. Rec.* 291, 1362–1388 (2008).

Witmer, L. M., Ridgely, R. C., Dufeau, D. L. & Semones, M. C. Using CT to peer into the past: 3D visualization of the brain and ear regions of birds, crocodiles, and nonavian dinosaurs in *Anatomical imaging: towards a new morphology* (ed. Endo, H. & Frey, R.) 67-87 (Springer, 2008).

Witmer, L. M. & Ridgely, R. C. New insights into the brain, braincase, and ear region of tyrannosaurs (Dinosauria, Theropoda), with implications for sensory organization and behavior. *Anat. Rec.* 292(9), 1266–1296. https://doi.org/10.1002/ar.20983 (2009).

Van Valen, L. Body size and numbers of plants and animals. *Evolution* 27(1), 27–35. https://doi.org/10.2307/2407116. JSTOR 2407116 (1973).

Voogd J. & Wylie, D. R. Functional and anatomical organization of floccular zones: a preserved feature in vertebrates. *J. Comp. Neurol*. 470(2), 107–112. https://doi.org/10.1002/cne.11022. (2004).

Zelenitsky, D. K., Therrien, F. & Kobayashi, Y. Olfactory acuity in theropods: palaeobiological and evolutionary implications. *Proc. R. Soc. B: Biol. Sci.* 276, 667–673 (2009).

Zelenitsky, D. K., Therrien, F., Ridgely, R. C., Mcgee, A. R. & Witmer, L. M. Evolution of olfaction in non-avian theropod dinosaurs and birds. *Proc. Biol. Sci.* 278, 3625–3634. https://doi.org/10.1098/rspb.2011.0238 (2011).

6. Publications and author contributions

The following (chronologically ordered) five articles constitute the base for this thesis; author contributions copied from the respective article in italics below.

I

Schade, M., Rauhut, O. W. M. & Evers, S. W. Neuroanatomy of the spinosaurid *Irritator challengeri* (Dinosauria: Theropoda) indicates potential adaptations for piscivory. *Sci. Rep.* 10, 9259. https://doi.org/10.1038/s41598-020-66261-w (2020).

"M.S. and O.W.M.R. designed the project. M.S. organized the CT scans and segmented the data. S.W.E. prepared the figures. M.S., O.W.M.R. and S.W.E. interpreted the data and wrote the manuscript."

II

Schade, M., Stumpf, S., Kriwet, J., Kettler, C. & Pfaff, C. Neuroanatomy of the nodosaurid *Struthiosaurus austriacus* (Dinosauria: Thyreophora) supports potential ecological differentiations within Ankylosauria. *Sci. Rep.* 12, 144. https://doi.org/10.1038/s41598-021-03599-9 (2022a).

"M.S., S.S., J.K. and C.P. designed the project. S.S. conducted the CT scans and M.S. segmented the data. M.S. and S.S. prepared the figures. M.S., S.S., J.K. and C.P. interpreted the data and wrote the manuscript. C.K. produced the photogrammetric models."

III

Schade, M. & Ansorge, J. New thyreophoran dinosaur material from the Early Jurassic of northeastern Germany. *PalZ* 96. https://doi.org/10.1007/s12542-022-00605-x (2022).

"MS designed the project and segmented the CT data. JA unearthed GG 504 and prepared the specimen. MS and JA prepared the figures, interpreted the data and wrote the manuscript."

IV

Schade, M., Knötschke, N., Hörnig, M. K., Paetzel, C. & Stumpf, S. Neurovascular anatomy of dwarf dinosaur implies precociality in sauropods. *eLife* 11, e82190. https://doi.org/10.7554/eLife.82190 (2022b).

"Marco Schade, Conceptualization, Resources, Data curation, Software, Formal analysis, Investigation, Visualization, Methodology, Writing – original draft, Project administration, Writing – review and editing; Nils Knötschke, Supervision, Validation, Investigation, Writing – original draft; Marie Hörnig, Resources, Software, Investigation, Visualization, Methodology, Writing – original draft; Carina Paetzel, Software, Formal analysis, Investigation, Visualization, Methodology, Writing – original draft; Sebastian Stumpf, Software, Formal analysis, Investigation, Visualization, Methodology, Writing – original draft, S.S. prepared the figures and contributed to the manuscript"

V

Schade, M., Evers, S. W., Foth, C., Moleman, O. & Rauhut, O. W. M. A reappraisal of the cranial osteology of the spinosaurid *Irritator challengeri* (Dinosauria: Theropoda). *Palaeontol. Electron.* (in review).

"MS and OWMR designed the project. MS organized CT scans. MS segmented the medical and micro CT data. OM segmented the medical CT data and produced the cranial rearrangement and videos. MS, OM, CF, SWE and OWMR coded and scored phylogenetic characters, and OWMR performed the cladistic analyses. SWE performed the character optimization. CF and SWE calibrated the time-tree and performed character rate analyses. MS, OM, CF, SWE and OWMR interpreted the data, prepared the figures, discussed the phylogeny and wrote the manuscript."

Marco Schade *Prof. Dr. Ingelore Hinz-Schallreuter*

I

Schade, M., Rauhut, O. W. M. & Evers, S. W. Neuroanatomy of the spinosaurid *Irritator challengeri* (Dinosauria: Theropoda) indicates potential adaptations for piscivory. *Sci. Rep.* 10, 9259. https://doi.org/10.1038/s41598-020-66261-w (2020).

SCIENTIFIC REPORTS
nature research

Check for updates

OPEN

Neuroanatomy of the spinosaurid *Irritator challengeri* (Dinosauria: Theropoda) indicates potential adaptations for piscivory

Marco Schade[1,2] ✉, Oliver W. M. Rauhut[2,3,4] & Serjoscha W. Evers[5]

Spinosauridae, a theropod group characterized by elongated snouts, conical teeth, enlarged forelimbs, and often elongated neural spines, show evidence for semiaquatic adaptations and piscivory. It is currently debated if these animals represent terrestrial carnivores with adaptations for a piscivorous diet, or if they largely lived and foraged in aquatic habitats. The holotype of *Irritator challengeri*, a nearly complete skull from the late Early Cretaceous Santana Formation of northeastern Brazil, includes one of the few preserved spinosaurid braincases and can provide insights into neuroanatomical structures that might be expected to reflect ecological affinities. We generated digital models of the neuroanatomical cavities within the braincase, using computer tomography (CT) data. The cranial endocast of *Irritator* is generally similar to that of other non-maniraptoriform theropods, with weakly developed distinctions of hindbrain and midbrain features, relatively pronounced cranial flexures and relatively long olfactory tracts. The endosseous labyrinth has a long anterior semicircular canal, a posteriorly inclined common crus and a very large floccular recess fills the area between the semicircular canals. These features indicate that *Irritator* had the ability for fast and well-controlled pitch-down head movements. The skull table and lateral semicircular canal plane are strongly angled to one another, suggesting a downward angling of approximately 45° of the snout, which reduces interference of the snout with the field of vision of *Irritator*. These neuroanatomical features are consistent with fast, downward snatching movements in the act of predation, such as are needed for piscivory.

Spinosauridae is a large-bodied theropod group within Megalosauroidea known from the Cretaceous, although their phylogenetic relationships indicate that the clade must have originated in the Jurassic[1]. Spinosaurids are characterized by a long and slender skull, conical teeth, strongly developed forelimbs with exceptionally large thumb claws and elongated neural spines[2–6]. Due to superficial similarities in cranial form with piscivorous Crocodilia, such as the gharial, and the wealth of fossil fish within the assemblages they were found in, spinosaurids were repeatedly associated with a semiaquatic lifestyle and piscivory [e.g.[3,7–12]]. Direct evidence for piscivory comes from acid-etched fish scales in the stomach contents of *Baryonyx walkeri*[3], although the same individual also includes terrestrial dinosaur bones of a juvenile ornithopod. Predation on pterosaurs has also been shown for spinosaurids[13]. Thus, direct evidence for spinosaurid diets indicates a mix, or opportunistic behaviour with a tendency towards relatively small prey items. Additional evidence to support semiaquatic adaptations beyond dietary preference in spinosaurids comes from: isotope signals acquired from tooth enamel of samples from different geographical contexts, which show that spinosaurids spent a significant amount of their lifetime in water[8,14,15]; the suspected elevated position of the orbits in the skull[12]; the occurrence of pachyostosis in the femur of a specimen referred to *Spinosaurus aegyptiacus*[10]; though see[16] for taxonomic identification]; and the presence of a fluke-like tail that was probably used for aquatic, tail-propelled locomotion in the same specimen of *S. aegyptiacus*[17].

[1]Institute of Geography and Geology, Palaeontology and Historical Geology, University of Greifswald, 17489, Greifswald, Germany. [2]Department of Earth and Environmental Sciences, Palaeontology and Geobiology, Ludwig-Maximilians-Universität, 80333, München, Germany. [3]Bayerische Staatssammlung für Paläntologie und Geologie, Staatliche Naturwissenschaftliche Sammlungen Bayerns (SNSB), 80333, München, Germany. [4]GeoBioCenter, Ludwig-Maximilians-Universität, 80333, München, Germany. [5]Department of Geosciences, University of Fribourg, 17000, Fribourg, Switzerland. ✉e-mail: marco.schade@stud.uni-greifswald.de

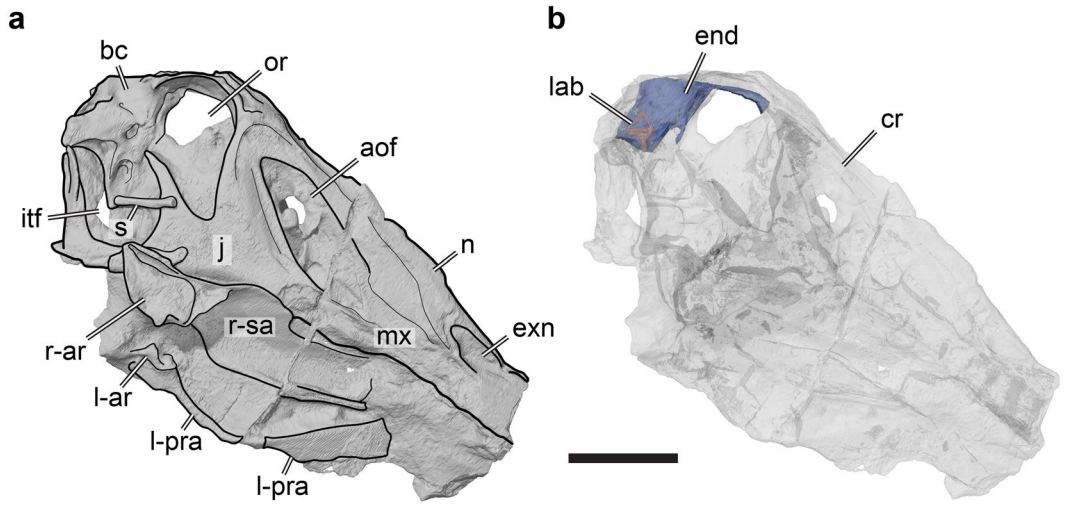

Figure 1. 3D renderings of the holotype fossil of *Irritator challengeri* (SMNS 58022) in right lateral view. (**a**) solid rendering of the skull with interpretative line drawing indicating gross anatomy; (**b**) transparent rendering of the skull with solid rendering of the cranial endocast and endosseous labyrinth. Note that the skull is inclined according to the 'alert' head pos-ture inferred by lateral semicircular canal horizontality (see text for details). Scale bar equals 100 mm. Abbreviations: aof, antorbital fenestra; ar, articular; bc, brain-case; cr, cranium; end, cranial endocast; exn, external naris; itf, infratemporal fenestra; j, jugal; l-, indicates left element; lab, endosseous labyrinth; mx, maxilla; n, nasal; or, orbit; pra, prearticular; r-, indicates right element; s, stapes; sa, surangular.

Spinosaurid material beyond isolated teeth is rare, making partial skeletons and especially skull remains particularly valuable to test for the presence of ecological adaptations. So far, the only spinosaurid taxon for which an almost complete skull is known is *Irritator challengeri* (SMNS 58022; Staatliches Museum für Naturkunde Stuttgart, Stuttgart, Germany) from the Aptian–Albian Santana Formation of Brazil[18,19] (Fig. 1). Modern methodological advances, such as computer tomography (CT) scanning methods, can reveal new details of specimens, which in turn give insights into unknown aspects of spinosaurid functional anatomy, ecology and evolution.

The braincase of vertebrates houses the brain and is closely associated with essential sensory organs [see for theropods e.g.[20–26]]. In addition, the braincase provides muscle attachment sites for the jaw and neck muscles, and directly articulates via the first neck vertebra with the postcranial skeleton. Equipped with bony crests as display devices, braincases can even be important for assessing behavioral questions[24].

In this study, we use CT scanning of the well-preserved braincase *of Irritator challengeri* to reveal its neuroanatomy. *I. challengeri* may represent the apex predator of the Santana Formation, which is one of the most important Early Cretaceous (Aptian–Albian) fossil lagerstätten from South America. The outer morphology of its braincase will be described elsewhere. The digital reconstructions of the endocast and inner ear give new insights into neuroanatomical features and associated sensory organs of this animal, and enable ecological implications to be hypothesized.

Results

Cranial endocast and innervation. The cranial endocast of SMNS 58022 is generally similar to that of other non-maniraptoriform theropods, in that many features of the hindbrain and midbrain (e.g. cerebellum and optic lobes) are not confidently perceivable as distinct structures on the surface of the endocast (Fig. 2). This indicates a poor direct correspondence between neural tissues and endocranial cavity surface, as in many other reptiles including crocodiles, lepidosaurs, and turtles [e.g.[27–30]]. A much closer brain-braincase correspondence is realized in strongly encephalised groups, which include some coelurosaurs, avian theropods, pterosaurs, or mammaliforms [e.g.[31–37]]. The endocast of SMNS 58022 is less tubular than that of crocodiles or many non-avialan coelurosaurs [e.g.[24,29]]. Instead, pontine and cephalic flexures are more pronounced, resulting in a midbrain section of the endocast that is relatively strongly angled between the hindbrain and forebrain (Fig. 2a). This is consistent with observations for basal tetanurans and ceratosaurs [e.g.[20,23,25,38,39]]. Near the cephalic flexure, the endocast of SMNS 58022 shows a weakly developed dural peak (Fig. 2a). However, because of a damage on the parietal, an accurate reconstruction of the area in which the pineal gland would be expected cannot be provided. As in other basal tetanurans and ceratosaurs [e.g.[20,23]], but unlike coelurosaurs[24], the dorsal middle cerebral vein exits the cranial endocast well below the level of the dural peak (Fig. 2a,b) in SMNS 58022.

In the forebrain, the cerebral hemispheres are distinguishable as laterally expanded but weakly delimited bulbs on the dorsolateral surface of the endocast of SMNS 58022 (Fig. 2). The impressions of the olfactory tracts are preserved along the ventral surface of the frontals. The conjoined impressions of the olfactory tracts and bulbs are around 55 mm in length. Anteriorly, the olfactory tract gets wider and diverges into distinct olfactory bulbs, which are dorsally separated by a shallow sulcus (Fig. 2b,d). Long olfactory tracts are considered plesiomorphic within theropods[24], and are shortened in theropods closer to the avian crown than basal tetanurans[24]. The full extent of the olfactory bulbs could not be reconstructed for SMNS 58022, due to insufficient preservation

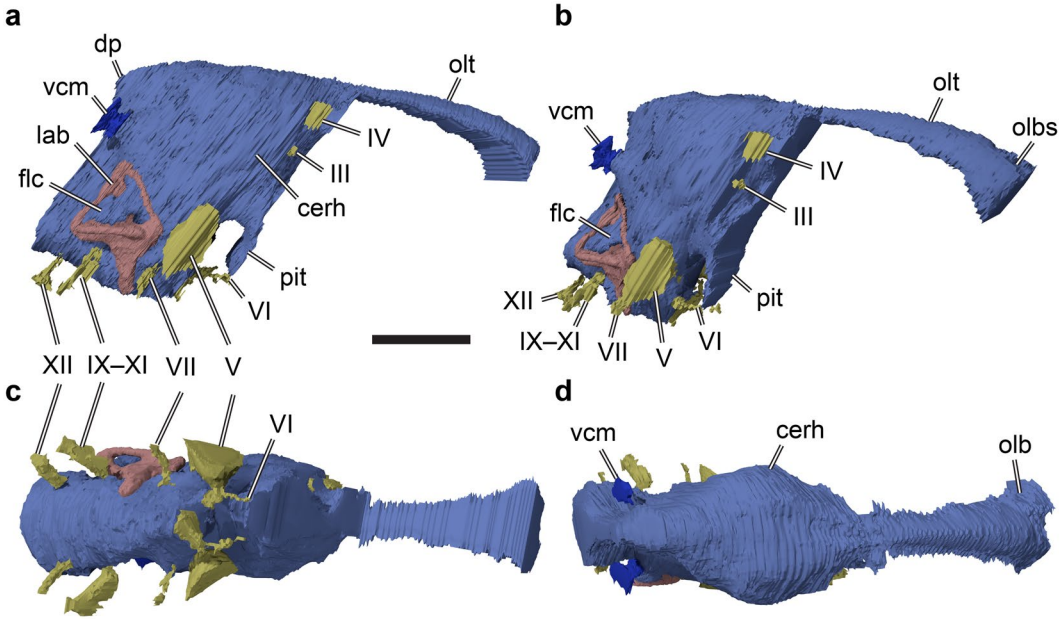

Figure 2. 3D rendering of the cranial endocast, cranial nerves, endosseous labyrinth, and as-sociated structures of the holotype fossil of *Irritator challengeri* (SMNS 58022). (**a**) right lat-eral view; (**b**) oblique view, roughly anterolaterally oriented; (**c**) ventral view; (**d**) dorsal view. Scale bar equals 30 mm. Abbreviations: cerh, cerebral hemisphere; dp, dural peak; flc, floc-cular recess; III, oculomotor nerve; IV, trochlear nerve; IX–XI, endocast of the metotic fissure, holding the glossopharyngeal (IX), vagus (X), and accessory (XI) nerves; lab, endosseous lab-yrinth; olb, olfactory bulb; olbs, olfactory bulb sulcus; olt, olfactory tract; pit, pituitary; V, trigeminal nerve; VI, abducens nerve; VII, facial nerve; vcm, dorsal middle cerebral vein; XII, hypoglossal nerve.

anteriorly. Ventral to the base of the olfactory tracts, the orbitosphenoid captures the courses of the cranial nerves III (oculomotor nerve) and IV (trochlear nerve) (Fig. 2a,b). Anteroventrally in the forebrain, the impression of the pituitary fossa is clearly visible in SMNS 58022 (Fig. 2a,b). Although no clear cerebral carotid canal could be identified, the paired abducens nerve (CN VI) canals could be reconstructed (Fig. 2a–c). The position of the foramen for the trigeminal nerve (CN V) is posterodorsal to the abducens canal. The respective foramen is large and clearly visible externally[19]. The facial nerve (CN VII) originates anteriorly to the position of the cochlear duct, whereas the metotic foramen and recessus scalae tympani for CN IX–XI is found posterior to the cochlear duct (Fig. 2a–c). Hypoglossal nerve (CN XII) canals were identified on both sides, whereas Sues *et al.*[19] were only able to locate one such foramen externally, on the left side of the specimen.

In the midbrain region, somewhat posteroventrally to the cerebral expansion, the endocast shows a poster-oventrally directed flap that projects off the cerebellum, the floccular lobe (flocculus in the following; Figs. 2a,b, 3a–d). The flocculus of SMNS 58022 is very large; it projects posteriorly into the space confined by the posterior semicircular canal and secondary common crus of the endosseous labyrinth, and extends laterally to the level of the lateral semicircular canal. Thus, the flocculus of *Irritator challengeri* is much larger than that of other basal tetanurans [e.g.[20,22,25]], and even most coelurosaurs [e.g.[40]], but is similar in size to taxa that reportedly have large flocculi (e.g. *Conchoraptor gracilis*[26]).

The medulla oblongata in the hindbrain is relatively broad mediolaterally, and connected with the foramen magnum.

The volume of the endocranial cavity was measured to be approximately 80 cm^3 (measured as suggested in[23]).

Endosseous labyrinth. The endosseous labyrinth of SMNS 58022 is composed of the dorsally positioned vestibular system that includes the semicircular canals, and a ventrally tapering cochlear duct (Fig. 3). The coch-lear duct is relatively long and dorsoventrally as tall as the semicircular canal system (Fig. 3a,e). It is gently ven-tromedially inclined (Fig. 3c,d,g,h). The vertical semicircular canals are strongly asymmetrical: the common crus is posteriorly directed rather than strictly dorsally (Fig. 3e). As a consequence, the posterior semicircular canal forms a low and relatively short arc, whereas the anterior semicircular canal is long and posterodorsally forms a 180° turn to reach the common crus. The course of the posterior semicircular canal does not lie in a single vertical plane, but the midpart of the canal is slightly bowed anterolaterally. In many tetrapods, the posterior portion of the lateral semicircular canal and the ventral portion of the posterior semicircular canal intersect, and form a singular cavity, the secondary common crus[30]. In SMNS 58022, the posterior and lateral semicircular canal also intersect, but the courses of the individual paths of the membranous ducts within the intersection are still clearly visible in the endosseous labyrinth model as impressions within the secondary common crus. Although these impressions are difficult to see in standard orientation figures of the endosseous labyrinth model (Fig. 3d,h), they are clearly visible in the actual 3D model (see[41]). The posterior semicircular canal arcs ventrally underneath the lateral semicircular canal, which curves medial to the posterior canal toward the common crus. The imprints of

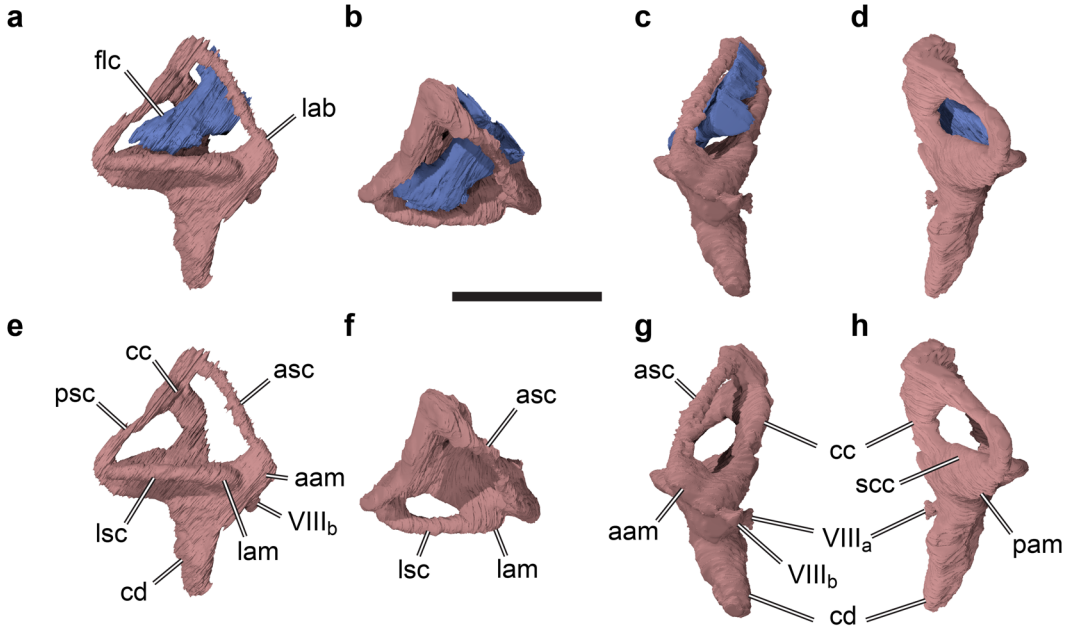

Figure 3. 3D rendering of right endosseous labyrinth and floccular recess of the holotype fossil of *Irritator challengeri* (SMNS 58022). (**a**)–(**d**), 3D renderings including the floccular re-cess; (**e**)–(**f**), excluding floccular recess. (**a**), (**e**), lateral view; (**b**), (**f**), dorsal view; (**c**), (**g**), anterior view; (**d**), (**h**), posterior view. Scale bar equals 20 mm. Abbreviations: aam, anterior ampulla; asc, anterior semicircular canal; cc, common crus; cd, cochlear duct; flc, floccular recess; lab, en-dosseous labyrinth; lam, lateral ampulla; lsc, lateral semicircular canal; pam, posterior am-pulla; psc, posterior semicircular canal; scc, secondary common crus; VIIIa, medial branch of vestibulocochlear nerve; VIIIb, anterior branch of vestibulocochlear nerve.

the posterior LSC and ventral PSC portions provide evidence that the semicircular ducts were relatively widely separated in life, as is the case in many modern birds, in which a secondary common crus is largely absent[42].

Pneumatic cavities. Pneumatic cavities in the braincase of SMNS 58022 are present, but hard to delimitate within our CT data. This is in part because some pneumatic cavities, particularly the caudal tympanic recess within the paroccipital process, and a recess directly ventral to the brain within the basioccipital, tentatively identified as the medial subcondylar recess [see [24,43] for theropod braincase pneumaticity], are interrupted by extensive webbing of laminae. Seemingly, there are more pneumatic recesses present within the braincase of SMNS 58022, including minor cavities within the basioccipital and the prootic, as well as a basisphenoid recess and a subsellar recess within the basisphenoid. In very general terms, the extent of braincase pneumaticity seems to be higher than in ceratosaurs[23,44], but less than in tyrannosaurs[24].

Discussion

Auditory capabilities. Auditory capability and cochlear duct length have been hypothesized to be correlated among extant archosaurs[45]. We used the equations derived by Walsh *et al.*[45] alongside digital measurements (cochlear duct length = 18.1 mm; basicranium length = 75.3 mm) to infer the mean hearing frequency (1950 Hz) and frequency band width (3196 Hz) for *Irritator challengeri*. We only consider these values as rough guidance, but the resulting frequency range between c. 350–3550 Hz places *I. challengeri* around the lower end of the sensitivity range inferred for modern birds, but above that for crocodiles[45]. Furthermore, the estimates are in approximate agreement with those calculated for other theropod dinosaurs [e.g.[40]]. Additional cues for the auditory capabilities can possibly be inferred from pneumaticity. Increased volume achieved by extensive tympanic pneumaticity, as observed in extant Aves and Crocodilia, but also tyrannosaurs and many maniraptoran theropods[46], is thought to impact impedance matching of the middle ear by reducing the acoustic stiffness and improving stapes vibration. These effects facilitate the reception of low frequencies, as well as the amplification of frequency-depending sounds[24,29,47]. The lesser degree of tympanic pneumatization of SMNS 58022, which probably represents a symplesiomorphy shared with other basal tetanurans, might indicate that the middle ear of *I. challengeri* was less specialized than those of tyrannosaurs. It is noteworthy that the stapes of SMNS 58022 is relatively more robust than in some other basal tetanurans, such as *Allosaurus* spp.[48,49], which might negatively affect the efficiency of the acoustic transformer ratio, and thus of impedance matching, of *I. challengeri*.

Vestibular anatomy as a guide to ecological reconstructions?. It is currently unclear how informative labyrinth geometry is for inferring habitat ecology in reptiles. The semicircular canals, which are the focus of most studies that test for such correlations, are used in gaze stabilization by detecting angular accelerations of the head as inputs to the vestibulo-ocular (VOR) and vestibulo-collic (VCR) reflexes[50]. Endolymphatic flow within the inner ear organ is determined by semicircular canal geometry, and the shape of the vestibular organ is therefore expected to vary depending on locomotor mode, as has been found for many mammal groups [e.g.[51–54]].

Functional changes in vestibular anatomy are expected to be largest in groups that experienced strong ecological transitions, such as the evolution of secondarily marine lifestyles or flight. However, for both these transitions, no characteristic shape change uniquely linked to either ecological adaptation has yet been found. In birds, studies that test for ecological signals in the vestibular anatomy so far fail to find correlations with flight ability or style. For instance, the size of the floccular lobe does not indicate flight ability[35]. Benson *et al*.[42] found little locomotor signal within the semicircular canal system size or semicircular canal shape of birds. They suggest that other constraints, such as visual acuity, head size, and spatial constraints within the cranium could instead determine the major variation associated with labyrinth shape[42]. Some studies have reported potential aquatic adaptations to the endosseous labyrinth in non-dinosaurian reptiles[30,55–57]. However, the hypothesis that aquatic tetrapods have low aspect ratios (i.e. comparatively dorsoventrally low and anteroposteriorly long labyrinths[55];) is not supported by more recently collected data[30]. Additionally, thick endosseous semicircular canals, although found in several secondarily marine groups[30,56,57], can also be present in highly terrestrial animals[30]. Furthermore, the endosseous labyrinths of phylogenetically shallow marine lineages, such as penguins or seals seem to be influenced more strongly by other factors like phylogeny (penguins:[55,56]; neodiapsids:[58]), or neck agility (seals:[59]), rather than habitat ecology.

Despite the above-mentioned reservations against clear ecological signals in the vestibular anatomy of reptiles, potential functional adaptations of the dinosaurian labyrinth have been reported throughout the literature. For instance, changes in labyrinth geometry associated with the evolution of bipedality within dinosaurs, particularly the elongation of the vertical semicircular canals, have been recorded for dinosaurs[60]. On the other hand, these changes could not be found in an ontogenetic labyrinth series of the dinosaur *Massospondylus carinatus*[61], which experiences a change from quadrupedality to bipedality during ontogeny[62].

Spinosaurids are deeply nested within the Theropoda, a clade of obligate bipedal, comparatively agile, and terrestrial animals. Even if spinosaurids had a semiaquatic ecology [e.g.[10]], it is quite possible that ancestral constraints on the theropodan bauplan dominate the shape of the spinosaurid labyrinth [e.g.[58]]. Therefore, semiaquatic adaptations are not necessarily expected to be overly obvious, or present at all, and their absence cannot be taken as strong evidence against semiaquatic lifestyles. In the following, we discuss and interpret three aspects of the neuroanatomy of *Irritator challengeri* that have been the focus of many studies that try to synthesize ecological adaptations from neuroanatomical structures: the size of the floccular recess, the size of the anterior semicircular canal, and the relative orientation of the lateral semicircular canal.

Behavioral interpretations of neuroanatomy. SMNS 58022 shows enlarged floccular recesses. The flocculus is important in the control and coordination of head, eye, and neck movements during gaze stabilization, by being involved in processing the vestibulo-ocular (VOR) and vestibulo-collic (VCR) reflexes[33,35,51]. Additionally, the flocculus plays a role in the reflex control of neck movements[63]. Although the floccular recess may also house non-neural tissues[35], floccular size has been interpreted to be grossly indicative of the amount of neural tissue and, by inference, the amount of respective signal procession[33]. A small flocculus endocast is conversely not necessarily indicative of a small amount of respective neural tissue, because the floccular lobe also extends within the cerebellum of extant birds[29,35]. However, a reduction in floccular size in the abelisaurid certosaurian *Majungasaurus crenatissimus* has been interpreted to indicate a decreased reliance on quick movement and sophisticated gaze-stabilization mechanisms in this taxon[23], though not necessarily in other abelisaurids[44,64]. In pterosaurs, enlarged floccular recesses have been interpreted as an adaptation to eye-guided pursuit hunting of fish, albeit aerially[33]. Within non-avian theropod dinosaurs, large floccular recesses are common among coelurosaurs, but this structure seems relatively smaller in basal tetanurans [e.g.[20,26,40,44]]. Among birds, flocculus sizes vary. It is noteworthy that particularly large flocculus sizes have been noted for many waterbirds (Procellariiformes, i.e. albatrosses and kin; Phaethoniformes, i.e. tropicbirds; Charadriiformes, i.e. gulls and kind; Anseriformes, i.e. ducks, geese, and swans; Gaviiformes, i.e. loons) and birds with particularly long necks (Rheiformes, i.e. Rhea; Ciconiiformes, i.e. storks)[35,64]. However, Falconiformes (falcons) and some Passeriformes (perching birds) also have large floccular sizes[35]. Although interpretations of floccular sizes are not straightforward [e.g.[35]], we interpret the large floccular size of *Irritator challengeri* as indicative for the relative importance of VOR and VCR coordination, particularly because large floccular sizes are unusual for the inferred phylogenetic position of spinosaurids.

Additional possible behavioural clues come from the semicircular canal system, particularly the anterior and lateral semicircular canals. In *Irritator challengeri*, the anterior semicircular canal is particularly long, with its length being furthermore increased by the posterodorsally inclined common crus. As the anterior semicircular canal is more sensitive to pitch-down movements of the head than the other semicircular canals[65,66], we suggest that this kind of sensitivity was particularly important for *I. challengeri*. Research suggests that 'alert' head orientation can be inferred for animals by aligning the plane of the lateral semicircular canal with a horizontal plane paralleling the ground[33,50,66–68]. Arranging the lateral semicircular canal in SMNS 58022 horizontally, its skull is inclined downwards at approximately 45° (Fig. 1b). This represents a rather strong ventral orientation of the snout tip, and could be interpreted to maximize the field of binocular vision by avoiding obstruction by the elongated snout [see also [24]]. This approach of inferring head posture has been criticized[69] based on data that show that modern birds have a range of realized orientation values of the lateral semicircular canal that deviate from horizontality by up to c. 20° to either side of the horizontal plane[67]. However, the same data show that birds with long beaks, such as storks, tend to have labyrinths that are pitched downward with their lateral semicircular canal planes[67,69], which would even increase the downward inclination inferred for *I. challengeri*. Even extremely upward pitched labyrinth orientations of 20° would result in a strong ventral inclination of the head of *I. challengeri* by approximately 25°. Furthermore, strong downward orientation of the snout of *I. challengeri* is independently supported by the slightly posteroventrally rotated occipital condyle. Therefore, we think that a strong

downward orientation of approximately 45° is supported for *I. challengeri* despite the caution that is warranted when making inferences about head orientation[69].

The above features – particularly a good eye-head coordination, sensitivity for pitch-down movements, and a ventrally inclined snout facilitating three-dimensional vision – are features that are presumably important for pursuit hunters, particularly for animals that hunt prey that is small and agile in comparison to their own body size. These findings are consistent with data from skull mechanics and functional anatomy in spinosaurids[7,70]. Although the known direct evidence for predation in spinosaurids[3,13] indicates an opportunistic feeding behaviour, fish might have played an important role in the diet of these animals. The 'alert' head posture of *Irritator challengeri*, in which the snout is held downward, furthermore possibly allowed the animal to tuck its snout into the water, while the retracted nares and eyes were not submerged. Possible mechanoreceptor foramina similar to those of crocodiles[71] have been identified for spinosaurids[10], although such structures can also be found in clearly terrestrial theropods[72]. The enlarged anterior semicircular canal facilitated fast downward movements, which were coordinated in part by a large floccular recess, and in conjunction allowed snapping movements during hunting of small prey. This functional hypothesis requires fast neck movements. Thus, independent skeletal evidence in support of our interpretation might come from the morphology of the cervical vertebrae of spinosaurids. Although this part of the skeleton is not preserved in *I. challengeri*, certain features of spinosaurid cervical morphology are consistently present among different members of the group, justifying the use of comparative evidence[1,16]. Spinosaurids have comparatively long anterior and mid-cervical centra[16], which make their necks considerably longer than those of other large-bodied theropods. Strong ventral rugosities on the mid-cervical to posterior centra of the spinosaurid *Sigilmassasaurus brevicollis* have been interpreted as osteological correlates for strong dorsoventral flexion musculature[16]. All of this evidence indicates a specialization of these gigantic predators on considerably smaller and elusive prey, including fish, which is remarkably different from that of other large-sized theropods, such as tyrannosaurids or carcharodontodsaurids [e.g.[73–75]], providing further evidence for niche partitioning between coeval spinosaurid and non-spinosaurid theropod taxa.

Conclusions

Irritator challengeri, the first spinosaurid for which neuroantomical features are documented, has a cranial endocast that shows features consistent with the inferred phylogenetic position of spinosaurids as basal tetanurans. These include weakly demarcated brain regions, elongate olfactory tracts and pronounced cranial flexures. *I. challengeri* has an enlarged floccular recess, which is an unusual feature for basal tetanurans. The vestibular part of the endosseous labyrinth is characterized by a large anterior semicircular canal. A large flocculus and anterior semicircular canal indicate that *I. challengeri* could move its head downwards in a fast and coordinated fashion. The lateral semicircular canal orientation suggests a downward inclined snout posture, which enables unobstructed, stereoscopic forward vision, important for distance perception and thus precise snatching movements of the snout. The suite of neuroanatomically facilitated behavioural capabilities inferred for *I. challangeri* are those expected for animals that mostly hunt small and agile prey. Although these prey items could be small terrestrial animals, our interpretations are consistent with, and corroborate independent evidence for the hypothesis for an at least partially piscivorous diet of spinosaurids.

Materials and Methods

The holotype and only known specimen of *Irritator challengeri* (SMNS 58022) is an almost complete skull (Fig. 1). It is about 55 cm long and well preserved, lacking only the premaxillae and a few other skull bones, especially of the splanchocranium. The specimen has suffered from slight transverse compression and disarticulation of the posterolateral parts of the skull roof, although some of the disarticulated elements are preserved in displaced positions within the skull, such as the postorbital[19].

We scanned SMNS 58022 originally with a medical Siemens Somatom Force CT scanner (dual source) (voltage: 120 kV, X-ray tube current: 1365 μA, exposure time: 154 ms, voxel size: 0.703123 mm ×0.703124 mm ×3 mm) in the German Heart Centre in Munich. This scan was the base for all digital reconstructions shown herein, except the inner ear and flocculus, which were visible but poorly resolved in the original scan. In order to get higher resolution data for the labyrinth reconstruction, we conducted a second scan focused only on the braincase, using a Zeiss Metrotom 1500 (voltage: 180 kV, X-ray tube current: 1800 μA, exposure time: 250 ms, voxel size: 0.09713 mm) in a subsidiary of Zeiss in Essingen. Digital segmentation and measurements were produced with Amira (5.6.). We used manual segmentation to create our models. Although the density contrast between the cranium and sediment infill of internal spaces was relatively weak, the boundary between bone surface and sediment infill is clearly visible in the slice data. 3D models of the high-resolution flocculus and endosseous labyrinth were aligned with the respective low-resolution structures in Blender 2.79b to get composite figures of models from both scans. A composite neuroanatomical model, as well as individual 3D models and the two CT scans are deposited online[41].

Data availability

The CT slice data and 3D files of SMNS 58022, are published online[41], in the repository MorphoSource, Project P 951: https://www.morphosource.org/Detail/ProjectDetail/Show/project_id/951.

Received: 26 February 2020; Accepted: 18 May 2020;
Published online: 09 June 2020

References

1. Carrano, M. T., Benson, R. B. J. & Sampson, S. D. The phylogeny of Tetanurae (Dinosauria: Theropoda). *J. Syst. Palaeontol.* **10**, 211–300, https://doi.org/10.1080/14772019.2011.630927 (2012).
2. Stromer, E. Ergebnisse der Forschungsreisen Prof. Stromers in den Wüsten Ägyptens. II Wirbeltier-Reste der Baharije-Stufe (unterstes Cenoman). 3. Das Original des Theropoden Spinosaurus aegyptiacus nov. gen., nov. spec. *Abh. Math.-Phys. Kl, K. Bayer. Akad. Wiss.* **28**, 1–32 (1915).
3. Charig, A. J. & Milner, A. C. *Baryonyx walkeri*, a fish-eating dinosaur from the Wealden of Surrey. *J. Syst. Palaeontol.* **53**, 11–70 (1997).
4. Sereno, P. C. *et al*. A long-snouted predatory dinosaur from Africa and the evolution of spinosaurids. *Science* **282**, 1298–1302 (1998).
5. Sasso, C. D., Maganuco, S., Buffetaut, E. & Mendez, M. A. New information on the skull of the enigmatic theropod *Spinosaurus*, with remarks on its size and affinities. *J. Vertebr. Paleontol*. **25**, 888–896; https://doi.org/10.1671/0272-4634(2005)025[0888:NIOTSO]2.0.CO;2 (2005).
6. Allain, R., Xaisanavong, T., Richir, P. & Khentavong, B. The first definitive Asian spinosaurid (Dinosauria: Theropoda) from the Early Cretaceous of Laos. *Sci. Nat*. **99**, 369–377, https://doi.org/10.1007/s00114-012-0911-7 (2012).
7. Rayfield, E. J., Milner, A. C., Xuan, V. B. & Young, P. G. Functional morphology of spinosaur 'crocodile-mimic' dinosaurs. *J. Vertebr. Paleontol*. **27**, 892–901; https://doi.org/10.1671/0272-4634(2007)27[892:FMOSCD]2.0.CO;2 (2007).
8. Amiot, R. *et al*. Oxygen isotope evidence for semi-aquatic habits among spinosaurid theropods. *Geology* **38**, 139–142, https://doi.org/10.1130/G30402.1 (2010).
9. Läng, E. *et al*. Unbalanced food web in a Late Cretaceous dinosaur assemblage. *Palaeogeogr. Palaeoclimatol. Palaeoecol.* **381-382**, 26–32, https://doi.org/10.1016/j.palaeo.2013.04.011 (2013).
10. Ibrahim, N. *et al*. Semiaquatic adaptations in a giant predatory dinosaur. *Science* **345**, 1613–1616, https://doi.org/10.1126/science.1258750 (2014).
11. Hone, D. W. E. & Holtz, T. R. Jr. A century of spinosaurs - a review and revision of the Spinosauridae with comments on their ecology. *Acta Geol. Sin-Engl.* **91**, 1120–1132, https://doi.org/10.1111/1755-6724.13328 (2017).
12. Arden, T. M. S., Klein, C. G., Zouhri, S. & Longrich, N. R. Aquatic adaptation in the skull of carnivorous dinosaurs (Theropoda: Spinosauridae) and the evolution of aquatic habits in spinosaurids. *Cretac. Res.* **93**, 275–284, https://doi.org/10.1016/j.cretres.2018.06.013 (2018).
13. Buffetaut, E., Martill, D. M. & Escuillié, F. Pterosaurs as part of a spinosaur diet. *Nature* **430**, 33 (2004).
14. Amiot, R. *et al*. Oxygen isotope composition of continental vertebrate apatites from Mesozoic formations of Thailand; environmental and ecological significance. *Geol. Soc. Spec. Publ. Special Publication* **315**(1), 271–283, https://doi.org/10.1144/SP315.19 (2009).
15. Amiot, R. *et al*. Oxygen and carbon isotope compositions of middle Cretaceous vertebrates from North Africa and Brazil: Ecological and environmental significance. *Palaeogeogr. Palaeoclimatol. Palaeoecol.* **297**, 439–451, https://doi.org/10.1016/j.palaeo.2010.08.027 (2010).
16. Evers, S. W., Rauhut, O. W. M., Milner, A. C., McFeeters, B. & Allain, R. A reappraisal of the morphology and systematic position of the theropod dinosaur *Sigilmassasaurus* from the "middle" Cretaceous of Morocco. *PeerJ* **3**, e1323, https://doi.org/10.7717/peerj.1323 (2015).
17. Ibrahim, N. *et al*. Tail-propelled aquatic locomotion in a theropod dinosaur. *Nature* **581**, 67–70 (2020).
18. Martill, D. M., Cruickshank, A. R. I. & Frey, E. A new crested maniraptoran dinosaur from the Santana Formation (Lower Cretaceous) of Brazil. *J. Geol. Soc.* **153**, 5–8 (1996).
19. Sues, H.-D., Frey, E., Martill, D. M. & Scott, D. M. *Irritator challengeri*, a spinosaurid (Dinosauria: Theropoda) from the Lower Cretaceous of Brazil. *J. Vertebr. Paleontol*. **22**, 535–547; https://doi.org/10.1671/0272-4634(2002)022[0535:ICASDT]2.0.CO;2 (2002).
20. Rogers, S. W. Exploring dinosaur neuropaleobiology: viewpoint computed tomography scanning and analysis of an *Allosaurus fragilis* endocast. *Neuron* **21**, 673–679 (1998).
21. Rogers, S. W. *Allosaurus*, crocodiles, and birds: evolutionary clues from spiral computed tomography of an endocast. *Anat. Rec.* **257**, 162–173 (1999).
22. Franzosa, J. & Rowe, T. Cranial endocast of the Cretaceous theropod dinosaur *Acrocanthosaurus atokensis*. *J. Vertebr. Paleontol.* **25**, 859–864 (2005).
23. Sampson, S. D. & Witmer, L. M. Craniofacial anatomy of *Majungasaurus crenatissimus* (Theropoda: Abelisauridae) from the Late Cretaceous of Madagascar. *J. Vertebr. Paleontol*. **27**, 32–104; https://doi.org/10.1671/0272-4634(2007)27[32:CAOMCT]2.0.CO;2 (2007).
24. Witmer, L. M. & Ridgely, R. C. New insights into the brain, braincase, and ear region of tyrannosaurs (Dinosauria, Theropoda), with implications for sensory organization and behavior. *Anat. Rec. (Hoboken, N.J.: 2007)* **292**(9), 1266–1296, https://doi.org/10.1002/ar.20983 (2009).
25. Paulina-Carabajal, A. & Canale, J. I. Cranial endocast of the carcharodontosaurid theropod *Giganotosaurus carolinii* Coria & Salgado, 1995. *N. Jb. Geol. Paläont. Abh.* **258**(2), 249–256 (2010).
26. Balanoff, A. M., Bever, G. S. & Norell, M. A. Reconsidering the avian nature of the oviraptorosaur brain (Dinosauria: Theropoda). *PLoS One* **9**(12), e113559, https://doi.org/10.1371/journal.pone.0113559 (2014).
27. Hopson, J. A. Paleoneurology in *Biology of the Reptilia* (ed. Gans, C.) 39-146 (Academic Press, 1979).
28. Rogers, S.W. Reconstructing the behaviors of extinct species: an excursion into comparative paleoneurology. *Am. J. Med. Genet.* **134A**, 349–356; 0.1002/ajmg.a.30538 (2005).
29. Witmer, L. M., Ridgely, R. C., Dufeau, D. L. & Semones, M. C. Using CT to peer into the past: 3D visualization of the brain and ear regions of birds, crocodiles, and nonavian dinosaurs in *Anatomical imaging: towards a new morphology* (ed. Endo, H. & Frey, R.) 67-87 (Springer, 2008).
30. Evers, S. W. *et al*. Neurovascular anatomy of the protostegid turtle *Rhinochelys pulchriceps* and comparisons of membranous and endosseous labyrinth shape in an extant turtle. *Zool. J. Linnean. Soc.* **187**, 800–828, https://doi.org/10.1093/zoolinnean/zlz063 (2019).
31. Jerison, H. J. Evolution of the brain and intelligence (Academic Press, 1973).
32. Iwaniuk, A. N. & Nelson, J. E. Can endocranial volume be used as an estimate of brain size in birds? *Can. J. Zool.* **80**, 16–23, https://doi.org/10.1139/Z01-204 (2002).
33. Witmer, L. M., Chatterjee, S., Franzosa, J. & Rowe, T. Neuroanatomy of flying reptiles and implications for flight, posture and behaviour. *Nature* **425**, 950–953, https://doi.org/10.1038/nature02048 (2003).
34. Rowe, T. B., Macrini, T. E. & Luo, Z.-X. Fossil evidence on the origin of the mammalian brain. *Science* **332**, 955–957, https://doi.org/10.1126/science.1203117 (2011).
35. Walsh, S. A. *et al*. Avian cerebellar floccular fossa size is not a proxy for flying ability in birds. *PLoS One* **8**(6), e67176, https://doi.org/10.1371/journal.pone.0067176 (2013).
36. Balanoff, A. M. *et al*. Best practices for digitally constructing endocranial casts: examples from birds and their dinosaurian relatives. *J. Anat*. **229** (**2**), https://doi.org/10.1111/joa.12378 (2015).
37. Balanoff, A. M. & Bever, G. S. The role of endocasts in the study of brain evolution in *Evolution of nervous systems* (ed. Kaas, J.) 223–241; https://doi.org/10.1016/B978-0-12-804042-3.00023-3 (2017).

38. Sanders, R. K. & Smith, D. K. The endocranium of the theropod dinosaur *Ceratosaurus* studied with computed tomography. *Acta Palaeontol. Pol.* **50**(3), 601–616 (2005).
39. Saveliev, S. V. & Alifanov, V. R. A new study of the brain of the predatory dinosaur *Tarbosaurus bataar* (Theropoda, Tyrannosauridae). *Paleontol. J.* **41**(3), 281–289 (2007).
40. Lautenschlager, S., Rayfield, E. J., Altangerel, P., Zanno, L. E. & Witmer, L. M. The endocranial anatomy of therizinosauria and its implications for sensory and cognitive function. *PLoS One* **7**, e52289, https://doi.org/10.1371/journal.pone.0052289 (2012).
41. Schade, M., Rauhut, O. W. M. & Evers, S. W. Project: Schade *et al*. Irritator challengeri SMNS 58022 neuroanatomy. MorphoSource, available at https://www.morphosource.org/Detail/ProjectDetail/Show/project_id/951 (2020).
42. Benson, R. B. J., Starmer-Jones, E., Close, R. A. & Walsh, S. A. Comparative analysis of vestibular ecomorphology in birds. *J. Anat.* **231**, 990–1018, https://doi.org/10.1111/joa.12726 (2017).
43. Witmer, L. M. & Ridgely, R. C. The Cleveland tyrannosaur skull (*Nanotyrannus* or *Tyrannosaurus*): new findings based on CT scanning, with special reference to the braincase. *Kirtlandia* **57**, 61–81 (2010).
44. Paulina-Carabajal, A. & Filippi, L. Neuroanatomy of the abelisaurid theropod *Viavenator*: The most complete reconstruction of a cranial endocast and inner ear for a South American representative of the clade. *Cretac. Res.* **83**, 84–94, https://doi.org/10.1016/j.cretres.2017.06.013 (2018).
45. Walsh, S. A., Barrett, P. M., Milner, A. C., Manley, G. & Witmer, L. M. Inner ear anatomy is a proxy for deducing auditory capability and behaviour in reptiles and birds. *Proc. R. Soc. B* **276**, 1355–1360 (2009).
46. Witmer, L. M. & Ridgley, R. C. The paranasal air sinuses of predatory and armored dinosaurs (Archosauria: Theropoda and Ankylosauria) and their contribution to cephalic structure. *Anat. Rec.* **291**, 1362–1388 (2008).
47. Sobral, G. & Müller, J. Archosaurs and their kin: the ruling reptiles in *Evolution of the vertebrate ear* (ed. Clack, J. A., Fay, R. R. & Popper, A. N.) 285–326 (Springer, 2016).
48. Madsen, J. H. J. *Allosaurus fragilis*: a revised osteology. *Utah Geological and Mineralogical Survey Bulletin* **109**, 3–163 (1976).
49. Chure, D. J. & Loewen, M. A. Cranial anatomy of *Allosaurus jimmadseni*, a new species from the lower part of the Morrison Formation (Upper Jurassic) of Western North America. *PeerJ* **8**, e7803, https://doi.org/10.7717/peerj.7803 (2020).
50. Spoor, F. & Zonneveld, F. Comparative review of the human bony labyrinth. *Yearbook of Physical Anthropology* **41**, 211–251 (1998).
51. Spoor, F. *et al*. The primate semicircular canal system and locomotion. *PNAS.* **104**, 10808–10812 (2007).
52. Cox, P. G. & Jeffery, N. Semicircular canals and agility: the influence of size and shape measures. *J. Anat.* **216**, 37–47, https://doi.org/10.1111/j.1469-7580.2009.01172.x (2010).
53. Pfaff, C., Martin, T. & Ruf, I. Bony labyrinth morphometry indicates locomotor adaptations in the squirrel-related clade (Rodentia, Mammalia). *Proc. R. Soc. B.* **282**, 20150744, https://doi.org/10.1098/rspb.2015.0744 (2015).
54. Pfaff, C., Czernym, S., Nagel, D. & Kriwet, J. Functional morphological adaptations of the bony labyrinth in marsupials (Mammalia, Theria). *J. Morphol.* **278**, 742–749, https://doi.org/10.1002/jmor.20669 (2017).
55. Georgi, J. A. & Sipla, J. S. Comparative and functional anatomy of balance in aquatic reptiles and birds in *Sensory evolution on the threshold: adaptations in secondarily aquatic vertebrates* (ed. Thewissen, J. G. M. & Nummela, S.) 233–256 (University of California Press, 2008).
56. Neenan, J. M. *et al*. Evolution of the sauropterygian labyrinth with increasingly pelagic lifestyles. *Curr. Biol. CB* **27**, 3852–3858.e3, https://doi.org/10.1016/j.cub.2017.10.069 (2017).
57. Schwab, J. A. *et al*. Inner ear sensory system changes as extinct crocodylomorphs transitioned from land to water. *PNAS*, 202002146 (2020).
58. Dudgeon, T. W., Maddin, H. C., Evans, D. C. & Mallon, J. C. The internal cranial anatomy of *Champsosaurus* (Choristodera: Champsosauridae): Implications for neurosensory function. *Sci. Rep.* **10**, 7122 (2020).
59. Spoor, F. & Thewissen, J. G. M. Comparative and functional anatomy of balance in aquatic mammals in Sensory evolution on the threshold, adaptations in secondarily aquatic vertebrates. (ed. Thewissen, J. G. M. & Nummela, S.) 65-81 (University of California Press, 2008).
60. Georgi, J. A., Sipla, J. S. & Forster, C. A. Turning semicircular canal function on its head: dinosaurs and a novel vestibular analysis. *Plos One* **8**(3), e58517, https://doi.org/10.1371/journal.pone.0058517 (2013).
61. Neenan, J. M., Chapelle, K. E. J., Fernandez, V. & Choiniere, J. N. Ontogeny of the *Massospondylus* labyrinth: implications for locomotory shifts in a basal sauropodomorph dinosaur. *Palaeontology* **62**, 255–265, https://doi.org/10.1111/pala.12400 (2019).
62. Chapelle, K. E. J. *et al*. A quantitative method for inferring locomotory shifts in amniotes during ontogeny, its application to dinosaurs and its bearing on the evolution of posture. *Palaeontology* 1–14; https://doi.org/10.1111/pala.12451 (2019).
63. De Zeeuw, C. I. & Koekkoek, S. K. E. Signal processing in the C2 module of the flocculus and its role in head movement control. *Prog. Brain Res.* **114**, 299–321 (1997).
64. Cerroni, M. A. & Paulina-Carabajal, A. Novel information on the endocranial morphology of the abelisaurid theropod *Carnotaurus sastrei*. *C. R. Palevol.* **18**, 985–995, https://doi.org/10.1016/j.crpv.2019.09.005 (2019).
65. Sipla, J. S. The semicircular canals of birds and non-avian theropod dinosaurs. PhD Thesis, Stony Brook University (2007).
66. Wilson, V.J. & Melville-Jones, G. Mammalian vestibular physiology (Springer, 1979).
67. Dujim, M. On the head posture in birds and its relation to some anatomical features. *Proceedings of the Koninklijke Nederlandse Akademie Van Wetenschappen, Series C. Biological and Medical Sciences* **54**, 260–271 (1951).
68. Hullar, T. E. Semicircular canal geometry, afferent sensitivity, and animal behavior. *Anat. Rec.* **288A**, 466–472, https://doi.org/10.1002/ar.a.20304 (2006).
69. Marugán-Lobón, J., Chiappe, L. M. & Farke, A. A. The variability of inner ear orientation in saurischian dinosaurs: testing the use of semicircular canals as a reference system for comparative anatomy. *PeerJ* **1**, e124 (2013).
70. Rauhut, O. W. M. Morphology and mechanics of the jaws of spinosaurid theropods (Dinosauria): implications for predation. *Ameghiana* **38**(**4**) Suplemento-Resumenes (2001).
71. George, I. D. & Holliday, C. M. Trigeminal nerve morphology in *Alligator mississippiensis* and its significance for crocodyliform facial sensation and evolution. *Anat. Rec.* **296**, 670–680, https://doi.org/10.1002/ar.22666 (2013).
72. Barker, C. T., Naish, D., Newham, E., Katsamenis, O. L. & Dyke, G. Complex neuroanatomy in the rostrum of the Isle of Wight theropod *Neovenator salerii*. *Sci. Rep.* **7**, 3749, https://doi.org/10.1038/s41598-017-03671-3 (2017).
73. Rayfield, E. J. Cranial mechanics and feeding in *Tyrannosaurus rex*. *Proc. R. Soc. Lond. B. Biol. Sci.* **271**(1547), 1451–1459, https://doi.org/10.1098/rspb.2004.2755 (2004).
74. Rayfield, E. J. Using finite-element analysis to investigate suture morphology: a case study using large carnivorous dinosaurs. *Anat. Rec. A. Discov. Mol. Cell. Evol. Biol.* **283**(2), 349–365, https://doi.org/10.1002/ar.a.20168 (2005).
75. Rayfield, E. J. Structural performance of tetanuran theropod skulls, with emphasis on the Megalosauridae, Spinosauridae and Carcharodontosauridae. *Special Papers in Palaeontology* **86**, 241–253 (2011).

Acknowledgements
We thank the German Heart Centre in Munich (especially Jacqueline Jendick and Cornelia Pankalla) and Zeiss in Essingen (especially Nicole Kreuzer) for the CT-scans of the skull of *Irritator*. Furthermore, we are deeply grateful for the help of the Cytology and Evolutionary Biology group of the Zoological Institute and Museum, University Greifswald (especially Marie Hörnig and Steffen Harzsch) and the Freunde der Bayerischen Staatssammlung für Paläontologie und Geologie München e.V. (especially Martin Nose). Additionally, Lehre@LMU (especially Tanja Schulz-Mirbach), the chair of Paleontology and Historical Geology (especially Ingelore Hinz-Schallreuter and Stefan Meng), Gertrud Rößner, Christoph Kettler and Benjamin Englich supported this project. Susannah Maidment, Neil Gostling and Chris Barker allowed provided access to material of *Baryonyx*. Gabriela Sobral and Cathrin Pfaff are thanked for discussions. We thank Rainer Schoch for access to SMNS 58022 and permission to loan the specimen in order to conduct CT scans. We also thank Stephan Lautenschlager, Matt White, and an anonymous reviewer for very constructive comments that improved an earlier version of this MS, as well as Heather Smith for editorial handling of our submission.

Author contributions
M.S. and O.W.M.R. designed the project. M.S. organized the CT scans and segmented the data. S.W.E. prepared the figures. M.S., O.W.M.R. and S.W.E. interpreted the data and wrote the manuscript.

Competing interests
The authors declare no competing interests.

Additional information
Correspondence and requests for materials should be addressed to M.S.

Reprints and permissions information is available at www.nature.com/reprints.

Publisher's note Springer Nature remains neutral with regard to jurisdictional claims in published maps and institutional affiliations.

II

Schade, M., Stumpf, S., Kriwet, J., Kettler, C. & Pfaff, C. Neuroanatomy of the nodosaurid *Struthiosaurus austriacus* (Dinosauria: Thyreophora) supports potential ecological differentiations within Ankylosauria. *Sci. Rep.* 12, 144. https://doi.org/10.1038/s41598-021-03599-9 (2022a).

scientific reports

Check for updates

OPEN

Neuroanatomy of the nodosaurid *Struthiosaurus austriacus* (Dinosauria: Thyreophora) supports potential ecological differentiations within Ankylosauria

Marco Schade[1,2,3]✉, Sebastian Stumpf[4], Jürgen Kriwet[4], Christoph Kettler[5] & Cathrin Pfaff[4]✉

Nodosauridae is a group of thyreophoran dinosaurs characterized by a collar of prominent osteoderms. In comparison to its sister group, the often club-tailed ankylosaurids, a different lifestyle of nodosaurids could be assumed based on their neuroanatomy and weaponry, e.g., regarding applied defensive strategies. The holotype of the nodosaurid *Struthiosaurus austriacus* consists of a single partial braincase from the Late Cretaceous of Austria. Since neuroanatomy is considered to be associated with ecological tendencies, we created digital models of the braincase based on micro-CT data. The cranial endocast of *S. austriacus* generally resembles those of its relatives. A network of vascular canals surrounding the brain cavity further supports special thermoregulatory adaptations within Ankylosauria. The horizontal orientation of the lateral semicircular canal independently confirms previous appraisals of head posture for *S. austriacus* and, hence, strengthens the usage of the LSC as proxy for habitual head posture in fossil tetrapods. The short anterior and angular lateral semicircular canals, combined with the relatively shortest dinosaurian cochlear duct known so far and the lack of a floccular recess suggest a rather inert lifestyle without the necessity of sophisticated senses for equilibrium and hearing in *S. austriacus*. These observations agree with an animal that adapted to a comparatively inactive lifestyle with limited social interactions.

Thyreophora are ornithischian dinosaurs, comprising iconic taxa like *Stegosaurus* and *Ankylosaurus*[1]. Ankylosauria thrived at least since the Middle Jurassic and some of their representatives witnessed the end-Cretaceous mass extinction[1]. These globally distributed quadruped herbivores were heavily armoured living fortresses; partly either equipped with a club tail (ankylosaurids[2]) or a collar of hypertrophied spikes on their neck and shoulders (nodosaurids[3]). Potential palaeoenvironmental[4] and food preferences[5], together with features of their nasal passages[6], jaw mechanics[7,8] and osteoderms[9], may indicate different lifestyles for both groups.

Since the brain and associated neuroanatomical structures of vertebrates leave perceivable traces, which are possibly ecologically informative, it is worthwhile to thoroughly examine the braincase of nodosaurids in order to compare it to ankylosaurids. Whereas complete braincase material among early-diverging thyreophorans is only known from *Scelidosaurus harrisoni*[10], neurocranial material of stegosaurs[11,12], and ankylosaurs (e.g.[13–15]) is more common. The heavily armored skull roofs of the latter likely improved their preservation potential.

Struthiosaurus is a European nodosaurid with an estimated body length of up to three metres, known from cranial and postcranial material of Campanian to Maastrichtian age[16–22]. As currently accepted, *Struthiosaurus* comprises three species: *S. austriacus* from the early Campanian of Austria[16–18], *S. languedocensis* from the early Campanian of France[22], and *S. transylvanicus* from the Maastrichtian of Romania[23,24]. In addition, skeletal remains referred to *Struthiosaurus* sp. were reported from late Campanian to early Maastrichtian deposits of

[1]Institute of Geography and Geology, Palaeontology and Historical Geology, University of Greifswald, 17489 Greifswald, Germany. [2]Zoological Institute and Museum, Cytology and Evolutionary Biology, University of Greifswald, 17489 Greifswald, Germany. [3]Department of Earth and Environmental Sciences, Palaeontology and Geobiology, Ludwig-Maximilians-Universität, 80333 Munich, Germany. [4]Department of Palaeontology, Faculty of Earth Sciences, Geography and Astronomy, University of Vienna, 1090 Vienna, Austria. [5]Department of Geology, Faculty of Earth Sciences, Geography and Astronomy, University of Vienna, 1090 Vienna, Austria. ✉email: marco.schade@stud.uni-greifswald.de; cathrin.pfaff@univie.ac.at

Spain[20,21]. The potentially oldest fossil record of *Struthiosaurus* is represented by a single right humerus from the Santonian of Hungary[25]. The type species of *Struthiosaurus*, *S. austriacus*, is based on fragmentary cranial and postcranial remains of at least three individuals of different ontogenetic stages that were recovered during the nineteenth century from early Campanian continental coal-bearing beds of Muthmannsdorf, Austria, referred to the Grünbach Formation (see[18] for overview).

The holotype specimen of *S. austriacus*, a partial braincase (IPUW 2349/6; Fig. 1), was scanned with the aid of a micro-CT; its superficial morphology has been previously described[16,17,26]. The segmentation of the internal structures provides new insights into the neuroanatomy and behavioral capacities of this Late Cretaceous (Campanian) armoured dinosaur from Austria.

Results

Cranial endocast, innervation and blood supply. As in most non-maniraptoriform dinosaur braincases (e.g.[27–29]), features of the midbrain and hindbrain are not securely identifiable as imprints on the endocast of IPUW 2349/6 (Figs. 2, 3). This suggests little correlation of the brain and respective soft tissues with the surface of the endocranial cavity in the living animal, which is similar to extant reptiles (e.g., crocodiles and turtles[30,31]).

Although not completely preserved, the endocranial cavity suggests great angles of both the cerebral and the pontine flexure in IPUW 2349/6, matching the condition in other ankylosaurs and stegosaurs[11–13,32]. The endocast shows a slight dural peak (Fig. 2A), where the pineal gland would be expected, similar to the condition in the ankylosaur *Kunbarrasaurus ieversi*[14]. The presence of the cartilage-filled pit in the supraoccipital, expressed as an anteroventrally inclined ridge on the cranial endocasts of *Struthiosaurus austriacus*, *S. transylvanicus*[17] and the nodosaurid *Hungarosaurus* sp.[32], is barely discernable in the digital endocast of IPUW 2349/6. Ventral to the pineal, around the mid-height of the brain endocast, the dorsal middle cerebral vein could be reconstructed on the right side (Fig. 2E,F; vcm). Additionally, at least two large canals, tentatively assigned to the transverso-occipital vein[13], traverse each paroccipital process and the prootic mainly anteroposteriorly; without any obvious connection to another endocranial structure (Fig. 2A,C,E). More delicate and complex networks of canals are present further anterodorsally and may belong to the posterior branching plexus[13]. Possibly, the expanding mediolateral width of the anterodorsal endocast marks the otherwise barely delineated cerebral hemispheres. Anteroventrally, the posterior portion of the pituitary fossa is preserved, together with the ventrolaterally directed internal carotid artery (Fig. 3A,B; pit; ic). Around the preserved mid-length, each internal carotid artery branch is connected to another vascular duct of uncertain identity, leading in a posterodorsolateral direction. The canal for the abducens nerve (Fig. 3A,B; CN VI) is situated posterolaterally to the pituitary fossa. While the facial nerve opening (CN VII) is situated anteriorly to the cochlear duct, the columellar recess, the metotic foramen (for CN IX-XI and jugular vein) and the hypoglossal nerve openings (CN XII) are situated posterior to the cochlear duct. Due to the fact that the specimen is strongly traversed by breakages, the canals for CN VII and IX-XI likely appear slightly too large in our reconstruction, but certainly approximate the course of the respective canals. However, for the same reason, the exact position and course of the CN XII openings and canals could not be established with certainty, but are estimated on the basis of internal and external characteristics. The micro-CT data suggest the presence of two CN XII openings per side, which are largely obscured by cracks on the outside (Figs. 1J,K, 2E,F, 3C,D). While Pereda-Suberbiola and Galton[16] identified two foramina on the left side of the specimen as the openings for CN XII, our reconstruction suggests that the more ventrally situated foramen actually represents the metotic foramen. In posterior view, medially to the left metotic foramen, another foramen seems to be situated (Fig. 1J,K) but the micro-CT data show that this is just a superficial damage. The midbrain of IPUW 2349/6 does not possess a floccular recess. Posteriorly, the foramen magnum is connected to the mediolaterally wide medulla oblongata. The incomplete endocranial cavity comprises a volume of around 12 cm^3 (measured according to Sampson and Witmer[33]).

Endosseous labyrinth. The vestibular system is ventrally connected to the cochlea and together they form the completely preserved endosseous labyrinth of IPUW 2349/6 (Fig. 4). The anterior semicircular canal is dorsoventrally slightly higher and anteroposteriorly wider than the posterior semicircular canal (Fig. 4A). The vertical semicircular canals are thick and short in relation to the complete vestibular system. In dorsal view, they enclose an angle of 91° in the right vestibular system and 98° at the left vestibular system. The common crus, uniting the anterior and posterior semicircular canal, is slightly posteriorly inclined. In dorsal view, the relatively thick lateral semicircular canal projects posterolaterally and arcs towards the posterior ampulla, producing a very acute angle on its distal-most corner (Fig. 4C). The cochlear duct is strikingly short on both sides, being dorsoventrally shorter than the vestibular system (Fig. 4E). The cochlear duct projects anteroventrolaterally and is strongly tapered distally.

Auditory capabilities. In order to very roughly estimate the auditory capability of *S. austriacus*, we digitally measured the dorsoventral cochlear duct length (c. 5.9 mm; as outlined by Walsh et al.[34]) and the anteroposterior basicranial length (c. 40.5 mm; measured between the anterior-most preserved part of the sella turcica and the distal-most part of the occipital condyle). Following the equations of Walsh et al.[34], we calculate the mean hearing frequency of *S. austriacus* as 1230 Hz and the frequency bandwidth as 1868 Hz (between 296 and 2164 Hz).

Discussion

Neurovascularanatomy and ecological affinities. The presence of widely distributed vascular canals in the holotypic neurocranium of *Struthiosaurus austriacus* adds to the diversity of patterns within Thyreophora[6,13,14,35]. Conversely to *Bissektipelta archibaldi*[13], these canals are not obviously interconnected with each other or the cavity that once contained the brain, and are located closer to the endosseous labyrinth in *S.*

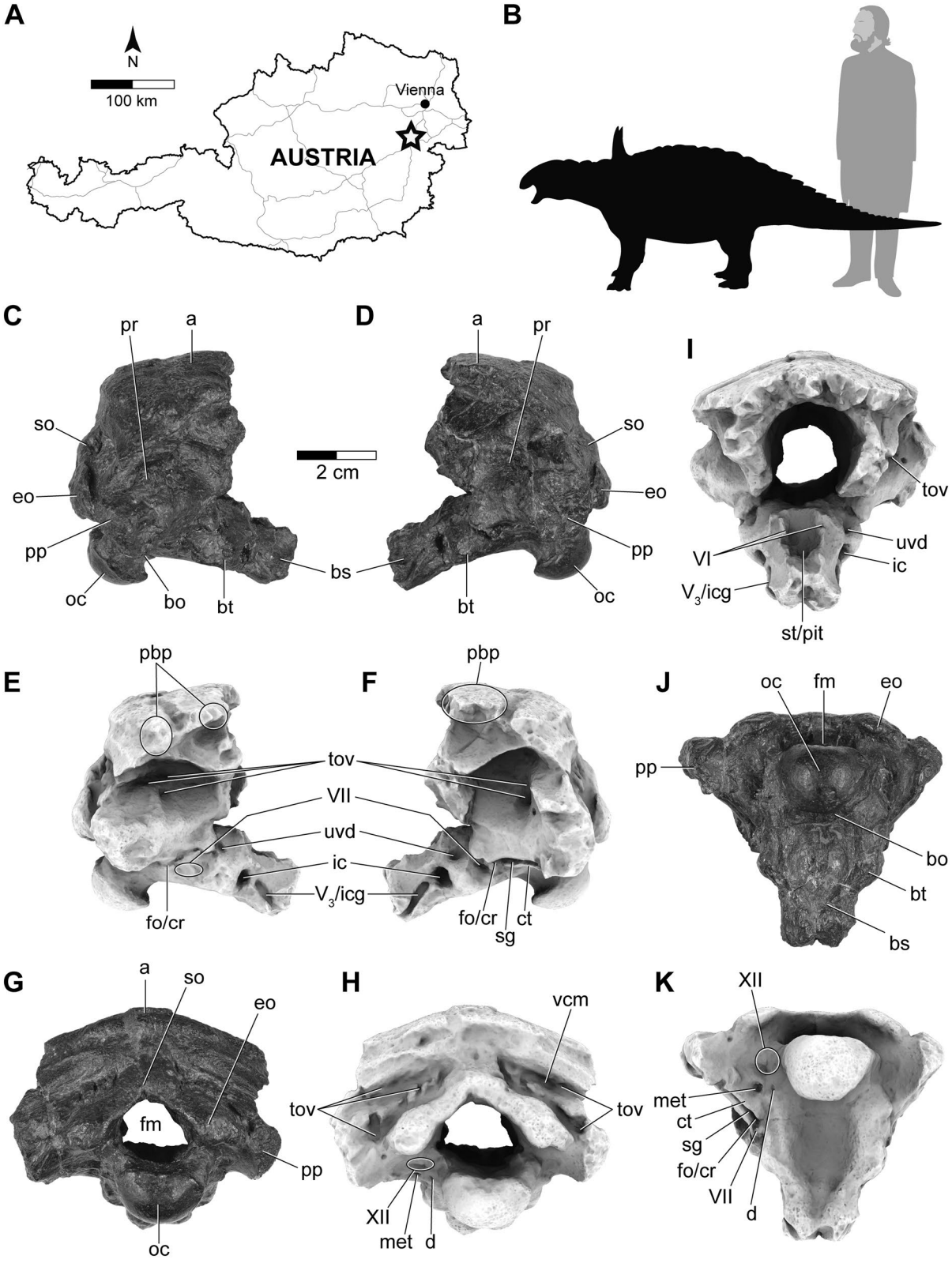

Figure 1. (**A**) Outline drawing of Austria with a star marking Muthmannsdorf, the type locality of *Struthiosaurus austriacus*. (**B**) Silhouette of *Struthiosaurus austriacus* (measuring 2.7 m in length here; copyright: Fabrizio De Rossi) and a human for comparison. Photographs (**C**,**D**,**G**,**J**) and ambient occlusion photogrammetric models (**E**,**F**,**H**,**I**,**K**) of the holotype specimen of *Struthiosaurus austriacus*, IPUW 2349/6, in (**C**,**E**) right lateral, (**D**,**F**) left lateral, (**I**) anterior, (**J**,**K**) ventral and (**G**,**H**) posterior views. a, armour; bo, basioccipital; bs, basisphenoid; bt, basal tuber; ct, crista tuberalis; d, damage; fm, foramen magnum; fo/cr, fenestra ovalis/columellar recess; met, metotic foramen; pbp, posterior branching plexus; sg, stapedial groove; st/pit, sella turcica/pituitary; tov, transverso-occipital vein; uvd, uncertain vascular duct; V_3/icg, groove for the mandibular branch of the trigeminal nerve or for the internal carotid; VI, abducens nerve; VII, facial nerve; vcm, dorsal middle cerebral vein; XII, hypoglossal nerve.

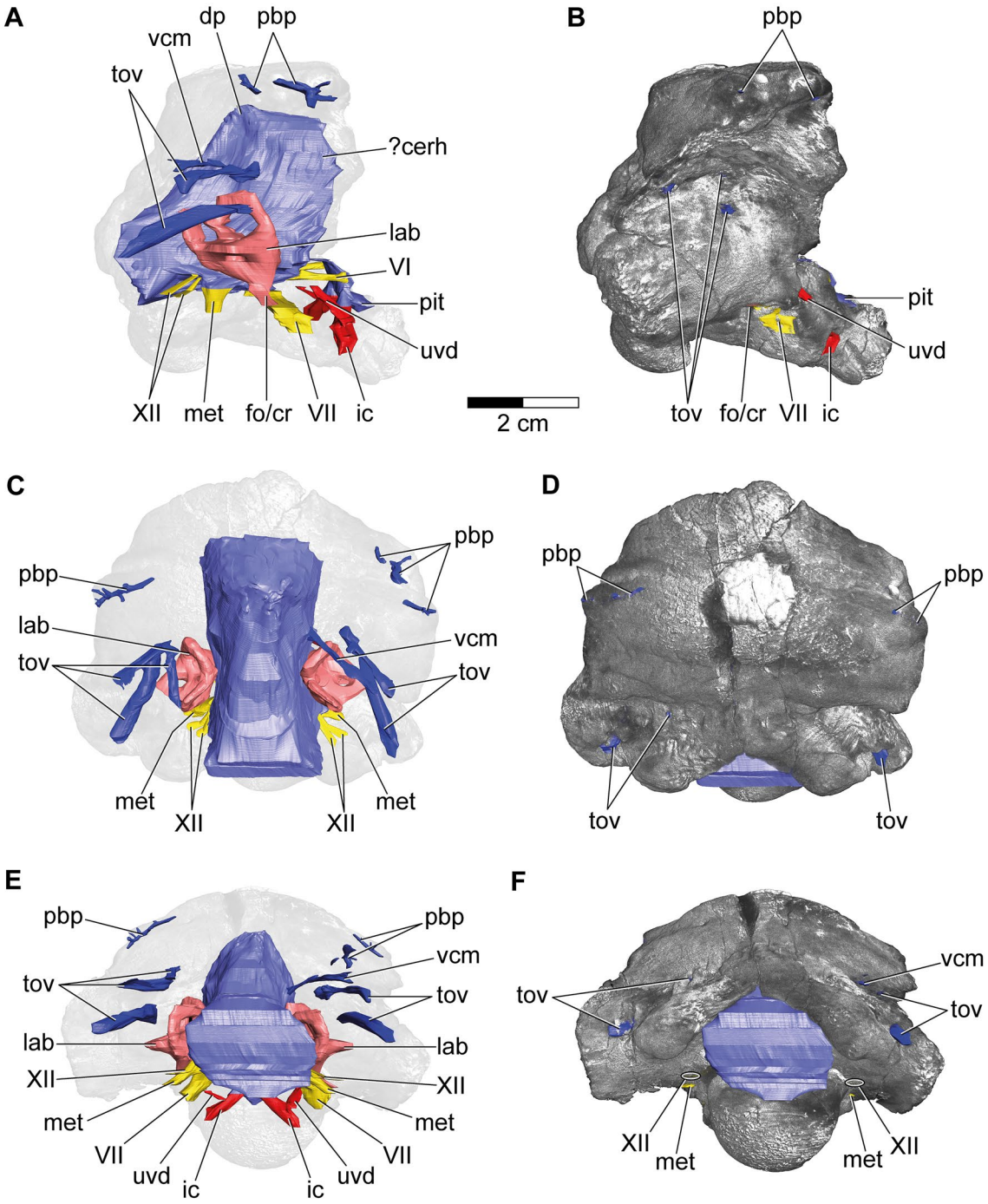

Figure 2. 3D model of the cranial endocast with endosseous labyrinths and neurovascular canals of the holotype specimen of *Struthiosaurus austriacus*, IPUW 2349/6, without (**A**,**C**,**E**) and with (**B**,**D**,**F**) a volume rendering of the braincase in (**A**,**B**) right lateral, (**C**,**D**) dorsal and (**E**,**F**) posterior aspects. ?cerh, possible cerebral hemisphere; dp, dural peak; fo/cr, fenestra ovalis/columellar recess; met, metotic foramen; lab, endosseous labyrinth; pbp, posterior branching plexus; pit, pituitary; tov, transverso-occipital vein; uvd, uncertain vascular duct; VI, abducens nerve; VII, facial nerve; vcm, dorsal middle cerebral vein; XII, hypoglossal nerve.

austriacus. As other authors suggested[6,13,35], a complex network of blood supply tissue within the braincase could have contributed to remodelling of skull bones and armour, and thermoregulation of the brain. Additionally, the posterodorsolaterally directed duct on each internal carotid artery branch found in *S. austriacus* likely played a role in thermoregulation[35].

The endosseous labyrinth of vertebrates detects head movements, making it critical in gaze stabilization during locomotion (e.g.[36]). Currently, it is a matter of debate to what extent the morphology of the semicircular canals is a proxy for certain ecological affinities within Archosauromorpha[37,38]. Few endosseous labyrinths of

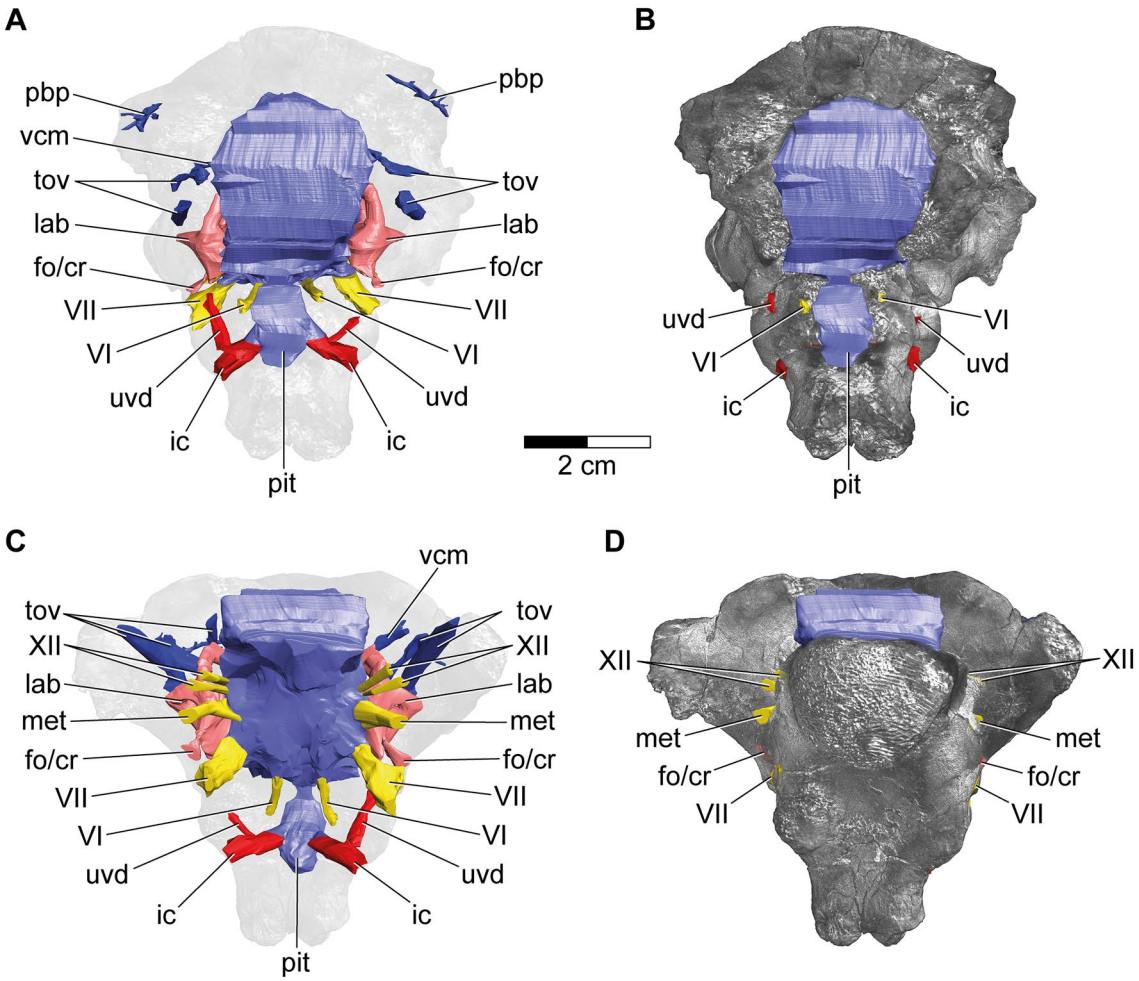

Figure 3. 3D model of the cranial endocast with endosseous labyrinths and neurovascular canals of the holotype specimen of *Struthiosaurus austriacus*, IPUW 2349/6 without (**A**,**C**) and with (**B**,**D**) a volume rendering of the braincase in (**A**,**B**) anterior and (**C**,**D**) ventral views. fo/cr, fenestra ovalis/columellar recess; met, metotic foramen; lab, endosseous labyrinth; pbp, posterior branching plexus; pit, pituitary; tov, transverso-occipital vein; uvd, uncertain vascular duct; VI, abducens nerve; VII, facial nerve; vcm, dorsal middle cerebral vein; XII, hypoglossal nerve.

ankylosaur taxa are known, of which all possess relatively short and thick semicircular canals, as seen in the early-diverging ankylosaur *Kunbarrasaurus ieversi*[14], the ankylosaurids *B. archibaldi*[13], *Euoplocephalus tutus*[39] (and probably *T. teresae*[15]), and the nodosaurid *Pawpawsaurus campbelli*[40]. Hence, including *S. austriacus*, only two nodosaurid endosseous labyrinths are known to date and both display an anterior semicircular canal, which is just slightly longer than the respective posterior semicircular canal. This contrasts the condition seen in *K. ieversi*[14], *B. archibaldi*[13] and *E. tutus*[39], clearly showing a relatively longer ASC. Long semicircular canals are thought to be more sensitive for head movements[33], and hence potentially related to neck mobility[41,42]. The unique and conspicuously acute angle at mid-length of the lateral semicircular canal of *S. austriacus* did probably impede a continuous endolymphatic flow, causing insensitivity in comparison to the usual rounded condition. Furthermore, the combination of a longer ASC in two ankylosaurid taxa (*B. archibaldi* and *E. tutus*), as well as the presence of a floccular recess (*E. tutus* and *T. teresae*), may render ankylosaurids superior in VOR (vestibulo-ocular reflex) and VCR (vestibulo-collic reflex) procession in comparison to nodosaurids. This could be associated with a more active kind of protective behaviour in ankylosaurids, involving digging and targeting usage of their tail clubs[2,15,43,44].

Because of its involvement in processing VOR/VCR, the flocculus is a critical structure of the cerebellum for control and coordination of head, eye, and neck movements[41,45,46]. Although the size of the floccular fossa has been found to fail as a proxy for ecology or behavior in certain extant mammals and birds[47], it has repeatedly been used to tentatively establish such a meaning for fossil taxa (e.g.[15,33,48]). Additionally, ontogeny possibly plays a role in the expression of the flocculus on the endocast[28]. A lack of a floccular recess is common for ankylosaurs, except for a group within Ankylosaurinae[13,15], and no floccular recess has been found in any nodosaurid endocast so far[32,40]. However, a floccular recess is present in the ankylosaurine ankylosaurids *E. tutus*[14,39] and *T. teresae*[40]. Furthermore, braincase endocasts of the stegosauruids *Stegosaurus*[11] and *Kentrosaurus*[12] share slight lateral

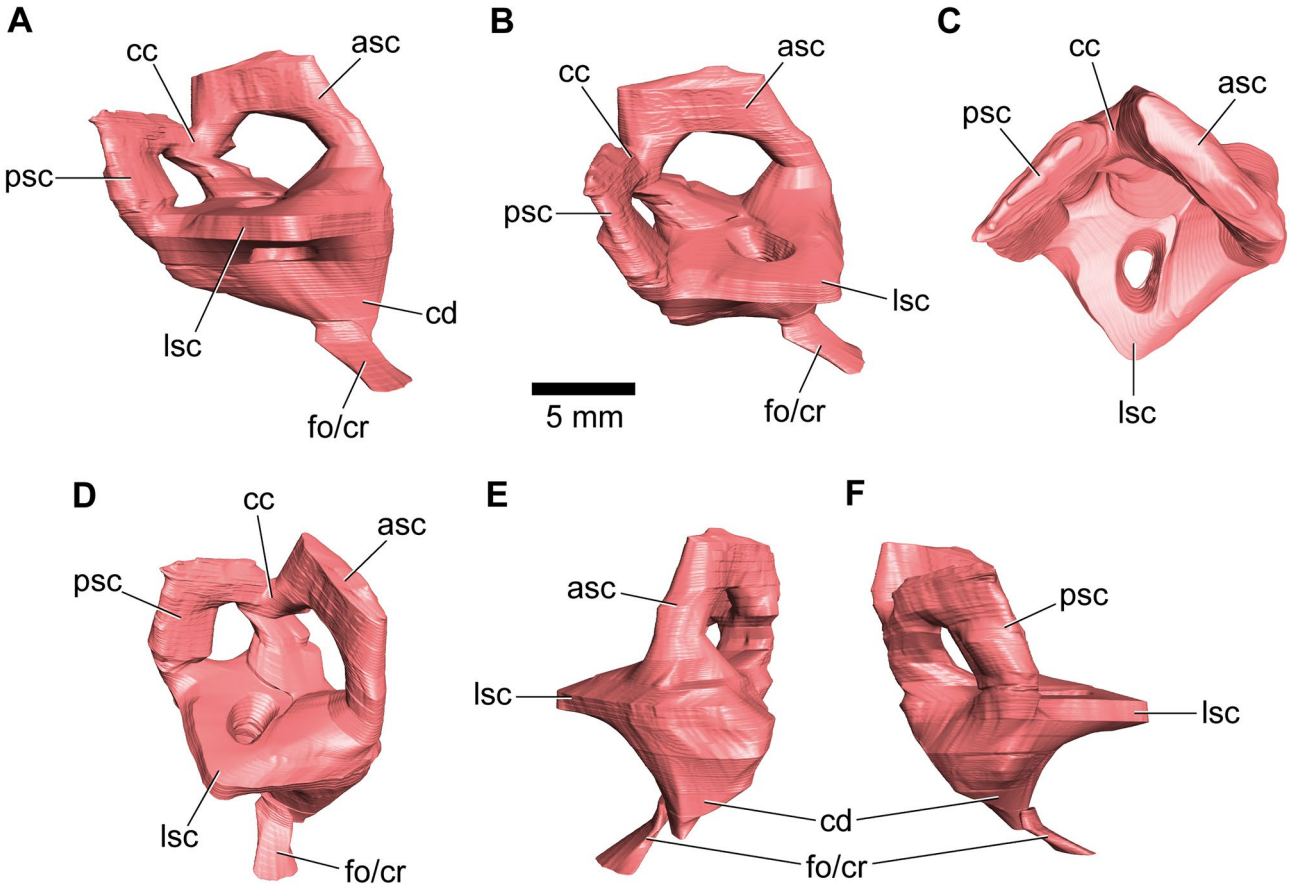

Figure 4. 3D model of the right endosseous labyrinth of the holotype specimen of *Struthiosaurus austriacus*, IPUW 2349/6, in (**A**) lateral, (**B**) posterodorsolateral, (**C**) dorsal, (**D**) anterodorsolateral, (**E**) anterior and (**F**) posterior views. asc, anterior semicircular canal; cc, common crus; cd, cochlear duct; fo/cr, fenestra ovalis/columellar recess; lsc, lateral semicircular canal; psc, posterior semicircular canal.

eminences, which have been identified as floccular recesses (however, not present in all *Stegosaurus* specimens[14]), and both taxa have spiked tails, which were very likely proper defensive means[49,50]. Arbour and Currie[2] reported a stepwise acquisition of clubbed tails in ankylosaurids, leading to a handle first (interlocking vertebrae produce a stiffened tail) and a knob second (fusion of distal-most osteoderms) model. Just like nodosaurids, some early-diverging ankylosaurids show no handle or knob adaptations[2]. Only ankylosaurine ankylosaurids show both, a handle and a knob, producing a functional tail club[2]. It is conspicuous that endocasts of thyreophoran taxa with a formidable weapon on the tail (*Stegosaurus*, *Kentrosaurus*, *Euoplocephalus* and *Tarchia*; although a tail club has only been referred to *Tarchia*[2,51]) bear a floccular recess as well[11,12,39,40]. In contrast, nodosaurids and early-diverging ankylosaurids neither show a distinct floccular recess[13,32,40], nor a tail club[2] for which targeting would have been useful. Nodosaurids bear long spikes around their neck and shoulder[3] (which likely rather limited their neck mobility[42]) in addition to osteoderms with relatively thicker cancellous cores[52]; an involvement in thermoregulation and display has been hypothesized for ankylosaur armor[9]. While ankylosaurids tend to bear armours only with bulky osteoderms, nodosaurids additionally possess proximodistally very elongated elements[3,53], may producing an armour with a comparably passive protective/offensive utility[9].This may suggest a more passive defense tactic through simple hunker down behavior in nodosaurids with less reliance on coordination-related (VOR/VCR) neural tissue (in contrast to[32]). Regarding the demonstrably well vascularized neurocranium of ankylosaurs[6,13], the putative hypertrophied cerebellum in endocasts of *Hungarosaurus* sp.[32] and *Struthiosaurus transylvanicus*[17] may rather represent areas of extensive blood supply and other soft tissues. Possibly, the flocculus independently developed a larger size because of its neurologic involvement[54] in VOR/VCR in the actively defending stegosaurs and late-diverging ankylosaurids (ankylosaurines).

The orientation of the lateral semicircular canal as a proxy for head posture is not necessarily straightforward[55,56]. However, our reconstructions suggest a strongly posteroventrally inclined occipital condyle (c. 55°; Figs. 1C, 2B) for *S. austriacus* when the LSC is horizontally arranged. Hence, this independently supports the findings of Pereda-Suberbiola and Galton[17], who compared the skull roof and basisphenoid of *S. austriacus* with *Panoplosaurus mirus*, signifying a habitually slightly inclined snout in both taxa.

Auditory capacities and sound production. Following the procedure of Walsh et al.[34], the auditory acuity of *S. austriacus* seems somewhat superior to that of turtles. Paulina-Carabajal et al.[40] considered the cochlea

to be relatively short in the nodosaurid *P. campbelli* because of the ventrally situated fenestra ovalis, which marks the border of the vestibular system and the cochlea. However, this contrasts with the practice of Walsh et al.[34], who included the fenestra ovalis in the cochlear duct length. Animals are likely to perceive sounds they are able to produce themselves (Walsh et al.[34] and references therein). Because ankylosaurids seem to possess longer cochlear ducts than nodosaurids, it has been hypothesized that ankylosaurids had more sophisticated sound producing and perception capabilities in comparison to nodosaurids[15,40]. The presence of relatively shorter and less convoluted nasal passages, which are possibly involved in sound production, in the nodosaurid *P. mirus*, compared to the ankylosaurid *E. tutus*, potentially supports this interpretation[6,30,40,42]. Nonetheless, the nasal passages of ankylosaurs may have mainly served as adaptation for thermal homeostasis of the brain by vascular tissues shedding excess heat into the nasal passages (being seemingly more efficient in *E. tutus* than in *P. mirus*[6]). The extremely short cochlear duct of *S. austriacus* (in fact the shortest found in a dinosaur so far) may further support inferior auditory capabilities of nodosaurids in comparison to ankylosaurids.

Conclusions

Whereas nodosaurids and ankylosaurids were lumbering[57,58], heavily armoured[9,52] and low-browsing[5] animals, mainly relying on large guts (possibly for fermentation) to digest[53], nodosaurids possibly preferred coastal or fluvial environments[4] and are suspected for having evolved jaw biomechanics delivering stronger bite forces[7,8] (potentially for tougher plant material), and the gut content of a nodosaurid hints to a selective feedings style[5]. Furthermore, the combination of a relatively short cochlear duct[40], the lack of a floccular recess[13,17,32,40], a short ASC[40], less elaborated nasal passages[6], the obligate absence of a tail club[2], but thickened osteoderms[9,52] in nodosaurids indicate different ecological adaptations in comparison to ankylosaurids. Hence, nodosaurids were possibly less reliant on their sense of hearing, applied a less active style of self-defense and, apparently, occupied different ecological niches than ankylosaurids. The new findings of the neuroanatomy of *Struthiosaurus austriacus* seem to add to this differentiation.

Materials and methods

The holotype specimen of *Struthiosaurus austriacus*, IPUW 2349/6, represents an incomplete braincase that is traversed by breakages but not deformed, preserving the posterior part of the skull roof, most of the occipital region and part of the basicranium. It is about 55 mm in mediolateral width and measures 50 mm anteroposteriorly and dorsoventrally. Although already described elsewhere[16,17,26], micro-CT-based neuroanatomical accounts for IPUW 2349/6 have never been made.

We scanned IPUW 2349/6 using the desktop micro-computed tomography device (micro-CT) SkyScan/Bruker 1173 housed in the Department of Palaeontology, University of Vienna (voltage: 130 kV, X-ray tube current: 61 μA, exposure time: 1249 ms, filter: brass 0.25 mm, voxel size: 0.032904 mm). Digital segmentation and measurements were produced utilizing the software Amira (6.1), based on bmp image files, which were exported using DataViewer 1.5.4.0. (Skyscan/Bruker). The micro-CT data were manually segmented to create 3D models, which were mirrored afterwards. The density contrast between the fossil and the sediment within was relatively weak, but whereas the respective cavities were still clearly discernable, it was not possible to distinguish individual bones and sutures of the neurocranium. The photogrammetry models are based on 122 photographs and were created with Agisoft (1.7.2).

Data availability

The micro-CT slice data, neuroanatomical and photogrammetry models of IPUW 2349/6, are published online, in the repository MorphoSource (Project: Struthiosaurus austriacus-IPUW 2349/6-Schade et al. 2021 neuro anatomy//MorphoSource).

Received: 17 August 2021; Accepted: 6 December 2021
Published online: 07 January 2022

References

1. Thompson, R. S., Parish, J. C., Maidment, S. C. R. & Barrett, P. M. Phylogeny of the ankylosaurian dinosaurs (Ornithischia: Thyreophora). *J. Syst. Palaeontol.* **10**(2), 301–312 (2012).
2. Arbour, V. M. & Currie, P. J. Ankylosaurid dinosaur tail clubs evolved through stepwise acquisition of key features. *J. Anat.* **227**, 514–523. https://doi.org/10.1111/joa.12363 (2015).
3. Brown, C. M. An exceptionally preserved armored dinosaur reveals the morphology and allometry of osteoderms and their horny epidermal coverings. *PeerJ* **5**, e4066. https://doi.org/10.7717/peerj.4066 (2017).
4. Butler, R. J. & Barrett, P. M. Palaeoenvironmental controls on the distribution of Cretaceous herbivorous dinosaurs. *Sci. Nat.* **95**, 1027–1032 (2008).
5. Brown, C. M. *et al.* Dietary palaeoecology of an Early Cretaceous armoured dinosaur (Ornithischia; Nodosauridae) based on floral analysis of stomach contents. *R. Soc. Open Sci.* **7**, 200305. https://doi.org/10.1098/rsos.200305 (2020).
6. Bourke, J. M., Porter, W. R. & Witmer, L. M. Convoluted nasal passages function as efficient heat exchangers in ankylosaurs (Dinosauria: Ornithischia: Thyreophora). *PLoS ONE* **13**, e0207381. https://doi.org/10.1371/journal.pone.0207381 (2018).
7. Mallon, J. C. & Anderson, J. S. The functional and palaeoecological implications of tooth morphology and wear for the megaherbivorous dinosaurs from the dinosaur park formation (Upper Campanian) of Alberta, Canada. *PLoS ONE* **9**(6), e98605. https://doi.org/10.1371/journal.pone.0098605 (2014).
8. Ősi, A., Prondvai, E., Mallon, J. & Bodor, E. R. Diversity and convergences in the evolution of feeding adaptations in ankylosaurs (Dinosauria: Ornithischia). *Hist. Biol.* **29**(4), 539–570. https://doi.org/10.1080/08912963.2016.1208194 (2017).
9. Hayashi, S., Carpenter, K., Scheyer, T. M., Watanabe, M. & Suzuki, D. Function and evolution of ankylosaur dermal armor. *Acta Palaeontol. Pol.* **55**(2), 213–228 (2010).
10. Norman, D. B. *Scelidosaurus harrisonii* from the Early Jurassic of Dorset, England: Cranial anatomy. *Zool. J. Linn. Soc.* **188**(1), 1–81. https://doi.org/10.1093/zoolinnean/zlz074 (2019).

11. Galton, P. M. Endocranial casts of the plated dinosaur *Stegosaurus* (Upper Jurassic, Western USA): A complete undistorted cast and the original specimens of Othniel Charles Marsh. In *The Armored Dinosaurs* (ed. Carpenter, K.) 103–129 (Indiana University Press, 2001).
12. Galton, P. M. Skull bones and endocranial casts of stegosaurian dinosaur *Kentrosaurus* Hennig, 1915 from Upper Jurassic of Tanzania, East Africa. *Geol. Palaeontol.* **22**, 123–143 (1988).
13. Kuzmin, I. *et al.* The braincase of *Bissektipelta archibaldi*—new insights into endocranial osteology, vasculature, and paleoneurobiology of ankylosaurian dinosaurs. *Biol. Commun.* **65**(2), 85–156. https://doi.org/10.21638/spbu03.2020.201 (2020).
14. Leahey, L. G., Molnar, R. E., Carpenter, K., Witmer, L. M. & Salisbury, S. W. Cranial osteology of the ankylosaurian dinosaur formerly known as *Minmi* sp. (Ornithischia: Thyreophora) from the Lower Cretaceous Allaru Mudstone of Richmond, Queensland, Australia. *PeerJ* **3**, e1475. https://doi.org/10.7717/peerj.1475 (2015).
15. Paulina-Carabajal, A., Lee, Y. N., Kobayashi, Y., Lee, H. J. & Currie, P. J. Neuroanatomy of the ankylosaurid dinosaurs *Tarchia teresae* and *Talarurus plicatospineus* from the Upper Cretaceous of Mongolia, with comments on endocranial variability among ankylosaurs. *Palaeogeogr. Palaeoclimatol. Palaeoecol.* **494**, 135–146. https://doi.org/10.1016/j.palaeo.2017.11.030 (2018).
16. Pereda-Suberbiola, X. & Galton, P. M. On the taxonomic status of the dinosaur *Struthiosaurus austriacus* Bunzel from the Late Cretaceous of Austria. *C. R. Acad. Sci. Paris II* **315**, 1275–1280 (1992).
17. Pereda-Suberbiola, X. & Galton, P. M. Revision of the cranial features of the dinosaur *Struthiosaurus austriacus* Bunzel (Ornithischia: Ankylosauria) from the Late Cretaceous of Europe. *Neues Jahrb. Geol. Palaontol. Abh.* **191**, 173–200 (1994).
18. Pereda-Suberbiola, X. & Galton, P. M. Reappraisal of the nodosaurid ankylosaur *Struthiosaurus austriacus* Bunzel from the Upper Cretaceous Gosau Beds of Austria. In *The Armored Dinosaurs* (ed. Carpenter, K.) 173–210 (Indiana University Press, 2001).
19. Pereda-Suberbiola, X. A revised census of European Late Cretaceous nodosaurids (Ornithischia: Ankylosauria): Last occurrence and possible extinction scenarios. *Terra Nova* **4**, 641–648 (1992).
20. Pereda-Suberbiola, X. Ankylosaurian dinosaur remains from the Upper Cretaceous of Laño (Iberian Peninsula). *Est. Mus. Cienc. Nat. de Álava* **14**(Número especial 1), 273–288 (1999).
21. Pereda-Suberbiola, X., Astibia, H. & Buffetaut, E. New remains of the armoured dinosaur *Struthiosaurus* from the Late Cretaceous of the Iberian peninsula (Lafio locality, Basque-Cantabric Basin). *Bull. Soc. Géol. Fr.* **166**, 207–211 (1995).
22. Garcia, G. & Pereda-Suberbiola, X. A new species of *Struthiosaurus* (Dinosauria: Ankylosauria) from the upper cretaceous of Villeveyrac (Southern France). *J. Vertbr. Paleontol* **23**(1), 156–165 (2003).
23. Nopcsa, F. Dinosaurierreste aus Siebenbürgen V. *Geologica Hungarica, Series Palaeontologica* **4**, 1–76 (1929).
24. Codrea, V. *et al.* More than just Nopcsa's Transylvanian dinosaurs: A look outside the Haţeg Basin. *Palaeogeogr. Palaeoclimatol. Palaeoecol.* **293**, 391–405. https://doi.org/10.1016/j.palaeo.2009.10.027 (2010).
25. Ősi, A. & Prondvai, E. Sympatry of two ankylosaurs (*Hungarosaurus* and cf. *Struthiosaurus*) in the Santonian of Hungary. *Cretac. Res.* **44**, 30–38. https://doi.org/10.1016/j.cretres.2013.03.006 (2013).
26. Bunzel, E. Die Reptilfauna der Gosaformation in der Neuen Welt bei Wiener-Neustadt. *Abhandlungen der Kaiserlich-Königlichen Geologischen Reichsanstalt.* **5**, 1–18 (1871).
27. Franzosa, J. & Rowe, T. Cranial endocast of the Cretaceous theropod dinosaur *Acrocanthosaurus atokensis*. *J. Vertebr. Paleontol.* **25**, 859–864 (2005).
28. Witmer, L. M. & Ridgely, R. C. New insights into the brain, braincase, and ear region of tyrannosaurs (Dinosauria, Theropoda), with implications for sensory organization and behavior. *Anat. Rec.* **292**(9), 1266–1296. https://doi.org/10.1002/ar.20983 (2009).
29. Schade, M., Rauhut, O. W. M. & Evers, S. W. Neuroanatomy of the spinosaurid Irritator challengeri (Dinosauria: Theropoda) indicates potential adaptations for piscivory. *Sci. Rep.* **10**(9259), 1613–1616. https://doi.org/10.1038/s41598-020-66261 (2020).
30. Witmer, L. M., Ridgely, R. C., Dufeau, D. L. & Semones, M. C. Using CT to peer into the past: 3D visualization of the brain and ear regions of birds, crocodiles, and nonavian dinosaurs. In *Anatomical imaging: towards a new morphology* (eds Endo, H. & Frey, R.) 67–87 (Springer, 2008).
31. Evers, S. W. *et al.* Neurovascular anatomy of the protostegid turtle *Rhinochelys pulchriceps* and comparisons of membranous and endosseous labyrinth shape in an extant turtle. *Zool. J. Linn. Soc.* **187**, 800–828. https://doi.org/10.1093/zoolinnean/zlz063 (2019).
32. Ősi, A., Pereda Suberbiola, X. & Földes, T. Partial skull and endocranial cast of the ankylosaurian dinosaur *Hungarosaurus* from the Late Cretaceous of Hungary: Implications for locomotion. *Palaeontol. Electro.* **17**(1), 18p (2014).
33. Sampson, S. D. & Witmer, L. M. Craniofacial anatomy of *Majungasaurus crenatissimus* (Theropoda: Abelisauridae) from the Late Cretaceous of Madagascar. *J. Vertebr. Paleontol.* **27**, 32–104. https://doi.org/10.1671/0272-4634(2007)27[32:CAOMCT]2.0.CO;2 (2007).
34. Walsh, S. A., Barrett, P. M., Milner, A. C., Manley, G. & Witmer, L. M. Inner ear anatomy is a proxy for deducing auditory capability and behaviour in reptiles and birds. *Proc. R. Soc. B* **276**, 1355–1360 (2009).
35. Porter, W. R. & Witmer, L. M. Vascular patterns in the heads of dinosaurs: Evidence for blood vessels, sites of thermal exchange, and their role in physiological thermoregulatory strategies. *Anat. Rec.* **303**, 1075–1103. https://doi.org/10.1002/ar.24234 (2019).
36. Benson, R. B. J., Starmer-Jones, E., Close, R. A. & Walsh, S. A. Comparative analysis of vestibular ecomorphology in birds. *J. Anat.* **231**, 990–1018. https://doi.org/10.1111/joa.12726 (2017).
37. Bronzati, M. *et al.* Deep evolutionary diversification of semicircular canals in archosaurs. *Curr. Biol.* **31**(12), 2520-2529.e6. https://doi.org/10.1016/j.cub.2021.03.086 (2021).
38. Hanson, M., Hoffman, E. A., Norell, M. A. & Bhullar, B. S. The early origin of a birdlike inner ear and the evolution of dinosaurian movement and vocalization. *Science* **372**(6542), 601–609. https://doi.org/10.1126/science.abb4305 (2021).
39. Miyashita, T., Arbour, V. M., Witmer, L. M. & Currie, P. J. The internal cranial morphology of an armoured dinosaur *Euoplocephalus* corroborated by X-ray computed tomographic reconstruction. *J. Anat.* **219**, 661–675. https://doi.org/10.1111/j.1469-7580.2011.01427.x (2011).
40. Paulina-Carabajal, A., Lee, Y. N. & Jacobs, L. L. Endocranial morphology of the primitive nodosaurid dinosaur *Pawpawsaurus campbelli* from the Early Cretaceous of North America. *PLoS ONE* **11**, e0150845. https://doi.org/10.1371/journal.pone.0150845 (2016).
41. Spoor, F. & Thewissen, J. G. M. Comparative and functional anatomy of balance in aquatic mammals. In *Sensory Evolution on the Threshold, Adaptations in Secondarily Aquatic Vertebrates* (eds Thewissen, J. G. M. & Nummela, S.) 65–81 (University of California Press, 2008).
42. Sobral, G. & Müller, J. Archosaurs and their kin: The ruling reptiles. In *Evolution of the Vertebrate Ear* (eds Clack, J. A. *et al.*) 285–326 (Springer, 2016).
43. Arbour, V. M. Estimating impact forces of tail club strikes by ankylosaurid dinosaurs. *PLoS ONE* **4**(8), e6738. https://doi.org/10.1371/journal.pone.0006738 (2009).
44. Park, J. Y. *et al.* A new ankylosaurid skeleton from the Upper Cretaceous Baruungoyot Formation of Mongolia: Its implications for ankylosaurid postcranial evolution. *Sci. Rep.* **11**, 4101. https://doi.org/10.1038/s41598-021-83568-4 (2021).
45. Witmer, L. M., Chatterjee, S., Franzosa, J. & Rowe, T. Neuroanatomy of flying reptiles and implications for flight, posture and behaviour. *Nature* **425**, 950–953. https://doi.org/10.1038/nature02048 (2003).
46. Walsh, S. A. *et al.* Avian cerebellar floccular fossa size is not a proxy for flying ability in birds. *PLoS ONE* **8**(6), e67176. https://doi.org/10.1371/journal.pone.0067176 (2013).
47. Ferreira-Cardoso, S. *et al.* Floccular fossa size is not a reliable proxy of ecology and behaviour in vertebrates. *Sci. Rep.* **7**(1), 2017. https://doi.org/10.1038/s41598-017-01981-0 (2005).

48. Ezcurra, M. D. *et al.* Enigmatic dinosaur precursors bridge the gap to the origin of Pterosauria. *Nature* **588**(7838), 445–449. https://doi.org/10.1038/s41586-020-3011-4 (2020) (**Epub 2020 Dec 9**).
49. Carpenter, K., Sanders, F., McWhinney, L. A. & Wood, L. Evidence for predator–prey relationships: examples for *Allosaurus* and *Stegosaurus*. In *The Carnivorous Dinosaurs* (ed. Carpenter, K.) 325–350 (Indiana University Press, 2005).
50. Mallison, H. CAD assessment of the posture and range of motion of *Kentrosaurus aethiopicus* HENNIG 1915. *Swiss. J. Geosci.* **103**, 211–233. https://doi.org/10.1007/s00015-010-0024-2 (2010).
51. Arbour, V. M., Lech-Hernes, N. L., Guldberg, T. E., Hurum, J. H. & Currie, P. J. An ankylosaurid dinosaur from Mongolia with in situ armour and keratinous scale impressions. *Acta Palaeontol. Pol.* **58**(1), 55–64. https://doi.org/10.4202/app.2011.0081 (2013).
52. Scheyer, T. M. & Sander, P. M. Histology of ankylosaur osteoderms: Implications for systematics and function. *J. Vertebr. Paleontol.* **24**, 874–893 (2004).
53. Carpenter, K. Ankylosauria. In *The Complete Dinosaur* 2nd edn (eds Brett-Surman, M. K. *et al.*) 505–526 (Indiana University Press, 2012).
54. Jerison, H. J. *Evolution of the brain and intelligence* 482 (Academic Press, 1973).
55. Marugan-Lobon, J., Chiappe, L. M. & Farke, A. A. The variability of inner ear orientation in saurischian dinosaurs: Testing the use of semicircular canals as a reference system for comparative anatomy. *PeerJ* **1**, e124 (2013).
56. Benoit, J. *et al.* A test of the lateral semicircular canal correlation to head posture, diet and other biological traits in "ungulate" mammals. *Sci. Rep.* **10**, 19602. https://doi.org/10.1038/s41598-020-76757-0 (2020).
57. Coombs, W. P. Jr. Forelimb muscles of the Ankylosauria (Reptilia, Ornithischia). *J. Paleontol.* **52**, 642–657 (1978).
58. Maidment, S. C. R. & Barrett, P. M. Osteological correlates for quadrupedality in ornithischian dinosaurs. *Acta Palaeontol. Pol.* **59**(1), 53–70 (2014).

Acknowledgements

We thank Marie Hörnig, Jakob Krieger, Steffen Harzsch and Ingelore Hinz-Schallreuter (all University of Greifswald, Germany), together with Benjamin Englich (Dinosaurierpark Münchehagen, Germany) and Fabrizio De Rossi (University of Vienna, Austria) for their support. We very much appreciate the dedicated and focused advisory opinions of Susannah Maidment and an anonymous reviewer, which improved an earlier version of the manuscript, as well as Tom Langen for editorial processing of this article. M.S. is supported by the Bogislaw scholarship, University of Greifswald. Open access funding provided by the University of Vienna.

Author contributions

M.S., S.S., J.K. and C.P. designed the project. S.S. conducted the CT scans and M.S. segmented the data. M.S. and S.S. prepared the figures. M.S., S.S., J.K. and C.P. interpreted the data and wrote the manuscript. C.K. produced the photogrammetric models.

Competing interests

The authors declare no competing interests.

Additional information

Correspondence and requests for materials should be addressed to M.S. or C.P.

III

Schade, M. & Ansorge, J. New thyreophoran dinosaur material from the Early Jurassic of northeastern Germany. *PalZ* 96. https://doi.org/10.1007/s12542-022-00605-x (2022).

PalZ
https://doi.org/10.1007/s12542-022-00605-x

RESEARCH PAPER

New thyreophoran dinosaur material from the Early Jurassic of northeastern Germany

Marco Schade[1,2,3] · **Jörg Ansorge**[1]

Received: 10 November 2021 / Accepted: 30 December 2021

Abstract
Thyreophora is a clade of globally distributed herbivorous ornithischian dinosaurs. The earliest forms are known from the Early Jurassic, and their latest surviving representatives witnessed the end-Cretaceous mass extinction. Throughout their evolutionary history, these 'shield bearers' became lumbering quadrupeds, evolved a wide array of bony armor, plates and spikes, as well as sweeping tail weapons in the form of tail clubs and thagomizers. An isolated new thyreophoran osteoderm from a Lower Jurassic Konservatlagerstätte near Grimmen is described and, with the aid of micro-CT data, compared to an osteoderm of the early diverging thyreophoran *Emausaurus ernsti* from a different stratigraphic horizon at the same locality.

Keywords Dinosauria · Thyreophora · Toarcian · Early Jurassic · Germany

Introduction

Only a few dinosaur remains are known from the Lower Jurassic of Europe, including the Sinemurian *Scelidosaurus harrisonii* Owen 1859 from Dorset, England and *Lusitanosaurus liasicus* Lapparent and Zbyszewski 1957 of similar age from Portugal. Lower Toarcian fossils comprise *Ohmdenosaurus liasicus* Wild 1978 from Ohmden near Holzmaden, South Germany, the fragment of a putative megalosaurian vertebra in an Ahrensburg drift boulder (von Huene 1966) and the remains of *Emausaurus ernsti* Haubold 1990 from Grimmen in northeastern Germany, and some potential gravisaurian sauropod bone fragments from the latter locality (Stumpf et al. 2015). Here, we report an isolated thyreophoran osteoderm from Grimmen and compare it with osteoderms of *Scelidosaurus* and *Emausaurus*.

The clay pit near Grimmen (northeastern Germany) is well known for its rich assemblage of lower Toarcian marine and terrestrial fossils (e.g., Ernst 1967, 1991; Haubold 1990; Ansorge 1996, 2003, 2007; Stumpf et al. 2015; Stumpf 2016; Konwert and Stumpf 2017). The abandoned clay pit displays Upper Liassic sediments (Fig. 1), although badly accessible nowadays. The lower Toarcian "Green Series" clay was mined for the production of light expanded clay aggregate (LECA) until 1995. The clay deposit was dislocated and elevated by Pleistocene glacial advances from nearby source rocks on the top of the Grimmen anticline. In the result, the Jurassic clay is intercalated as a giant drift within Pleistocene tillites (Ernst 1991; J.A., pers. obs.). The clay itself is highly deformed, folded and fractured in a way that detailed lithological observations are difficult. The oldest sediments exposed are upper Pliensbachian sands. Following a hiatus, resulting from a sea-level low stand, the lower Toarcian (*tenuicostatum* zone) is built of about 1 m coarse- to fine-grained sand of shallow-marine origin. Within the sand, a thin clay layer contains carbonate concretions with ammonites, indicating that this is part of the *semicelatum* subzone. On the sand follows a heterolithic sediment of about 0.60 m thickness, regarded as Posidonia shale equivalent by Ernst (1967). At the top of this unit, carbonate concretions occur from which the holotype of *Emausaurus* was prepared (Ernst

Handling Editor: Hans-Dieter Sues.

✉ Marco Schade
marco.schade@stud.uni-greifswald.de

Jörg Ansorge
ansorge@uni-greifswald.de

[1] Institute of Geography and Geology, Palaeontology and Historical Geology, University of Greifswald, 17489 Greifswald, Germany

[2] Zoological Institute and Museum, Cytology and Evolutionary Biology, University of Greifswald, 17489 Greifswald, Germany

[3] Department of Earth and Environmental Sciences, Palaeontology and Geobiology, Ludwig-Maximilians-Univer sität, 80333 München, Germany

Published online: 19 January 2022

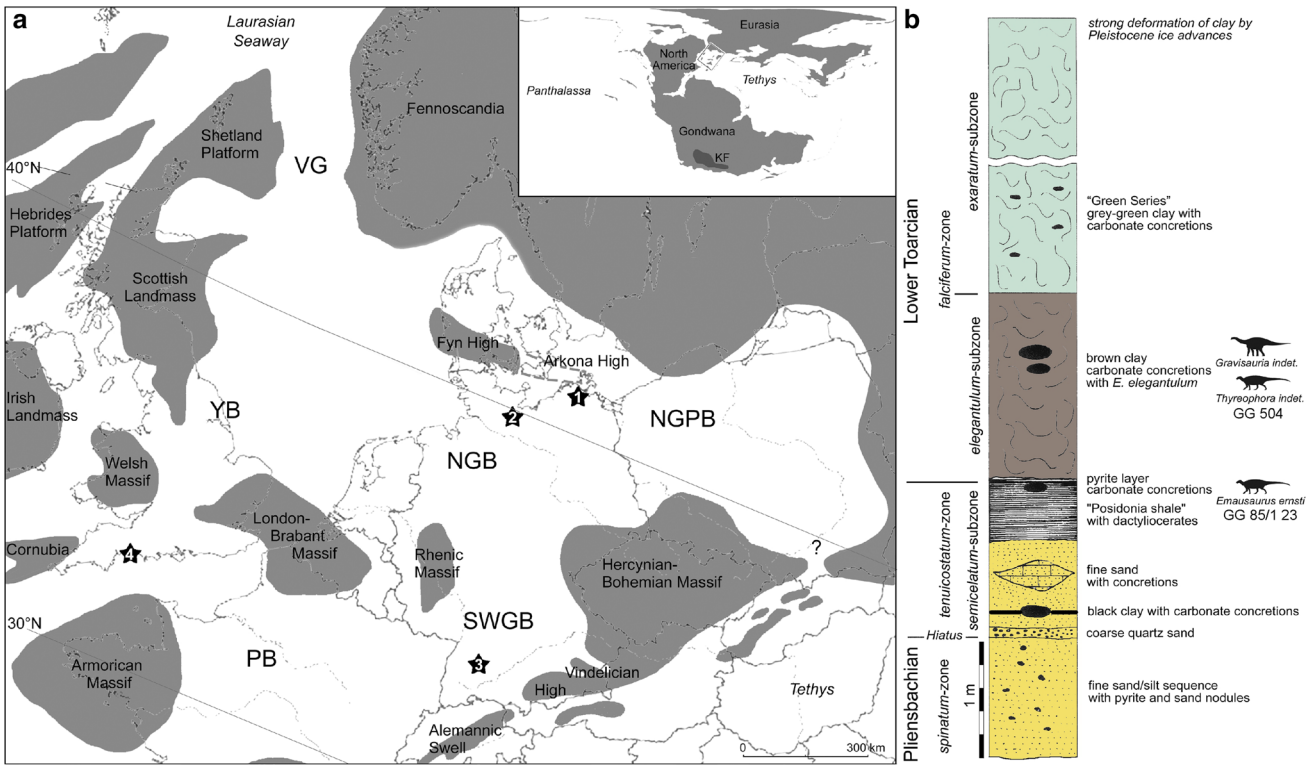

Fig. 1 **a** Lower Jurassic palaeogeography of central Europe with dinosaur find spots. 1. Grimmen, 2. Ahrensburg, 3. Ohmden, 4. Lyme Regis. *NGPB* Northeast German Polish Basin, *NGB* North German Basin, *SWGB* South West German Basin, *PB* Paris Basin, *YB* Yorkshire Basin, *VG* Viking Graben; **b** schematic profile of the Grimmen section, modified after Ansorge 2007, with occurrences of dinosaur remains

1967, 1991; Haubold 1990). The Posidonia shale equivalent is overlain by a brown clay containing laminated carbonate concretions with the ammonite *Eleganticeras elegantulum* (*elegantulum* subzone of *falciferum* zone), drift wood, as well as the potential gravisaurian remains published by Stumpf et al. (2015), and the osteoderm described herein. A comparison of the mineralogical attributes of the bones indicate that the gravisaurian remains probably do not originate from the horizon with insect-bearing carbonate concretions of the "Green Series" clay of *exaratum* subzone, contradicting Stumpf et al. (2015). In addition to the terrestrial tetrapods, the presence of abundant insects (Ansorge 1996, 2003) and a single spider (Selden & Dunlop 2014) indicates a rather short distance to the mainland or certain islands. A possible source might be the Arkona high (an island in the extension of the Ringköping-Fyn high to the southeast; Seidel 2019), rather than the more distal Scandinavian mainland.

Institutional abbreviations

BRSMG, Bristol City Museum and Gallery, Bristol, UK; GG, Greifswalder Geologische Sammlungen, University of Greifswald, Greifswald, Germany; MNA, Museum of Northern Arizona, Flagstaff, USA; YPM, Peabody Museum of Natural History, Yale University, New Haven, USA.

Materials and methods

J.A. found the broken pieces of the new thyreophoran osteoderm GG 504 in 2017 and subsequently prepared them. Fracture surfaces of the bone pieces were moistened with alcohol to enhance visibility of details for macro-photography. To reveal its inner structure, we scanned the osteoderm GG 85/1 23, belonging to the holotype of *Emausaurus ernsti*, using the micro-computed tomography device MicroXCT-200 housed in the Department of Cytology and Evolutionary Biology, University of Greifswald. Parameters—voltage: 60 kV, X-ray tube current: 133 µA, exposure time: 5 s, voxel size: 0,0,465,132 mm. The figures showing CT data were produced utilizing the software Amira (6.1),

Fig. 2 GG 504, osteoderm of an unknown thyreophoran dinosaur. **a** top view of the slightly convex side; **b** view on the acute edge, showing the inclination of the osteoderm and its base towards the less convex side; **c** cross section of the proximodistal mid-length; **d** intertrabecular spaces filled with aragonite; **e** magnified part of a cross section. *ae* acute edge, *al* aragonitic layers, *be* blunt edge, *co* cortex

based on tiff files (16 bit). GG 504 and GG 85/1 23 are housed in the paleontological collection of the Institut für Geographie und Geologie in Greifswald, Germany.

Description

gen. et sp. indet. (GG 504) Figs. 2, 3, 4.

The partial osteoderm GG 504 consists of five matching fragments. Assembled, the specimen measures some 15.5 cm proximodistally (Figs. 2a, 3a); judging from the

Fig. 3 GG 504, osteoderm of an unknown thyreophoran dinosaur. **a** top view of the pronounced convex side; **b** base in proximal view; **c** close-up of striated cortex shown in **a**; **d** magnified cortex; **e** close-up of section close to the base shown in **a**. *co* cortex, *ob* offset base, *sd* slight depression

slightly converging edges, maybe around one fourth of the original length is missing. Whereas both sides show a proximodistally oriented striation (appearing wrinkled under the microscope; Fig. 3a, c, d), the slightly convex side possesses a more roughened and irregular surface proximally. The rugose base seems to have been slightly offset from the rest of the osteoderm. The base of the osteoderm is proximally slightly convex in top

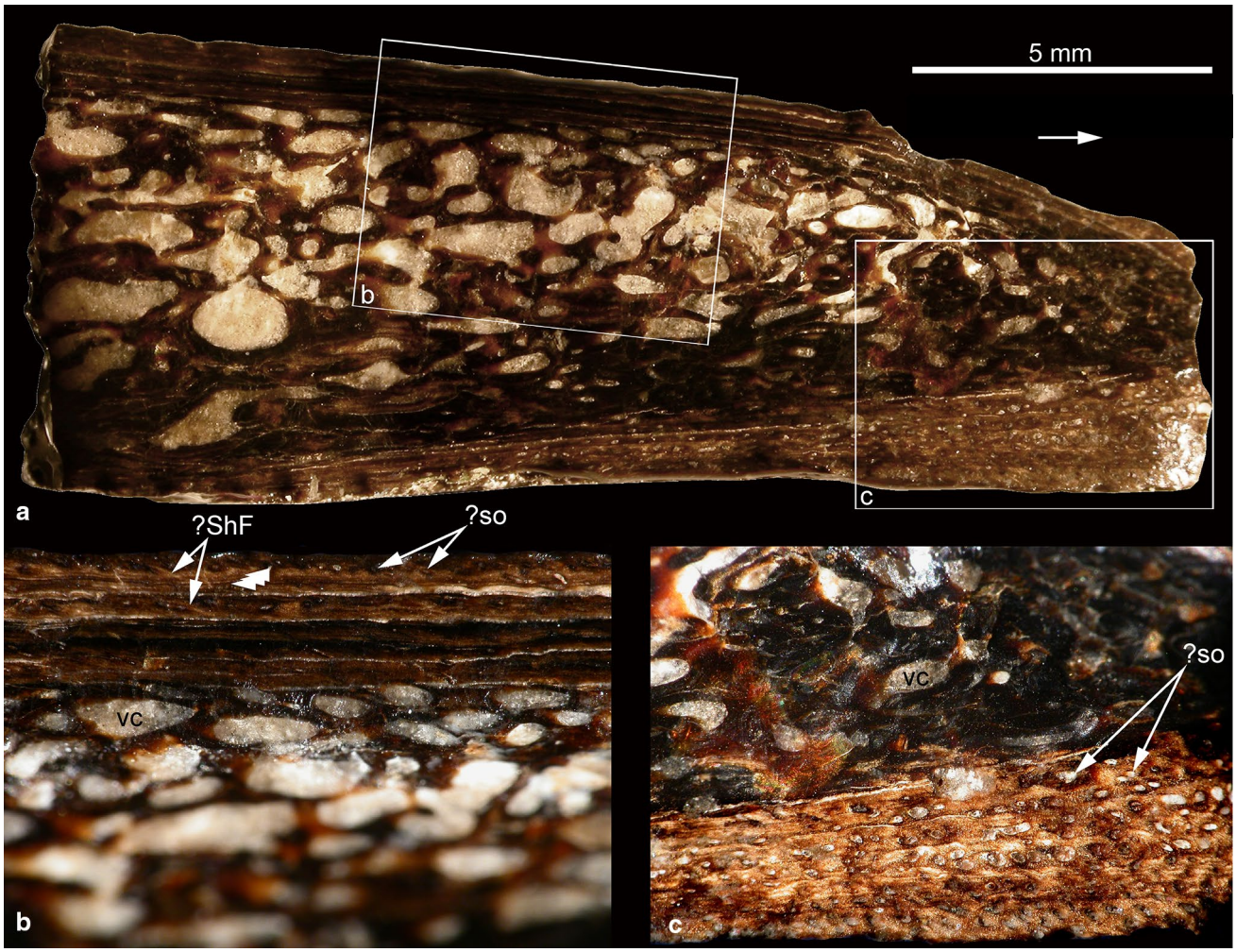

Fig. 4 GG 504, osteoderm of an unknown thyreophoran dinosaur. **a** magnified section of the distal-most fragment, arrow points towards former apex; **b** close-up of cortex from the pronounced convex side shown in **a**, arrows without lines hint towards potential LAGs; **c** close-up of cortex from the slightly convex side shown in **a**. *?ShF* potential Sharpey's fibers, *?so* potential secondary osteons, *vc* vascular cavities

view. In proximal view, the base has shallow depressions that extend from one side to the other, and very small, irregularly placed vascular foramina seem to be visible (Fig. 3b). In the top view, the osteoderm is widest proximally between both edges and becomes narrower distally. Its proximal thickness measures some 2 cm. The thickness gradually decreases distally and towards both edges, while the maximum thickness is not situated at the mid-width, producing an asymmetrical cross section (Fig. 2c). Furthermore, one side appears only slightly convex, whereas the other side is more pronounced convex. The whole osteoderm is slightly inclined or bent towards the less convex side; this is also perceivable on the base (Fig. 2b). The edges seem to have been sub-parallel proximally and gradually converged distally; however, the distal-most part of the osteoderm might have been rather blunt. In cross section, one edge is more acute than the other (Fig. 2c). There is a thin and laminated cortex surrounding potential Haversian bone, which is transitioning to larger vascular cavities towards the core (Figs. 2c, e; 4); the latter two structures are made up by a network of trabeculae. Whereas the cortex of the slightly convex side tends to be thicker and more porous—in cross section—than of the pronounced convex side (although the surfaces of both seem to be intact), potential secondary osteons, lines of arrested growth (LAG) and low-angled Sharpey's fibers seem to be present on both sides (Figs. 2c; 4). Best seen in the laminated cortex of the clearly convex side, layers of the actual cortex are occasionally separated from each other by thin layers of aragonite (Figs. 2c, e; 4a, b). In some places, LAGs seem perceivable, but not to a degree that allows secure and continuous counting (Fig. 4b). The spaces created by the trabeculae (vascular cavities and/or erosion cavities; Scheyer and Sander 2004; Scheyer et al.

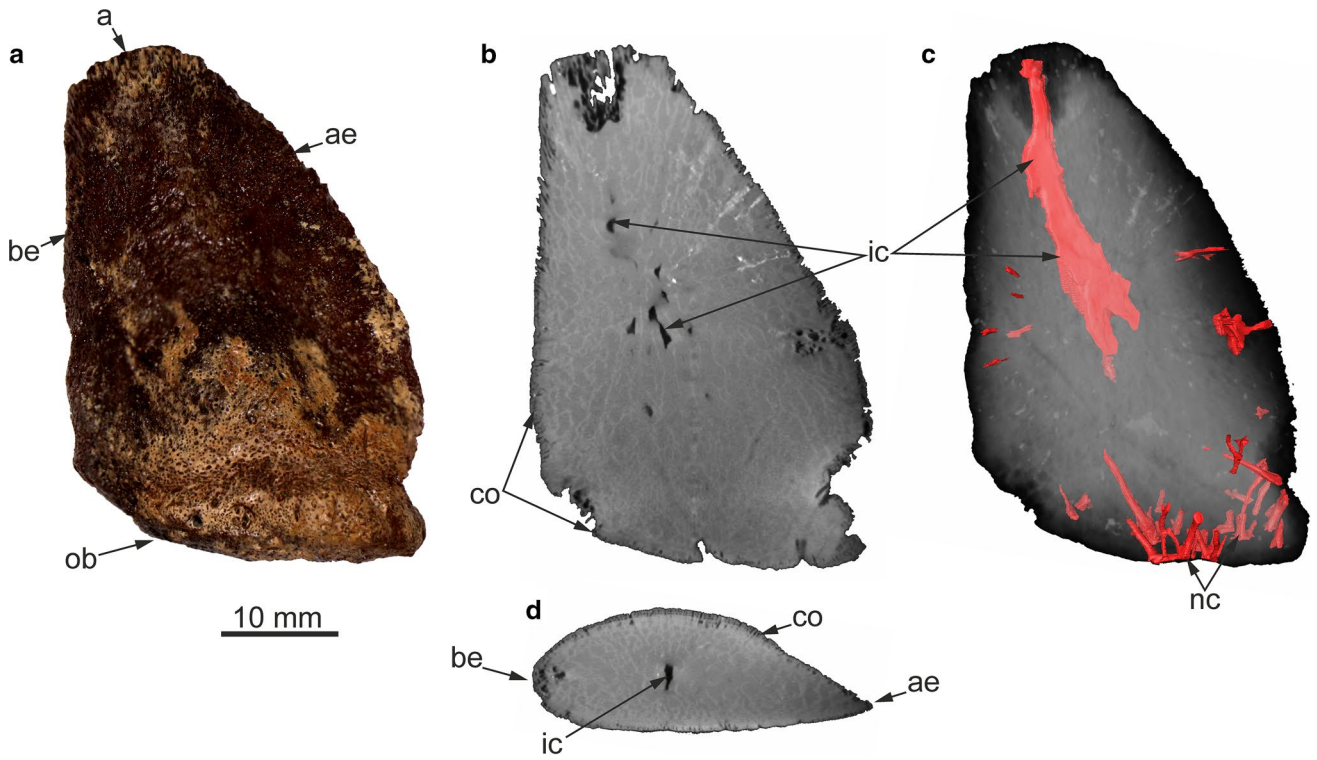

Fig. 5 **a** GG 85/1 23, osteoderm of the *Emausaurus ernsti* holotype; **b** sagittal(?) micro-CT slice close to the mid-width; **c** volume rendering with segmented vascular structures; **d** transverse(?) micro-CT slice close to the proximodistal mid-length. The convex side faces towards the observer in **a**–**c**. *a* apex, *ae* acute edge, *be* blunt edge, *co* cortex, *ic* internal cavity with potential apical canal, *nc* nutritive canals, *ob* offset base

2013) are filled with aragonitic crystals (Fig. 2d); they are largest close to the core of the osteoderm and become smaller distally in all directions. Furthermore, the cortex occupies more of the cross-sectional surface in relation to the cancellous bone toward the former apex of the osteoderm. Fractions close to the offset base suggest that GG 504 bears a thin basal cortex (Fig. 3e).

Emausaurus ernsti Haubold, 1990 (GG 85/1 23), Fig. 5.

The largest (around 4.5 cm proximodistally) and almost completely preserved osteoderm of *Emausaurus*, GG 85/1 23, resembles GG 504 in many aspects. However, the rugose base of GG 85/1 23 shows more and larger vascular foramina, is more clearly offset from the rest of the osteoderm, and the sides, still showing very slight striations in some places in Haubold (1990) and photographs prior to the latest preparation of 2013, appear rather porous nowadays. Furthermore, although the edges of GG 504 slightly converge, one edge of GG 85/1 23 is more or less straight and blunt, whereas the other edge is convex in outline, more acute, and gives the osteoderm a somewhat inclined appearance (Fig. 5a). The CT data of GG 85/1 23 suggest a thin cortex, also at the base (Fig. 5b, d). Additionally, canals from the abundant foramina at the base of GG 85/1 23 could be traced to one fourth of the proximodistal length of the osteoderm (Fig. 5c). Furthermore, there are vascular canals on both sides and both edges as well. One large cavity with a respective canal seems to have reached between the proximodistal mid-length of the osteoderm and the eroded apex. However, whereas the distal-most extent of this canal might represent a preservational artifact, the trabecular network is clearly more wide spaced in the core of the osteoderm and shows increasingly smaller inter-trabecular spaces distally in all directions.

Discussion

Although GG 85/1 23 is almost completely preserved and certainly represents an osteoderm, the isolated and incomplete nature of GG 504 may open up the possibility that it is not an osteoderm. Some long bones, like those of dinosaurs, can be very wide on the epiphyses and very narrow on the diaphysis. Furthermore, the proximal aspect of GG 504 shows shallow depressions, which resemble the epiphysis of some long bones; however, osteoderm bases seem to be variable in thyreophorans, being longitudinally concave as in some osteoderms of *Scutellosaurus lawleri*

(MNA.V.175; Breeden et al. 2021), funnel-like concave as in some osteoderms of *Emausaurus* (Haubold 1990), or convex as is the case in GG 85/1 23. Additionally, GG 504 has prominently striated sides and—for a long bone—sharp edges, as well as an exceptionally thin (between the sides) and wide (between the edges) cross section in relation to the base. Also, the thin and somewhat elongate nature of GG 504 may resemble a broken neural spine or transverse process. In both cases, the putative base of GG 504 would then represent the somewhat thickened and roughened distal end of such a neural arch projection. Across the vertebral column in many taxa, transverse processes and neural spines can change their appearance considerably, e.g. in respect to their general morphology, orientation, thickness, lamination (e.g., Wilson 1999; Evers et al. 2015); and obviously, there is a lot of interspecific variation as well. The asymmetrical morphology (differently convex sides, inclination to one side, differently developed cortex) of GG 504 seems to exclude a sagittal position as neural spine. Furthermore, GG 504 would be much wider anteroposteriorly distally than it would be proximally, which is rather not typical for neural spines. Also, neural spines often show irregular textures on their anterior and posterior edges; such features are absent in GG 504. Considering transverse processes, often they show sub-parallel anterior and posterior edges, are dorsoventrally thickened because of the centrodiapophyseal laminae (sensu lato) and the diapophysis is rather sub-circular (and not elongated oval like the putative base of GG 504). The—from one side to the other—thin shape, as well as the slightly converging and relatively sharp edges, and again, the width relation between the putative base and distal portion of GG 504 make it unlikely to represent a transverse process. However, since long bones, neural spines and transverse processes (as well as the rest of their skeleton) are very diverse across Mesozoic terrestrial and marine reptiles (e.g., Sues 2019), these options cannot be excluded with absolute certainty.

Still, the specimens GG 504 and GG 85/1 23 most probably represent a comparably elongated and flat type of osteoderm. In addition to thyreophorans, other archosauriforms can bear dermal armor as well, but are unlikely to represent the owner of GG 504 and GG 85/1 23, based on morphological and/or geological age (e.g., Scheyer and Sander 2004; Curry Rogers et al. 2011; Desojo et al. 2013).

Following most phylogenetic analyses (e.g., Thompson et al. 2012; Raven & Maidment 2017), *Scutellosaurus* (Early Jurassic, USA), *Emausaurus* and *Scelidosaurus* (Early Jurassic, UK) represent early diverging thyreophorans, and are sister taxa to Eurypoda (which comprise Ankylosauria and Stegosauria; but see Norman 2020c). Although there is no consensus of what exactly is smooth or rugose, it seems that, within Ankylosauria, ankylosaurids (partly club-tailed) and nodosaurids (spike-shouldered) possess rather rugose surfaces on their osteoderms (e.g., Scheyer and Sander 2004; Hayashi et al. 2010), whereas early diverging thyreophoran osteoderms can show rugose and smooth surfaces (Norman, 2020b). Scheyer and Sander (2004: fig. 12) reported a relatively thin cortex in *Scelidosaurus*. Furthermore, they mention that osteoderms of *Scutellosaurus* are similar to what is known about the external and internal characteristics of *Scelidosaurus* osteoderms. Early diverging thyreophoran and ankylosaurid osteoderms share a basal cortex, which is absent in nodosaurids (Scheyer and Sander 2004; Main et al. 2005; Hayashi et al. 2010).

The pattern of numerous independent vascular canals in GG 85/1 23 differs from the condition found in a dorsal plate of *Stegosaurus* (specimen YPM 57,716) in that no 'main channel' is present from which other vascular canals branch off (Farlow et al. 2010). However, both osteoderms resemble each other in the restriction of the largest vascular canals to a relatively proximal part of the osteoderm (Farlow et al. 2010). Furthermore, osteoderms situated in the neck region of early diverging thyreophorans, stegosaurs, and ankylosaurs can be somewhat similar in appearance (e.g., Chengkai et al. 2007; Maidment et al. 2015; Brown 2017; Norman 2020b). Hence, because of the geological setting (no ankylosaur or stegosaur is known from Lower Jurassic deposits) they were found in, their overall morphology and their detailed characteristics (smooth surface with striations, thin cortex, basal cortex), early diverging thyreophoran affinities for GG 504 and GG 85/1 23 are assumed and, respectively, supported herein.

Concerning the former anatomical position and orientation of GG 504 and GG 85/1 23, it is worth noting that neither was found in articulation and that GG 504 is incompletely preserved. Norman (2020b) pointed out that the osteoderms of the early diverging thyreophoran *Scelidosaurus* vary considerably with respect to their position on the body and ontogeny. The usual overall arrangement of ankylosaur osteoderms constitutes a streamlined pattern with most osteoderms being posteriorly inclined (contrasted by protruding spike-like osteoderms on the neck and shoulders of the nodosaurid *Edmontonia longiceps* (e.g., Brown et al. 2017). Furthermore, osteoderms similar to the elongated and flat type as GG 504 and GG 85/1 23 are, at least in some taxa, flat to slightly convex dorsally and clearly convex ventrally, which can be observed on the fully articulated neck and shoulder region of the nodosaurid *Borealopelta markmitchelli* (Brown 2017). Hence, there may be two details helpful to orient an isolated osteoderm: inclination (anterior/posterior), and the convexity or concavity of both sides (dorsal/ventral). The acuteness of both edges seems to be no reliable proxy for an anterior or posterior direction (M.S., pers. obs. on osteoderms of *Emausaurus*). In comparison to the specimen BRSMG LEGL 0004 of *Scelidosaurus*, GG 504 might match the morphology of a large osteoderm on the lateral neck base with slightly converging edges (Norman

2020b: figs. 8, 22). Hence, GG 504 is herein interpreted as representing a lateral osteoderm of the neck or shoulder region of an early diverging thyreophoran. If this assignment is correct, GG 504 possibly belongs to an individual much larger than the juvenile *Scelidosaurus* specimen BRSMG LEGL 0004 and *Emausaurus*.

Haubold (1990) interpreted GG 85/1 23 as a right parasagittal osteoderm. However, it seems that osteoderms can be more variable morphologically, the more anterior they are situated (Brown 2017). Whereas ankylosaurids tend to possess bulkier and less protruding osteoderms (e.g., Arbour and Currie 2013), a comparable shape to GG 85/1 23 is found in osteoderms of the neck and shoulder region of nodosaurids (e.g., Brown 2017) and—more importantly—the head, neck and shoulder region of *Scelidosaurus* (Norman 2020a, b). In fact, the occipital osteoderms of the latter (BRSMG LEGL 0004) are strikingly similar in outline, and the 'waisted zone' between the porous base and the distal osteoderm (Norman 2020a: fig. 16; b: figs. 18, 19). However, the lateral edges of the occipital osteoderms are slightly laterally curved in *Scelidosaurus*, whereas the respective edge of GG 85/1 23 is straight. Additionally, it is not clear if the dorsal and ventral sides of the occipital osteoderms in *Scelidosaurus* are concave, straight or convex, and if the medial and lateral edges are similarly developed as in GG 85/1 23 in respect to their acuteness. The fossae where the occipital osteoderms attach to the posterodorsal aspects of the supraoccipital, opisthotic, parietal and squamosal in *Scelidosaurus* make up 65% of the mediolateral skull width (Norman 2020a). Based on the reconstruction of Haubold (1990), this width would be 70% in *Emausaurus*. Hence, the likely socio-sexual component of keratinous sheaths on thyreophoran osteoderms (which are similar to cranial horns of extant bovids because of their external structure in bearing a relatively smooth surface with slight grooves or striations, and small foramina, which hint towards having been nutritive for the potentially keratinous caps, e.g., Main et al. 2005; Farlow et al. 2010; Brown et al. 2017; Brown 2017; Norman 2020a, b) may render the holotype of *Emausaurus* a sub-adult and not a juvenile.

Acknowledgements We thank Marie Hörnig, Steffen Harzsch, Ingelore Hinz-Schallreuter and Stefan Meng (all University of Greifswald, Germany) for their help and support. M.S. was supported with the Bogislaw scholarship, funded by the University of Greifswald. We also thank Hans-Dieter Sues and Benjamin Breeden for very helpful comments, which improved an earlier version of this manuscript, as well as Mike Reich for editorial handling of this article.

Author contributions MS designed the project and segmented the CT data. JA unearthed GG 504 and prepared the specimen. MS and JA prepared the figures, interpreted the data and wrote the manuscript.

Funding Open Access funding enabled and organized by Projekt DEAL.

Declarations

Conflict of interests The authors declare no competing interests.

References

Ansorge, J. 1996. Insekten aus dem oberen Lias von Grimmen (Vorpommern, Norddeutschland). *Neue Paläontologische Abhandlungen* 2: 1–132.

Ansorge, J. 2003. Insects from the Lower Toarcian of Middle Europe and England. Proceedings of the Second Palaeoentomological Congress, Kraków 2001. *Acta Zoologica Cracoviensia* 46 (Suppl. Fossil Insects): 291 – 310.

Ansorge, J. 2007. Lower Jurassic clay pit of Klein Lehmhagen near Grimmen. In Geo-Pomerania Excursion guide, eds. R.-O. Niedermeyer, R. Dobracki, and K. Schütze. *Biuletyn Państwowego Instytutu Geologicznego* 424: 37–41.

Arbour, V.M., and P.J. Currie. 2013. *Euoplocephalus tutus* and the diversity of ankylosaurid dinosaurs in the Late Cretaceous of Alberta, Canada, and Montana, USA. *PLoS ONE* 8 (5): e62421. https://doi.org/10.1371/journal.pone.0062421.

Breeden, B.T., III., T.J. Raven, R.J. Butler, T.B. Rowe, and S.C.R. Maidment. 2021. The anatomy and palaeobiology of the early armoured dinosaur *Scutellosaurus lawleri* (Ornithischia: Thyreophora) from the Kayenta Formation (Lower Jurassic) of Arizona. *Royal Society Open Science* 8: 201676. https://doi.org/10.1098/rsos.201676.

Brown, C.M., D.M. Henderson, J. Vinther, I. Fletcher, A. Sistiaga, J. Herrera, and R.E. Summons. 2017. An exceptionally preserved three-dimensional armored dinosaur reveals insights into coloration and Cretaceous predator-prey dynamics. *Current Biology*. https://doi.org/10.1016/j.cub.2017.06.071.

Brown, C.M. 2017. An exceptionally preserved armored dinosaur reveals the morphology and allometry of osteoderms and their horny epidermal coverings. *PeerJ* 5 e4066. https://doi.org/10.7717/peerj.4066.

Chengkai, J., C.A. Foster, X. Xing, and J.M. Clark. 2007. The first stegosaur (Dinosauria, Ornithischia) from the Upper Jurassic Shishugou formation of Xinjiang, China. *Acta Geologica Sinica (english Edition)* 81: 351–356.

de Lapparent, A.F., and G. Zbyszewski. 1957. Les dinosauriens du Portugal Mémoires Des Services Géologiques Du Portugal. *Nouvelle Série* 2: 1–63.

Desojo, J.B., A.B. Heckert, J.W. Martz, W.G. Parker, R.R. Schoch, B.J. Small, and T. Sulej. 2013. Aetosauria: a clade of armoured pseudosuchians from the Late Triassic continental beds. In *Anatomy, phylogeny and palaeobiology of early archosaurs and their kin*, eds. S.J. Nesbitt, J.B. Desojo, and R.B. Irmis. Geological Society, London, Special Publications 389: 203–239.

Ernst, W. 1967. Die Liastongrube Grimmen. Sediment Makrofauna Und Stratigraphie. Ein Überblick. *Geologie* 16: 550–569.

Ernst, W. 1991. Der Lias im Ton-Tagebau bei Grimmen (Vorpommern). *Fundgrube* 27: 171–183.

Evers, S.W., O.W.M. Rauhut, A.C. Milner, B.McFeeters, and R. Allain. 2015. A reappraisal of the morphology and systematic position of the theropod dinosaur *Sigilmassasaurus* from the "middle" Cretaceous of Morocco. *PeerJ* 3:e1323; https://doi.org/10.7717/peerj.1323.

Farlow, J.O., S. Hayashi, and G.J. Tattersall. 2010. Internal vascularity of the dermal plates of *Stegosaurus* (Ornithischia, Thyreophora). *Swiss Journal of Geosciences* 103: 173–185. https://doi.org/10.1007/s00015-010-0021-5.

Haubold, H. 1990. Ein neuer Dinosaurier (Ornithischia, Thyreophora) aus dem unteren Jura des Nördlichen Mitteleuropa. *Revue de Paléobiologie* 9: 149–177.

Hayashi, S., K. Carpenter, T.M. Scheyer, M. Watabe, and D. Suzuki. 2010. Function and evolution of ankylosaur dermal armor. *Acta Palaeontologica Polonica* 55 (2): 213–228.

Konwert, M., and S. Stumpf. 2017. Exceptionally preserved Leptolepidae (Actinopterygii, Teleostei) from the late Early Jurassic Fossil-Lagerstätten of Grimmen and Dobbertin (Mecklenburg-Western Pomerania, Germany). *Zootaxa* 4243 (2): 249–296. https://doi.org/10.11646/zootaxa.4243.2.2.

Maidment, S.C, C. Brassey, P.M. Barrett. 2015. The postcranial skeleton of an exceptionally complete individual of the plated dinosaur *Stegosaurus stenops* (Dinosauria: Thyreophora) from the Upper Jurassic Morrison Formation of Wyoming, U.S.A. *PLoS One* 10(10):e0138352. https://doi.org/10.1371/journal.pone.0138352.

Main, R., A. De Ricqlès, J. Horner, and K. Padian. 2005. The evolution and function of thyreophoran dinosaur scutes: implications for plate function in stegosaurs. *Paleobiology* 31 (2): 291–314. https://doi.org/10.1666/0094-8373(2005)031[0291:TEAFOT]2.0.CO;2.

Norman, D.B. 2020a. *Scelidosaurus harrisonii* from the Early Jurassic of Dorset, England: the dermal skeleton. *Zoological Journal of the Linnean Society* 190 (1): 1–53. https://doi.org/10.1093/zoolinnean/zlz085.

Norman, D.B. 2020a. *Scelidosaurus harrisonii* from the Early Jurassic of Dorset, England: cranial anatomy. *Zoological Journal of the Linnean Society* 188(1): 1–81. https://doi.org/10.1093/zoolinnean/zlz074.

Norman, D.B. 2020c. *Scelidosaurus harrisonii* (Dinosauria: Ornithischia) from the Early Jurassic of Dorset, England: biology and phylogenetic relationships. *Zoological Journal of the Linnean Society* 191(1): 1–86. https://doi.org/10.1093/zoolinnean/zlaa061.

Owen, R. 1859. Palaeontology. In *Encyclopaedia Britannica, 8th edn*. Edinburgh: Adam & Charles Black, 91–176.

Raven, T.J., and S.C.R. Maidment. 2017. A new phylogeny of Stegosauria (Dinosauria: Ornithischia). *Palaeontology* 60: 401–408.

Rogers, K.C., M. D'Emic, R. Rogers, M. Vickaryous, and A. Cagan. 2011. Sauropod dinosaur osteoderms from the Late Cretaceous of Madagascar. *Nature Communications* 2 (1): 564. https://doi.org/10.1038/ncomms1578.

Scheyer, T.M., and P.M. Sander. 2004. Histology of ankylosaur osteoderms: implications for systematics and function. *Journal of Vertebrate Paleontology* 24: 874–893.

Scheyer, T.M., J.B. Desojo, and I.A. Cerda. 2013. Bone histology of phytosaur, aetosaur, and other archosauriform osteoderms (Eureptilia, Archosauromorpha). *The Anatomical Record* 297: 240–260.

Seidel, E. 2019. The Tectonic Evolution of the German offshore area, as part of the Trans-European Suture Zone (North and East of Rügen Island). PhD thesis, University of Greifswald. https://epub.ub.uni-greifswald.de/frontdoor/index/index/year/2019/docId/3033.

Selden, P.A., and J.A. Dunlop. 2014. The first fossil spider (Araneae: Palpimanoidea) from the Lower Jurassic (Grimmen, Germany). *Zootaxa* 3894 (1): 161–168. https://doi.org/10.11646/zootaxa.3894.1.13.

Stumpf, S. 2016. New information on the marine reptile fauna from the lower Toarcian (Early Jurassic) "Green Series" of North-Eastern Germany. *Neues Jahrbuch Für Geologie Und Paläontologie, Abhandlungen* 280 (1): 87–105.

Stumpf, S., J. Ansorge, and W. Krempien. 2015. Gravisaurian sauropod remains from the marine late Early Jurassic (Lower Toarcian) of North-Eastern Germany. *Geobios* 48 (3): 271–279. https://doi.org/10.1016/j.geobios.2015.04.001.

Sues, H.D. 2019. *The rise of reptiles: 320 million years of evolution*. Baltimore: Johns Hopkins University Press.

Thompson, R.S., J.C. Parish, S.C.R. Maidment, and P.M. Barrett. 2012. Phylogeny of the ankylosaurian dinosaurs (Ornithischia: Thyreophora). *Journal of Systematic Palaeontology* 10 (2): 301–312.

von Huene, F. 1966. Ein Megalosauriden-Wirbel des Lias aus norddeutschem Geschiebe. *Neues Jahrbuch Für Geologie Und Paläontologie, Monatshefte* 1966 (1): 318–319.

Wild, R. 1978. Ein Sauropoden-Rest (Reptilia, Saurischia) aus dem Posidonienschiefer (Lias, Toarcium) von Holzmaden. *Stuttgarter Beiträge zur Naturkunde. Serie B (geologie Und Paläontologie)* 41: 1–15.

Wilson, J.A. 1999. A nomenclature for vertebral laminae in sauropods and other saurischian di- nosaurs. *Journal of Vertebrate Paleontology* 19: 639–653. https://doi.org/10.1080/02724634.1999.10011178

IV

Schade, M., Knötschke, N., Hörnig, M. K., Paetzel, C. & Stumpf, S. Neurovascular anatomy of dwarf dinosaur implies precociality in sauropods. *eLife* 11, e82190. https://doi.org/10.7554/eLife.82190 (2022b).

RESEARCH ARTICLE

Neurovascular anatomy of dwarf dinosaur implies precociality in sauropods

Marco Schade[1,2]*, Nils Knötschke[3], Marie Hörnig[2], Carina Paetzel[2], Sebastian Stumpf[4]

[1]University of Greifswald, Institute of Geography and Geology, Palaeontology and Historical, Greifswald, Germany; [2]University of Greifswald, Zoological Institute and Museum, Cytology and Evolutionary Biology, Greifswald, United States; [3]Mineralientage, Oberhaching, Germany; [4]University of Vienna, Department of Palaeontology, Vienna, Austria

Abstract Macronaria, a group of mostly colossal sauropod dinosaurs, comprised the largest terrestrial vertebrates of Earth's history. However, some of the smallest sauropods belong to this group as well. The Late Jurassic macronarian island dwarf *Europasaurus holgeri* is one of the most peculiar and best-studied sauropods worldwide. So far, the braincase material of this taxon from Germany pended greater attention. With the aid of micro-computed tomography (microCT), we report on the neuroanatomy of the nearly complete braincase of an adult individual, as well as the inner ears of one other adult and several juveniles (the latter also containing novel vascular cavities). The presence of large and morphologically adult inner ears in juvenile material suggests precociality. Our findings add to the diversity of neurovascular anatomy in sauropod braincases and buttress the perception of sauropods as fast-growing and autonomous giants with manifold facets of reproductive and social behaviour. This suggests that – apart from sheer size – little separated *Europasaurus* from its large-bodied relatives.

***For correspondence:** marco.schade@stud.uni-greifswald.de

Competing interest: See page 17

Funding: See page 17

Preprinted: 04 August 2022
Received: 26 July 2022
Accepted: 11 November 2022

Reviewing Editor: Nizar Ibrahim, University of Portsmouth, United Kingdom

Introduction

Sauropoda is a taxon of saurischian dinosaurs and comprise popular taxa like *Diplodocus*, *Giraffatitan*, and *Argentinosaurus* (***Bates et al., 2016***). Sauropods were diverse and had a worldwide distribution (e.g., ***Bates et al., 2016***; ***Pol et al., 2021b***). Sauropods likely originated in the Late Triassic (e.g., ***Rauhut et al., 2020***; ***Pol et al., 2021b***) and their geologically youngest representatives vanished during the end-Cretaceous mass extinction event (e.g., ***Curry Rogers and Forster, 2001***; ***Bates et al., 2016***). Whereas bipedal early sauropodomorphs were probably capable of swiftly tracking down prey (***Müller et al., 2021***), the later evolutionary history of the group is characterized by an unrivaled increase in body size (among land-dwelling vertebrates), accompanied with herbivory, an extreme elongation in neck length and graviportal quadrupedality (e.g., ***Sander et al., 2011***; ***Bates et al., 2016***; ***Bronzati et al., 2018***).

While fossil braincases are generally rare, studies of sauropod endocrania are nevertheless numerous (e.g., ***Janensch, 1935***; ***Carabajal, 2012***; ***Knoll et al., 2015***), serving as a good base for comparisons. Potentially, aspects of lifestyle can be inferred from morphological details of cavities that once contained the brain, inner ear, and other associated neurovascular structures within the bony braincase of fossil vertebrates (e.g., ***Neenan et al., 2017***; ***Schwab et al., 2020***; ***Schwab et al., 2021***; ***Ezcurra et al., 2020***; ***Hanson et al., 2021***; ***Choiniere et al., 2021***; however, see also ***Benson et al., 2017***; Evers et al., 2019; ***Bronzati et al., 2021***; ***David et al., 2022***). Furthermore, ontogenetically induced morphological shifts of neuroanatomy can hint towards different ecological tendencies within a species, for example, in respect to bipedal or quadrupedal locomotion (***Bullar et al., 2019***).

The middle Kimmeridgian (Late Jurassic) sauropod *Europasaurus* (represented by a single species, *E. holgeri*) is regarded as an unequivocal example of insular dwarfism (although, see ***Lokatis and Jeschke, 2018***, for a critical view on the concept of the island rule) with paedomorphic features, having reached adult body lengths of nearly 6 m and weighing about 800 kg (***Sander et al., 2006***; ***Stein et al., 2010***; ***Carballido and Sander, 2013***; ***Marpmann et al., 2014***). From this taxon, a great number of cranial and postcranial fossil bones are known (housed in the Dinosaurier-Freilichtmuseum Münchehagen/Verein zur Förderung der Niedersächsischen Paläontologie e.V., Rehburg-Loccum, Münchehagen, Germany; DFMMh/FV), of which the latter hint to at least 21 individuals of different ontogenetic stages (***Scheil et al., 2018***). The fossils come from shallow-marine carbonate rocks of the Langenberg quarry, assigned to the Süntel Formation, having formed in the Lower Saxony basin (see ***Zuo et al., 2018***).

The paratype specimen of *Europasaurus*, DFMMh/FV 581.1, comprises a largely complete, articulated and probably mature braincase, with DFMMh/FV 581.2 and 3 representing the respective detached parietals (***Figures 1–3***; ***Figure 1—figure supplements 1–4***). The outer morphology of this material has previously been described (***Marpmann et al., 2014***). For this study, the parietals were rearticulated with the preserved neurocranium and subsequently documented with micro-computed tomography (microCT). The endocranial cavities which once housed the brain, inner ears, and other soft neuroanatomical structures, such as nerves and blood supply, were then manually segmented. The articulated specimens DFMMh/FV 581.1, 2, and 3 measure about 120 mm in mediolateral width, 80 mm anteroposteriorly, and 100 mm dorsoventrally.

Additionally, the specimens DFMMh/FV 1077 (***Figure 4***; ***Figure 4—figure supplements 1 and 2***; adult fragmentary braincase, complete inner ear), DFMMh/FV 466+205 (***Figures 5 and 6***; ***Figure 5—figure supplement 1***; ***Figure 7—figure supplements 1 and 2***; ***Figure 8—figure supplements 1 and 2***; juvenile prootic and otoccipital, nearly complete inner ear; the common bond of these two specimens has not been recognized in former studies; ***Marpmann et al., 2014***), DFMMh/FV 964 and DFMMh/FV 561 (***Figure 7***; ***Figure 7—figure supplements 1 and 2***; prootics of uncertain maturity, anterior labyrinth), DFMMh/FV 981.2, DFMMh/FV 898, and DFMMh/FV 249 (***Figure 8***; ***Figure 8—figure supplements 1 and 2***; juvenile otoccipitals, posterior labyrinth) were documented with microCT. Since the isolated specimens contain different parts of the endosseous labyrinths, cranial nerves and vascular cavities, the respective digital models were reconstructed in order to describe, compare, and contextualize their characteristics. Whereas the smallest of these specimens (DFMMh/FV 898) hints to an approximate posterior skull width of under 5 cm, the largest specimens DFMMh/FV 581.1 and DFMMh/FV 1077 suggest a mediolateral width of about 14 cm.

The microCT data and our digital reconstructions (Europasaurus holgeri - neuroanatomy - DFMMh/FV - Schade et al. 2023 // MorphoSource) of different *Europasaurus* individuals add to the knowledge of diversity of dinosaur neuroanatomy and allow a better understanding of ontogenetic development. We discuss our findings in context of insights into the lifestyle of this long-necked insular dwarf from the Late Jurassic of Germany.

Results

Cranial endocast, innervation, and blood supply

As is generally the case in non-maniraptoriform dinosaurs (e.g., ***Witmer and Ridgely, 2008a***; ***Witmer and Ridgely, 2009***; ***Knoll et al., 2015***; ***Knoll et al., 2021***), many characteristics of the mid- and hindbrain are not perceivable with certainty (however, see ***Evans, 2005***; ***Morhardt, 2016***; ***Fabbri et al., 2017***) on the braincase endocast of DFMMh/FV 581.1 (***Figure 1A***), which implies scarce correlation of the actual brain and the inner surface of the endocranial cavity (see ***Watanabe et al., 2019***, for ontogenetic variations in recent archosaurs).

This endocast suggests low angles in the cerebral and pontine flexures. There is a prominent dorsal expansion, spanning from around the posterodorsal skull roof to approximately the anteroposterior mid-length of the endocast (***Figures 1 and 2***). In posterior view, the dorsal expansion is T-shaped with a more or less straight top and dorsolateral beams that become dorsoventrally higher and gradually lead over anteriorly to the area where the posterior part of the cerebral hemispheres are expected. In lateral view, the posterior-most extent of the dorsal expansion is separated from the dorsal margin of the medulla oblongata by a concavity. Anterolaterally to this concavity, the eminence for the vena

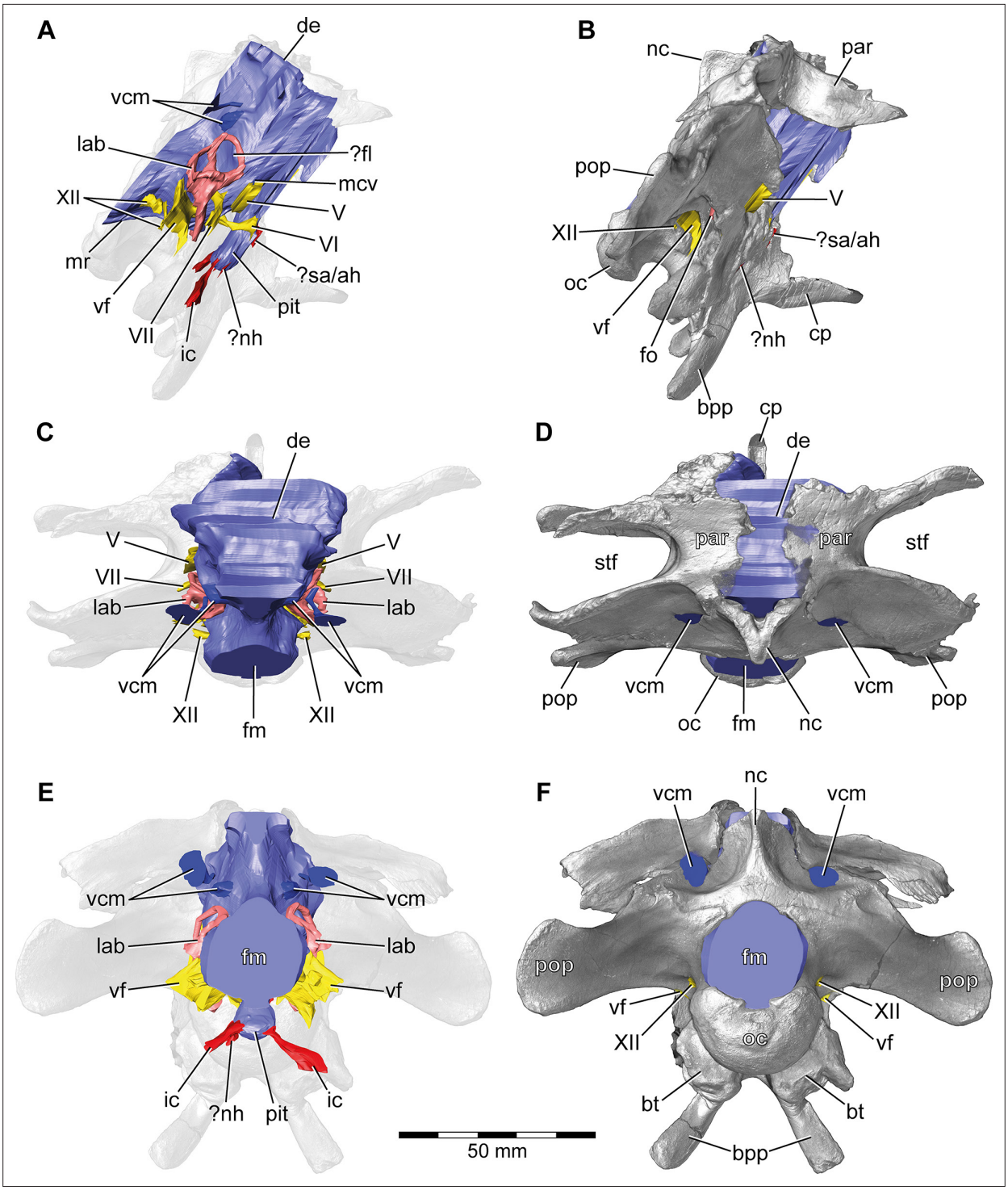

Figure 1. *Europasaurus holgeri*, 3D model of the braincase endocast with endosseous labyrinths and neurovascular canals of DFMMh/FV 581.1, 2, and 3 with transparent (**A,C,E**) and covering (**B,D,F**) volume rendering of the bony braincase in (**A,B**) right lateral, (**C,D**) dorsal, and (**E,F**) posterior view. Note that scale mainly applies to posterior perspective (**E,F**).?fl, potential floccular recess; ?nh, potential canal for the neurohypophysis; ?sa/ah, potential sphenoidal artery/canal for the adenohypophysis; bpp, basipterygoid process; bt, basal tuber; cp, cultriform process; de, dorsal expansion; ic, internal carotid; fm, foramen magnum; fo, fenestra ovalis; lab, endosseous labyrinth; mcv, mid cerebral vein; mr, medial ridge; nc, sagittal nuchal crest; oc, occipital condyle; par, parietal; pit, pituitary; pop, paroccipital process; stf, supratemporal fenestra; vcm, vena capitis media; vf, vagal foramen; V, trigeminal nerve; VI, abducens nerve; VII, facial nerve; XII, hypoglossal nerve.

The online version of this article includes the following figure supplement(s) for figure 1:

Figure 1 continued on next page

Figure 1 continued

Figure supplement 1. *Europasaurus holgeri*, close-up of left lateral aspect of DFMMh/FV 581.1.

Figure supplement 2. *Europasaurus holgeri*, close-up of anterior endocranial floor of DFMMh/FV 581.1 in dorsal view.

Figure supplement 3. *Europasaurus holgeri*, close-up of 3D model of anterior endocranial floor of DFMMh/FV 581.1 in dorsal view.

Figure supplement 4. *Europasaurus holgeri*, close-up of right posterior endocranial wall of DFMMh/FV 581.1, viewed through the foramen magnum.

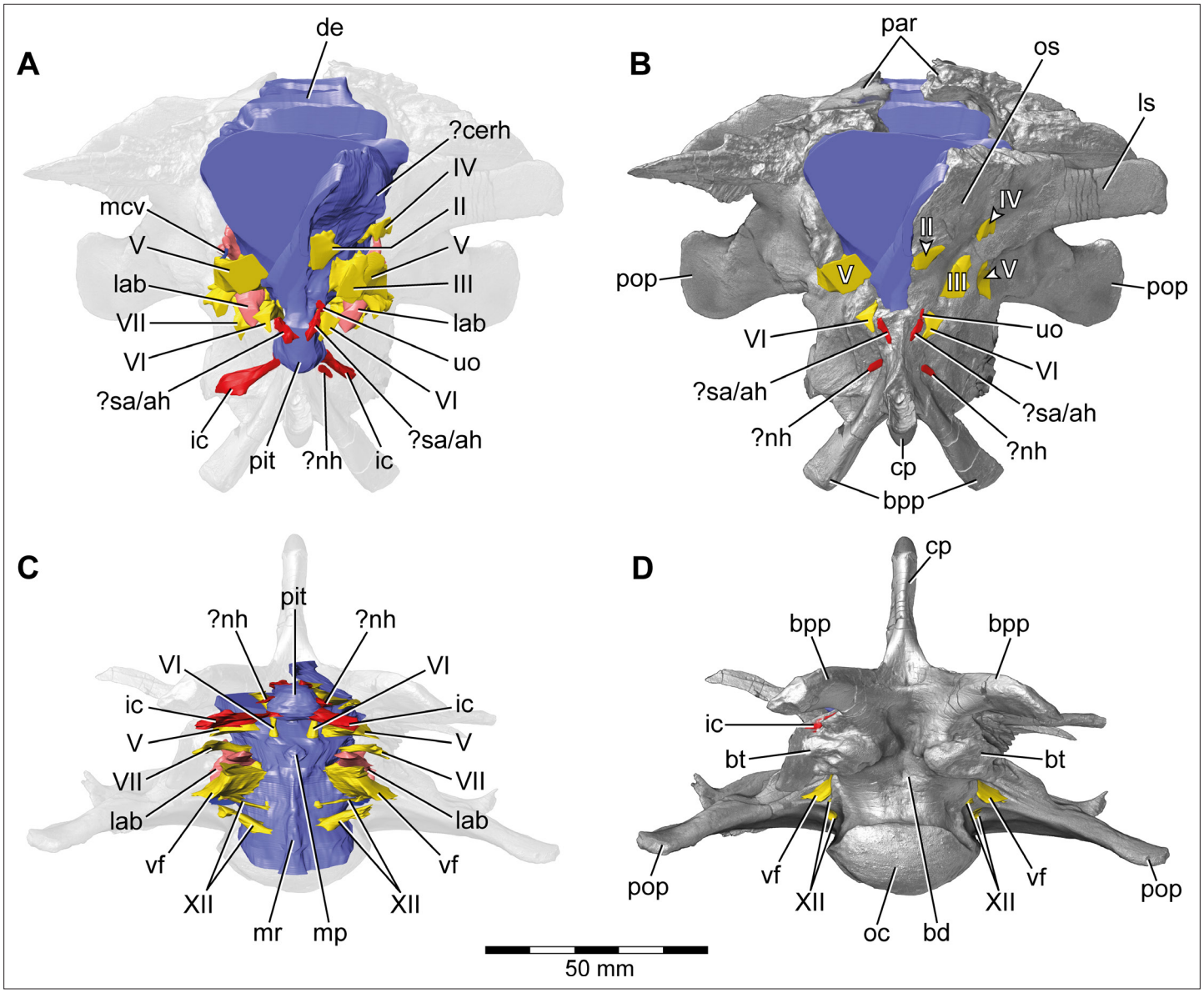

Figure 2. *Europasaurus holgeri*, 3D model of the braincase endocast with endosseous labyrinths and neurovascular canals of DFMMh/FV 581.1, 2, and 3 with transparent (**A,C**) and covering (**B,D**) volume rendering of the bony braincase in (**A,B**) anterior (**C,D**) and ventral view. Note that scale mainly applies to ventral perspective (**C,D**). ?cerh, potential cerebral hemisphere; ?nh, potential canal for the neurohypophysis; ?sa/ah, potential sphenoidal artery/canal for the adenohypophysis; bd, blind depression; bpp, basipterygoid process; bt, basal tuber; cp, cultriform process; de, dorsal expansion; ic, internal carotid; fm, foramen magnum; lab, endosseous labyrinth; ls, laterosphenoid; mcv, mid cerebral vein; mp, median protuberance; mr, medial ridge; oc, occipital condyle; os, orbitosphenoid; par, parietal; pit, pituitary; pop, paroccipital process; uo, unclear opening; vf, vagal foramen; II, optic nerve; III, oculomotor nerve; IV, trochlear nerve; V, trigeminal nerve; VI, abducens nerve; VII, facial nerve; XII, hypoglossal nerve.

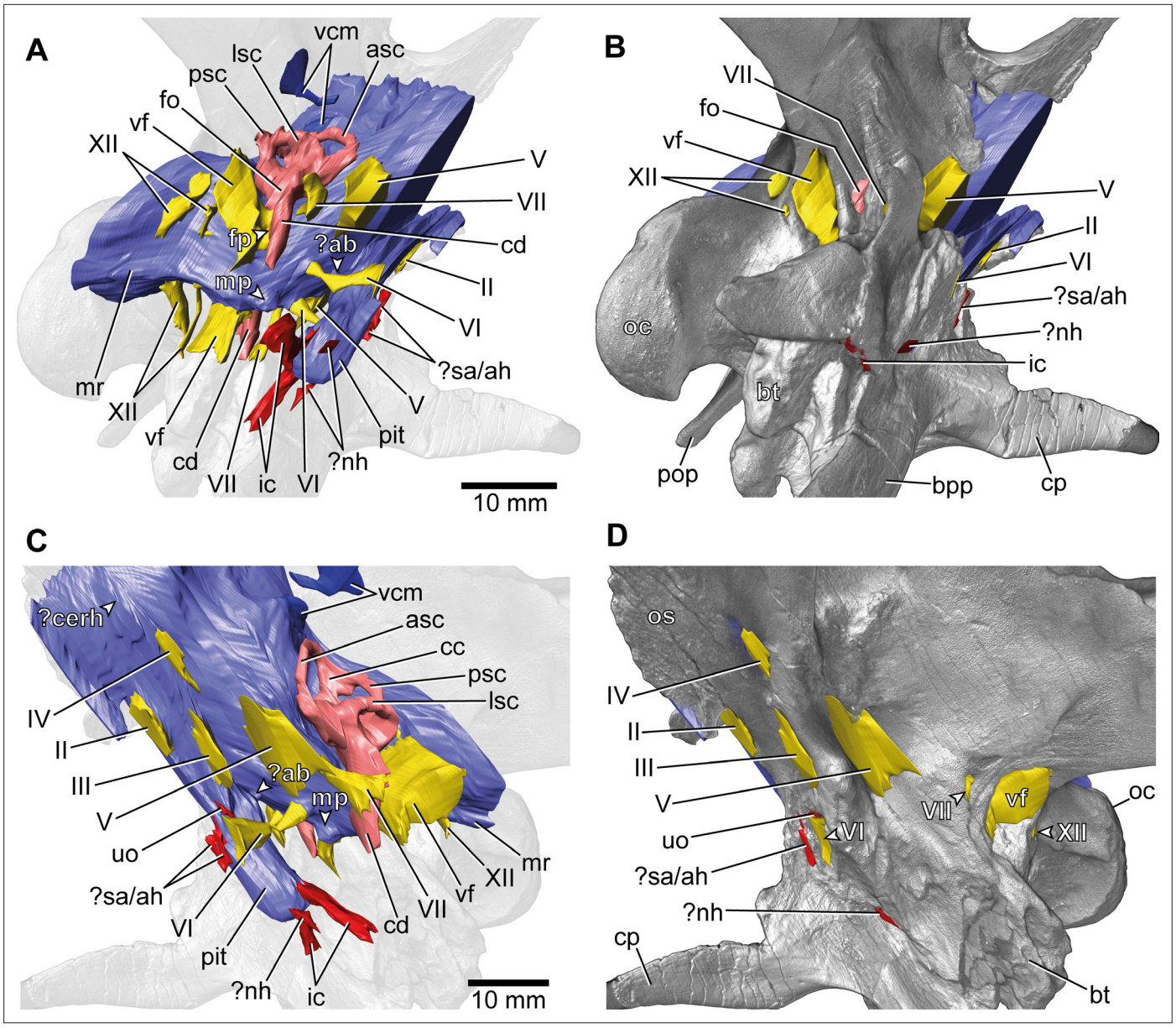

Figure 3. *Europasaurus holgeri*, 3D model of the braincase endocast with endosseous labyrinths and neurovascular canals of DFMMh/FV 581.1, 2, and 3 with transparent (**A,C**) and covering (**B,D**) volume rendering of the bony braincase in (**A,B**) right ventrolateral and (**C,D**) left lateral view. ?ab, potential basilar artery; ?cerh, potential cerebral hemisphere; ?nh, potential canal for the neurohypophysis; ?sa/ah, potential sphenoidal artery/canal for the adenohypophysis; bpp, basipterygoid process; bt, basal tuber; cp, cultriform process; ic, internal carotid; fo, fenestra ovalis; fp, fenestra pseudorotunda; mp, median protuberance; mr, medial ridge; oc, occipital condyle; os, orbitosphenoid; pit, pituitary; pop, paroccipital process; uo, unclear opening; vcm, vena capitis media; vf, vagal foramen; II, optic nerve; III, oculomotor nerve; IV, trochlear nerve; V, trigeminal nerve; VI, abducens nerve; VII, facial nerve; XII, hypoglossal nerve.

capitis media is present. Although the respective openings are identifiable on DFMMh/FV 581.1 (close to a kink on the posterodorsal contact between the parietals and the supraoccipital, called 'external occipital fenestra for the caudal middle cerebral vein' in ***Marpmann et al., 2014***), only an approximate reconstruction of the course of the veins was possible (due to low contrast in the microCT data; ***Figures 1 and 3***). There is a large semicircular depression on the posterodorsolateral aspect of the endocast, being anterodorsally bordered by the dorsal expansion and anteroventrally by the eminence of the vena capitis media. On the anterodorsal skull roof, a mediolateral expansion of the endocast possibly marks the position of the cerebral hemisphere (***Figures 2 and 3***). In lateral view, there is a distinct ventral step on top of the endocast (also present in many other sauropod taxa; see,

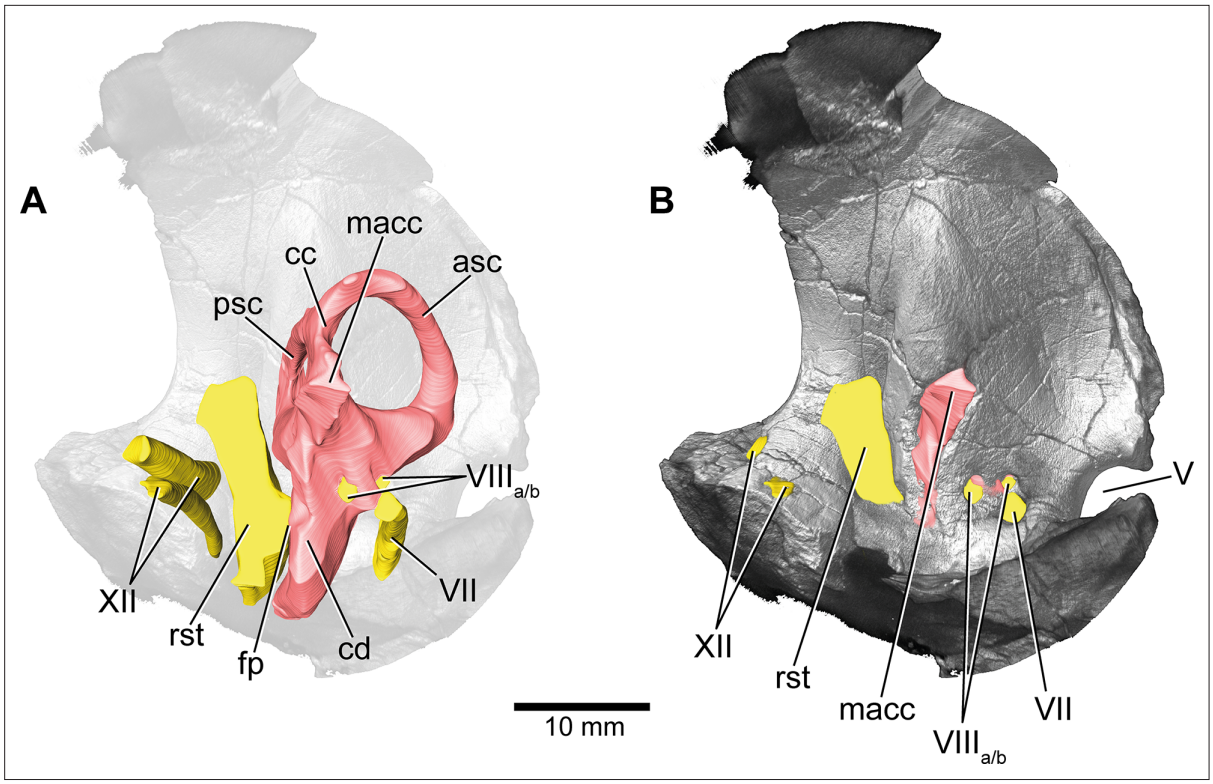

Figure 4. *Europasaurus holgeri*, 3D model of the left endosseous labyrinth region in DFMMh/FV 1077 with transparent (**A**) and covering (**B**) volume rendering of the bony braincase in medial view. asc, anterior semicircular canal; cc, common crus; cd, cochlear duct; fp, fenestra pseudorotunda; lsc, lateral semicircular canal; macc, medial aspect of common crus; psc, posterior semicircular canal; rst, recessus scalae tympani; V, trigeminal nerve opening; VII, facial nerve; VIIIa/b, both branches of the vestibulocochlear nerve; XII, hypoglossal nerve.

The online version of this article includes the following figure supplement(s) for figure 4:

Figure supplement 1. *Europasaurus holgeri*, fragmentary braincase DFMMh/FV 1077 in (**A**) ventral and (**B**) posterior view. fm, foramen magnum; fo, fenestra ovalis; nc, nuchal crest; oc, occipital condyle; pop, paroccipital process; vf, vagal foramen; V, trigeminal nerve opening; VII, facial nerve opening; XII, hypoglossal nerve opening.

Figure supplement 2. *Europasaurus holgeri*, close-up of medial aspect of the fragmentary braincase DFMMh/FV 1077.

e.g., ***Knoll and Schwarz-Wings, 2009***; ***Carabajal, 2012***; ***Knoll et al., 2013***), between the anteriormost part of the dorsal expansion and the posterior part of the cerebral hemispheres, followed by a slight ascent in anterior direction. The left side of the endocast suggests that the cerebral hemisphere impressions are delimited approximately by the contact between the orbitosphenoid and the laterosphenoid anteriorly, and by the trochlear nerve (CN IV) ventrally. Anteriorly, the orbitosphenoid bears a prominent medial incision for the optic nerve (CN II). Posteroventrally to the optic nerve canal and anteroventrally to the trochlear nerve canal, the canal of the oculomotor nerve (CN III) is situated. On the anteroventral aspect of the endocast, the pituitary reaches about as far ventrally as the ventralmost margin of the medulla oblongata, producing an angle of about 50° to the lateral semicircular canal (LSC) of the endosseous labyrinth (see ***Paulina-Carabajal et al., 2020***). On the anterodorsal aspect of the pituitary, two small and dorsolaterally diverging canals of uncertain identity branch off (***Figures 1–3***; ***Marpmann et al., 2014*** labelled the openings as carotid artery: Figure 13D). In the titanosaur specimen CCMGE 628/12457 and *Sarmientosaurus*, structures of a similar position were identified as sphenoidal arteries (***Sues et al., 2015***; ***Martínez et al., 2016***). However, in *Bonatitan* and the titanosaur braincase MPCA-PV-80, anterolateral openings on the pituitary, close to the abducens nerve (CN VI) canal, have been assigned to canals leading to the adenohypophysis (***Carabajal, 2012***). Posterolaterally to these canals, the abducens nerve (CN VI) canals trend in an anteroposterior direction (***Figures 1–3***; ***Figure 1—figure supplements 1–3***). The specimen DFMMh/FV 581.1 suggests a natural connection between the pituitary fossa and the left CN VI canal, close to its anterior opening. This condition may be due to breakage, since the microCT data suggests a continuous wall on the right

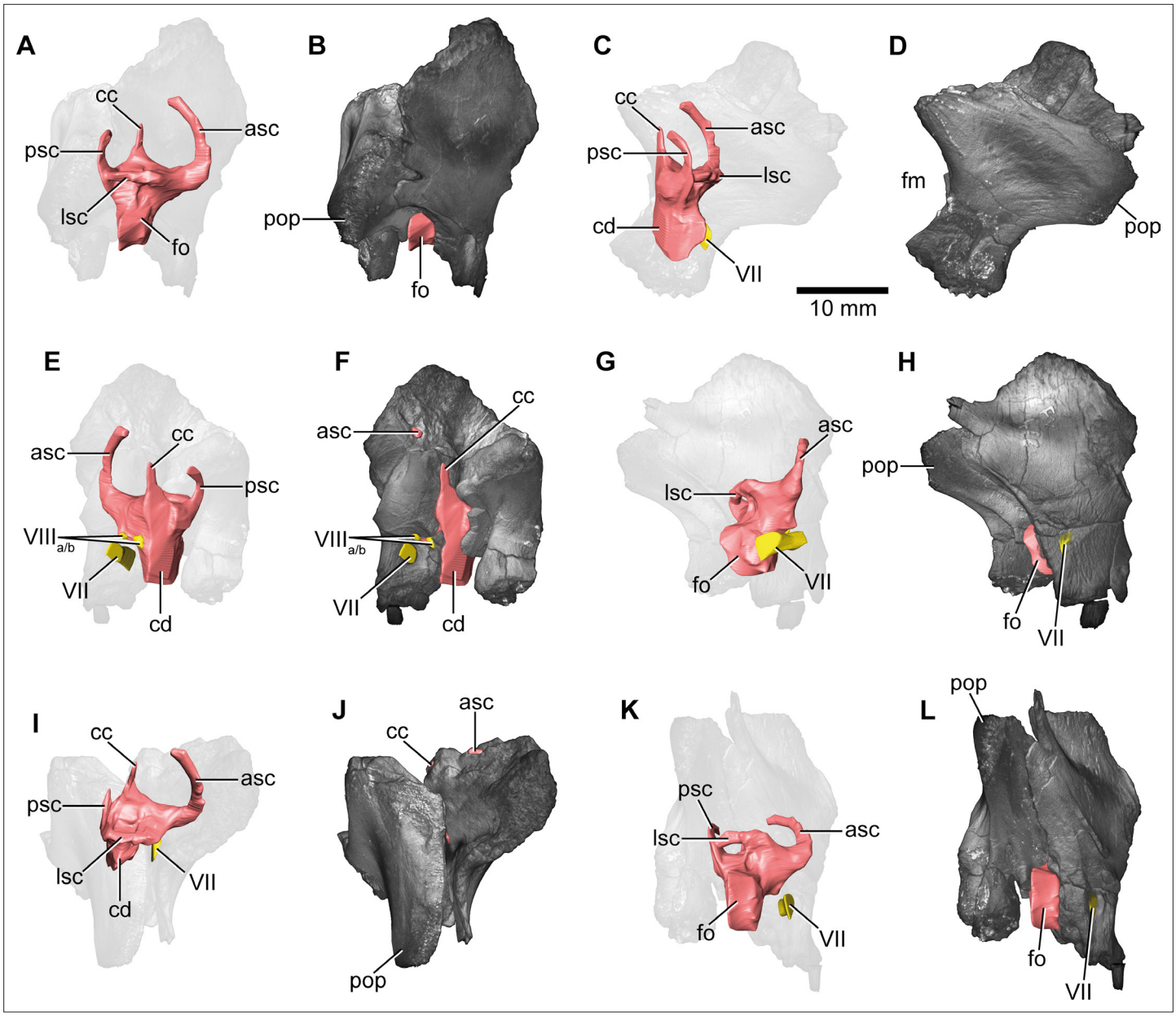

Figure 5. *Europasaurus holgeri*, 3D model of the right endosseous labyrinth in DFMMh/FV 466+205 with transparent (**A,C,E,G,I,K**) and covering (**B,D,F,H,J,L**) volume rendering of the bony braincase remains in (**A,B**) lateral, (**C,D**) posterior, (**E,F**) medial, (**G,H**) anterolateroventral, (**I,J**) dorsolateral, and (**K,L**) lateroventral view; in respect to the endosseous labyrinth. Note that scale mainly applies to posterior perspective (**C,D**), and that VII and VIIIa/b are not shown in (**A**) and (**B**). asc, anterior semicircular canal; cc, common crus; cd, cochlear duct; fm, foramen magnum; fo, fenestra ovalis; lsc, lateral semicircular canal; pop, paroccipital process; psc, posterior semicircular canal; VII, facial nerve; VIIIa/b, both branches of the vestibulocochlear nerve.

The online version of this article includes the following figure supplement(s) for figure 5:

Figure supplement 1. *Europasaurus holgeri*, isolated otoccipital (DFMMh/FV 205; **A,B**) and prootic (DFMMh/FV 466; **C,D**) in (**A**) posterior, (**B**) anterior, (**C**) lateral, and (**D**) medial view; prootic and otoccipital conjoined in (**E**) posterolateral, (**F**) lateral, (**G**) medial, (**H**) dorsal, and (**I**) ventral view.

side. In ventrolateral view, the left side of DFMMh/FV 581.1 shows an additional small medial opening dorsally within the depression for CN VI (***Figures 2A, B and 3C, D***; ***Figure 1—figure supplements 1–3***). Because of its smooth curvature, this opening seems natural, but for preservational reasons this is not visible on the right side of the specimen. On the ventrolateral part of the pituitary, two short canals of uncertain identity are branching off ventrolaterally (***Figures 1–3***; ***Figure 1—figure supplement 1***; in *Bonatitan*, anterolateral canals on the ventral portion of the pituitary have been identified

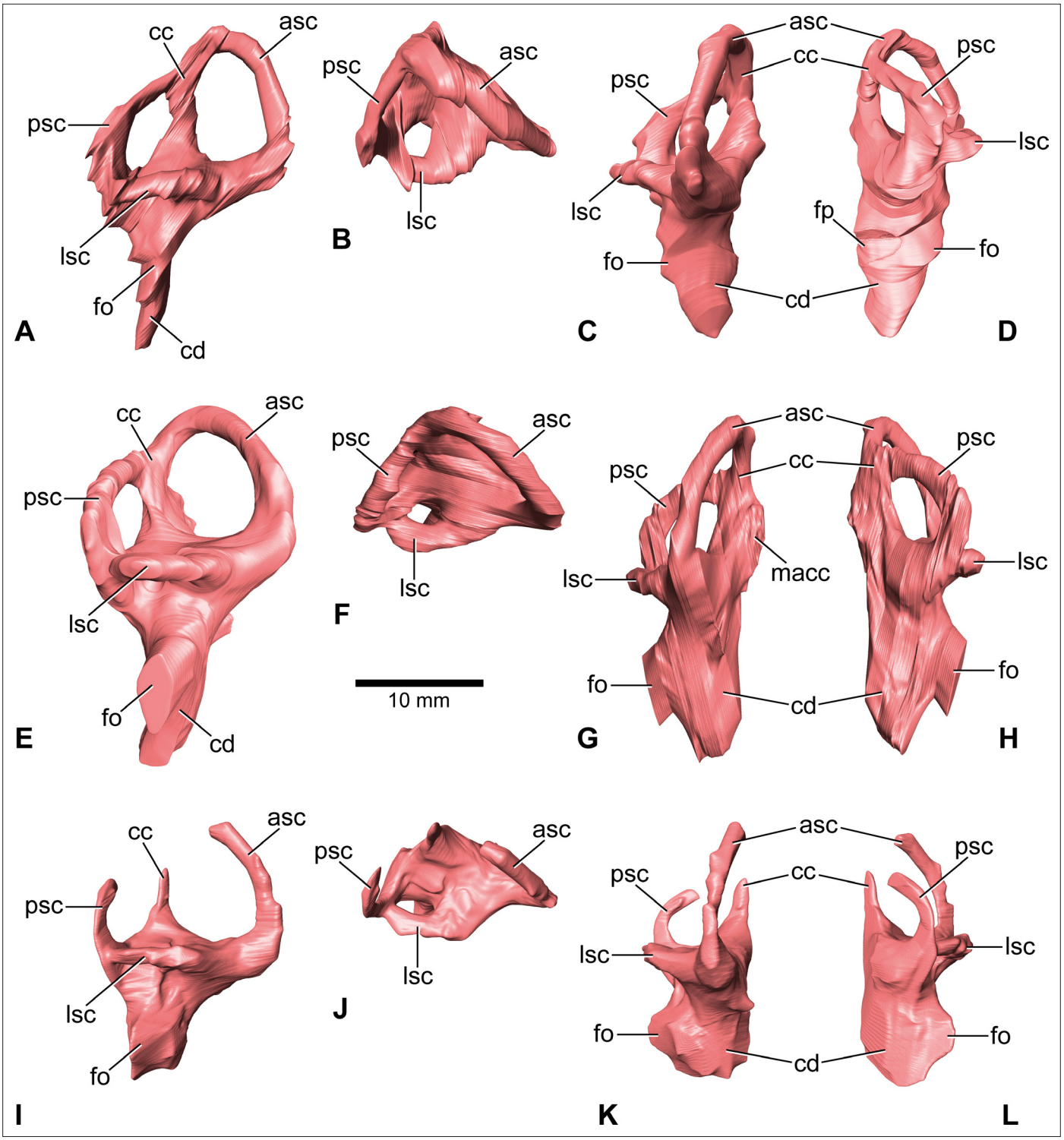

Figure 6. *Europasaurus holgeri*, 3D models of the endosseous labyrinth of DFMMh/FV 581.1 (**A–D**), DFMMh/FV 1077 (**E–H**; note that this model is mirrored) and DFMMh/FV 466+205 (**I–L**) in (**A,E,I**) lateral, (**B,F,J**) dorsal, (**C,G,K**), anterior and (**D,H,L**) posterior view. Note that scale mainly applies to dorsal perspective (**B,F,J**). asc, anterior semicircular canal; cc, common crus; cd, cochlear duct; fo, fenestra ovalis; fp, fenestra pseudorotunda; lsc, lateral semicircular canal; macc, medial aspect of common crus; psc, posterior semicircular canal.

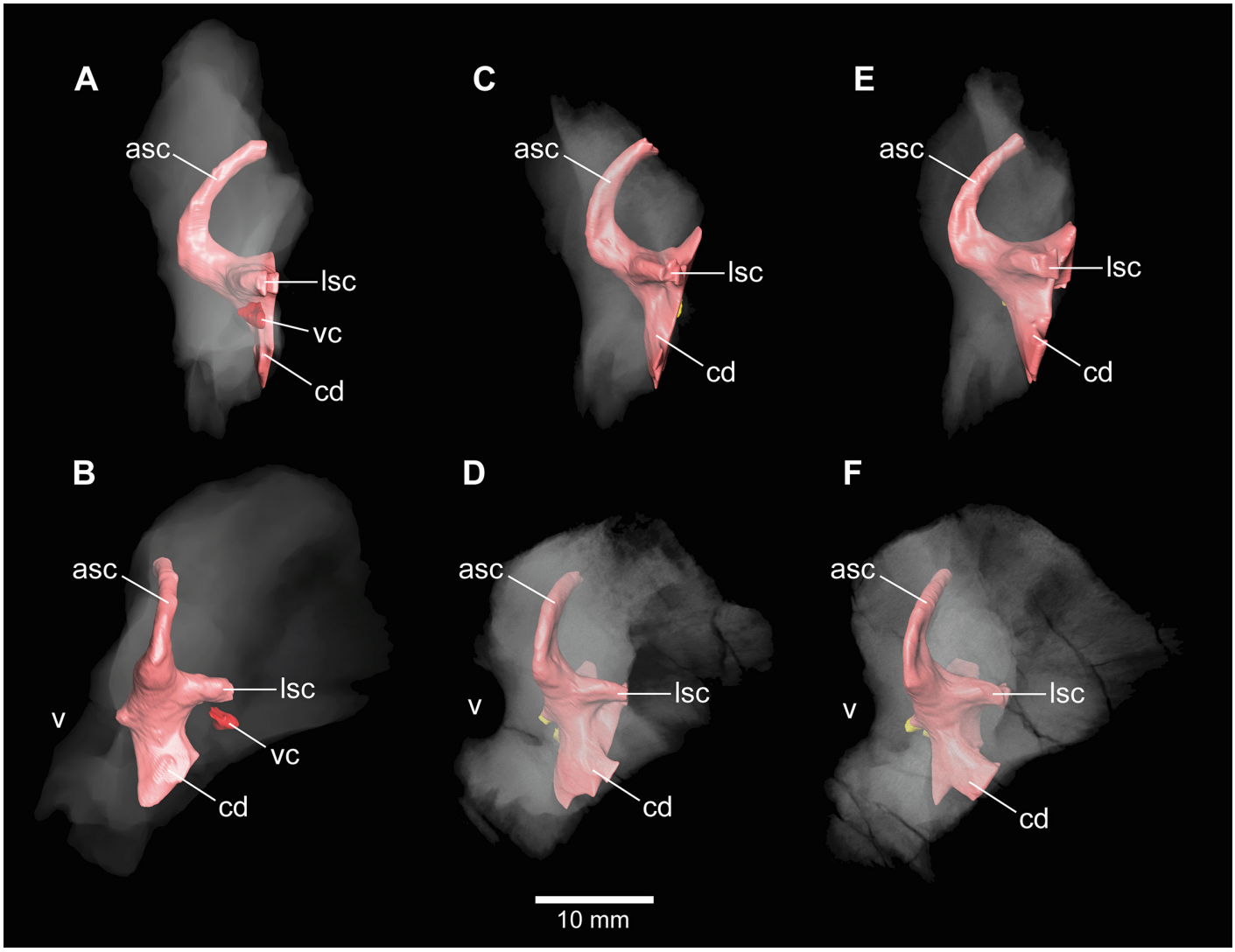

Figure 7. *Europasaurus holgeri*, 3D models of the anterior portions of the endosseous labyrinth in (**A**,**B**; note that this model is mirrored) DFMMh/FV 466, (**C,D**) DFMMh/FV 561 and (**E,F**) DFMMh/FV 964 in (**A,C,E**) lateral and (**B,D,F**) anterolateral view; in respect to the endosseous labyrinth. Note that scale mainly applies to anterolateral perspective (**B,D,F**). asc, anterior semicircular canal; cd, cochlear duct; lsc, lateral semicircular canal; vc, vascular cavity; V, trigeminal nerve opening.

The online version of this article includes the following figure supplement(s) for figure 7:

Figure supplement 1. *Europasaurus holgeri*, isolated prootics (DFMMh/FV 466, **A**,**B**; DFMMh/FV 964, **C**,**D**; DFMMh/FV 561, **E,F**) in (**A,C,E**) lateral and (**B,D,F**) medial view.

Figure supplement 2. *Europasaurus holgeri*, 3D models of isolated prootics and inner features (DFMMh/FV 466, **A**; DFMMh/FV 561, **B**; DFMMh/FV 964, **C**) in (**A–C**) medial view. Note that models are not scaled. asc, anterior semicircular canal; lab, endosseous labyrinth; lsc, lateral semicircular canal; vc, vascular cavity.

as leading to the neurohypophysis; ***Carabajal, 2012***). Directly behind, the pituitary bears the long internal carotid canals, branching off ventrolaterally as well.

The endosseous labyrinth is situated within an anteroventrally inclined lateral depression of the endocast, directly ventral to the vena capitis media eminence. Here, an opening is present, leading to the medial aspect of the common crus in DFMMh/FV 581.1 and 1077 (the opening is considerably larger in the latter specimen; ***Figures 4 and 6***; ***Figure 1—figure supplement 4***; ***Figure 4—figure supplement 2***). Whereas the trigeminal (CN V), facial (CN VII), and vestibulocochlear (CN VIII; two openings) nerve canals are mainly anterior to the endosseous labyrinth, the vagal foramen (=jugular foramen for CN IX-XI and jugular vein) and two canals for the hypoglossal nerves are situated

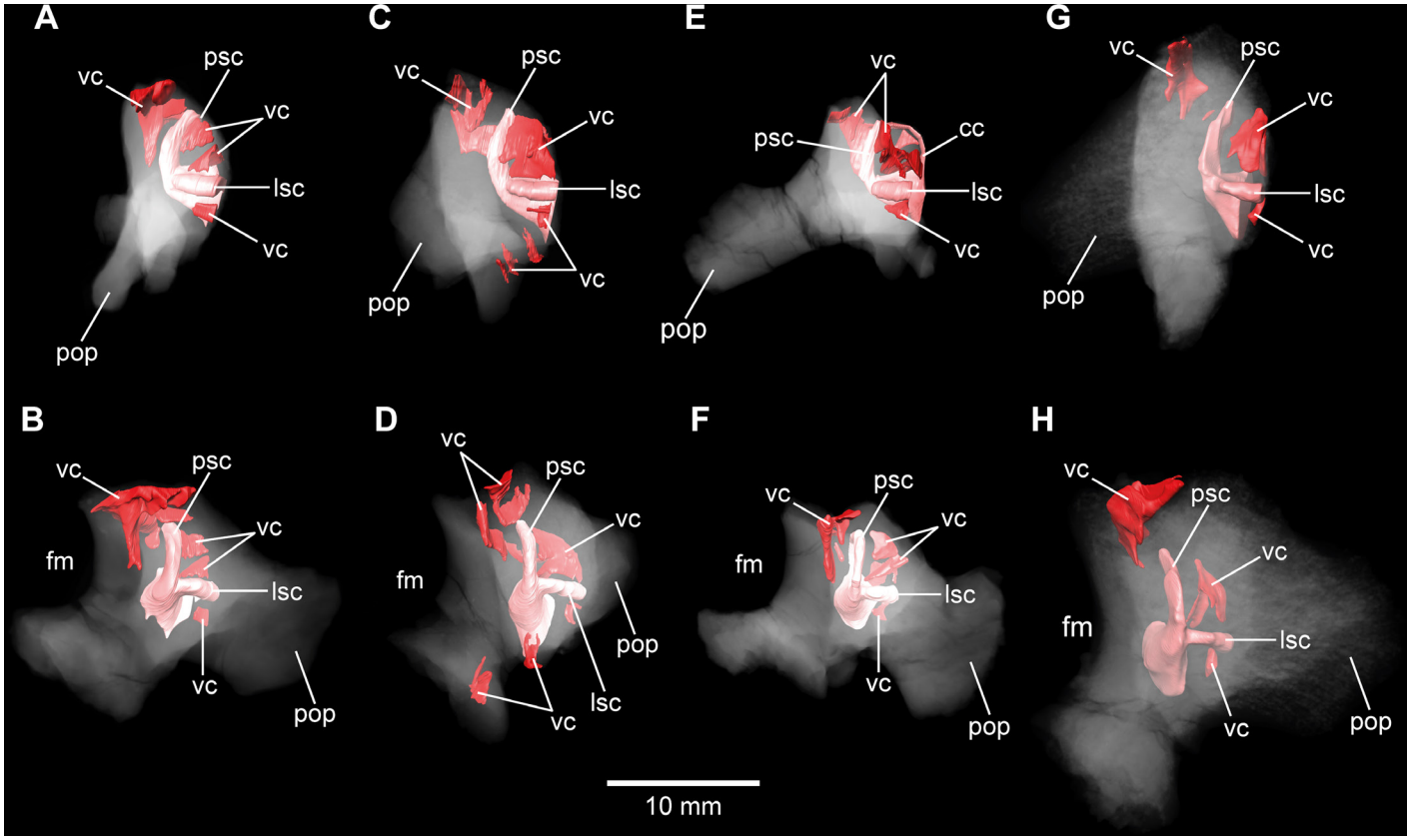

Figure 8. *Europasaurus holgeri*, 3D models of the posterior portions of the endosseous labyrinth in (**A,B**) DFMMh/FV 898, (**C,D**) DFMMh/FV 981.2, (**E,F**) DFMMh/FV 249, and (**G,H**) DFMMh/FV 205 in (**A,C,E,G**) anterolateral and (**B,D,F,H**) posterior view. Note that scale mainly applies to posterior perspective (**B,D,F,H**). fm, foramen magnum; lsc, lateral semicircular canal; pop, paroccipital process; psc, posterior semicircular canal; vc, vascular cavity.

The online version of this article includes the following figure supplement(s) for figure 8:

Figure supplement 1. *Europasaurus holgeri*, isolated otoccipitals (DFMMh/FV 898, **A**,**B**; DFMMh/FV 981.2, **C**,**D**; DFMMh/FV 249, **E**,**F**; DFMMh/FV 205, **G**,**H**) in (**A,C,E,G**) posterior and (**B,D,F,H**) anterior view.

Figure supplement 2. *Europasaurus holgeri*, 3D models of isolated otoccipitals and inner features (DFMMh/FV 898, **A**; DFMMh/FV 981.2, **B**,**C**; DFMMh/FV 249, **D**; DFMMh/FV 205, **E**) in (**A,B,D,E**) anterodorsomedial and (**C**) ventral view. Note that models are not scaled. cc, common crus; fm, foramen magnum; lab, endosseous labyrinth; lsc, lateral semicircular canal; pop, paroccipital process; psc, posterior semicircular canal; vc, vascular cavity.

posterior to the cochlear duct (***Figures 1–3***). Within the depression for CN V, dorsally, a very small opening for the mid-cerebral vein is situated on both sides of DFMMh/FV 581.1. However, only the right canal could approximately be reconstructed (***Figures 1A and 2A***). Dorsal to the right slit-like opening for CN VII, a small depression is present in DFMMh/FV 581.1. The microCT data do not suggest penetration. Whereas the posterior canals for the hypoglossal nerve (CN XII) are clearly discernable in the microCT data, the anterior ones are not as obvious to detect. However, because of the expression of their respective openings on the actual fossil, their course could be established. ***Marpmann et al., 2014***, only identified one hypoglossal canal (CN XII). However, the specimens considered herein support the presence of two openings on each side. Furthermore, anterior to the proximal openings of the anterior CN XII canals, one depression each is visible in DFMMh/FV 581.1, however, the microCT data do not suggest a penetration. Anterodorsally to the endosseous labyrinth, the cerebellum appears as a mediolaterally expanded part of the endocast, almost reaching the trigeminal nerve (CN V) anteriorly and being delimited by the eminence of the vena capitis media posterodorsally (***Figure 1A***). Furthermore, a small floccular recess is present close to the mid-length of the anterior semicircular canal (ASC) in DFMMh/FV 581.1. The ventral aspect of the endocast is anterodorsally inclined and bears a medial ridge (figures becoming mediolaterally narrower in anterior direction; ***Figures 1A, 2C,3A***), reaching between the foramen magnum and the anteroventral

portion of the endocast (not considering the pituitary). Posteroventral to the abducens nerve (CN VI), a single median protuberance is present on the endocast, produced by a fossa on the floor of the endocranial cavity (***Figures 2C and 3***; ***Figure 1—figure supplements 2 and 3***). In addition, anterodorsally to the proximal openings for the abducens nerve (CN VI), a single median opening is present on the braincase floor, producing a connection to the pituitary fossa (probably for vascularization; see ***Carabajal, 2012***; ***Sues et al., 2015***, for arguments on arterial or venous identity). The general osteological configuration of the endocranial floor (***Figure 1—figure supplements 2 and 3***) seems very similar in the macronarian *Giraffatitan* (***Janensch, 1935***: Figure 117). The anterodorsally incomplete endocranial cavity of DFMMh/FV 581.1, 2, and 3 comprises a volume of about 35 cm^3 (including the pituitary fossa). On the ventral aspect of DFMMh/FV 581.1, a small funnel-like depression anterior to the occipital condyle ends blindly (***Figure 2D***).

Endosseous labyrinth

Both vestibular systems are preserved and are ventrally connected to the respective cochlea in DFMMh/FV 581.1 (the semicircular canals of the left inner ear were only vaguely perceptible in some places). Whereas only the left endosseous labyrinth is preserved in DFMMh/FV 1077, only the right one is preserved within DFMMh/FV 466+205. The following description is based on the mentioned endosseous labyrinths (***Figure 6***). The vertical semicircular canals are relatively long and slender. Dorsoventrally, the ASC reaches considerably higher than the posterior one, and the ASC occupies more of the anteroposterior length of the vestibular system. The common crus is dorsally slightly posteriorly inclined (where preserved). While the posterior semicircular canal (PSC) forms a low arc, the ASC turns about 180° to contact the common crus dorsomedially. The medial aspect of the common crus is exposed to the endocranial cavity in DFMMh/FV 581.1 and DFMMh/FV 1077 (***Figures 4 and 6G***; ***Figure 1—figure supplement 4***; ***Figure 4—figure supplement 2***). The angle between the ASC and the PSC amounts 80° (measured in dorsal view with the common crus as fixpoint). The LSC is anteroposteriorly short. In dorsal view, its anterior ampulla appears posteriorly shifted, producing a medially concave gap between the ASC and LSC (***Figure 6B,F,J***). Such a medial concavity is also present between the LSC and the PSC (best seen in dorsal view). The cochlear duct is approximately as high as the vestibular system dorsoventrally, points anteroventrally and very slightly medially (in DFMMh/FV 581.1 and 1077). In lateral view, the cochlear duct is anteroposteriorly slender with sub-parallel anterior and posterior margins. However, mediolaterally, the cochlear duct is very wide, resulting in an elongated oval-shaped cross-section. The fenestra ovalis (***Figures 1A, B, 2A, B and 6***; ***Figure 4—figure supplement 1***) is situated close to the dorsoventral mid-length of the lateral aspect of the cochlear duct (in DFMMh/FV 581.1 and DFMMh/FV 1077). This is also true for the anteroposteriorly oriented fenestra pseudorotunda (***Figures 4 and 6D***; ***Figure 1—figure supplement 4***), lying on the posteromedial aspect of the cochlear duct. The hiatus acusticus expresses as an anteromedially open notch (similar to the theropod *Irritator*; ***Schade et al., 2020***) on the actual fenestra pseudorotunda in DFMMh/FV 581.1 (***Figure 1—figure supplement 4***).

Auditory capabilities

To get a rough idea of the audition of *Europasaurus*, we measured the dorsoventral cochlear duct length of DFMMh/FV 581.1 (c. 16 mm; as outlined by ***Walsh et al., 2009***; however, see ***Witmer and Ridgely, 2008a***; ***Paulina-Carabajal et al., 2016***) and the anteroposterior basicranial length (c. 55 mm; from the anterodorsal part of the pituitary fossa to the posterior-most part of the occipital condyle). Based on the equations of ***Walsh et al., 2009***, our estimate of the mean hearing frequency of *Europasaurus* yields a value of 2225 Hz and a frequency bandwidth of 3702 Hz (374–4076 Hz). The auditory capabilities of the Late Triassic early-diverging sauropodomorph *Thecodontosaurus* from England was estimated by same means with a mean frequency of 1893 Hz and a band width of 3089 Hz (349–3438 Hz; ***Ballell et al., 2021***).

Inner ears and cavities of incomplete specimens

In addition to DFMMh/FV 581.1, 2, and 3 (***Figures 1–3*** and ***Figure 6A–D***; ***Figure 1—figure supplements 1–4***), eight other braincase specimens (that hold parts of the endosseous labyrinth), assigned to *Europasaurus*, were scanned and analysed. DFMMh/FV 1077 (***Figures 4 and 6E–H***; ***Figure 4—figure supplements 1 and 2***) contains a complete left endosseous labyrinth and was categorized

as belonging to an osteological mature individual in ***Marpmann et al., 2014***; as DFMMh/FV 581.1, 2, and 3. Furthermore, there are two right elements (***Figures 5, 6I–L, 7A,B, 8G,H***; ***Figure 5—figure supplement 1***; ***Figure 7—figure supplements 1A, B and 2A***; ***Figure 8—figure supplements 1G, H and 2E***; DFMMh/FV 205, a fragmentary otoccipital, and DFMMh/FV 466, a fragmentary prootic) that were originally found some 10 cm apart from each other in the sedimentary matrix. Whereas DFMMh/FV 205 was thought to belong to a juvenile, DFMMh/FV 466 was supposed to belong to a considerably older individual (both estimations are mainly based on size and surface texture; ***Marpmann et al., 2014***). However, DFMMh/FV 205 and DFMMh/FV 466 articulate well with each other and jointly contain most of the endosseous labyrinth and the dorsal portion of the lagena, all in a meaningful manner in respect to size, position, and orientation of its compartments. DFMMh/FV 466 is of similar size and texture as the other prootics considered here. DFMMh/FV 205 is considerably smaller than the otoccipitals in the adult specimens. Hence, DFMMh/FV 466+205 are herein interpreted to belong to the same juvenile individual. Furthermore, there are two left fragmentary prootics (***Figure 7C–F***; ***Figure 7—figure supplement 1C–F***, ***Figure 7—figure supplement 2B, C***; DFMMh/FV 561 and DFMMh/FV 964) containing most of the ASC, the ventral base of the common crus, the anterior ampulla of the LSC, and the anterior base of the lagena; both specimens were assigned to relatively mature individuals (***Marpmann et al., 2014***). The three right fragmentary otoccipitals DFMMh/FV 249, DFMMh/FV 898, and DFMMh/FV 981.2 (***Figure 8A–F***; ***Figure 8—figure supplements 1A–F and 2A–D***) contain at least the posterior parts of the LSC and the lagena, as well as most of their PSCs; these specimens were assigned to immature individuals (***Marpmann et al., 2014***).

In general, the morphology of the inner ears contained within these isolated specimens is consistent to what can be observed in DFMMh/FV 581.1 and DFMMh/FV 1077. Since ***Marpmann et al., 2014***, used the vascularization (indicated by surface texture) of *Europasaurus* specimens as a critical character in judging the relative maturity, the inner cavities surrounding the endosseous labyrinths were examined herein.

No discrete cavities could be found in DFMMh/FV 581.1, DFMMh/FV 1077, DFMMh/FV 964, and DFMMh/FV 561 (all considered to represent more or less mature individuals). The otocipitals DFMMh/FV 249, DFMMh/FV 898, and DFMMh/FV 981.2 and the articulated specimens DFMMh/FV 205 (otoccipital) and DFMMh/FV 466 (prootic) show very similar, or corresponding, patterns of inner cavities (***Figures 7 and 8***; ***Figure 7—figure supplement 2***; ***Figure 8—figure supplement 2***). All four otoccipitals show dorsoventrally deep cavities posterodorsal to anteromedial to the PSC, close to the articulation surface with the supraoccipital (except for DFMMh/FV 205, in which this cavity network is not as much extended anteriorly). There are T- (DFMMh/FV 898 and DFMMh/FV 981.2), V- (DFMMh/FV 205), or X- (DFMMh/FV 249) shaped (in cross-section in anterior view), dorsoventrally high and mediolaterally thin structures anterior to the PSC and dorsal to the LSC (close to the articulation surface with the prootic). Additionally, all four otoccipital specimens bear relatively small cavities ventral to the LSC (again, close to the articulation surface with the prootic). DFMMh/FV 981.2 shows dorsoventrally high cavities posteroventrally to the endosseous labyrinth (close to the articulation surface with the basioccipital). Generally, the cavities, likely of vascular purpose, of DFMMh/FV 205 seem not as large and extensive as in the other three otoccipitals. This coincides with their size and assumed relative maturity (DFMMh/FV 205 being the largest, smoothest and, hence, most mature of them[17]). Whereas DFMMh/FV 466 bears a small cavity ventral to the LSC (corresponding to the respective cavity in the otocipital DFMMh/FV 205), no other unequivocal cavities could be found, which is surprising when the V-shaped cavity close to the prootic contact of DFMMh/FV 205 is considered.

Discussion

Comparison of neurovascular anatomy and potential ecological implications

Although not as prominent as in *Dicraeosaurus* (***Janensch, 1935***; ***Paulina Carabajal et al., 2018***) and some specimens of *Diplodocus* (***Witmer and Ridgely, 2008a***), the position and morphology of the dorsal expansion of *Europasaurus* gives a rather 'upright' or sigmoidal appearance to the endocast (***Figure 1A***; see also ***Paulina-Carabajal et al., 2020***). This is partly explained by the (preservational) lack of its olfactory bulb and tract. The first cranial nerve is not expected to be very long in many sauropods, especially in the closely related macronarian taxa *Camarasaurus* and *Giraffatitan* (***Witmer***

and Ridgely, 2008a; *Knoll and Schwarz-Wings, 2009*; see also *Müller, 2021*). In contrast, the braincase endocast is rather tubular in some taxa, for example, the early-diverging sauropodomorph *Buriolestes* (*Müller et al., 2021*), the rebbachisaurid *Nigersaurus* (*Sereno et al., 2007*), and the titanosaur specimen MCCM-HUE-1667 (*Knoll et al., 2015*). Instead, the endocast of *Europasaurus* seems to be most similar to *Giraffatitan* (*Janensch, 1935*; *Knoll and Schwarz-Wings, 2009*) (formerly *Brachiosaurus brancai*, see *Paul, 1988*; *Taylor, 2009*).

Contrary to other sauropod taxa (e.g., *Spinophorosaurus*, *Diplodocus*, *Camarasaurus*, and *Sarmientosaurus*; see *Witmer et al., 2008b*; *Knoll et al., 2012*; *Martínez et al., 2016*), there are no discrete canals for vascular features such as, for example, the rostral middle cerebral vein or the orbitocerebral vein on the endocast of *Europasaurus*.

A ventral ridge on the medulla, as seen in *Europasaurus* (*Figures 1A, 2C, 3A*), seems to be present, although not as pronounced, in *Thecodontosaurus* (*Ballell et al., 2021*), the early-diverging sauropod specimen OUMNH J13596 (*Bronzati et al., 2018*), *Spinophorosaurus* (*Knoll et al., 2012*), *Camarasaurus* (*Witmer and Ridgely, 2008a*) and, potentially, *Giraffatitan* (*Janensch, 1935*; *Knoll and Schwarz-Wings, 2009*) as well.

Although not obvious on the endocast (*Knoll and Schwarz-Wings, 2009*), *Giraffatitan* seems to bear a median fossa posteromedially to the proximal CN VI openings (*Janensch, 1935*: Figure 117); the respective protuberance in *Europasaurus* marks a distinct kink on the endocast (*Figures 2C and 3*; *Figure 1—figure supplements 2 and 3*).

The endocast of *Europasaurus* bears two pairs of canals on the ventrolateral aspect of the pituitary, the posterior of which is interpreted to represent the internal carotid here (*Figures 1A, 2,3*; *Figure 1—figure supplement 1*; in accordance with *Marpmann et al., 2014*: Figure 13A). Whereas structures identified as the craniopharyngeal canal are present anterior to the carotid artery in the titanosaur specimen CCMGE 628/12457 (*Sues et al., 2015*) and the diplodocid specimen MMCh-Pv-232 (assigned to *Leinkupal*; *Garderes et al., 2022*), they are situated posteriorly in *Apatosaurus* (*Balanoff et al., 2010*; see also *Carabajal, 2012*, and *Paulina Carabajal et al., 2014*, for subcondylar foramina in the vicinity of the internal carotid arteries). However, in these taxa, the craniopharyngeal canal is a singular median canal. This may render the anterior of the two pairs of canals on the ventral aspect of the pituitary in *Europasaurus* the canals for the neurohypophysis (*Carabajal, 2012*). The pituitary of the *Europasaurus* endocast of DFMMh/FV 581.1 does not project much more ventrally than the posteroventral margin of the medulla oblongata. The pituitary is slightly higher dorsoventrally than the ASC (*Figure 1A*). Usually in sauropods, the pituitary is large and inclined posteroventrally, reaching much more ventrally than the ventral margin of the hindbrain (see, e.g., *Knoll and Schwarz-Wings, 2009*; *Martínez et al., 2016*; see also *Sues et al., 2015* for an extreme reached in the titanosaur specimen CCMGE 628/12457 with a short ASC and an enormous pituitary). The finding of a relatively small pituitary fossa in *Europasaurus* and early-diverging sauropodomorphs seem to support a close connection of body and pituitary size, as suggested by some authors (*Nopcsa, 1917*; *Edinger, 1942*; *Müller et al., 2021*). The microCT data of DFMMh/FV 581.1 suggest that the right CN VI canal closely passes by the pituitary fossa without a penetration, whereas the left CN VI canal tangents on the pituitary fossa and opens into the latter (*Figure 1—figure supplement 3*). The feature of the CN VI canals not penetrating the pituitary fossa seems typical for titanosaurs (e.g., *Carabajal, 2012*; *Knoll et al., 2015*; *Paulina-Carabajal et al., 2020*). Whereas *Knoll and Schwarz-Wings, 2009* note such a penetration or connection on the endocast of MB.R.1919, *Janensch, 1935*, originally described penetrating canals in the *Giraffatitan* specimens S 66 (on which the endocast MB.R.1919 is based) and Y 1. However, the specimen t 1 seems to show CN VI canals rather passing by the pituitary fossa. This may suggest a certain role of individual expressions (*Giraffatitan*), asymmetries (*Europasaurus*), and/or represents a phylogenetically potentially reasonable intermediate state (nonetheless, this feature may also be prone to preservational bias).

The endosseous labyrinth of *Europasaurus* (*Figure 6*) is most similar to *Giraffatitan* (*Janensch, 1935*) and *Spinophorosaurus* (*Knoll et al., 2012*) in bearing a relatively long ASC and a long lagena. In dorsal view, the anterior ampulla of the short LSC in *Europasaurus* displays a medially concave gap between the ASC and LSC (*Figure 6B,F,J*). Similarly, a pronounced concavity is present between the LSC and the PSC (best seen in dorsal view). Both concave gaps (the ASC and the PSC project further laterally than the lateral outline of the LSC reaches medially) are similarly present in many Titanosauriformes (with the exception of FAM 03.064; *Knoll et al., 2019*): *Giraffatitan* (*Janensch,*

1935), *Malawisaurus* (*Andrzejewski et al., 2019*), *Sarmientosaurus* (*Martínez et al., 2016*), CCMGE 628/12457 (*Sues et al., 2015*), *Jainosaurus* (*Andrzejewski et al., 2019*), *Ampelosaurus* (*Knoll et al., 2013*), *Narambuenatitan* (*Paulina-Carabajal et al., 2020*), *Bonatitan*, *Antarctosaurus*, MCF-PVPH 765 and MGPIFD-GR 118 (*Carabajal, 2012*), but also in the rebbachisaurids *Limaysaurus* and *Nigersaurus* (*Paulina-Carabajal and Calvo, 2021*). In contrast to other sauropods, the anterior portion of the LSC, as well as its lateral-most extent (best seen in dorsal view), seems somewhat posteriorly shifted in the macronarians *Camarasaurus* (*Witmer and Ridgely, 2008a*) and *Europasaurus* (*Figure 6B,F,J*; for further discussion, see *Supplementary file 1*).

Although the mediolateral width of the lagena does not appear to be associated with auditory capabilities (*Walsh et al., 2009*), the lagena of *Europasaurus* is conspicuously thick mediolaterally, especially when compared to its anteroposterior slenderness (*Figure 6*). The calculated auditory capacities (based on *Walsh et al., 2009*) impute *Europasaurus* a relatively wide hearing range with a high upper frequency limit (among non-avian dinosaurs; *Lautenschlager et al., 2012*; *King et al., 2020*; *Sakagami and Kawabe, 2020*). *Walsh et al., 2009*, demonstrate a certain correlation between hearing range, complexity of vocalizing, and aggregational behaviour in extant reptiles and birds (see also *Gleich et al., 2005*; *Hanson et al., 2021*). Following their conclusions and other studies suggesting (age-segregated) gregariousness in sauropodomorphs on the basis of nesting sites, body, and ichnofossils (e.g., *Lockley et al., 2002*; *Sander et al., 2008*; *Myers and Fiorillo, 2009*; *Pol et al., 2021a*), it appears plausible that *Europasaurus* lived in groups with conspecifics (although it is not clear whether this took place perennial or seasonal, e.g., for 'brooding'), which made airborne communication crucial. Furthermore, taphonomic reasons (femora count suggests at least 21 individuals in close temporal and spatial connection with very young and very old individuals being rarely represented; *Scheil et al., 2018*) and evidence for two morphotypes in the cranial and postcranial material of *Europasaurus* may suggest some form of social cohesion (*Carballido and Sander, 2013*; *Marpmann et al., 2014*). However, while a given species is likely to perceive sounds within the frequency spectrum it is able to produce, it may be rather unlikely that the full range of frequencies that can be heard is covered by the sound production ability (see also *Walsh et al., 2009*; *Senter, 2008*). Habitat preferences potentially play a role as well: 'acoustically cluttered' habitats like forests seem associated with a tendency towards high-frequency intraspecific communication in recent mammals (*Charlton et al., 2019*). Together with tropic Late Jurassic conditions in Europe (*Armstrong et al., 2016*), this may be part of the explanation of the recovered auditory capacities of *Europasaurus*.

Fragmentary bones and their eco-ontogenetic meaning

An interesting issue are the different morphological ontogenetic stages of DFMMh/FV 466 and DFMMh/FV 205 mentioned in *Marpmann et al., 2014*. The authors considered the prootic DFMMh/FV 466 more mature than the otoccipital DFMMh/FV 205. Indeed, DFMMh/FV 466 is about as large as the prootics of DFMMh/FV 581.1, DFMMh/FV 1077, DFMMh/FV 964, and DFMMh/FV 561 (*Figure 7*; *Figure 7—figure supplement 1*), but the otoccipital DFMMh/FV 205 is much smaller than the ones in DFMMh/FV 581.1 and DFMMh/FV 1077 (and only slightly larger than DFMMh/FV 981.2, DFMMh/FV 898, and DFMMh/FV 249; *Figure 8*; *Figure 8—figure supplement 1*).

In addition to general size of the specimens, and build and rugosity of articular facets, *Marpmann et al., 2014* (see also *Benton et al., 2010*) defined the morphological ontogenetic stages also by bone surface smoothness, advocating for vascularization: the smoother the surface, the lesser the degree of vascularization and – in tendency – the more mature the individual bone. Our findings support this (*Figures 7 and 8*; *Figure 7—figure supplement 2*; *Figure 8—figure supplement 2*). While the bases of individual cavities described herein may represent depressions of articulation areas, their deep penetration into the bone is unambiguous. Apart from this, the described structures might represent sutures. However, the position and orientation of individual cavities do not conform to what would be expected. Since these cavities make sense in the frame of morphological ontogenetic stages used in *Marpmann et al., 2014*, they are considered as so far unknown vascular expressions of juvenile *Europasaurus* individuals here.

DFMMh/FV 466 and DFMMh/FV 205 articulate very well with each other, especially on their lateral aspects. Additionally, there are cavities ventral to the LSC that seem to have been continuous originally (*Figure 5*; *Figure 7A, B*; *Figure 8G, H*, *Figure 5—figure supplement 1*). However, whereas the fenestra ovalis is considerably smaller than the vagal foramen in DFMMh/FV 581.1 and DFMMh/FV

1077 (***Figure 3B***; ***Figure 4—figure supplement 1A***), it seems that in DFMMh/FV 466+205 this is vice versa (although this impression may be due to the fragmentary nature of the latter two specimens; ***Figure 5L***; ***Figure 5—figure supplement 1F***). If DFMMh/FV 466 and DFMMh/FV 205 are in articulation, there is a large gap on their common dorsal aspect (***Figure 5J***; ***Figure 5—figure supplement 1H***). Considering DFMMh/FV 581.1 and DFMMh/FV 1077 and for example, the braincase of *Massospondylus* (***Chapelle and Choiniere, 2018***), the supraoccipital usually occupies this gap. In case our interpretation of a common bond between DFMMh/FV 466 and DFMMh/FV 205 is misleading and they actually represent two differently matured individuals, it is still noticeable that the preserved parts of the conjoined endosseous labyrinth of DFMMh/FV 466 and DFMMh/FV 205 display the same features as DFMMh/FV 581.1 and DFMMh/FV 1077 and is anteroposteriorly almost as long as the latter two specimens (***Figures 5 and 6***; ***Supplementary file 1***). This suggests an allometric growth between the prootic and otoccipital: during growth, the prootic reaches the 'adult' size faster than the otoccipital, producing a surprisingly small paroccipital process (or a surprisingly large prootic) in juvenile individuals of *Europasaurus* (seemingly, also seen in *Massospondylus*; ***Sues et al., 2004***), containing a relatively large endosseous labyrinth (see also ***Fabbri et al., 2021***, for ontogenetic transformations in the cranium of sauropodomorphs). A relatively large immature endosseous labyrinth is also present in the ornithischians *Dysalotosaurus* (***Lautenschlager and Hübner, 2013***), *Psitaccosaurus* (***Bullar et al., 2019***), and *Triceratops* (***Morhardt, 2018***). Furthermore, the inner ear is relatively large in juveniles of *Massospondylus* (***Neenan et al., 2019***) and the extant, precocial ostrich (***Romick, 2013***), and stays morphologically relatively stable throughout ontogeny (see also ***Jeffery and Spoor, 2004***).

The vestibular apparatus detects movements with the aid of endolymphatic fluid and cilia contained within the semicircular canals, which is crucial for locomotion (see, e.g., ***Benson et al., 2017***). Thus, a relatively large and morphologically adult-like endosseous labyrinth in expectedly very young individuals of *Europasaurus* suggests that hatchlings had to be light on their feet very fast in this dwarfed sauropod taxon.

Conclusion

Europasaurus has a rather sigmoid general braincase endocast shape, with a comparably large dorsal expansion, two openings for CN XII, an angle of 50° between the pituitary fossa and the LSC, and the ASC is clearly dorsoventrally higher than the PSC (***Figures 1–4*** and ***Figure 6***). This and additional novel details, such as the highly uniform vascular cavities within the juvenile braincase material (***Figures 7 and 8***; ***Figure 7—figure supplement 2***; ***Figure 8—figure supplement 2***), add to our knowledge about dinosaur neuroanatomy. The relatively small pituitary fossa (***Figure 1A***) in an insular dwarf lends support to the idea of being a proxy for body size (***Nopcsa, 1917***; ***Edinger, 1942***; ***Müller et al., 2021***).

Many sauropods were extremely large land-dwellers as adults, and still, started as tiny hatchlings, indicating enormously fast growth rates (e.g., ***Carpenter, 1999***; ***Hallett and Wedel, 2016***; ***Curry Rogers et al., 2016***). The threat arising from the discrepancy of several tens of tons between adults and juveniles makes it, among other reasons, unlikely that these animals were able to take good care for their offspring (e.g., ***Sander et al., 2011***; ***Curry Rogers et al., 2016***). This implies a great mobility early in life (precociality in a broader sense; see ***Dial, 2003***; ***Iwaniuk and Nelson, 2003***) of sauropods (***Sander et al., 2011***). Although *Europasaurus* represents an island dwarf (adults were probably not as dangerous for their juveniles), having roamed islands not exceeding an area of three times modern-day Bavaria (***Sander et al., 2006***), this taxon seemingly retained precociality (and therefore potentially r-strategy; ***Sander et al., 2008***; ***Myers and Fiorillo, 2009***; ***Hallett and Wedel, 2016***) from its large-bodied ancestors. As also suggested by the taphonomic circumstances (***Sander et al., 2006***; ***Carballido and Sander, 2013***; ***Marpmann et al., 2014***; see also ***Supplementary file 1***), *Europasaurus* individuals likely stayed in a certain social cohesion, and potentially practiced colonial nesting as is known from other sauropodomorphs (***Lockley et al., 2002***; ***Sander et al., 2008***; ***Myers and Fiorillo, 2009***; ***Pol et al., 2021b***). In concert with the approximate auditory capabilities offered here, our findings add hints towards the nature of aggregation with a certain complexity of reproductive and social behaviours for these little real-life titans, thriving in Europe some 154 Ma.

Materials and methods

The articulated braincase specimen of *E. holgeri*, DFMMh/FV 581.1, together with both loose parietals (FV 581.2 and 3), represents a braincase that is traversed by breakages but not strongly deformed, lacking parts of the anterior and dorsomedial skull roof, as well as the anteromedial walls of the endocranial cavity. The articulated and assembled braincase lacks the frontals, the right orbitosphenoid and laterosphenoid. The parietals are anteriorly, posterodorsomedially, and posteriorly incomplete and somewhat deformed (if they fit posteromedially with the supraoccipital they do not fit with the supraoccipital, prootic and laterosphenoid further anteriorly, and vice versa). The braincase of, for example, the macronarian *G. brancai* suggests a plain posterior skull roof not exceeding the dorsal extent of the sagittal nuchal crest; this served as an orientation here.

Macro-photography

All specimens, except DFMMh/FV 581.1, 2, and 3, were documented using a Canon EOS 70D reflex camera equipped with a Canon EFS 10–135 mm objective, extension tubes (13 or 21 mm), and a Canon Macro Twin Lite MT-26EX-RT. Light was cross-polarized in order to reduce reflections of the specimen surface. Images were recorded in different focal planes (z-stacks) and subsequently fused with CombineZP (Alan Hadley). All obtained images were optimized for colour balance, saturation, and sharpness using Adobe Photoshop CS2.

Micro-computed tomography

MicroCT of DFMMh/FV 581.1, 2, and 3 (***Figures 1–3***; ***Figure 1—figure supplements 1–4***) was performed using a Metrotom 1500 (Carl Zeiss Microscopy GmbH, Jena, Germany) in a subsidiary of Zeiss in Essingen; 1804 images were recorded with binning 1 resulting in a DICOM data set (for further details of settings and voxel size, see ***Supplementary file 1***).

All other specimens (***Figures 4, 5, 7 and 8***; ***Figure 4—figure supplements 1 and 2***; ***Figure 5—figure supplement 1***, ***Figure 7—figure supplements 1 and 2***; ***Figure 8—figure supplements 1 and 2***) were documented with a Xradia MicroXCT-200 (Carl Zeiss Microscopy GmbH, Jena, Germany) of the Imaging Center of the Department of Biology, University of Greifswald; 1600 projection images were recorded each, using 0.39× objective lens, with binning 2 (for further details of settings and voxel size for each specimen, see ***Supplementary file 1***). The tomographic images were reconstructed with XMReconstructor software (Carl Zeiss Microscopy GmbH, Jena, Germany), binning 1 (full resolution) resulting in image stacks (TIFF format).

Digital segmentation and measurements were produced utilizing the software Amira (5.6), based on DICOM files (DFMMh/FV 581.1, 2, and 3) and tiff files (remaining material). The microCT data were manually segmented to create 3D surface models. In DFMMh/FV 581.1, 2, and 3, the X-ray absorption of the fossil and the sediment within is quite similar, resulting in low contrast in many places. Furthermore, for preservational reasons (lack of both frontals, right orbitosphenoid, laterosphenoid, and loose parietals), the extent of the digital model of the endocast was conservatively estimated on the skull roof and on the anterodorsal region; some asymmetries on the endocast are explained by this circumstance.

Acknowledgements

We are extremely thankful towards Zeiss in Essingen (especially Bastian Zwick and Stephan Tomaschko), the Universitätsmedizin in Greifswald (especially Christopher Nell) for actuating their CT devices for the fossils of *Europasaurus*; further microCT were performed at the Imaging Center of the Department of Biology, University of Greifswald (DFG INST 292/119-1 FUGG; DFG INST 292/120-1 FUGG). We thank Michael 'Ede' Kenzler, Jakob Krieger, Georg Brenneis, Jennifer Legat, Steffen Harzsch, and Ingelore Hinz-Schallreuter (all University of Greifswald, Germany), together with Benjamin Englich (Dinosaurierpark Münchehagen, Germany) and Serjoscha Evers (University of Fribourg) for their support and discussions.

Additional information

Competing interests

Nils Knötschke: Nils Knötschke is affiliated with Mineralientage. The author has no financial interests to declare. The other authors declare that no competing interests exist.

Funding

Funder	Grant reference number	Author
Universität Greifswald	Bogislaw scholarship	Marco Schade
Deutsche Forschungsgemeinschaft	DFG INST 292/119-1 FUGG	Marie Hörnig
Deutsche Forschungsgemeinschaft	DFG INST 292/120-1 FUGG	Marie Hörnig

The funders had no role in study design, data collection and interpretation, or the decision to submit the work for publication.

Author contributions

Marco Schade, Conceptualization, Resources, Data curation, Software, Formal analysis, Investigation, Visualization, Methodology, Writing – original draft, Project administration, Writing – review and editing; Nils Knötschke, Supervision, Validation, Investigation, Writing – original draft; Marie Hörnig, Resources, Software, Investigation, Visualization, Methodology, Writing – original draft; Carina Paetzel, Software, Formal analysis, Investigation, Visualization, Methodology, Writing – original draft; Sebastian Stumpf, Software, Formal analysis, Investigation, Visualization, Methodology, Writing – original draft, S.S. prepared the figures and contributed to the manuscript

Author ORCIDs

Marco Schade http://orcid.org/0000-0003-1658-6854
Sebastian Stumpf http://orcid.org/0000-0002-1945-2387

Additional files

Supplementary files

- Supplementary file 1. Supplementary information, scan details, and measurements.
- MDAR checklist

Data availability

The microCT data and neuroanatomical models of all fossil specimens depicted herein are published online, in the repository MorphoSource (Europasaurus holgeri - neuroanatomy - DFMMh/FV - Schade et al. 2023 // MorphoSource).

The following dataset was generated:

Author(s)	Year	Dataset title	Dataset URL	Database and Identifier
Marco S	2022	Europasaurus holgeri - neuroanatomy - DFMMh/FV - Schade et al. 2023	https://www.morphosource.org/projects/000445173?locale=en	morphosource, 000445173

References

Andrzejewski KA, Polcyn MJ, Winkler DA, Gomani Chindebvu E, Jacobs LL. 2019. The braincase of malawisaurus dixeyi (sauropoda: titanosauria): a 3D reconstruction of the brain endocast and inner ear. *PLOS ONE* **14**:e0211423. DOI: https://doi.org/10.1371/journal.pone.0211423, PMID: 30759166

Armstrong HA, Wagner T, Herringshaw LG, Farnsworth AJ, Lunt DJ, Harland M, Imber J, Loptson C, Atar EFL. 2016. Hadley circulation and precipitation changes controlling black shale deposition in the late Jurassic boreal seaway. *Paleoceanography* **31**:1041–1053. DOI: https://doi.org/10.1002/2015PA002911

Balanoff AM, Bever GS, Ikejiri T. 2010. The braincase of apatosaurus (dinosauria: sauropoda) based on computed tomography of a new specimen with comments on variation and evolution in sauropod neuroanatomy. *American Museum Novitates* **3677**:1–32. DOI: https://doi.org/10.1206/591.1

Ballell A, King JL, Neenan JM, Rayfield EJ, Benton MJ. 2021. The braincase, brain and palaeobiology of the basal sauropodomorph dinosaur thecodontosaurus antiquus . *Zoological Journal of the Linnean Society* **193**:541–562. DOI: https://doi.org/10.1093/zoolinnean/zlaa157

Bates KT, Mannion PD, Falkingham PL, Brusatte SL, Hutchinson JR, Otero A, Sellers WI, Sullivan C, Stevens KA, Allen V. 2016. Temporal and phylogenetic evolution of the sauropod dinosaur body plan. *Royal Society Open Science* **3**:150636. DOI: https://doi.org/10.1098/rsos.150636, PMID: 27069652

Benson RBJ, Starmer-Jones E, Close RA, Walsh SA. 2017. Comparative analysis of vestibular ecomorphology in birds. *Journal of Anatomy* **231**:990–1018. DOI: https://doi.org/10.1111/joa.12726, PMID: 29156494

Benton MJ, Csiki Z, Grigorescu D, Redelstorff R, Sander PM, Stein K, Weishampel DB. 2010. Dinosaurs and the island rule: the dwarfed dinosaurs from haţeg island. *Palaeogeography, Palaeoclimatology, Palaeoecology* **293**:438–454. DOI: https://doi.org/10.1016/j.palaeo.2010.01.026

Bronzati M, Benson RBJ, Rauhut OWM, Mannion P. 2018. Rapid transformation in the braincase of sauropod dinosaurs: integrated evolution of the braincase and neck in early sauropods? *Palaeontology* **61**:289–302. DOI: https://doi.org/10.1111/pala.12344

Bronzati M, Benson RBJ, Evers SW, Ezcurra MD, Cabreira SF, Choiniere J, Dollman KN, Paulina-Carabajal A, Radermacher VJ, Roberto-da-Silva L, Sobral G, Stocker MR, Witmer LM, Langer MC, Nesbitt SJ. 2021. Deep evolutionary diversification of semicircular canals in archosaurs. *Current Biology* **31**:2520–2529. DOI: https://doi.org/10.1016/j.cub.2021.03.086

Bullar CM, Zhao Q, Benton MJ, Ryan MJ. 2019. Ontogenetic braincase development in psittacosaurus lujiatunensis (dinosauria: ceratopsia) using micro-computed tomography. *PeerJ* **7**:e7217. DOI: https://doi.org/10.7717/peerj.7217, PMID: 31428535

Carabajal AP. 2012. Neuroanatomy of titanosaurid dinosaurs from the upper cretaceous of patagonia, with comments on endocranial variability within sauropoda. *Anatomical Record* **295**:2141–2156. DOI: https://doi.org/10.1002/ar.22572, PMID: 22961834

Carballido JL, Sander MP. 2013. Postcranial axial skeleton of europasaurus holgeri (dinosauria, sauropoda) from the upper jurassic of germany: implications for sauropod ontogeny and phylogenetic relationships of basal macronaria. *J. Syst. Palaeontol* **12**:335–387. DOI: https://doi.org/10.1080/14772019.2013.764935

Carpenter K. 1999. Eggs, Nests and Baby Dinosaurs: A Look at Dinosaur Reproduction. Indiana University Press.

Chapelle KEJ, Choiniere JN. 2018. A revised cranial description of *massospondylus carinatus* owen (dinosauria: sauropodomorpha) based on computed tomographic scans and A review of cranial characters for basal sauropodomorpha. *PeerJ* **6**:e4224. DOI: https://doi.org/10.7717/peerj.4224, PMID: 29340238

Charlton BD, Owen MA, Swaisgood RR. 2019. Coevolution of vocal signal characteristics and hearing sensitivity in forest mammals. *Nature Communications* **10**:2778. DOI: https://doi.org/10.1038/s41467-019-10768-y, PMID: 31239439

Choiniere JN, Neenan JM, Schmitz L, Ford DP, Chapelle KEJ, Balanoff AM, Sipla JS, Georgi JA, Walsh SA, Norell MA, Xu X, Clark JM, Benson RBJ. 2021. Evolution of vision and hearing modalities in theropod dinosaurs. *Science* **372**:610–613. DOI: https://doi.org/10.1126/science.abe7941, PMID: 33958472

Curry Rogers K, Forster CA. 2001. The last of the dinosaur titans: a new sauropod from madagascar. *Nature* **412**:530–534. DOI: https://doi.org/10.1038/35087566, PMID: 11484051

Curry Rogers K, Whitney M, D'Emic M, Bagley B. 2016. Precocity in a tiny titanosaur from the cretaceous of madagascar. *Science* **352**:450–453. DOI: https://doi.org/10.1126/science.aaf1509, PMID: 27102482

David R, Bronzati M, Benson RBJ. 2022. Comment on "the early origin of a birdlike inner ear and the evolution of dinosaurian movement and vocalization." *Science* **376**:eabl6710. DOI: https://doi.org/10.1126/science.abl6710, PMID: 35737763

Dial KP. 2003. Evolution of avian locomotion: correlates of flight style, locomotor modules, nesting biology, body size, development, and the origin of flapping flight. *The Auk* **120**:941. DOI: https://doi.org/10.1642/0004-8038(2003)120[0941:EOALCO]2.0.CO;2

Edinger T. 1942. The pituitary body in giant animals fossil and living: a survey and a suggestion. *The Quarterly Review of Biology* **17**:31–45. DOI: https://doi.org/10.1086/394644

Evans DC. 2005. New evidence on brain-endocranial cavity relationships in ornithischian dinosaurs. *Acta Palaeontologica Polonica* **50**:617–622.

Ezcurra MD, Nesbitt SJ, Bronzati M, Dalla Vecchia FM, Agnolin FL, Benson RBJ, Brissón Egli F, Cabreira SF, Evers SW, Gentil AR, Irmis RB, Martinelli AG, Novas FE, Roberto da Silva L, Smith ND, Stocker MR, Turner AH, Langer MC. 2020. Enigmatic dinosaur precursors bridge the gap to the origin of pterosauria. *Nature* **588**:445–449. DOI: https://doi.org/10.1038/s41586-020-3011-4, PMID: 33299179

Fabbri M, Mongiardino Koch N, Pritchard AC, Hanson M, Hoffman E, Bever GS, Balanoff AM, Morris ZS, Field DJ, Camacho J, Rowe TB, Norell MA, Smith RM, Abzhanov A, Bhullar B-AS. 2017. The skull roof tracks the brain during the evolution and development of reptiles including birds. *Nature Ecology & Evolution* **1**:1543–1550. DOI: https://doi.org/10.1038/s41559-017-0288-2, PMID: 29185519

Fabbri M, Navalón G, Mongiardino Koch N, Hanson M, Petermann H, Bhullar BA. 2021. A shift in ontogenetic timing produced the unique sauropod skull. *Evolution; International Journal of Organic Evolution* **75**:819–831. DOI: https://doi.org/10.1111/evo.14190, PMID: 33578446

Garderes JP, Gallina PA, Whitlock JA, Toledo N. 2022. Neuroanatomy of a diplodocid sauropod dinosaur from the lower cretaceous of patagonia, argentina. *Cretaceous Research* **129**:105024. DOI: https://doi.org/10.1016/j.cretres.2021.105024
Gleich O, Dooling RJ, Manley GA. 2005. Audiogram, body mass, and basilar papilla length: correlations in birds and predictions for extinct archosaurs. *Die Naturwissenschaften* **92**:595–598. DOI: https://doi.org/10.1007/s00114-005-0050-5, PMID: 16231131
Hallett M, Wedel MJ. 2016. The Sauropod Dinosaurs. Life in the Age of Giants. Johns Hopkins University Press.
Hanson M, Hoffman EA, Norell MA, Bhullar BAS. 2021. The early origin of a birdlike inner ear and the evolution of dinosaurian movement and vocalization. *Science* **372**:601–609. DOI: https://doi.org/10.1126/science.abb4305, PMID: 33958471
Iwaniuk AN, Nelson JE. 2003. Developmental differences are correlated with relative brain size in birds: a comparative analysis. *Canadian Journal of Zoology* **81**:1913–1928. DOI: https://doi.org/10.1139/z03-190
Janensch W. 1935. Die schädel der sauropoden brachiosaurus, barosaurus und dicraeosaurus aus den tendaguru-schichten deutsch-ostafrikas. *Palaeontographica, Suppl* **7**:147–298.
Jeffery N, Spoor F. 2004. Prenatal growth and development of the modern human labyrinth. *Journal of Anatomy* **204**:71–92. DOI: https://doi.org/10.1111/j.1469-7580.2004.00250.x, PMID: 15032915
King JL, Sipla JS, Georgi JA, Balanoff AM, Neenan JM. 2020. The endocranium and trophic ecology of velociraptor mongoliensis. *Journal of Anatomy* **237**:861–869. DOI: https://doi.org/10.1111/joa.13253, PMID: 32648601
Knoll F, Schwarz-Wings D. 2009. Palaeoneuroanatomy of brachiosaurus. *Annales de Paléontologie* **95**:165–175. DOI: https://doi.org/10.1016/j.annpal.2009.06.001
Knoll F, Witmer LM, Ortega F, Ridgely RC, Schwarz-Wings D. 2012. The braincase of the basal sauropod dinosaur spinophorosaurus and 3D reconstructions of the cranial endocast and inner ear. *PLOS ONE* **7**:e30060. DOI: https://doi.org/10.1371/journal.pone.0030060, PMID: 22272273
Knoll F, Ridgely RC, Ortega F, Sanz JL, Witmer LM. 2013. Neurocranial osteology and neuroanatomy of a late cretaceous titanosaurian sauropod from spain (ampelosaurus sp.). *PLOS ONE* **8**:e54991. DOI: https://doi.org/10.1371/journal.pone.0054991, PMID: 23355905
Knoll F., Witmer LM, Ridgely RC, Ortega F, Sanz JL. 2015. A new titanosaurian braincase from the Cretaceous " lo hueco " locality in Spain sheds light on neuroanatomical evolution within titanosauria. *PLOS ONE* **10**:e0138233. DOI: https://doi.org/10.1371/journal.pone.0138233, PMID: 26444700
Knoll F, Lautenschlager S, Valentin X, Díez Díaz V, Pereda Suberbiola X, Garcia G. 2019. First palaeoneurological study of a sauropod dinosaur from france and its phylogenetic significance. *PeerJ* **7**:e7991. DOI: https://doi.org/10.7717/peerj.7991, PMID: 31763068
Knoll F, Lautenschlager S, Kawabe S, Martínez G, Espílez E, Mampel L, Alcalá L. 2021. Palaeoneurology of the early cretaceous iguanodont proa valdearinnoensis and its bearing on the parallel developments of cognitive abilities in theropod and ornithopod dinosaurs. *The Journal of Comparative Neurology* **529**:3922–3945. DOI: https://doi.org/10.1002/cne.25224, PMID: 34333763
Lautenschlager S, Rayfield EJ, Altangerel P, Zanno LE, Witmer LM. 2012. The endocranial anatomy of therizinosauria and its implications for sensory and cognitive function. *PLOS ONE* **7**:e52289. DOI: https://doi.org/10.1371/journal.pone.0052289, PMID: 23284972
Lautenschlager S, Hübner T. 2013. Ontogenetic trajectories in the ornithischian endocranium. *Journal of Evolutionary Biology* **26**:2044–2050. DOI: https://doi.org/10.1111/jeb.12181, PMID: 23682701
Lockley MG, Schulp AS, Meyer CA, Leonardi G, Mamani DK. 2002. Titanosaurid trackways from the upper cretaceous of bolivia: evidence for large manus, wide-gauge locomotion, and gregarious behaviour. *Cret. Res* **23**:383–400. DOI: https://doi.org/10.1006/cres.2002.1006
Lokatis S, Jeschke JM. 2018. The island rule: an assessment of biases and research trends. *Journal of Biogeography* **45**:289–303. DOI: https://doi.org/10.1111/jbi.13160
Marpmann JS, Carballido JL, Sander MP, Knötschke N. 2014. Cranial anatomy of the late jurassic dwarf sauropod europasaurus holgeri (dinosauria, camarasauromorpha): ontogenetic changes and size dimorphism. *Journal of Systematic Palaeontology* **1**:875074. DOI: https://doi.org/10.1080/14772019.2013.875074
Martínez RDF, Lamanna MC, Novas FE, Ridgely RC, Casal GA, Martínez JE, Vita JR, Witmer LM. 2016. A basal lithostrotian titanosaur (dinosauria: sauropoda) with A complete skull: implications for the evolution and paleobiology of titanosauria. *PLOS ONE* **11**:e0151661. DOI: https://doi.org/10.1371/journal.pone.0151661
Morhardt AC. 2016. Doctoral dissertation: Gross Anatomical Brain Region Approximation (GABRA): Assessing Brain Size, Structure, and Evolution in Extinct Archosaurs. Ohio University.
Morhardt AC. 2018. Study of endocranial & ontogeny in the late cretaceous non-avian dinosaur genus triceratops using computed tomography & 3D visualization. Poster.
Müller R. 2021. Olfactory acuity in early sauropodomorph dinosaurs. *Historical Biology* **34**:1914600. DOI: https://doi.org/10.1080/08912963.2021.1914600
Müller RT, Ferreira JD, Pretto FA, Bronzati M, Kerber L. 2021. The endocranial anatomy of buriolestes schultzi (dinosauria: saurischia) and the early evolution of brain tissues in sauropodomorph dinosaurs. *Journal of Anatomy* **238**:809–827. DOI: https://doi.org/10.1111/joa.13350, PMID: 33137855
Myers TS, Fiorillo AR. 2009. Evidence for gregarious behavior and age segregation in sauropod dinosaurs. *Palaeogeography, Palaeoclimatology, Palaeoecology* **274**:96–104. DOI: https://doi.org/10.1016/j.palaeo.2009.01.002

Neenan JM, Reich T, Evers SW, Druckenmiller PS, Voeten D, Choiniere JN, Barrett PM, Pierce SE, Benson RBJ. 2017. Evolution of the sauropterygian labyrinth with increasingly pelagic lifestyles. *Current Biology* **27**:3852–3858. DOI: https://doi.org/10.1016/j.cub.2017.10.069, PMID: 29225027

Neenan JM, Chapelle KEJ, Fernandez V, Choiniere JN, Mannion P. 2019. Ontogeny of the massospondylus labyrinth: implications for locomotory shifts in a basal sauropodomorph dinosaur. *Palaeontology* **62**:255–265. DOI: https://doi.org/10.1111/pala.12400

Nopcsa FV. 1917. Über dinosaurier. 2. die riesenformen unter den dinosauriern centralblatt. *Für Mineralogie* **1917**:332–351.

Paul GS. 1988. The brachiosaur giants of the morrison and tendaguru with a description of a new subgenus, giraffatitan, and a comparison of the world's largest dinosaurs. *Hunteria* **2**:1–14.

Paulina-Carabajal A, Lee YN, Jacobs LL. 2016. Endocranial morphology of the primitive nodosaurid dinosaur pawpawsaurus campbelli from the early cretaceous of north america. *PLOS ONE* **11**:e0150845. DOI: https://doi.org/10.1371/journal.pone.0150845, PMID: 27007950

Paulina Carabajal A., Coria RA, Currie PJ, Koppelhus EB. 2018. A natural cranial endocast with possible dicraeosaurid (sauropoda, diplodocoidea) affinities from the lower Cretaceous of Patagonia. *Cretaceous Research* **84**:437–441. DOI: https://doi.org/10.1016/j.cretres.2017.12.001

Paulina-Carabajal A, Filippi L, Knoll F. 2020. Neuroanatomy of the titanosaurian sauropod narambuenatitan palomoi from the upper cretaceous of patagonia, argentina. *Pe APA* **20**:1–9.

Paulina Carabajal A, Carballido JL, Currie PJ. 2014. Braincase, neuroanatomy, and neck posture of amargasaurus cazaui (sauropoda, dicraeosauridae) and its implications for understanding head posture in sauropods. *Journal of Vertebrate Paleontology* **34**:870–882. DOI: https://doi.org/10.1080/02724634.2014.838174

Paulina-Carabajal A, Calvo JO. 2021. Re-description of the braincase of the rebbachisaurid sauropod limaysaurus tessonei and novel endocranial information based on CT scans. *Anais Da Academia Brasileira de Ciencias* **93**:e20200762. DOI: https://doi.org/10.1590/0001-3765202120200762, PMID: 33533794

Pol D, Mancuso AC, Smith RMH, Marsicano CA, Ramezani J, Cerda IA, Otero A, Fernandez V. 2021a. Earliest evidence of herd-living and age segregation amongst dinosaurs. *Scientific Reports* **11**:20023. DOI: https://doi.org/10.1038/s41598-021-99176-1, PMID: 34675327

Pol D, Otero A, Apaldetti C, Martínez RN. 2021b. Triassic sauropodomorph dinosaurs from south america: the origin and diversification of dinosaur dominated herbivorous faunas. *Journal of South American Earth Sciences* **107**:103145. DOI: https://doi.org/10.1016/j.jsames.2020.103145

Rauhut OWM, Holwerda FM, Furrer H. 2020. A derived sauropodiform dinosaur and other sauropodomorph material from the late triassic of canton schaffhausen, switzerland. *Swiss Journal of Geosciences* **113**:00360-8. DOI: https://doi.org/10.1186/s00015-020-00360-8

Romick CA. 2013. Undergraduate thesis: Ontogeny of the brain endocasts of Ostriches (Aves: Struthio camelus) with implications for interpreting extinct dinosaur endocasts. OhioLINK Electronic Theses and Dissertations Center.

Sakagami R, Kawabe S. 2020. Endocranial anatomy of the ceratopsid dinosaur triceratops and interpretations of sensory and motor function. *PeerJ* **8**:e9888. DOI: https://doi.org/10.7717/peerj.9888

Sander PM, Mateus O, Laven T, Knötschke N. 2006. Bone histology indicates insular dwarfism in a new late jurassic sauropod dinosaur. *Nature* **441**:739–741. DOI: https://doi.org/10.1038/nature04633, PMID: 16760975

Sander PM, Peitz C, Jackson FD, Chiappe LM. 2008. Upper cretaceous titanosaur nesting sites and their implications for sauropod dinosaur reproductive biology. *Palaeontogr. A* **284**:69–107.

Sander PM, Christian A, Clauss M, Fechner R, Gee CT, Griebeler EM, Gunga HC, Hummel J, Mallison H, Perry SF, Preuschoft H, Rauhut OWM, Remes K, Tütken T, Wings O, Witzel U. 2011. Biology of the sauropod dinosaurs: the evolution of gigantism. *Biological Reviews of the Cambridge Philosophical Society* **86**:117–155. DOI: https://doi.org/10.1111/j.1469-185X.2010.00137.x, PMID: 21251189

Schade M, Rauhut OWM, Evers SW. 2020. Irritator challengeri SMNS 58022 neuroanatomy. 00000C951. MorphoSource. https://www.morphosource.org/Detail/ProjectDetail/Show/project_id/951

Scheil M, Wings O, Knötschke N, Sander M. 2018. The Age Structure of the Europasaurus Holgeri Assemblage from the Langenberg Quarry, Upper Jurassic, Germany. Poster.

Schwab JA, Young MT, Neenan JM, Walsh SA, Witmer LM, Herrera Y, Allain R, Brochu CA, Choiniere JN, Clark JM, Dollman KN, Etches S, Fritsch G, Gignac PM, Ruebenstahl A, Sachs S, Turner AH, Vignaud P, Wilberg EW, Xu X, et al. 2020. Inner ear sensory system changes as extinct crocodylomorphs transitioned from land to water. *PNAS* **117**:10422–10428. DOI: https://doi.org/10.1073/pnas.2002146117, PMID: 32312812

Schwab JA, Young MT, Herrera Y, Witmer LM, Walsh SA, Katsamenis OL, Brusatte SL. 2021. The braincase and inner ear of 'metriorhynchus' cf. 'M.' brachyrhynchus – implications for aquatic sensory adaptations in crocodylomorphs. *Journal of Vertebrate Paleontology* **1**:1912062. DOI: https://doi.org/10.1080/02724634.2021.1912062

Senter P. 2008. Voices of the past: a review of paleozoic and Mesozoic animal sounds. *Historical Biology* **20**:255–287. DOI: https://doi.org/10.1080/08912960903033327

Sereno PC, Wilson JA, Witmer LM, Whitlock JA, Maga A, Ide O, Rowe TA. 2007. Structural extremes in a Cretaceous dinosaur. *PLOS ONE* **2**:e1230. DOI: https://doi.org/10.1371/journal.pone.0001230, PMID: 18030355

Stein K, Csiki Z, Rogers KC, Weishampel DB, Redelstorff R, Carballido JL, Sander PM. 2010. Small body size and extreme cortical bone remodeling indicate phyletic dwarfism in magyarosaurus dacus (sauropoda: titanosauria). *PNAS* **107**:9258–9263. DOI: https://doi.org/10.1073/pnas.1000781107, PMID: 20435913

Sues HD, Reisz RR, Hinic S, Raath MA. 2004. On the skull of massospondylus carinatus Owen, 1854 (dinosauria: sauropodomorpha) from the Elliot and clarens formations (lower Jurassic) of South Africa. *Annals of the Carnegie Museum* **73**:239–257. DOI: https://doi.org/10.5962/p.316084

Sues HD, Averianov A, Ridgely RC, Witmer LMT. 2015. Titanosauria (dinosauria, sauropoda) from the upper Cretaceous (turonian) bissekty formation of uzbekistan. *Journal of Vertebrate Paleontology* **35**:e889145. DOI: https://doi.org/10.1080/02724634.2014.889145

Taylor MP. 2009. A re-evaluation of brachiosaurus altithorax riggs 1903 (dinosauria, sauropoda) and its generic separation from giraffatitan brancai (janensch 1914) . *Journal of Vertebrate Paleontology* **29**:787–806. DOI: https://doi.org/10.1671/039.029.0309

Walsh SA, Barrett PM, Milner AC, Manley G, Witmer LM. 2009. Inner ear anatomy is a proxy for deducing auditory capability and behaviour in reptiles and birds. *Proceedings. Biological Sciences* **276**:1355–1360. DOI: https://doi.org/10.1098/rspb.2008.1390, PMID: 19141427

Watanabe A, Gignac PM, Balanoff AM, Green TL, Kley NJ, Norell MA. 2019. Are endocasts good proxies for brain size and shape in archosaurs throughout ontogeny? *Journal of Anatomy* **234**:291–305. DOI: https://doi.org/10.1111/joa.12918, PMID: 30506962

Witmer LM, Ridgely RC. 2008a. Structure of the brain cavity and inner ear of the centrosaurine ceratopsid dinosaur pachyrhinosaurus based on CT scanning and 3D visualization. Geoscienceworld.

Witmer LM, Ridgely RC, Dufeau DL, Semones MC. 2008b. Using CT to peer into the past: 3D visualization of the brain and ear regions of birds, crocodiles, and nonavian dinosaurs. Endo H, Frey R (Eds). *Anatomical Imaging: Towards a New Morphology*. Tokyo: Springer. p. 1–10. DOI: https://doi.org/10.1007/978-4-431-76933-0

Witmer LM, Ridgely RC. 2009. New insights into the brain, braincase, and ear region of tyrannosaurs (dinosauria, theropoda), with implications for sensory organization and behavior. *Anatomical Record* **292**:1266–1296. DOI: https://doi.org/10.1002/ar.20983, PMID: 19711459

Zuo F, Heimhofer U, Huck S, Luppold FW, Wings O, Erbacher J. 2018. Sedimentology and depositional sequences of a kimmeridgian carbonate ramp system, lower saxony basin, northern germany. *Facies* **64**. DOI: https://doi.org/10.1007/s10347-017-0513-0

Figures and figure supplements

Neurovascular anatomy of dwarf dinosaur implies precociality in sauropods

Marco Schade *et al*.

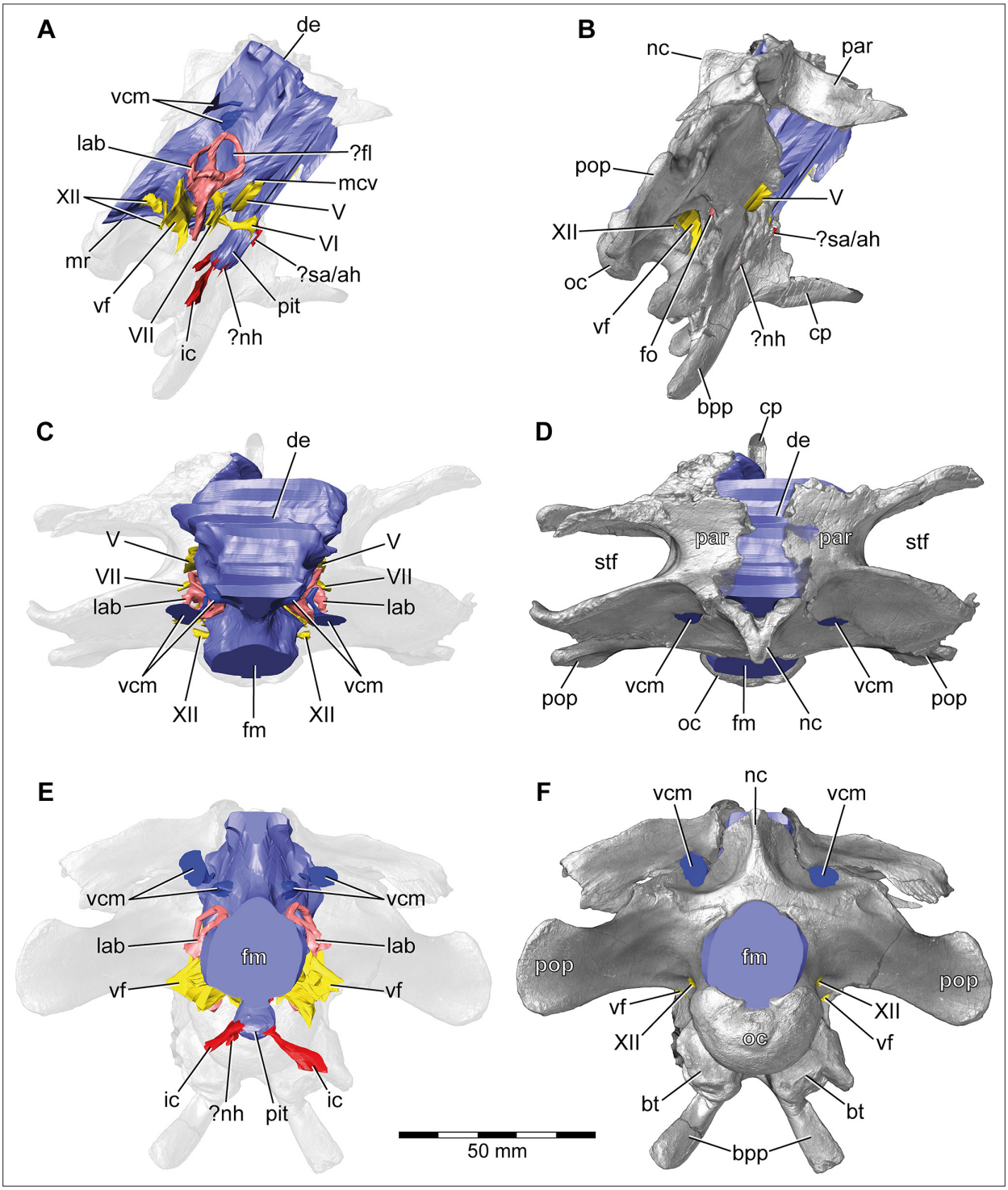

Figure 1. *Europasaurus holgeri*, 3D model of the braincase endocast with endosseous labyrinths and neurovascular canals of DFMMh/FV 581.1, 2, and 3 with transparent (**A,C,E**) and covering (**B,D,F**) volume rendering of the bony braincase in (**A,B**) right lateral, (**C,D**) dorsal, and (**E,F**) posterior view. Note that scale mainly applies to posterior perspective (**E,F**).?fl, potential floccular recess; ?nh, potential canal for the neurohypophysis; ?sa/ah, potential sphenoidal artery/canal for the adenohypophysis; bpp, basipterygoid process; bt, basal tuber; cp, cultriform process; de, dorsal expansion; ic, internal carotid; fm, foramen magnum; fo, fenestra ovalis; lab, endosseous labyrinth; mcv, mid cerebral vein; mr, medial ridge; nc, sagittal nuchal crest; oc, occipital condyle; par, parietal; pit, pituitary; pop, paroccipital process; stf, supratemporal fenestra; vcm, vena capitis media; vf, vagal foramen; V, trigeminal nerve; VI, abducens nerve; VII, facial nerve; XII, hypoglossal nerve.

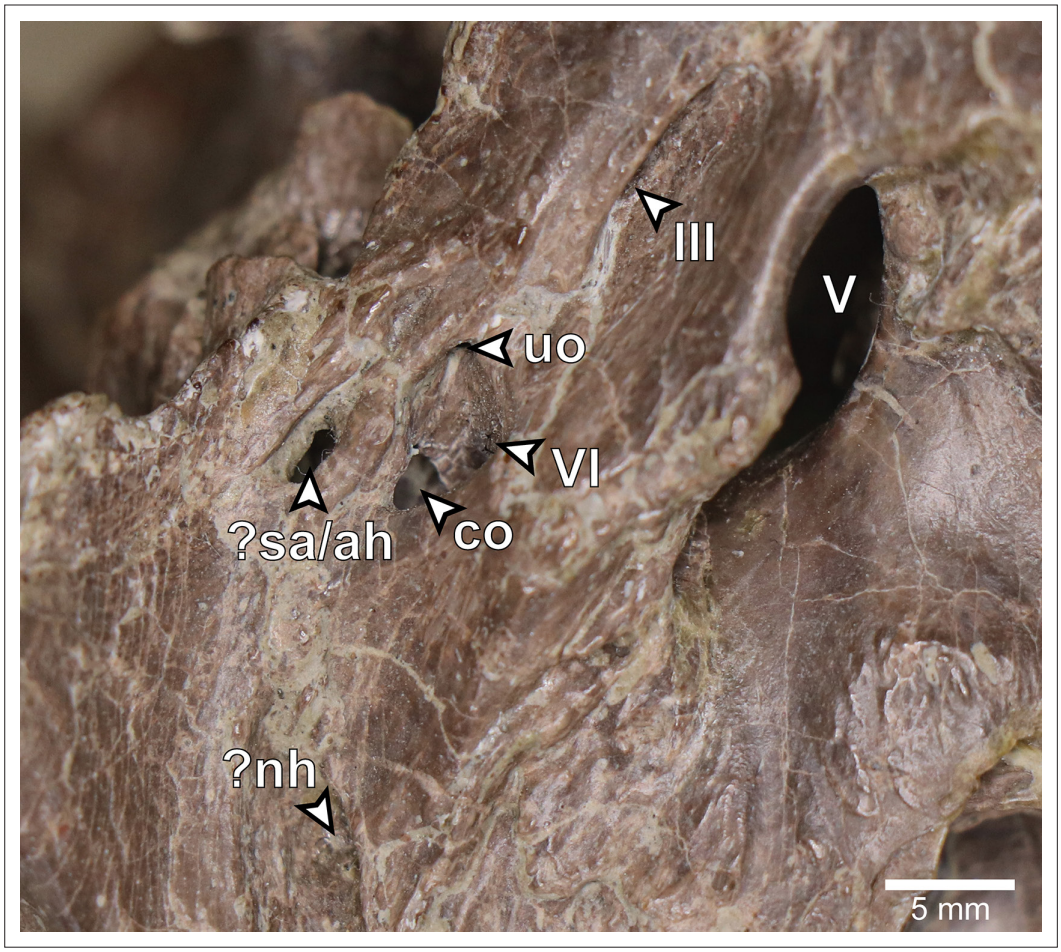

Figure 1—figure supplement 1. *Europasaurus holgeri*, close-up of left lateral aspect of DFMMh/FV 581.1. ?nh, potential opening for the neurohypophysis; ?sa/ah, potential sphenoidal artery opening/opening for adenohypophysis canal; co, connection between the abducens nerve canal (CN VI) and the pituitary fossa; uo, unclear opening; III, oculomotor nerve opening; V, trigeminal nerve opening; VI, abducens nerve opening.

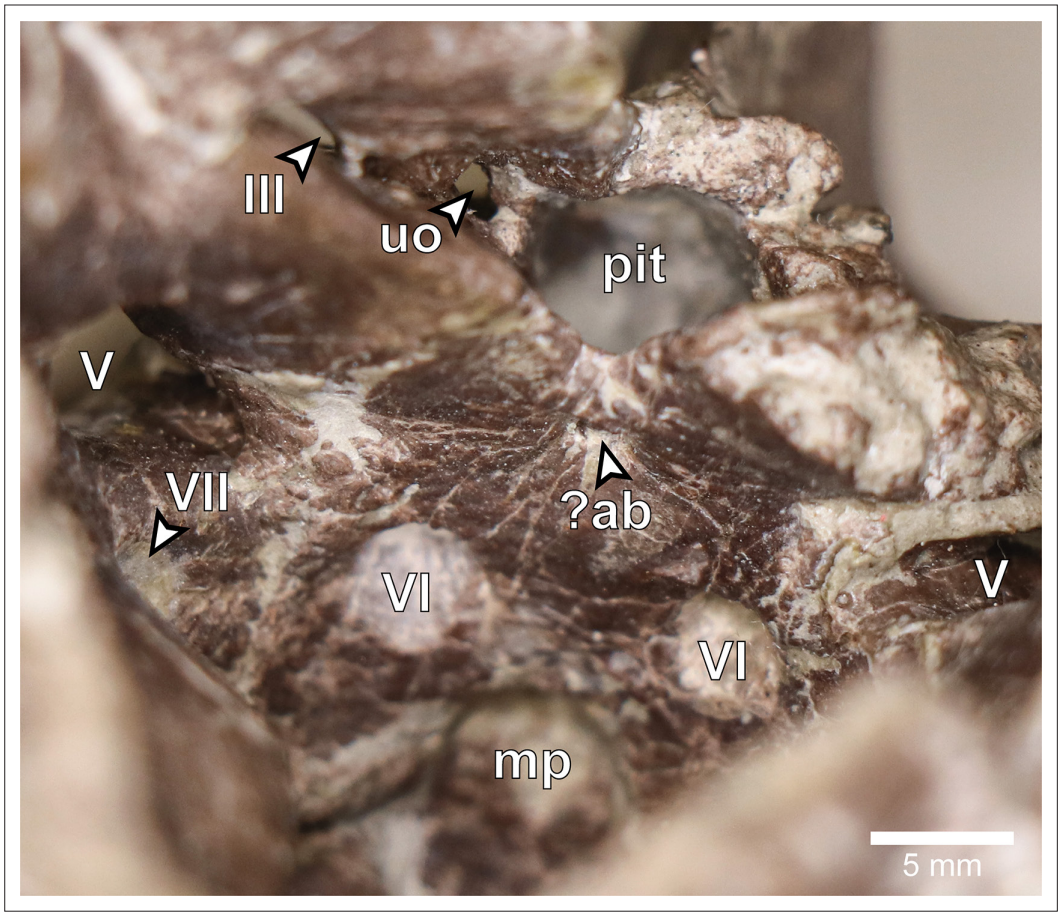

Figure 1—figure supplement 2. *Europasaurus holgeri*, close-up of anterior endocranial floor of DFMMh/FV 581.1 in dorsal view. ?ab, potential basilar artery opening; mp, median fossa producing the median protuberance on the ventral braincase endocast; pit, pituitary fossa; uo, unclear opening; III, oculomotor nerve opening; V, trigeminal nerve opening; VI, abducens nerve opening; VII, facial nerve opening.

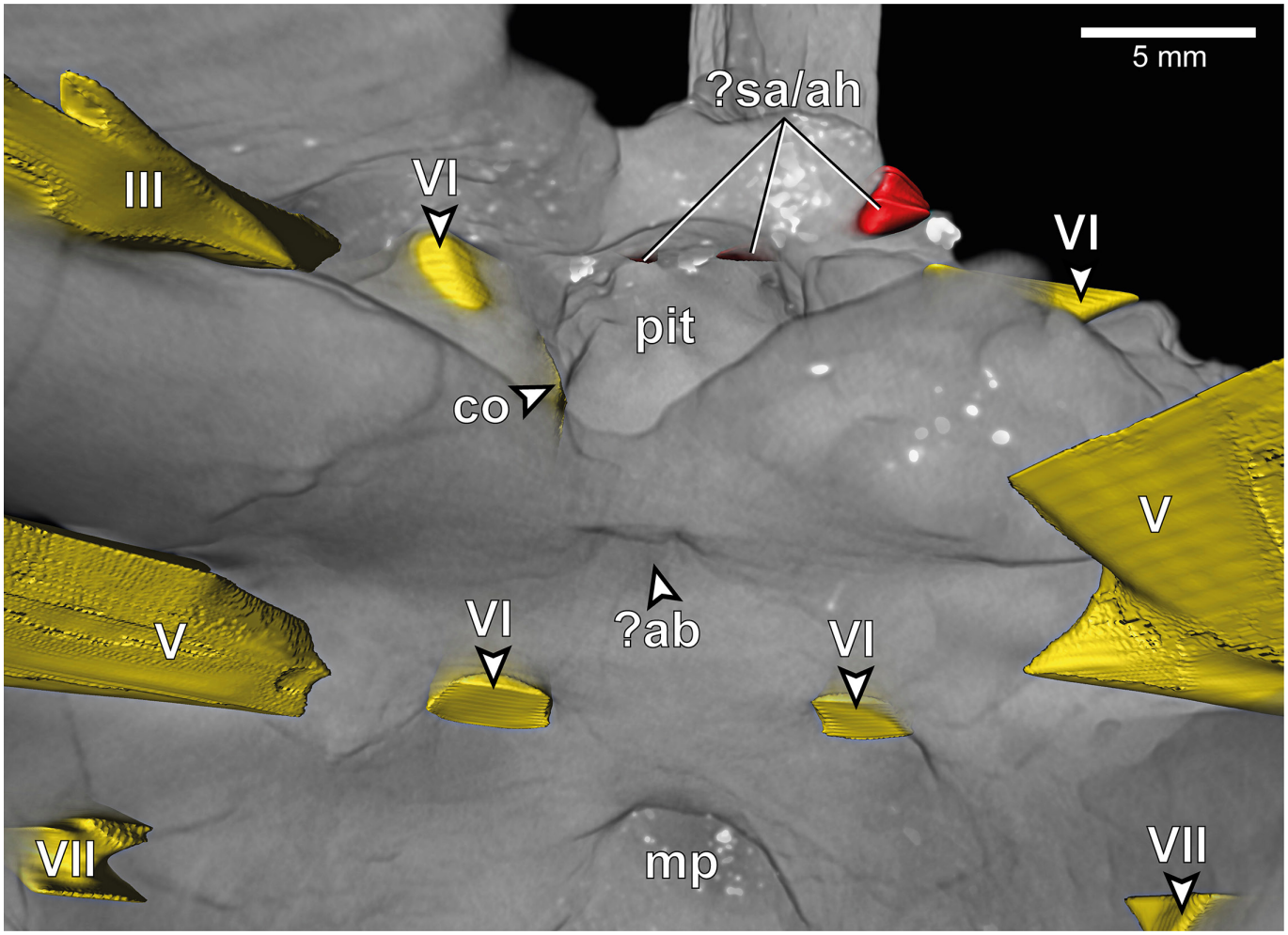

Figure 1—figure supplement 3. *Europasaurus holgeri*, close-up of 3D model of anterior endocranial floor of DFMMh/FV 581.1 in dorsal view. ?ab, potential basilar artery opening; ?sa/ah, potential sphenoidal artery opening/opening for adenohypophysis canal; co, connection between the abducens nerve canal (CN VI) and the pituitary fossa; mp, median fossa producing the median protuberance on the ventral braincase endocast; uo, unclear opening; pit, pituitary fossa; III, oculomotor nerve opening; V, trigeminal nerve opening; VI, abducens nerve opening; VII, facial nerve opening.

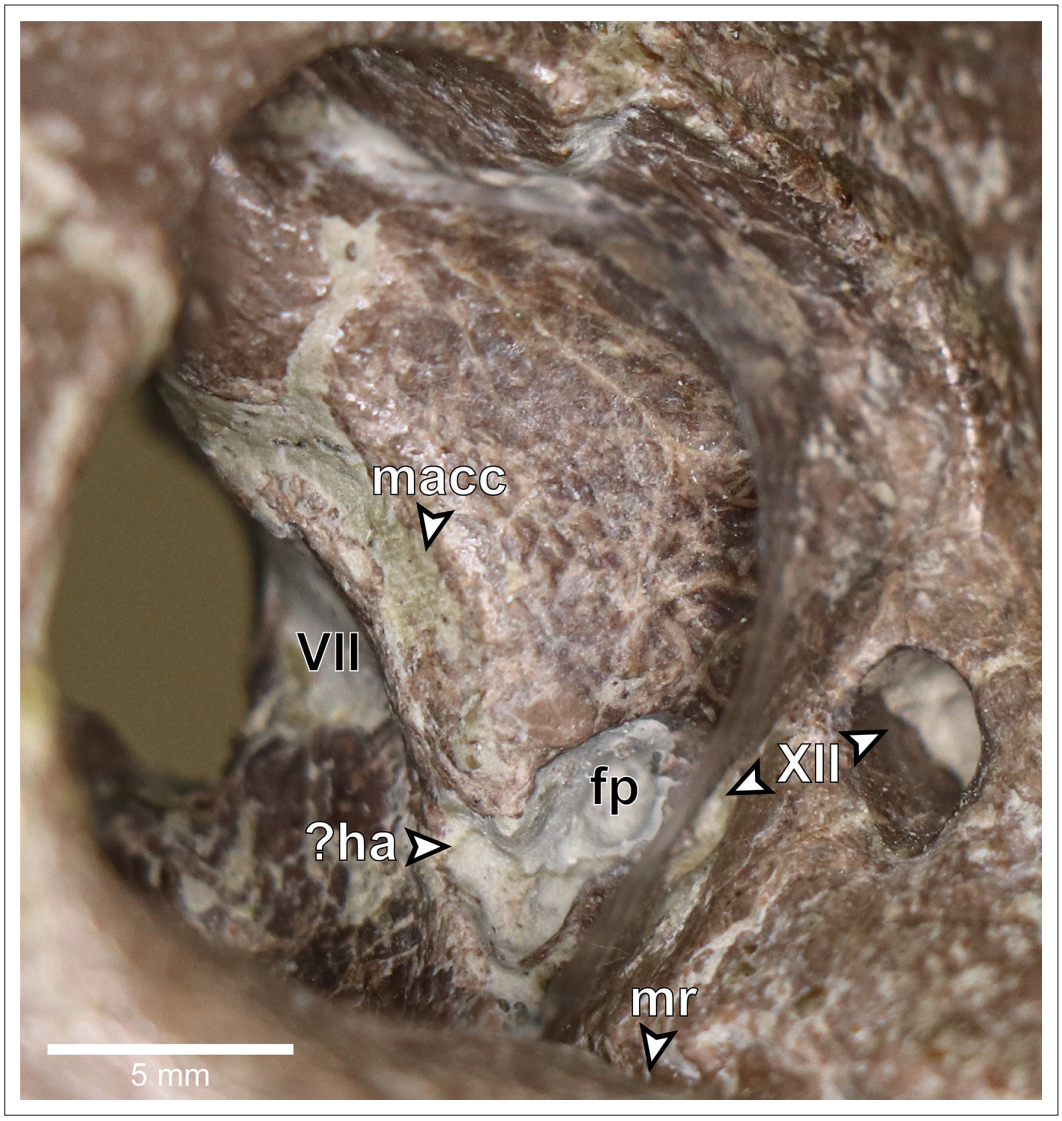

Figure 1—figure supplement 4. *Europasaurus holgeri*, close-up of right posterior endocranial wall of DFMMh/FV 581.1, viewed through the foramen magnum. ?ha, potential hiatus acusticus; fp, fenestra pseudorotunda; macc, medial aspect of common crus; mr, medial trough producing the medial ridge on the ventral braincase endocast; VII, facial nerve opening; XII, hypoglossal nerve openings.

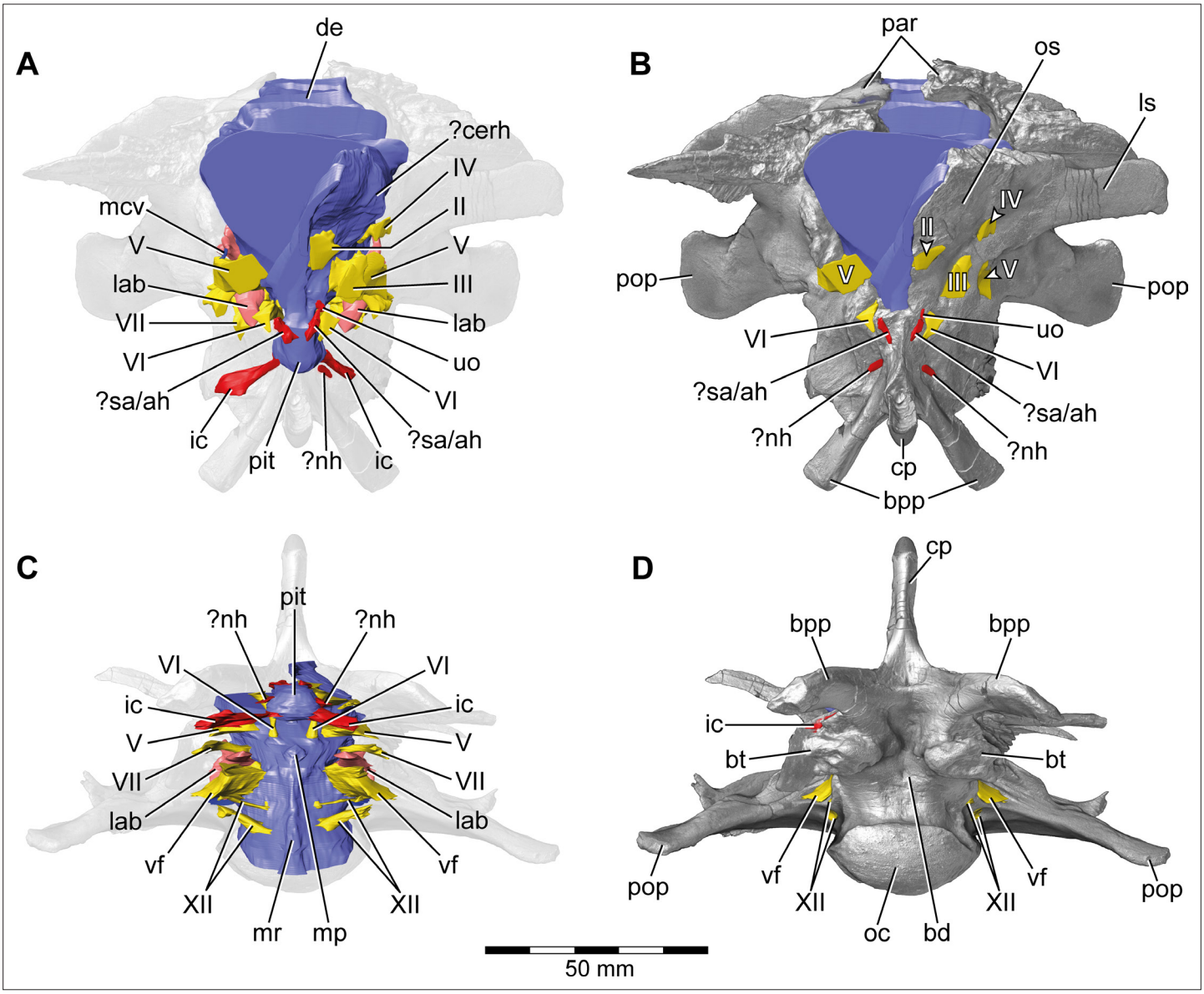

Figure 2. *Europasaurus holgeri*, 3D model of the braincase endocast with endosseous labyrinths and neurovascular canals of DFMMh/FV 581.1, 2, and 3 with transparent (**A,C**) and covering (**B,D**) volume rendering of the bony braincase in (**A,B**) anterior (**C,D**) and ventral view. Note that scale mainly applies to ventral perspective (**C,D**). ?cerh, potential cerebral hemisphere; ?nh, potential canal for the neurohypophysis; ?sa/ah, potential sphenoidal artery/canal for the adenohypophysis; bd, blind depression; bpp, basipterygoid process; bt, basal tuber; cp, cultriform process; de, dorsal expansion; ic, internal carotid; fm, foramen magnum; lab, endosseous labyrinth; ls; laterosphenoid; mcv, mid cerebral vein; mp, median protuberance; mr, medial ridge; oc, occipital condyle; os, orbitosphenoid; par, parietal; pit, pituitary; pop, paroccipital process; uo, unclear opening; vf, vagal foramen; II, optic nerve; III, oculomotor nerve; IV, trochlear nerve; V, trigeminal nerve; VI, abducens nerve; VII, facial nerve; XII, hypoglossal nerve.

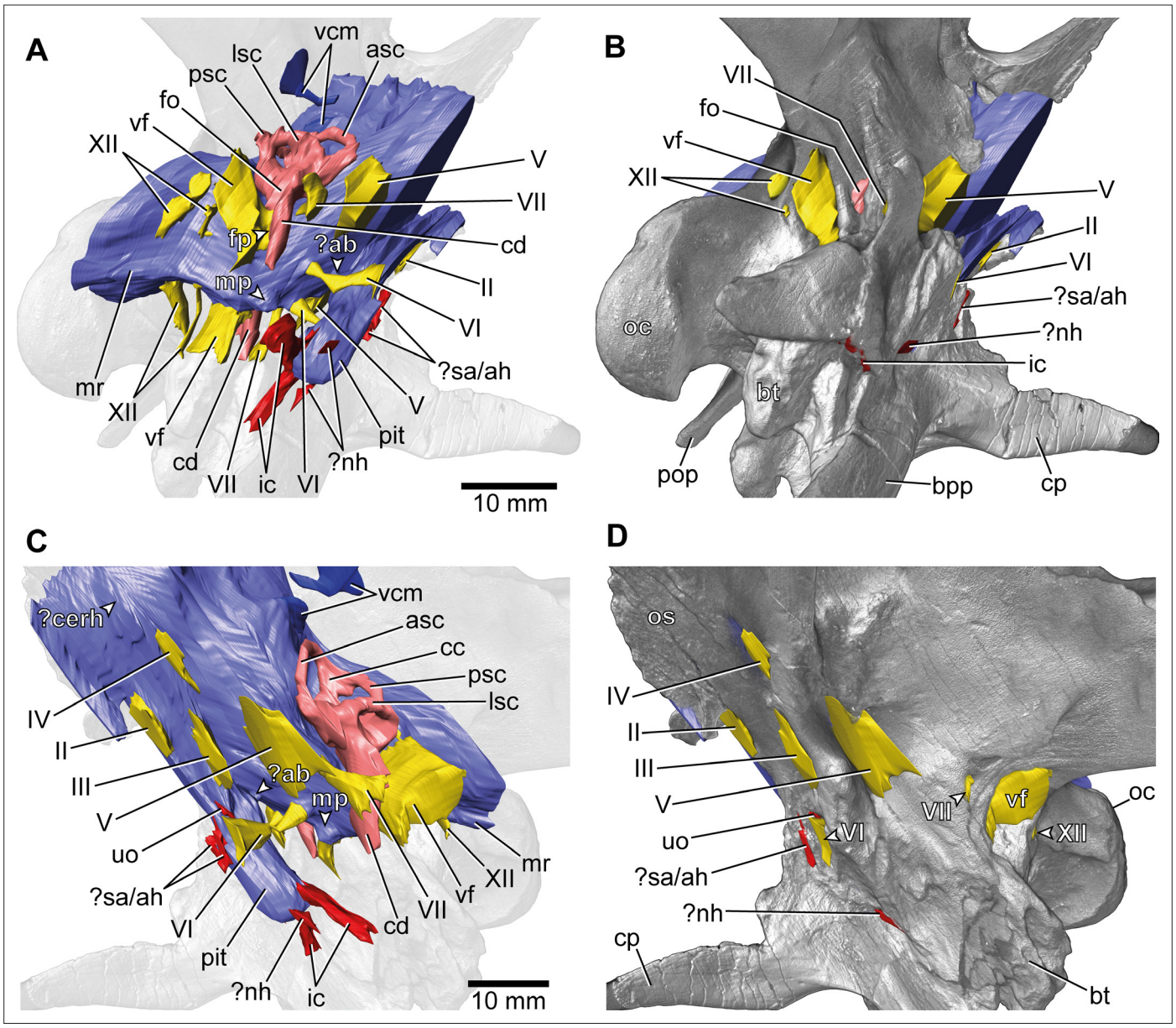

Figure 3. *Europasaurus holgeri*, 3D model of the braincase endocast with endosseous labyrinths and neurovascular canals of DFMMh/FV 581.1, 2, and 3 with transparent (**A,C**) and covering (**B,D**) volume rendering of the bony braincase in (**A,B**) right ventrolateral and (**C,D**) left lateral view. ?ab, potential basilar artery; ?cerh, potential cerebral hemisphere; ?nh, potential canal for the neurohypophysis; ?sa/ah, potential sphenoidal artery/canal for the adenohypophysis; bpp, basipterygoid process; bt, basal tuber; cp, cultriform process; ic, internal carotid; fo, fenestra ovalis; fp, fenestra pseudorotunda; mp, median protuberance; mr, medial ridge; oc, occipital condyle; os, orbitosphenoid; pit, pituitary; pop, paroccipital process; uo, unclear opening; vcm, vena capitis media; vf, vagal foramen; II, optic nerve; III, oculomotor nerve; IV, trochlear nerve; V, trigeminal nerve; VI, abducens nerve; VII, facial nerve; XII, hypoglossal nerve.

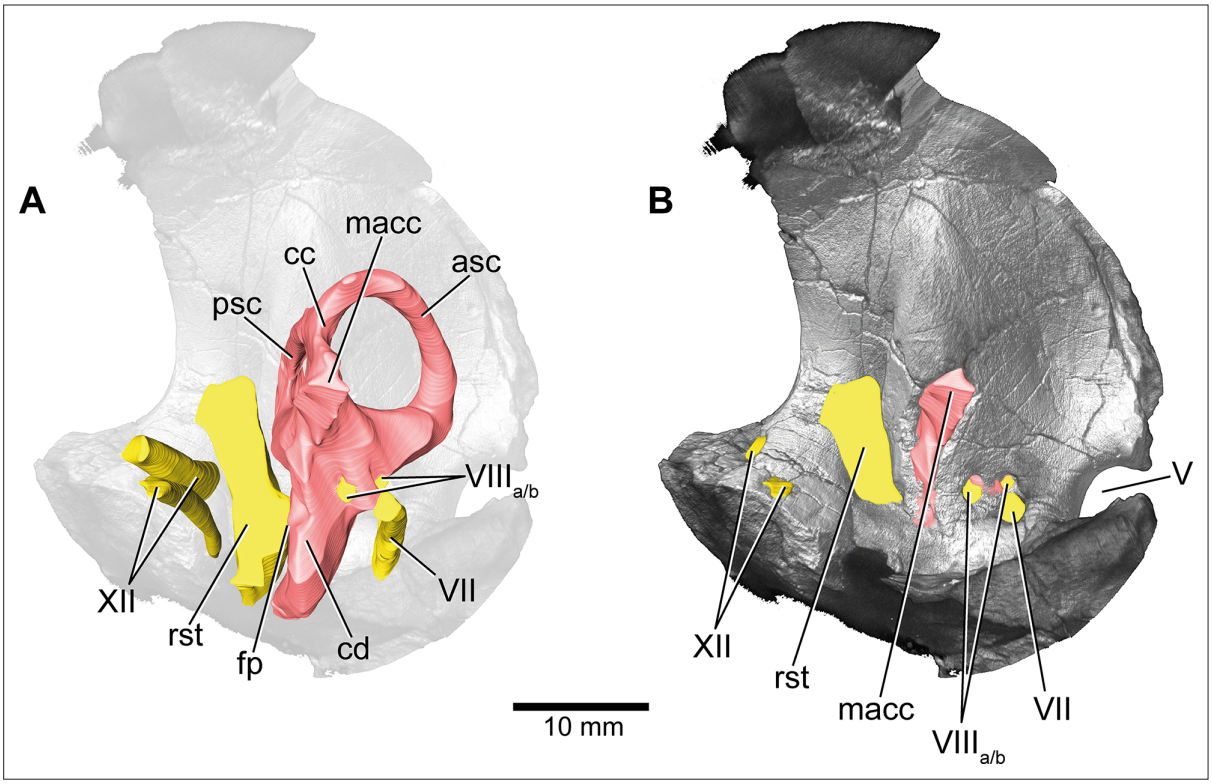

Figure 4. *Europasaurus holgeri*, 3D model of the left endosseous labyrinth region in DFMMh/FV 1077 with transparent (**A**) and covering (**B**) volume rendering of the bony braincase in medial view. asc, anterior semicircular canal; cc, common crus; cd, cochlear duct; fp, fenestra pseudorotunda; lsc, lateral semicircular canal; macc, medial aspect of common crus; psc, posterior semicircular canal; rst, recessus scalae tympani; V, trigeminal nerve opening; VII, facial nerve; VIIIa/b, both branches of the vestibulocochlear nerve; XII, hypoglossal nerve.

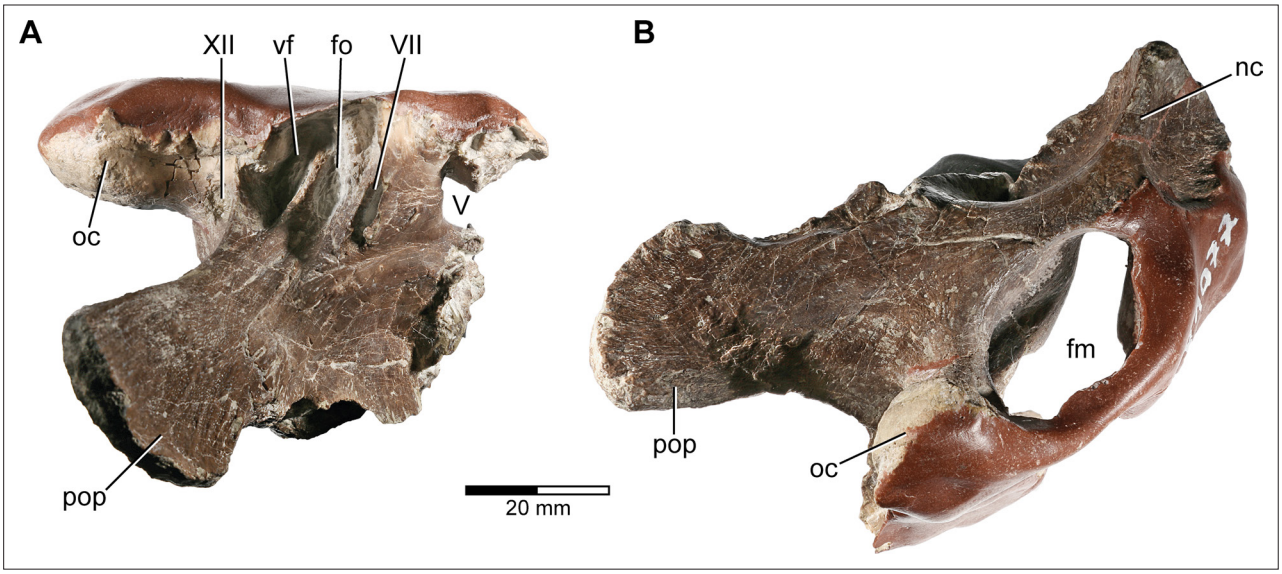

Figure 4—figure supplement 1. *Europasaurus holgeri*, fragmentary braincase DFMMh/FV 1077 in (**A**) ventral and (**B**) posterior view. fm, foramen magnum; fo, fenestra ovalis; nc, nuchal crest; oc, occipital condyle; pop, paroccipital process; vf, vagal foramen; V, trigeminal nerve opening; VII, facial nerve opening; XII, hypoglossal nerve opening.

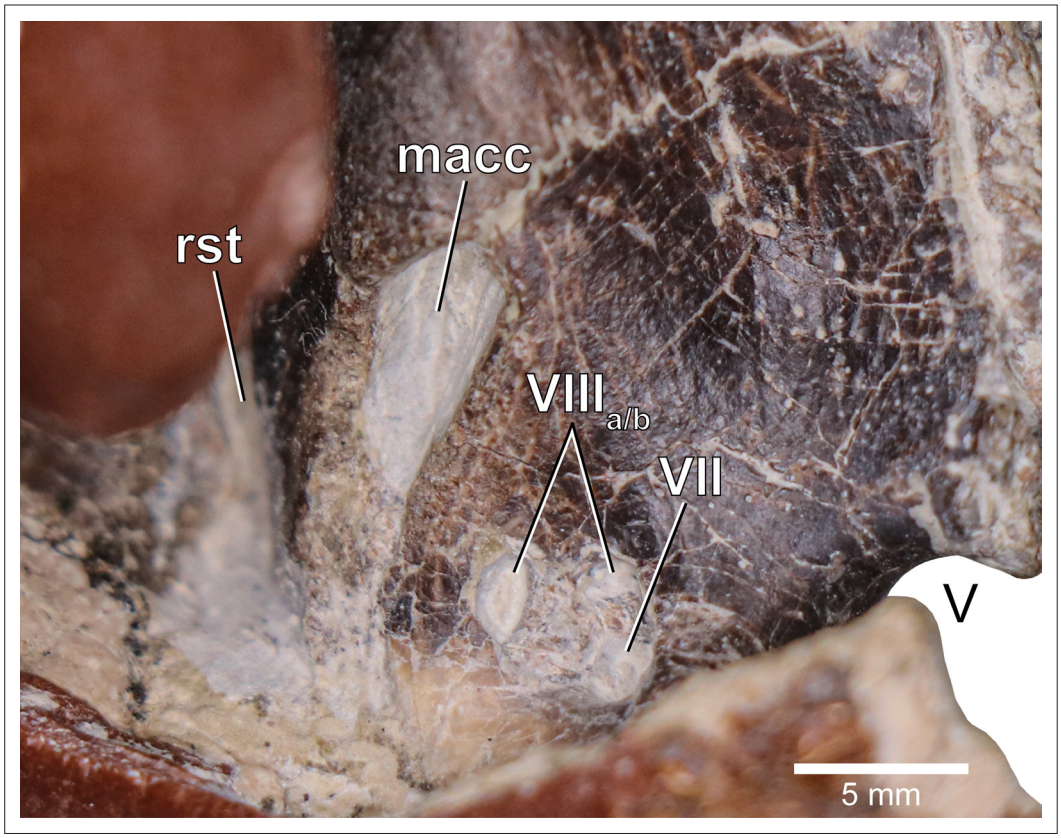

Figure 4—figure supplement 2. *Europasaurus holgeri*, close-up of medial aspect of the fragmentary braincase DFMMh/FV 1077. macc, medial aspect of common crus; rst, recessus scalae tympani; V, trigeminal nerve opening; VII, facial nerve opening; VIIIa/b, both openings of the vestibulocochlear nerve.

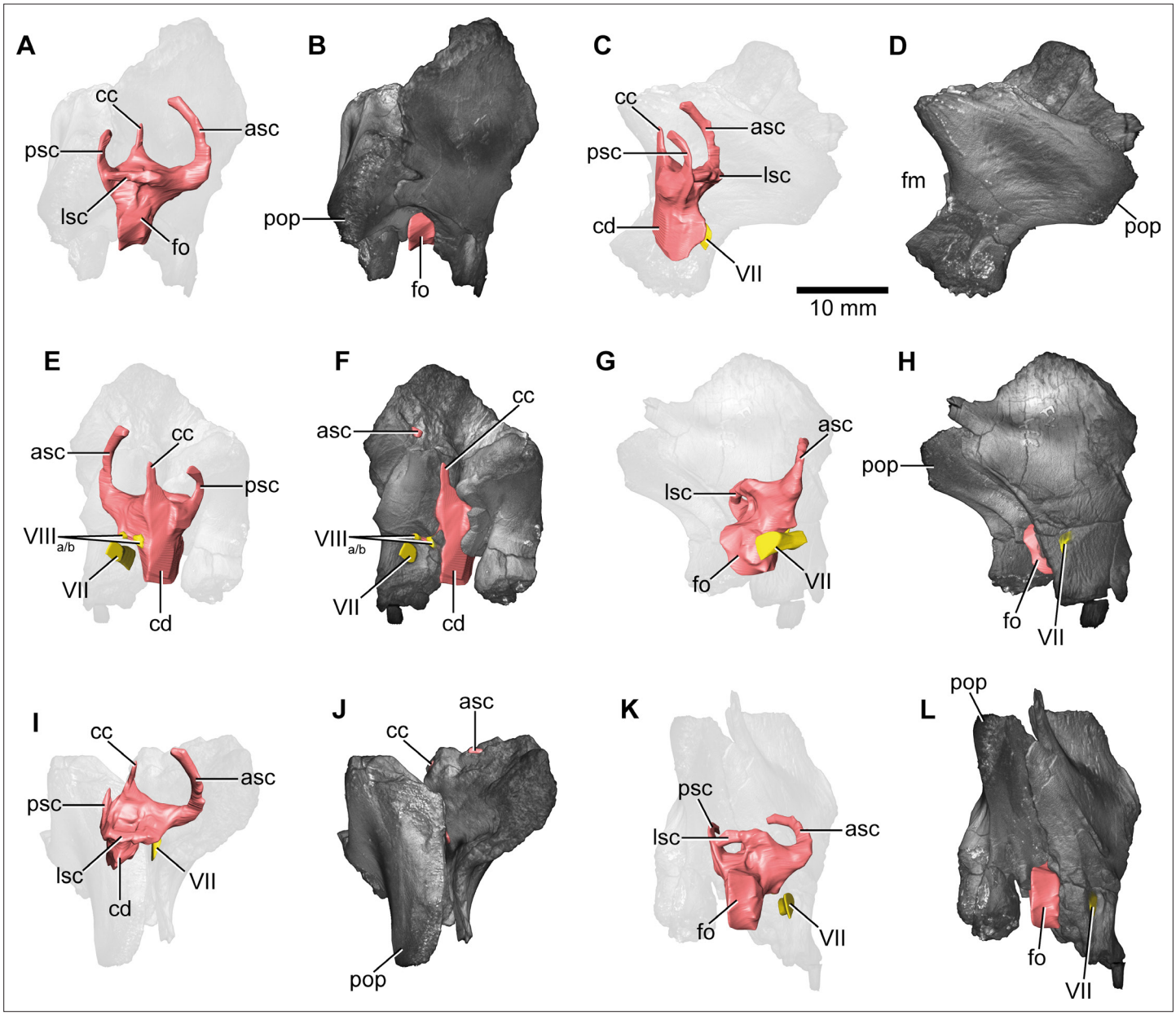

Figure 5. *Europasaurus holgeri*, 3D model of the right endosseous labyrinth in DFMMh/FV 466+205 with transparent (**A,C,E,G,I,K**) and covering (**B,D,F,H,J,L**) volume rendering of the bony braincase remains in (**A,B**) lateral, (**C,D**) posterior, (**E,F**) medial, (**G,H**) anterolateroventral, (**I,J**) dorsolateral, and (**K,L**) lateroventral view; in respect to the endosseous labyrinth. Note that scale mainly applies to posterior perspective (**C,D**), and that VII and VIIIa/b are not shown in (**A**) and (**B**). asc, anterior semicircular canal; cc, common crus; cd, cochlear duct; fm, foramen magnum; fo, fenestra ovalis; lsc, lateral semicircular canal; pop, paroccipital process; psc, posterior semicircular canal; VII, facial nerve; VIIIa/b, both branches of the vestibulocochlear nerve.

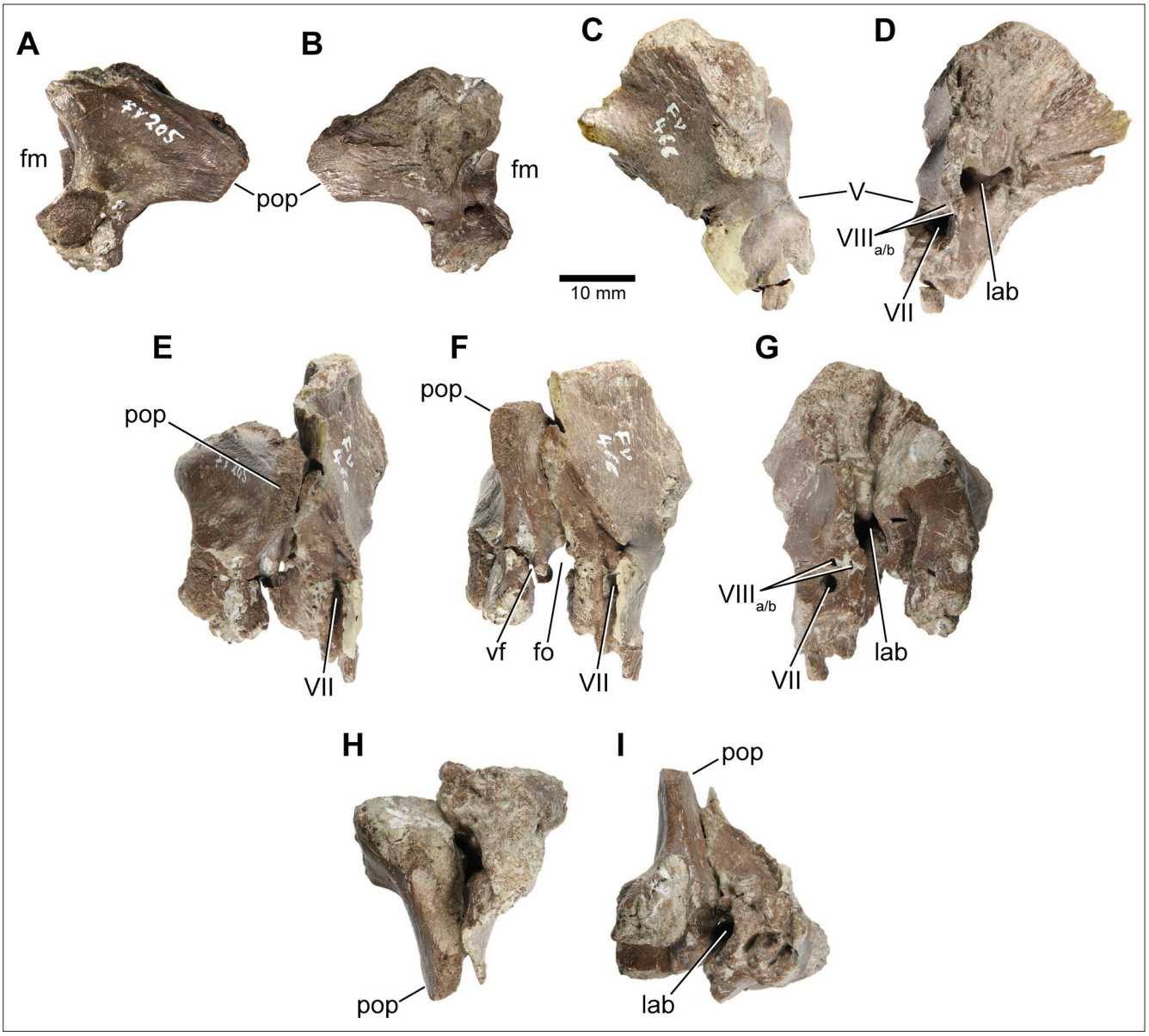

Figure 5—figure supplement 1. *Europasaurus holgeri*, isolated otoccipital (DFMMh/FV 205; **A,B**) and prootic (DFMMh/FV 466; **C,D**) in (**A**) posterior, (**B**) anterior, (**C**) lateral, and (**D**) medial view; prootic and otoccipital conjoined in (**E**) posterolateral, (**F**) lateral, (**G**) medial, (**H**) dorsal, and (**I**) ventral view. Note that scale mainly applies to (**A**) and (**B**). fm, foramen magnum; fo, fenestra ovalis; lab, endosseous labyrinth; pop, paroccipital process; vf, vagal foramen; V, trigeminal nerve opening; VII, facial nerve opening; VIIIa/b, both openings of the vestibulocochlear nerve.

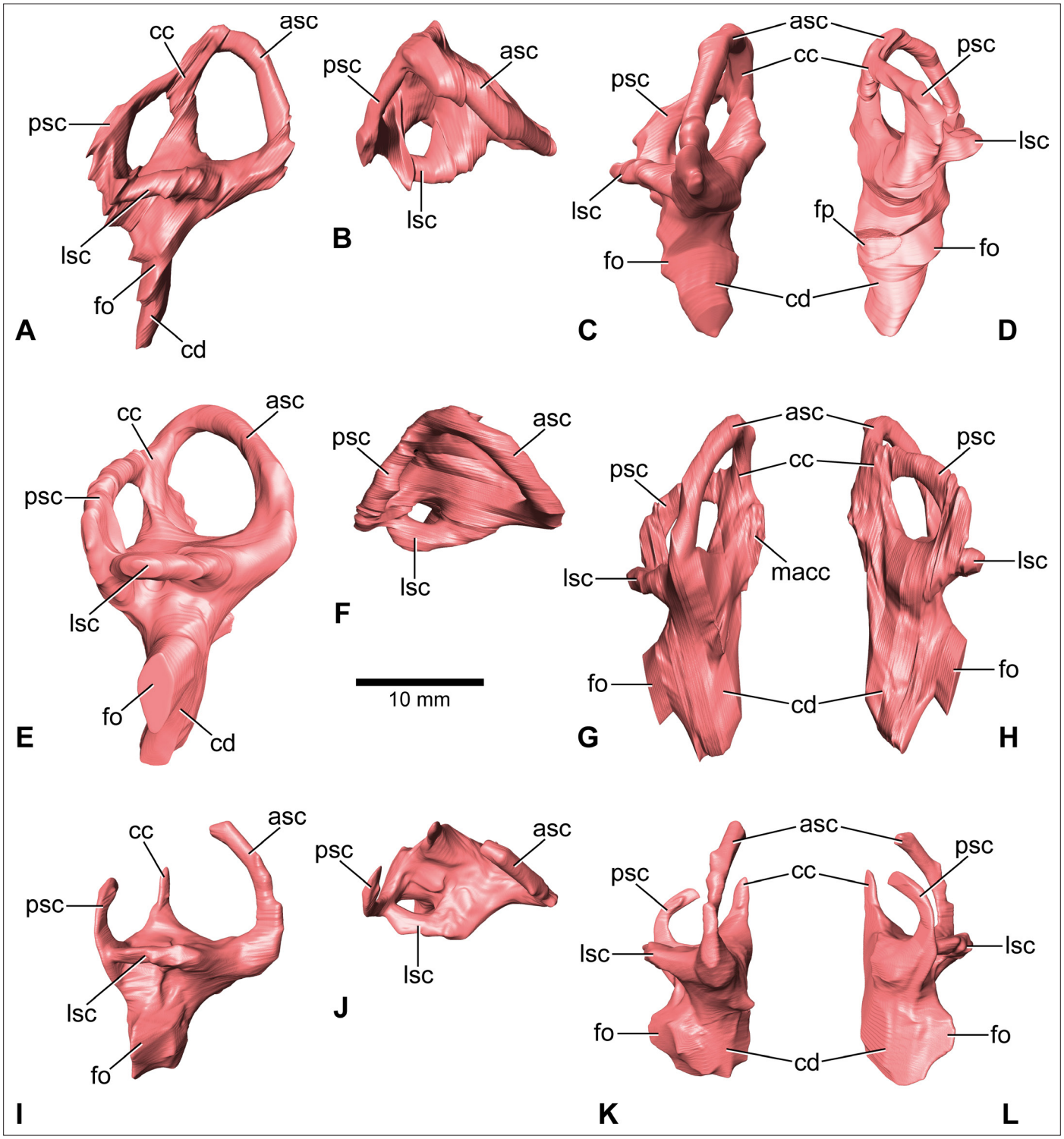

Figure 6. *Europasaurus holgeri*, 3D models of the endosseous labyrinth of DFMMh/FV 581.1 (**A–D**), DFMMh/FV 1077 (**E–H**; note that this model is mirrored) and DFMMh/FV 466+205 (**I–L**) in (**A,E,I**) lateral, (**B,F,J**) dorsal, (**C,G,K**), anterior and (**D,H,L**) posterior view. Note that scale mainly applies to dorsal perspective (**B,F,J**). asc, anterior semicircular canal; cc, common crus; cd, cochlear duct; fo, fenestra ovalis; fp, fenestra pseudorotunda; lsc, lateral semicircular canal; macc, medial aspect of common crus; psc, posterior semicircular canal.

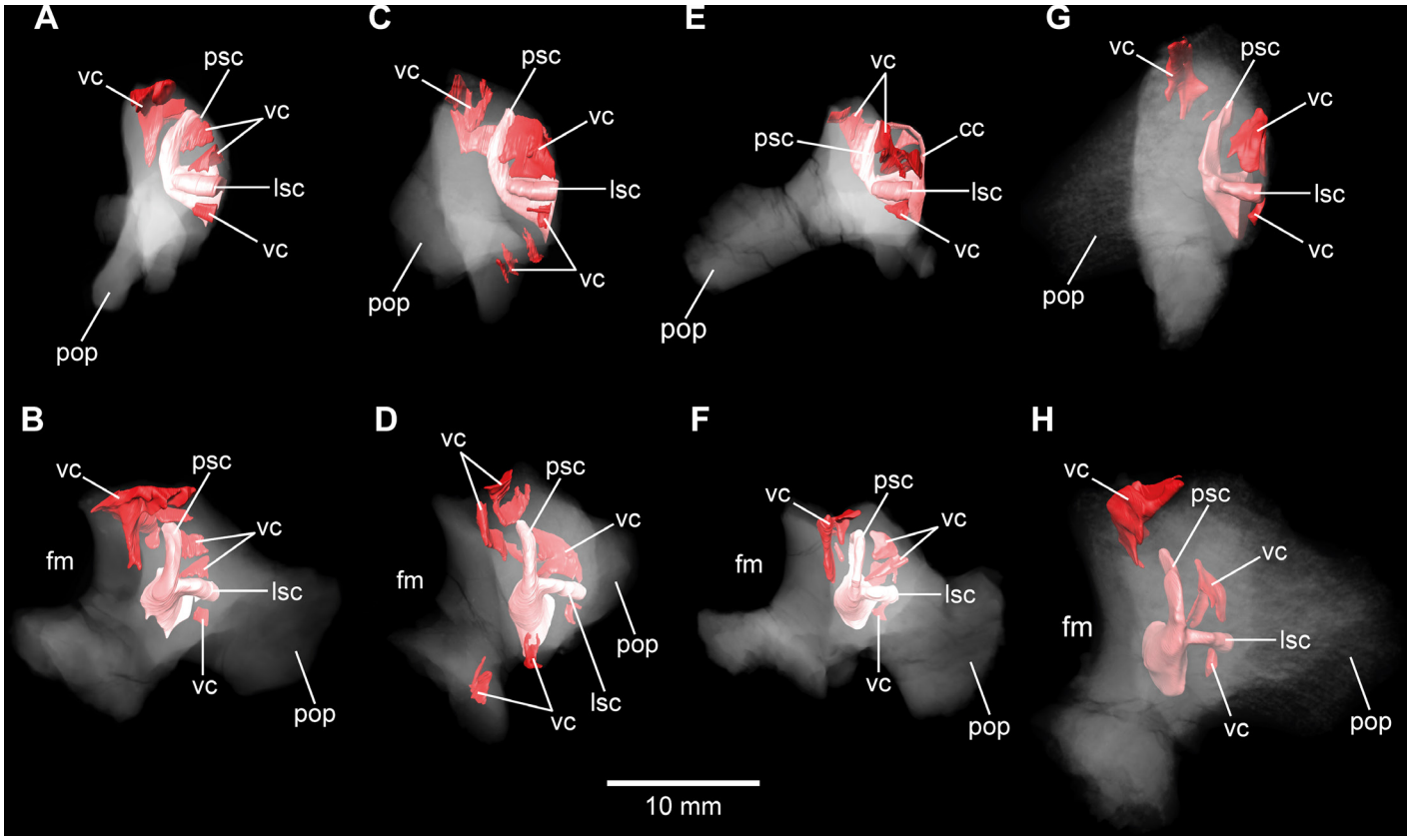

Figure 8. *Europasaurus holgeri*, 3D models of the posterior portions of the endosseous labyrinth in (**A,B**) DFMMh/FV 898, (**C,D**) DFMMh/FV 981.2, (**E,F**) DFMMh/FV 249, and (**G,H**) DFMMh/FV 205 in (**A,C,E,G**) anterolateral and (**B,D,F,H**) posterior view. Note that scale mainly applies to posterior perspective (**B,D,F,H**). fm, foramen magnum; lsc, lateral semicircular canal; pop, paroccipital process; psc, posterior semicircular canal; vc, vascular cavity.

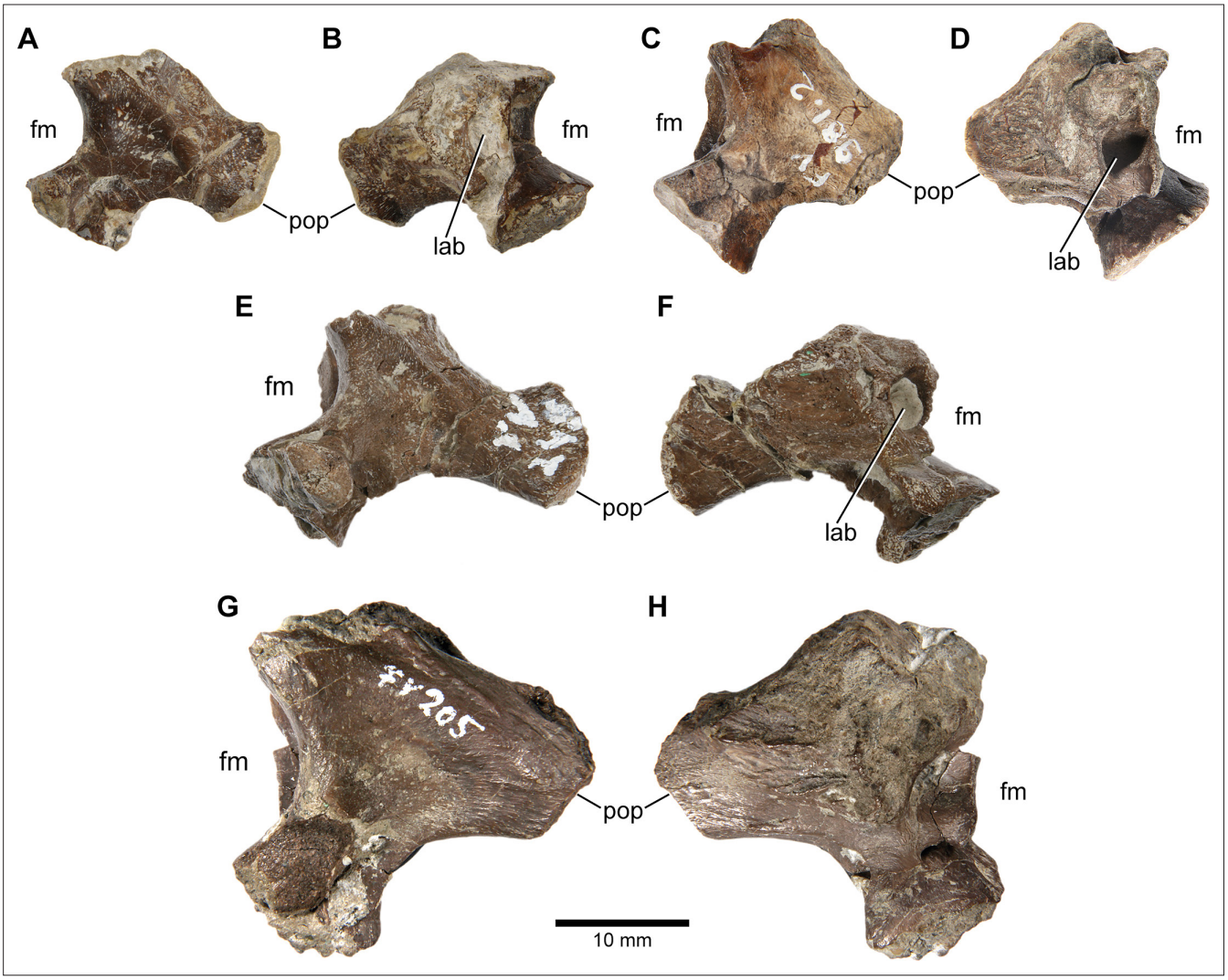

Figure 8—figure supplement 1. *Europasaurus holgeri*, isolated otoccipitals (DFMMh/FV 898, **A**,**B**; DFMMh/FV 981.2, **C**,**D**; DFMMh/FV 249, **E**,**F**; DFMMh/FV 205, **G**,**H**) in (**A**,**C**,**E**,**G**) posterior and (**B**,**D**,**F**,**H**) anterior view. Note that scale mainly applies to posterior perspective (**A**,**C**,**E**,**G**). fm, foramen magnum; lab, endosseous labyrinth; pop, paroccipital process.

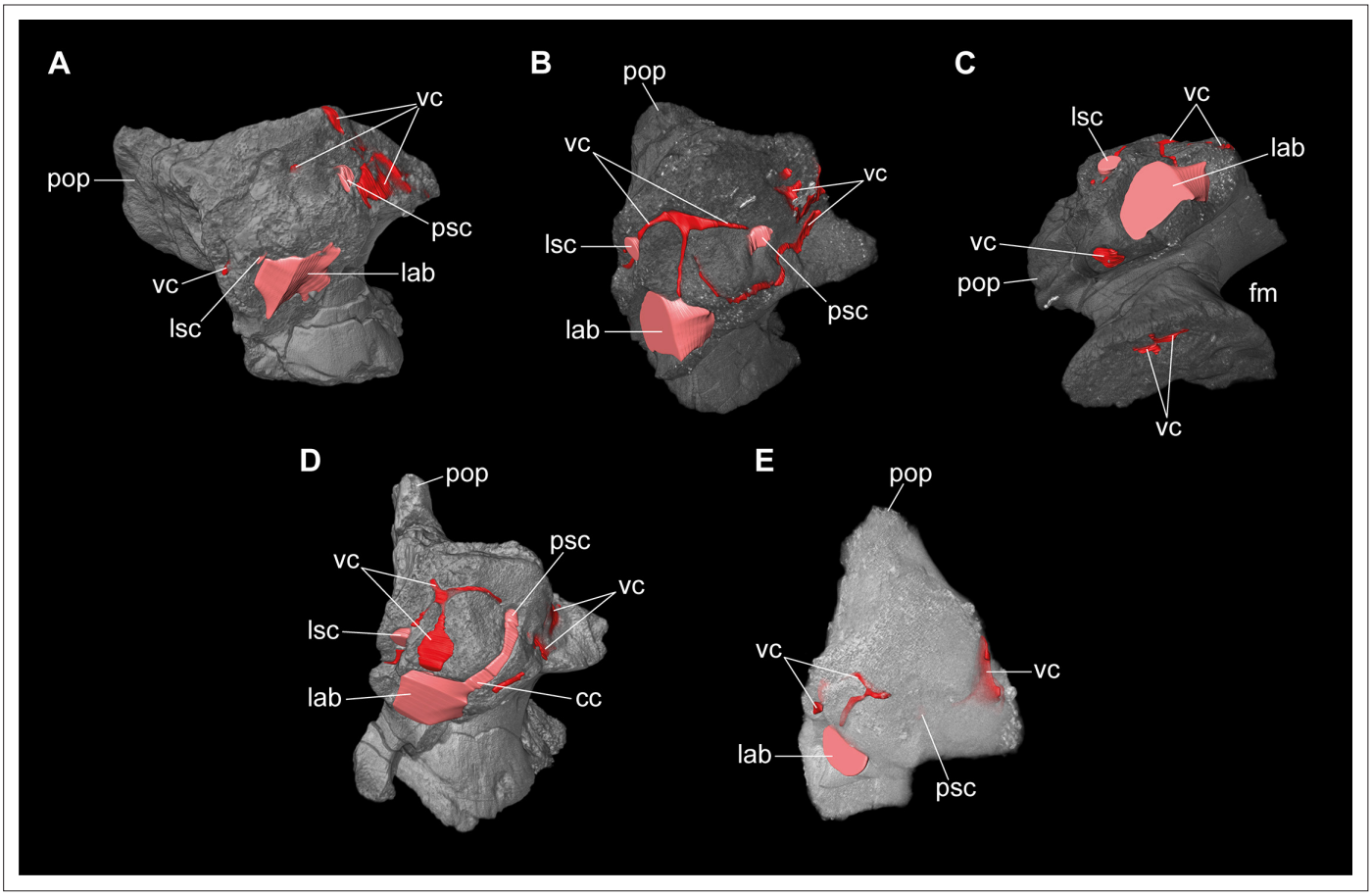

Figure 8—figure supplement 2. *Europasaurus holgeri*, 3D models of isolated otoccipitals and inner features (DFMMh/FV 898, **A**; DFMMh/FV 981.2, **B**,**C**; DFMMh/FV 249, **D**; DFMMh/FV 205, **E**) in (**A**,**B**,**D**,**E**) anterodorsomedial and (**C**) ventral view. Note that models are not scaled. cc, common crus; fm, foramen magnum; lab, endosseous labyrinth; lsc, lateral semicircular canal; pop, paroccipital process; psc, posterior semicircular canal; vc, vascular cavity.

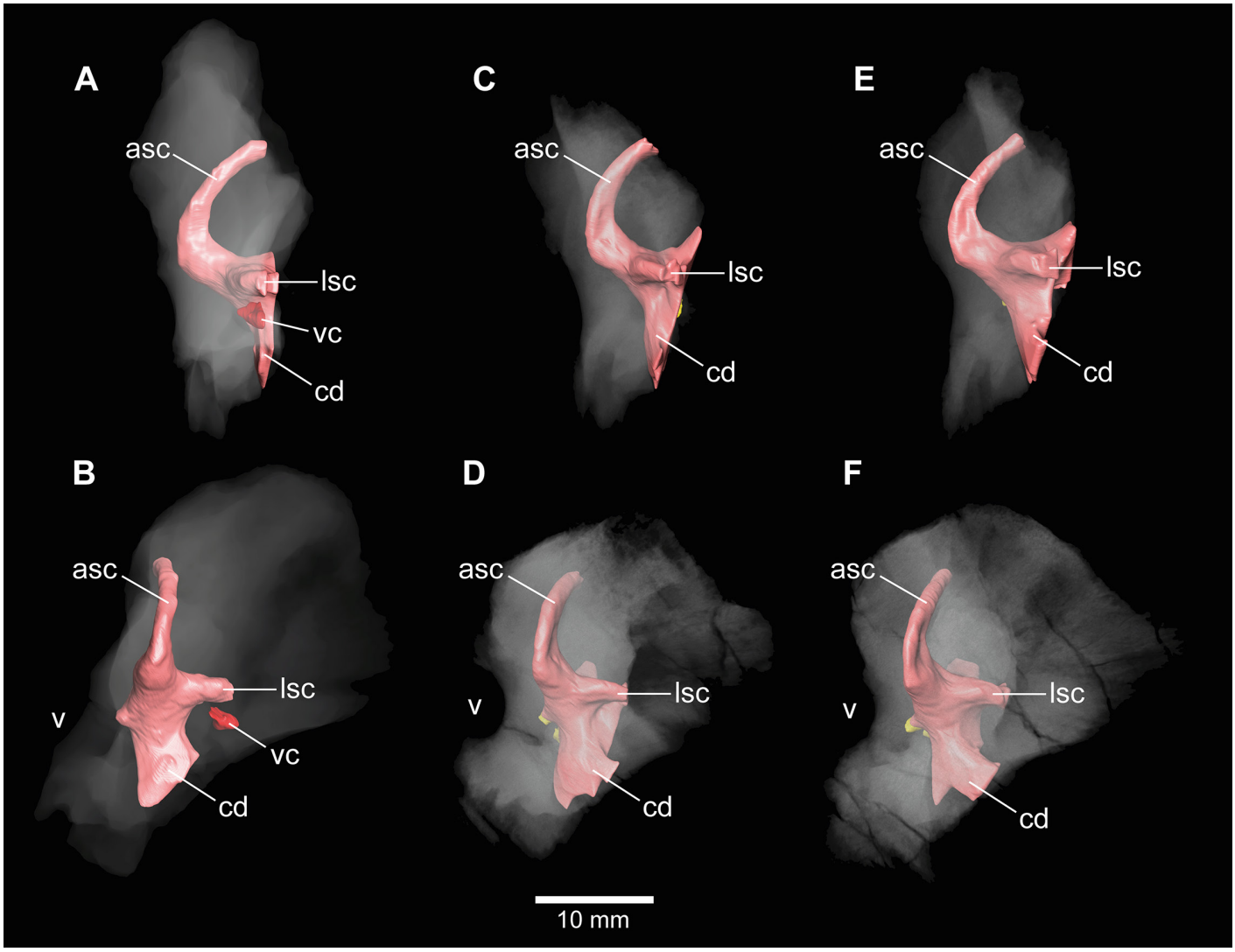

Figure 7. *Europasaurus holgeri*, 3D models of the anterior portions of the endosseous labyrinth in (**A**,**B**; note that this model is mirrored) DFMMh/FV 466, (**C,D**) DFMMh/FV 561 and (**E,F**) DFMMh/FV 964 in (**A,C,E**) lateral and (**B,D,F**) anterolateral view; in respect to the endosseous labyrinth. Note that scale mainly applies to anterolateral perspective (**B,D,F**). asc, anterior semicircular canal; cd, cochlear duct; lsc, lateral semicircular canal; vc, vascular cavity; V, trigeminal nerve opening.

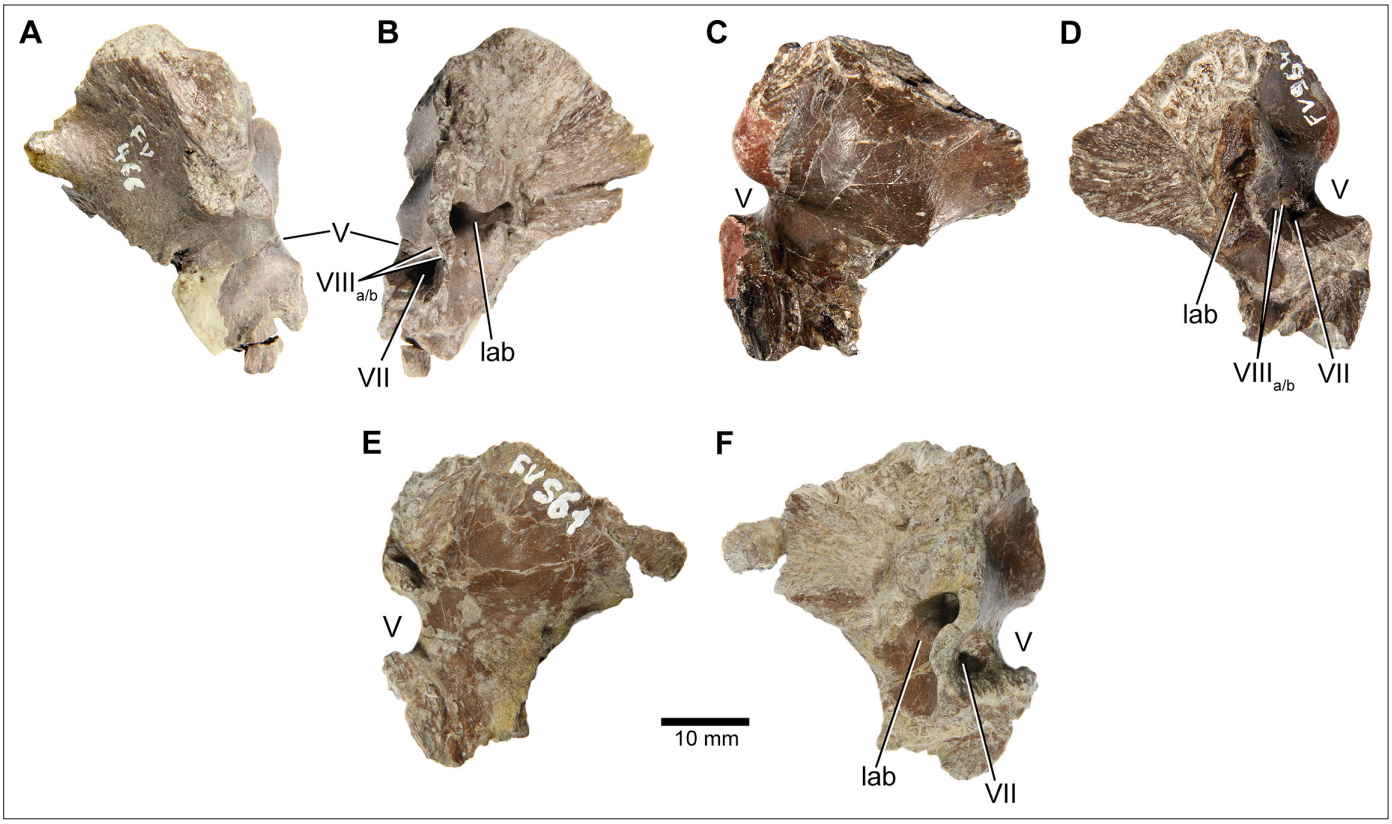

Figure 7—figure supplement 1. *Europasaurus holgeri*, isolated prootics (DFMMh/FV 466, **A**,**B**; DFMMh/FV 964, **C**,**D**; DFMMh/FV 561, **E**,**F**) in (**A**,**C**,**E**) lateral and (**B**,**D**,**F**) medial view. Note that scale mainly applies to lateral perspective (**A**,**C**,**E**). lab, endosseous labyrinth; V, trigeminal nerve opening; VII, facial nerve opening; VIIIa/b, both openings of the vestibulocochlear nerve.

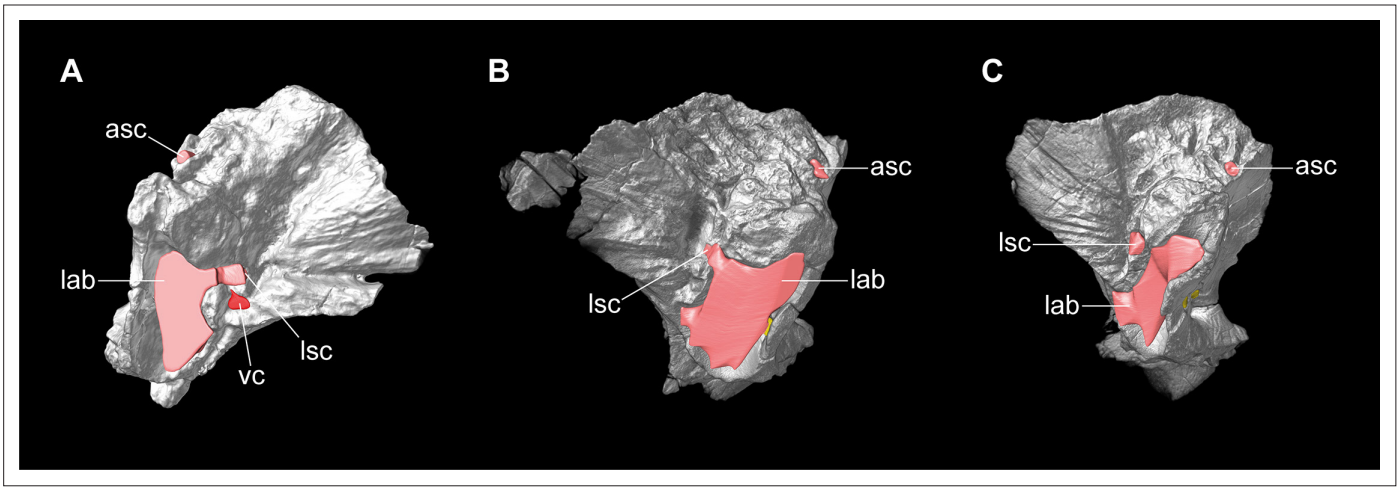

Figure 7—figure supplement 2. *Europasaurus holgeri*, 3D models of isolated prootics and inner features (DFMMh/FV 466, **A**; DFMMh/FV 561, **B**; DFMMh/FV 964, **C**) in (**A–C**) medial view. Note that models are not scaled. asc, anterior semicircular canal; lab, endosseous labyrinth; lsc, lateral semicircular canal; vc, vascular cavity.

V

Schade, M., Evers, S. W., Foth, C., Moleman, O. & Rauhut, O. W. M. A reappraisal of the cranial osteology of the spinosaurid *Irritator challengeri* (Dinosauria: Theropoda). *Palaeontol. Electron.* (in review).

A reappraisal of the cranial osteology of the spinosaurid *Irritator challengeri* (Dinosauria: Theropoda)

Marco Schade, Serjoscha W. Evers, Christian Foth, Olof Moleman & Oliver W. M. Rauhut

Marco Schade. University of Greifswald, Institute of Geography and Geology, Palaeontology and Historical Geology, Friedrich-Ludwig-Jahnstraße 17A, 17489, Greifswald, Germany and Zoological Institute and Museum, Cytology and Evolutionary Biology at University of Greifswald, Soldmannstraße 23, 17489 Greifswald, Germany. corresponding author. marco.schade@stud.uni-greifswald.de

Serjoscha W. Evers. University of Fribourg, Department of Geosciences, Ch. du Musée 6, 1700 Fribourg, Swiss.

Christian Foth. University of Fribourg, Department of Geosciences, Ch. du Musée 6, 1700 Fribourg, Swiss.

Olof Moleman. Alkmaar, Netherlands.

Oliver W. M. Rauhut. SNSB - Bayerische Staatssammlung für Paläontologie und Geologie; Department für Geo- und Umweltwissenschaften, Ludwig-Maximilians-Universität; GeoBioCenter, Ludwig-Maximilians-Universität; Richard-Wagner-Str. 10, 80333 Munich, Germany.

ABSTRACT

Although described almost three decades ago, the holotype of *Irritator challengeri* from the Lower Cretaceous Romualdo Formation of Brazil still represents the most complete spinosaurid skull known to science. Here, we present a detailed description of the skull of *Irritator* based on digital reconstructions from (micro)CT data. We segmented the full morphology of bones hidden by matrix, revealing the near-complete palatal complex and braincase, an unusual morphology of the retroarticular process, a large, ventrally inclined surangular shelf and tooth replacement. The digitally re-arranged skull implies a robust dentition, a field of binocular vision in front of the skull with an inclined snout orientation, a relatively weak but fast bite, as well as laterally spreading and rotating lower jaw rami during jaw opening. In order to investigate the peculiarity of spinosaurids, we modified an existing phylogenetic matrix of Tetanurae to account for new observations on the morphology of *Irritator* and analysed this using parsimony methods. Our phylogeny supports spinosaurids as megalosauroids and recovers a monophyletic Carnosauria. Despite a highly derived cranial morphology, spinosaurids do not show elevated rates of morphological evolution, so that their perceived aberrant skull morphology can be explained by accumulation of differences to other megalosauroids over an extended period of evolutionary time that is implied by the current ghost lineage at the base of spinosaurids. This study provides an in-depth look into the evolution and expression of the distinctiveness of spinosaurid cranial anatomy and refines our imagination of these specialized Mesozoic predators.

INTRODUCTION

The perception of spinosaurids as an aberrant group of large-bodied theropods, so far restricted to the Cretaceous, has experienced major shifts from “normal” terrestrial hunters with piscivorous affinities to a taxonomically diverse clade potentially encompassing representatives that foraged and pursued under water. Indeed, Spinosauridae are an unusual clade of theropods that includes some of the largest terrestrial predators in Earth’s history, such as *Spinosaurus* (Stromer, 1915; Therrien & Henderson, 2007; Hone & Holtz, 2017). However, whereas other giant theropods are interpreted as hypercarnivorous apex predators (e.g., Molnar & Farlow, 1992), spinosaurids show an aberrant skull morphology, indicating a different feeding ecology than in these taxa, being specialized on rather small prey items, maybe predominately fish (e.g., Taquet, 1984; Charig & Milner, 1997; Sereno et al., 1998; Rauhut, 2001; Buffetaut et al., 2004; Rayfield et al., 2007; Amiot et al., 2010; Rayfield, 2011; Ibrahim et al., 2014; Schade et al., 2020; Hone & Holtz, 2021). However, although the name-giving genus *Spinosaurus* was described more than 100 years ago (Stromer, 1915), the cranial osteology of spinosaurids is still rather poorly known.

Most spinosaurid specimens described so far have no or only very limited cranial remains. The original material of *Spinosaurus* only included the anterior ends of the mandibles and a fragment of the maxilla (Stromer, 1915), and only few and fragmentary cranial remains were referred to the clade up to the mid-1990ies (Taquet, 1984; Buffetaut, 1989, 1992). The most important specimen was the type of *Baryonyx walkeri*, which includes a complete premaxilla, partial maxilla, nasal, lacrimal, braincase, and several mandibular elements (Charig & Milner, 1986, 1997; see also Sereno et al., 1998). Premaxillae and braincase material is also known for the recently described *Riparovenator milnerae* and *Ceratosuchops inferodios* (Barker et al., 2021), and a snout and further isolated cranial elements, including a braincase

have been referred to *Suchomimus tenerensis* (Sereno et al., 1998; Hendrickx et al., 2016; Sereno et al., 2022), but these taxa lack detailed osteological descriptions. Other specimens mainly included partial snouts (Kellner & Campos, 1996; Taquet & Russell, 1998; Dal Sasso et al., 2005; Kellner et al., 2011; Isasmendi et al. 2022), or isolated cranial remains (e.g. Hendrickx et al., 2016; Ibrahim et al., 2014; Arden et al., 2019). The only spinosaurid known from an almost complete skull is the late Early Cretaceous Brazilian taxon *Irritator challengeri* (Figure 1).

The spinosaurid *Irritator* from the Araripe Basin of north-eastern Brazil was initially briefly described and assigned to Maniraptora by Martill et al. (1996). The authors examined the specimen with aid of computer tomography (CT), revealing that the upper jaw was artificially elongated, but, due to the technical limitations of CT devices at that time, little anatomical detail could be gathered from the scans. In the same year, Kellner (1996) suggested that *Irritator* actually represents a spinosaurid, which was later supported in a more detailed description of the specimen by Sues et al. (2002), after the skull had been more completely prepared. The spinosaurids *Irritator* and *Angaturama,* both from the Romualdo Member of the Santana Formation (as formerly considered, see below) of Brazil, were described within a period of one month (Martill et al., 1996; Kellner & Campos, 1996). It was hypothesized that both taxa may represent fragments of the same skull (Sereno et al. 1998), since they come from the same area and strata and represent largely complementary portions of the skull. However, Sales and Schultz (2017) pointed out that *Irritator* and *Angaturama* most probably do not represent the same individual, as both seem to preserve the 3rd maxillary tooth (though see below). In 2020, Schade et al. published the first study of a spinosaurid endocranium, based on the digital braincase endocast of *Irritator* derived from novel CT data. While this study provided information about

head posture and neuroanatomy, Schade et al. (2020) did not present new osteological information from their CT data.

Here, we present a new study of the skull of *Irritator* with the aid of digital segmentation, using the CT data published by Schade et al. (2020). In addition to studying the cranial elements from all sides, we were also able to rearrange the skull bones and mirror elements that are only present from one side (postorbital, quadratojugal, quadrate, squamosal, prearticular and angular). The result (Figure 2-4) is a digital model of the most complete spinosaurid skull known to science, which shows articulations of all the preserved skull bones and allows for further investigations, e.g., of the biomechanics of spinosaurid skulls.

MATERIAL AND METHODS

Segmentation and Digital Reconstruction

The principal specimen analysed here is the holotype skull of the spinosaurid theropod *Irritator challengeri*, SMNS 58022, from the Aptian Romualdo Formation of northeastern Brazil. Comparisons with other spinosaurid cranial material is based on first hand observations of *Baryonyx* (NHMUK R9951; MS, OWMR, SWE), *Suchomimus* (MNN GDF 501, referred premaxillae and maxillae cast, MNN GDF 214, referred braincase cast; MS; and original material of these specimens by OWMR, SWE), casts of FSAC KK 11888 ('neotype' of *Spinosaurus aegyptiacus*; SWE, OWMR), and a snout referred to *Spinosaurus* (MNHN SAM 124; OWMR). Additionally, we had a surface scan of the braincase cast referred to *Suchomimus* (MNN GDF 214), produced by MS, available for comparisons. Comparisons with

other non-avian theropods are based on first hand observations of many different specimens (MS, OWMR, CF, SWE) and the cited literature.

Originally, we scanned SMNS 58022 entirely with a medical Siemens Somatom Force (dual source) CT (voltage: 120 kV, X-ray tube current: 1365 µA, exposure time: 154 ms, voxel size: 0.703123 mm × 0.703124 mm × 3 mm) in the Deutsches Herzzentrum in Munich. Additionally, we conducted a second scan focused only on the braincase, using a Zeiss Metrotom 1500 (voltage: 180 kV, X-ray tube current: 1800 µA, exposure time: 250 ms, voxel size: 0.09713 mm) in the Carl Zeiss Industrielle Messtechnik GmbH in Essingen. Both scans were published on the online repository MorphoSource for a previous study that examined neuroanatomical features of SMNS 58022 (Schade et al., 2020; link below). While most of SMNS 58022 was reconstructed using medical CT data, the reconstruction of the braincase (excluding the frontals and parietals together with their respective inner cavities) is based on the micro CT scan. All elements were segmented manually independently by MS and OM, using Amira (5.6) and 3D slicer (4.10.2), respectively. MS worked with the medical and the micro CT data, while OM worked with the medical CT set only. The resulting models were compared to validate the anatomical reconstructions. SWE used the 3D models, resulting from the segmentation work of MS to produce figures of isolated elements with Blender (2.79b). OM used his models and the software Blender (2.91) to rearrange the skull bones into their original position. For this, OM mirrored the elements that are only present on one side (postorbital, quadratojugal, quadrate, squamosal, prearticular and angular) and arranged the bones according to their articular facets in cases of disarticulated elements. Additionally, minor retro-deformation was carried out for digital articulation of the skull bones (see Supplementary Data 1).

Phylogenetic analysis

To explore phylogenetic aspects of the cranial anatomy of spinosaurids, we modified the matrix of Rauhut & Pol (2019) for basal tetanurans. Several spinosaurid taxa were added, including the recently described taxa *Vallibonavenatrix* (Malafaia et al., 2020), *Ceratosuchops* and *Riparovenator* (Barker et al., 2021), and the poorly known *Oxalaia* (Kellner et al., 2011). Furthermore, we restricted the codings for *Spinosaurus aegyptiacus* to the original material described by Stromer (1915, 1936; Smith et al., 2006), and coded the referred specimens MSNM V 4047 (Dal Sasso et al., 2005), MNHN SAM 124 (Taquet & Russell, 1998) and FSAC KK 11888 (Ibrahim et al., 2014, 2020a, b) as separate operational taxonomic units (OTUs), as two of these (MSNM V 4047, MNHN SAM 124) lack overlap with the original type material, and the referral of FSAC KK 11888 to the same species as *Spinosaurus aegyptiacus* has not been firmly established (see Evers et al., 2015; Kellermann, 2021; Lacerda et al., 2021 contra Ibrahim et al., 2020a, Smyth et al., 2020). The character list was critically evaluated, with a focus on cranial characters. Eight of the original characters were deleted, several modified, and a total of 45 characters were added, either from other sources, or as new characters based on our comparisons of non-avian theropod taxa (see Results).

The final data matrix thus had 76 OTUs, scored for 395 morphological characters (Supplementary Data 2). Of the characters, 195 are craniodental characters, the rest concern the postcranium. Two OTUs, *Oxalaia* and MNHN SAM 124, were subsequently deleted, following safe taxonomic reduction criteria (Wilkinson, 1995), as they had very high amounts of missing data (99.7% and 95%, respectively), and all codings completely overlapped with those of MSNM V 4047. As in most

palaeontological data sets, missing data is rampant in the resulting data set of 74 taxa and 395 characters; the average proportion of coded characters per taxon is only 40%, with a range from 99% in *Allosaurus* to only 4% in *Angaturama*.

For a second analysis, we restricted the data matrix to craniodental characters only and deleted all OTUs for which no cranial material is known (Supplementary Data 3). In addition, several taxa with few cranial or dental material known could be deleted, following safe taxonomic reduction criteria, including *Coelurus*, *Condorraptor*, *Fukuiraptor*, *Magnosaurus*, *Megaraptor* (codings exclude the juvenile material described by Porfiri et al., 2014, as its referral to *Megaraptor* is not entirely certain; Porfiri, pers. comm. 2021), *Saurophaganax,* and "*Szechuanosaurus*" *zigongensis* (in addition to *Oxalaia* and MNHN SAM 124 as mentioned above). The resulting data matrix for cranial characters thus had 54 taxa scored for the 195 craniodental characters. Missing data is slightly less in this data set, with an average of 49% coded characters per OTU, ranging from 99.5% in *Allosaurus* to 8% in *Angaturama*, *Australovenator* and FSAC KK 11888.

The matrices were analysed under maximum parsimony in the phylogenetic software TNT (Goloboff & Catalano, 2016) under the traditional search option, using equally weighted parsimony, with 1’000 replicates of Wagner trees, followed by TBR branch swapping. From the resulting equally parsimonious trees (Supplementary Data 4,5), a strict consensus tree and reduced consensus trees were calculated, using the IterPCR method for the latter (Pol & Escapa, 2009), with the TNT command "pcrprune/>0;nelsen//{0};". Character support of internal nodes, as well as character transformations were evaluated using the trace character option in Mesquite (Maddison & Maddison, 2019). In order to evaluate the robustness of the results, we also carried out analyses using implied weights (with k=10; Goloboff et al., 2018) in

TNT (Supplementary Data 6) and evaluated the number of steps needed for alternative placements in Mesquite.

In order to show the temporal context of our phylogenetic results, we time-calibrated the reduced consensus tree (Supplementary Data 7) from the parsimony analysis using equal weighting and the full character dataset. We performed the time calibration in R v.3.6.0 (R Core Team). We used commands of the paleotree (Bapst, 2012), ape (Paradis & Schliep, 2019), phytools (Revell, 2012) and strap (Bell & Lloyd, 2014) packages for tree modification, visualization, and calibration (Supplementary Data 8). We employed the cal3 calibration method of Bapst (2013), treating age data as known age ranges for taxa (i.e., using the firstLast option in the dateTreatment argument). Age ranges were collected from the literature and are available as Supplementary Data 9. Polytomies of the reduced consensus tree were resolved at random for the calibration procedure, but were re-inserted manually after calibration. The cal3 protocol requires the input of an instantaneous branching, extinction, and sampling rate, and we used values that Benson et al. (2017) used for dinosaurs. We specified 100 iterations of the cal3 algorithm, and all 100 trees are available as Supplementary Data 10. We created a single tree from the 100 cal3 solutions by averaging the branch lengths and root times of the 100 starting trees (Supplementary Data 11,12) using the consensus.edges function of phytools (Revell, 2012) and custom code (Supplementary Data 8).

Character optimization

In order to calculate rates of cranial character evolution, we performed character state optimization in PAUP* 4.0a for Macintosh (Swofford, 2002), as PAUP* allows specification of the optimization criterion, whereas TNT only returns unambiguous

synapomorphies. Although we were only interested in cranial rates of evolution, we used the full matrix and reduced consensus tree from the analysis using the full matrix for this. The reason is that we put more credibility in the analysis using the full matrix. We performed the optimization using both accelerated transformations (ACCTRAN) and delayed transformations (DELTRAN). ACCTRAN and DELTRAN are end-members of a range of possible node positions in which a character state change can occur along a portion of the tree for which the transition cannot be known with certainty, which is either due to missing data or due to conflicting character states for a given character among sister taxa. As some character transformations are equivocal on a reduced consensus tree under both ACCTRAN and DELTRAN, but the algorithm of PAUP needs to make a decision about these transformations, the number of transformations evaluated using this software might differ slightly from those evaluated with Mesquite. Unambiguous character state transitions are those in which ACCTRAN and DELTRAN agree. We provide a full list of optimizations (organized by node, but also by character) in which unambiguous, ACCTRAN, and DELTRAN optimizations as found by PAUP are listed, as Supplementary Data 13. Contrasting ACCTRAN and DELTRAN is important especially for groups such as Spinosauridae, in which we have much missing data, and few taxa with extraordinary character coverage such as *Irritator*: Currently, many cranial character states that can only be observed in *Irritator* can either be autapomorphies of the species (under DELTRAN optimization), or spinosaurid synapomorphies (ACCTRAN). Only considering unambiguous synapomorphies (e.g., Rauhut & Pol, 2019; but see Rauhut, 2003, Carrano & Sampson, 2008; Rauhut & Carrano, 2016) is much less informative, as it disregards all of the concerned characters in the spinosaurid example, and thus underestimates the number of traits that are apomorphic among

the group, even if the exact nodal appearance of the character state conditions in question cannot be known given the data.

As character optimizations should be performed on a fully bifurcated tree, we resolved the polytomies of the reduced consensus tree derived from our TNT analysis using the full matrix. Hereby, we resolved the polytomy within Spinosaurinae by grouping specimens according to geographic provenance, resulting in the following in-group topology for Spinosaurinae: ((Angaturama, Irritator),(Spinosaurus aegyptiacus, MSNN V4047)). This topology implies close relationships between geographically proximate OTUs, which can be easier justified than resolving this polytomy at random. The other polytomies are not further relevant to the objectives of this study as they are relatively deeply nested within non-megalosauroid groups and alternative resolutions would not affect the results presented herein. The resolution of these polytomies is documented in the tree file stored in the nexus file that was used for optimization (Supplementary Data 14). PAUP* assigns numerical node labels to internal nodes of the provided phylogeny. For the purpose of communication and easier documentation of synapomorphies, we converted this into a taxonomic code for internal nodes. We used widely-used clade names (e.g., “Allosauria”) whenever possible, and these are consistent with the usage of these names in our phylogenetic figures (figure refs). For unnamed internal nodes, we used “Taxon A+Taxon B” to indicate a sister-group relationship between two specific taxa. Our code “Taxon A++Taxon C” denotes the most inclusive group that includes both taxon A and taxon C. Although our optimizations include all characters (Supplementary Data 13), we focus our synapomorphy discussions on cranial characters, as this is the partition of the matrix for which Irritator and our study provides new evidence.

Time calibration for character state transition rates of cranial evolution

In order to plot our phylogenetic results to absolute time and to assess character state transition rates, we generated a tree with branch lengths scaled to time. We performed the time calibration in R v.3.6.0 (R Core Team), and used the resolved reduced consensus tree described in the previous section (Supplementary Data 15). We again employed the cal3 calibration method of Bapst (2013), using the same procedure as described above, and documented in Supplementary Data 16. The resulting cal3-calibrated, polytomy-resolved, branch averaged reduced consensus tree was pruned to include only taxa with known cranial material. We identified four clades or grades ('groups' hereafter) for which we were interested in character transition rates of the cranial partition of the character-taxon matrix. The clades were Spinosauridae, Megalosauroidea (i.e., including spinosaurids), and Allosauroidea. Other major clades (e.g., Coelurosauria, Ceratosauria) were not included because they have relatively incomplete taxon coverage in our matrix and thus result in less fair comparisons. Besides the three clades mentioned above, we also used the paraphyletic grade of non-spinosaurid megalosauroids. This allowed us to compare rates within Spinosauridae with those of closely related megalosauroid taxa, even if these do not form a monophylum to the exclusion of spinosaurids. To compute a rate metric, we required a number of character state transitions for each group, to be contrasted with an evolutionary duration during which these were accumulated. Character state transitions were based on our optimization using PAUP* (Supplementary Data 13; see above) and counted for all four groups, whereby the number of character state changes for a group is the sum of the character state changes of its constituent groups and OTUs. Only ACCTRAN and unambiguous character state transitions were counted. The exception are two ambiguous cranial character state changes, which were optimized as spinosaurid synapomorphies

under DELTRAN but as Monolophosaurus+Spinosauridae synapomorphies under ACCTRAN. We counted these as synapomorphies of Spinosauridae, rather than as synapomorphies of the megalosauroid grade. Multiple character state changes for the same character within a group were counted as such, as each character state transition represents an evolutionary change. Because we only computed character state transition rates for the cranium, the pruning of taxa without skull material accounts for the bias that any OTU counts towards the evolutionary time of its group, but does not count towards the number of cranial character state transitions unless it also preserves cranial material. To get a duration of evolutionary time for each group, we summed the branch lengths of all branches within a given group, and also included the branch leading to that group from the next more inclusive node (i.e., groups were treated as stem-based). This was done in R using commands from the Claddis package (Lloyd 2016). Character state transition rates were then computed as the ratio of group-specific character state transitions and the total evolutionary time of the group. As the OTUs in our matrix have different levels of coverage in terms of positively scored cranial characters, we computed the proportion of scored cranial characters for all four groups as the ratio of scored cranial characters (i.e., no "?") to number of cranial characters (N = 195; see Supplementary Data 17). This value was used to produce a sampling-corrected per-group character transition rate with the unit 'character state transitions per Ma per scored character". These rate metrics represent fairer comparisons between groups than non-corrected rates. All calculations are documented in Supplementary Data 16.

Systematic Palaeontology

Theropoda Marsh, 1881

Tetanurae Gauthier, 1986

Megalosauroidea (Fitzinger, 1843)

Spinosauridae Stromer, 1915

Irritator challengeri Martill, Cruickshank, Frey, Small & Clarke, 1996

Holotype. SMNS 58022, largely complete skull, missing most of the premaxillae, anterior ends of the maxillae, and anterior parts of both mandibles.

Locality and horizon. Near Buxexé, close to Santana do Cariri, Ceará State, northeastern Brazil (see Sues et al., 2002: 535). Lower part of the Romualdo Formation (Santana Formation of some authors; see discussion in Arai & Assine, 2020) of the Santana Group, late Aptian (Arai & Assine, 2020).

Emended diagnosis. The original diagnosis of *Irritator challengeri* by Martill et al. (1996: 5) consisted of a list of skull characters, most of which are common in non-avian theropods (e.g., “tooth replacement mesolingual”, “maxilla straight with more than 11 teeth”, “orbit ovoid”, “stapes very thin, stick-like with expanded and flattened ends”) or at least not unique to *Irritator* (e.g., “anterior maxillary teeth are straight, elongate, with suboval cross section and unserrated anterior and posterior carinae”, “nasal opening oval, sited some way back from tip of snout”, “infratemporal fenestra almost as large as orbit”) and is thus of limited help to distinguish this species from other theropods.

Sues et al. (2002: 537) gave a shorter diagnosis for the species, based mainly on unique or at least very rare characters, but these authors also noted that the lack of cranial material for spinosaurids in general made any definite decision about the apomorphic status of characters tentative. Although some additional spinosaurid

cranial material has been described since (e.g., Dal Sasso et al., 2005; Kellner et al., 2011; Ibrahim et al., 2014, 2020; Hendrickx et al., 2016; Arden et al., 2019; Barker et al., 2021), the situation has not improved decisively, also since the taxonomic identity of many of these specimens is unclear. In the following emended diagnosis, we thus list characters that are tentatively regarded as apomorphic to *Irritator*, with characters that can be evaluated in at least one other spinosaurid specimen being indicated with an asterisk; future discoveries of more spinosaurid cranial material will have to show if the other characters represent autapomorphies of *Irritator* or synapomorphies of spinosaurids or a subclade thereof. In cases where characters represent a local apomorphy within theropods (i.e. they are present in some other, but distantly related taxa), other occurrences are noted in brackets.

Shelf-like subnarial fossa on the anterior ramus of the maxilla below the posterior end of the external nares* (absent in *Baryonyx*, *Suchomimus* and a snout referred to *Spinosaurus*; Charig & Milner, 1997; Sereno et al., 1998; Dal Sasso et al., 2005); widely spaced maxillary teeth, with distance between teeth subequal or greater than mesiodistal length of individual teeth in the anterior part of the maxilla and more closely spaced teeth posteriorly* (absent in *Baryonyx*, *Suchomimus* and a snout referred to *Spinosaurus*; Charig & Milner, 1997; Sereno et al., 1998; Taquet & Russell, 1998; Dal Sasso et al., 2005; similar in *Archaeopteryx*; Rauhut et al., 2018); posterodorsal end of ascending process of the maxilla tapering and undivided; ascending process extends further posterior than jugal ramus of the maxilla; jugal with slightly concave ventral margin; facet for contact with the laterosphenoid on postorbital very small and placed entirely on the anterior process of the postorbital (also present in *Dubreuillosaurus*; Allain, 2002); marked lateral ridge on the dorsal half of the squamosal process of the quadratojugal; lack of a well developed preotic pendant (=ala basisphenoidalis) in the braincase* (this structure is present in

Baryonyx, *Suchomimus, Ceratosuchops* and *Riparovenator;* Charig & Milner, 1997; MS, pers. obs. on cast, MNN GDF 214; Barker et al., 2021); pterygoid without ectopterygoid process; ectopterygoid with strongly reduced ventral recess (also present in *Ceratosaurus* and abelisaurids; Madsen & Welles, 2000; Sampson & Witmer, 2007) and very small medial pterygoid process; surangular with a broad and strongly ventrolaterally directed, posteriorly flange-like lateral shelf* (absent in *Camarillasaurus*; OR, pers. obs.).

DESCRIPTION

General description

While Sues et al. (2002) were only able to describe the outer morphology of the fossil, our (micro)CT data reveal inner cavities, the non-exposed sides of the skull bones and elements that are at least partly obscured by sedimentary matrix or other bones, some due to taphonomic displacement. Important new features could be revealed on the medial (e.g., maxillae) or lateral (e.g., right surangular) aspects of the cranial material. Some elements are only partly exposed on the fossil but are finely preserved (e.g., palatal elements, quadrate and squamosal, teeth). Furthermore, the right epipterygoid is visible in the specimen but was not mentioned before.

To facilitate comparability with other anatomical descriptions of non-avian theropods, we used anatomical direction terms for SMNS 58022 as if the animal held its skull horizontally.

Skull openings

As in most archosaurs, the most prominent skull openings of *Irritator* are the external naris, antorbital fenestra, orbit, infratemporal fenestra and the supratemporal fenestra (Figure 2A). Whereas the first three of these openings can be directly observed in the specimen, the shape of the temporal fenestrae can be estimated from a digital re-articulation of the bones that form large parts of their margins. The external naris is roughly oval, anteroposteriorly elongate and anteroventrally inclined. It is bordered by the premaxilla anteriorly, the nasal posterodorsally and posteriorly, and the maxilla ventrally. The maxillary surface in this region shows no recess for a process of either the nasal or premaxilla, suggesting that the maxillary contribution to the external naris is no artefact of breakage. The anterodorsal margin, which was most probably formed by the premaxilla, is not preserved. As in other spinosaurids, such as *Baryonyx* (Charig & Milner, 1986, 1997) and *Suchomimus* (Sereno et al., 1998), the external nares was obviously placed entirely posterior to the premaxillary body, although not to the degree seen in the snout referred to *Spinosaurus* by Dal Sasso et al. (2005).

The antorbital fenestra is elongate suboval in shape and steeply anteroventrally inclined. It is anteroventrally and anterodorsally bordered by the maxilla, and posteroventrally and posterodorsally by the lacrimal. In contrast to most non-avian theropods, the jugal does not participate in the antorbital fenestra. The orbit is reversed drop-shaped, being dorsally wider than ventrally, with the ventral part of the opening flexing slightly anteriorly. Anteriorly, the orbit is bordered by the lacrimal, while the prefrontal forms the anterodorsal margin. Dorsally, the orbit is bordered by the frontal, and posteriorly by the postorbital and the postorbital process of the jugal. The ventral margin is formed by the jugal. The infratemporal fenestra is nearly drop-shaped, being dorsoventrally taller than anteroposteriorly wide, and similar in size to the orbit. It is framed by the jugal anteriorly, the postorbital dorsally, the squamosal

posterodorsally and the quadratojugal posteriorly and posteroventrally. The supratemporal fenestra is irregularly oval-shaped and longer anteroposteriorly than wide mediolaterally (Figure 3B, Figure 4A). It is much smaller than the antorbital fenestra, orbit and the infratemporal fenestra. The parietal forms its anterior, medial and posterior margin. The postorbital forms the anterior and lateral margin and the squamosal is situated on the posterior corner of the supratemporal fenestra.

In ventral view, our cranial reconstruction reveals the previously unknown morphology of the palate in *Irritator* (Figure 2B, Figure 4B). The internal narial opening (choana) is displaced posteriorly and situated at the level of the anterior end of the antorbital fenestra; there is thus a partial secondary palate formed by the ventral parts of the maxillae and the vomer. The choana is a strongly anteroposteriorly elongated, anteriorly pointed, drop-shaped opening that is laterally and posteriorly bordered by the palatine, anterolaterally by the maxilla, and medially by the pterygoid and the vomer. The very small, subtriangular palatine fenestra (sometimes called the suborbital fenestra) is anteromedially framed by the palatine, medially by the pterygoid and posteriorly by the ectopterygoid. It is placed posterolateral to the internal choanae, at about the mid-length of the antorbital fenestra. The lateral and a small part of the anterior border are made up by the maxilla. The notably elongated subtemporal fenestra is surrounded by the ectopterygoid anteriorly, the pterygoid medially, the quadrate posteriorly, the quadratojugal posterolaterally and the jugal anterolaterally. It is by far the largest opening of the palate, and is placed below the posterior end of the antorbital fenestra, the orbit, and the anterior part of the infratemporal fenestra. Due to the anteroventral inclination of the quadrates, its posterior margin is placed entirely anterior to the supratemporal fenestra. Furthermore, the interpterygoid vacuity can be discerned. It is strongly elongated triangular in shape and becomes narrower

anteriorly. Laterally, the pterygoid makes up the border of the vacuity while the posterior margin is formed by the basisphenoid. Anteriorly, the interpterygoid vacuity extends to approximately the half-length of the ectopterygoid, at about the level of the posterior third of the antorbital fenestra.

Premaxilla

Solely the posterior portions of the narial processes of the paired premaxillae are preserved as a small, exceptionally thin cap on the anteriormost preserved portion of the maxillae on either side of the skull, whereas the premaxillary body and posterodorsal nasal process are missing (Figure 2A, Figure 3A). Because of the incomplete state of preservation, the detailed contacts with surrounding bones are not entirely clear. Usually, however, the premaxilla contacts the maxilla posterorventrally and the nasal posterodorsally and, possibly, the vomer ventromedially.

As the nares is placed entirely posterior to the premaxillary body, there is an undivided, dorsally placed posterior narial process of the premaxilla, as in *Baryonyx* and *Suchomimus* (Charig & Milner, 1986, 1997; Sereno et al., 1998), unlike the situation in most non-avian theropods, in which distinct nasal and subnarial processes extend posteriorly directly from the premaxillary body. The preserved posterior end of the narial process of the premaxilla overlaps the anterior ramus of the maxilla dorsally. Posteriorly, the process has a rounded notch that forms the anteriormost margin of the external naris, and thus represents the branching of the nasal and subnarial processes of the premaxilla. Since the nasal reaches far anteroventrally, it is possible that the premaxilla formed only a small portion of the anterodorsal margin of the external naris in lateral view in *Irritator*. This is also the

case in *Baryonyx* and *Suchomimus* in which the long posterodorsal nasal process of the premaxilla is flanked laterally by the anterodorsal premaxillary process of the nasal over most of its length (Charig & Milner, 1997, Sereno et al., 1998).

The preserved part of the premaxilla of *Irritator* clearly contributes to the margin of the external naris, as it is usual in theropods and also the case in *Baryonyx* and *Suchomimus* (Charig & Milner, 1997, Sereno et al., 1998), but not in a snout referred to *Spinosaurus* (MSNM V4047; Dal Sasso et al., 2005), in which the premaxilla is excluded from the naris. However, the preserved, posteriorly tapering subnarial process of the premaxilla is extremely short in *Irritator*, contrasting the more elongate process in *Baryonyx* and *Suchomimus* (Charig & Milner, 1997, Sereno et al., 1998).

Maxilla

Both maxillae are incomplete anteriorly, but many aspects of their morphology can be discerned (Figure 5,6). The right maxilla is heavily damaged on its lateral surface along the maxillary body. Here, an elongate, rectangular and toothed fragment is broken away from the rest of the bone (Figure 1B, Figure 6). The maxilla contacts the narial process of the premaxilla anterodorsally, the nasal dorsally, the palatine and vomer medially and the lacrimal and jugal posteriorly (Figure 2-4); the anterior articulation with the premaxillary body is missing.

The contact area with the lacrimal and jugal is damaged on both sides, but a piece of maxilla remains articulated with these bones on the right side. The ascending process of the right maxilla is broken along a large vertical fracture that separates the snout from the rest of the cranium, but the posterodorsally tapering end of both processes remains in articulation with the respective nasal and lacrimal. The left

maxillary body has a better surface preservation than the right pendant, but the ascending process is less well preserved. Furthermore, the posterior process of the left maxilla that articulates with the lacrimal and jugal is missing.

The maxilla is comparatively slender and low. The well developed ascending process has an anteroposteriorly long base and is inclined steeper (around 25°) than in *Suchomimus*, in which the process is almost horizontally orientated over its entire length (Sereno et al. 1998). The inclination of the ascending process is much steeper in other megalosaurs, such as *Afrovenator* (Sereno et al., 1994), *Dubreuillosaurus* (Allain, 2002), *Duriavenator* (Benson, 2008), and *Torvosaurus* (Hendrickx & Mateus, 2014). The entire anterodorsal margin of the process is gently convex and lacks a marked change in orientation, as it is present in coelophysids (e.g., Raath, 1977), *Monolophosaurus* (Zhao & Currie, 1993; Brusatte et al. 2010), the allosauroid *Asfaltovenator* (Rauhut & Pol, 2019), and many megalosaurids (e.g., Sereno et al., 1994; Allain, 2002; Benson, 2008; Hendrickx & Mateus, 2014; Rauhut et al., 2016). The ascending process of *Irritator* becomes very slender and tapers posteriorly and articulates with the nasal dorsomedially and with the lacrimal posteromedially, which the ascending process overlies laterally. In contrast to most non-avian theropods, the posterior end of the ascending process does not bifurcate to receive the anterior end of the lacrimal but tapers to a point, which laterally overlies an extensive articular facet on the lateral side of the anterior end of the lacrimal. Another very unusual feature of the maxilla of *Irritator* is that the ascending process extends further posteriorly than the jugal ramus of this bone, reflecting the strong anteroventral inclination of the ventral ramus of the lacrimal.

The elongated body of the maxilla of *Irritator* is morphologically similar to those of other known spinosaurids. As in these, this elongate shape is mainly caused by the

greatly elongated anterior ramus. The anterior ramus contacts the premaxilla anterior to the level of the external nares, as in other spinosaurids (Charig & Milner, 1986; Sereno et al., 1998; Dal Sasso et al., 2005). The maxilla forms most of the ventral and the posteroventral margin of this opening, as in a snout referred to *Spinosaurus* (Dal Sasso et al., 2005), but in contrast to *Suchomimus*, where most of the anteroventral border of the nares is formed by the subnarial process of the premaxilla, and the maxilla has only a small participation in the narial opening (Sereno et al., 1998). A narrow longitudinal groove with sharp lateral and medial margins is present on the dorsal surface of the maxilla anterior to the naris and below its anterior margin, marking the facet for the contact with the narial process of the premaxilla. Posterior to this groove, the dorsal surface of the maxilla forms a subnarial fossa in the form of a posteriorly widening shelf below the posterior part of the nares. In its anterior portion, the shelf is strongly laterodorsally directed, with the medial rim of the articular groove for the premaxilla forming a sharp medial rim of the shelf. This medial crest becomes lower posteriorly, and the shelf twists into a more dorsally facing position in its posterior part. Its lateral margin is formed by a low ridge that becomes more conspicuous posteriorly and leads into the anterodorsal margin of the ascending process of the maxilla. An intermaxillary contact is present ventrally in the anterior part of the anterior maxillary ramus, and the thin vomer is also contacted in this region. Together, these bones form a short secondary palate below the anteriorly narrow and posteriorly widening nasal vestibule. In anterior view, breakage reveals that the anterior maxillar rami are triangular in cross section and broadly contact each other dorsoventrally, except for their upper third where the anteroposteriorly long sinus of the nasal vestibule is situated. (Figure 3A) The anteromedial surface of each maxilla is slightly roughened for the articulation with the respective counterpart. Dorsal to the 4th preserved alveolus and posterior to the end

of the premaxillar subnarial process, the left maxilla is dorsoventrally narrowest, as the margin of the bone forms a concave notch along the margin of the external naris (Figure 5A-D).

In addition to the lacrimal contact of the ascending process, a second contact with the lacrimal is present ventral to the antorbital fenestra, where the maxilla bifurcates into a posterodorsal process that contacts and overlaps the anteroventral end of the lacrimal laterally, and a posteroventral process that additionally contacts the jugal, palatine, and possibly the ectopterygoid (Figure 2A, Figure 6A).

The lateral surface of the maxilla bears a single row of broadly spaced neurovascular foramina, each of which is positioned approximately between individual tooth positions (Figure 5A). There are at least seven neurovascular foramina on the lateral surface of the left maxilla, leading to the anteroposteriorly long neurovascular canal, which housed the trigeminal nerve and blood vessels. Due to the limits of resolution in the CT data and preservation, the neurovascular canals could not followed over their entire length in both maxillae. Such canals are also known from other spinosaurids (Rayfield et al., 2007), megalosaurs (Benson, 2008, Rauhut et al., 2020) and other non-avian theropods (Barker et al., 2017). Seemingly, unlike *Baryonyx* and *Suchomimus* (Charig & Milner, 1997, Sereno et al., 1998), *Irritator* does not bear one foramen per alveolus. On the left maxilla, the foramina in *Irritator* are approximately situated above the 2nd, 3rd, 5th and 6th preserved alveoli as well as between the 6th and 7th, above the 8th, and between the 9th and 10th. Additionally, the foramina tend to be dorsoventrally higher positioned the more anteriorly they are.

The antorbital fossa seems to have been small and mainly restricted to the anterior rim of the antorbital fenestra, although the medial wall of the fossa is incompletely preserved on both sides. In contrast to most non-avian theropods, but like in

Suchomimus (OR, SE, pers. obs., MNN GDF 501; Sereno et al. 1998), the fossa has a sharp and overhanging anterior and anteroventral rim and does not extend onto the jugal ramus of the maxilla. Dorsally, the fossa more gradually fades into the lateral surface of the process of the ascending process bordering the antorbital fenestra dorsally, but over most of the length of this process, its lateral surface is not notably depressed. Despite the damaged medial wall of the fossa, it seems almost certain that no distinct maxillary fenestra was present, as there would be very little space for such an opening. Ventrally, a natural rim of the medial lamina of the antorbital fossa is preserved and disappears below an overhanging lateral lamina in lateral view, being strongly indented anteriorly in the ventral part in medial view. In general, the medial wall gives a similar impression as in *Suchomimus* (Sereno et al. 1998), being more extensive dorsally than ventrally, although more extremely so than in the latter taxon, in which parts of the medial lamina are also visible on the ventral end of the antorbital fossa in lateral view. A feature revealed by the break of the right maxilla (see Sues et al., 2002: fig. 1B) and our CT data is the presence of a large antrum, invading the base of the ascending process and the anterior ramus of the maxilla from the anterior margin of the antorbital fenestra, and extending approximately from the 4^{th} to the 10^{th} preserved tooth position within the left maxilla (Figure 5B, D, E). The antrum is connected to the external antorbital fenestra (sensu Witmer, 1997) by a dorsoventrally large, posteriorly opening, funnel-like foramen, similar to the condition in *Suchomimus* (MNN GDF 501; Sereno et al., 1998) and *Wiehenvenator* (Rauhut et al., 2016), although both the antrum and the foramen are relatively smaller in the latter taxon, in accordance with the much less extensive base of the ascending process. A thin, dorsoventrally slightly medially convex wall borders the antrum medially and connects the dorsal margin of the alveolar maxillary body with the medial side of the anterodorsal margin of the ascending process (Figure 5E). Like

in *Allosaurus* (Madsen, 1976, Witmer, 1997), this medial wall is anterodorsally perforated by a large, oval opening that connects the antrum with the space just posterior to the internal naris (see also Sues et al., 2002). This opening is preserved on both sides, although the margins seem to be largely broken, and on the left side, the medial wall posterior to it is largely broken away. Sues et al. (2002) identified the large recess in the base of the ascending process as the maxillary antrum, but its position anterior to the antorbital space and its connection to the latter by a posteriorly opening foramen are more consistent with an interpretation as the promaxillary recess, with the foramen representing the promaxillary foramen. The left promaxillary recess reaches anteroventrally deep where it seems to meet the neurovascular canals ventral to the posterior margin of the external naris. This is similar to the condition in *Suchomimus* and the spinosaurid maxillar fragment ICMWS 2014.95 (OR, SE, pers. obs., MNN GDF 501; Munt et al., 2017).

The maxillary body and the elongate anterior ramus of *Irritator* form the tooth-bearing part of the bone. Ten tooth positions are preserved on the left side and twelve on the right side (though, see details in the dentition section). Sales & Schultz (2017) interpreted the alveoli they recognized to represent tooth positions 3 to 12 and suggested that the fourth maxillary tooth seems to generally be the largest in spinosaurids, and thus the second preserved alveolus of the left side in *Irritator* should represent this tooth position. However, the situation is not quite as clear as that: In *Baryonyx*, maxillary tooth positions 2 to 4 are of subequal size, with the third alveolus seemingly being slightly larger than the fourth (NHMUK R 9951; Charig & Milner, 1997), and in *Suchomimus*, maxillary tooth positions three to six are largest and approximately subequal in size (OR, pers. obs., MNN GDF 501; Sereno et al., 1998). Although the posterior part of each maxilla is damaged in *Irritator*, the alveolar size of the posteriormost preserved tooth position on the right side, along with the

geometrical arrangement of the skull bones in this area may suggest that no further teeth were present posterior to this tooth. Anteriorly, it is likely that additional maxillary teeth were once present.

A very unusual condition in *Irritator* is that the maxillary teeth are very widely spaced, with the space between individual teeth being more than the mesiodistal length of the alveoli (Figure 1, Figure 2, Figure 4B, Figure 5, Figure 6). Individual alveoli are almost round (Figure 5G), slightly longer mesiodistally than wide labiolingually, as in other spinosaurids, but unlike the rectangular alveoli of abelisaurids (e.g., Smith, 2007) or the much more elongate alveoli of most non-avian theropods. The depth of the alveoli extends to almost the dorsal margin of the maxillary body in the anterior ramus, but diminishes below the promaxillary recess (Figure 5B, D, Figure 6B, D).

The ventral surface of the maxilla between the alveoli forms a lateral lamina, a notable longitudinal trough, and a prominent, swollen medial ridge (Figure 4B, Figure 5F, G, Figure 6E). As in other spinosaurids (e.g., *Baryonyx*; NHMUK 9551; *Suchomimus*; GDF 501), this medial ridge represents a ventrally expanded paradental lamina (the lamina overhanging the nutrient groove at the dorsal end of the interdental plates; see Hendrickx & Mateus, 2014) that covers the interdental plates medially. The latter seem to be completely fused and are separated from the paradental lamina by a deep but narrow incision. The medial ridges formed by the swollen paradental laminae constitute the secondary palate below the nasal passage. Both medial ridges are close and in parallel to each other anteriorly, but diverge at the 4th preserved maxillary alveolus. The medial ridge reaches at least to the last preserved tooth positions . A similar ridge is also known from *Baryonyx, Suchomimus* and *Spinosaurus* (Charig & Milner, 1997, Sereno et al., 1998, Dal Sasso et al., 2005).

The medial surface of the maxilla bears a deep and anteroposteriorly long depression that receives the maxillary process of the palatine. This depression is positioned dorsal to the posterior portion of the median ridge, and extends anteriorly to the level of the middle portion of the promaxillary recess, at the space between the sixth and seventh preserved alveolus. Below the promaxillary recess, the alveolar part of the medial side of the maxilla bulges slightly medially, whereas the medial side of the anterior ramus is flat for the contact with the opposite side. A prominent lingual bar or lingual bulge, as it is present in many basal tetanuran theropods (Carrano et al., 2012) is absent.

In *Irritator*, the configuration of the maxilla, lacrimal and jugal excludes the jugal from the antorbital fenestra (Figure 1, Figure 2A), similar to the condition in *Ceratosaurus* where, however, this point is situated more posteriorly (Gilmore, 1920). The posteroventral contacts of the maxilla and the morphology of the respective maxillary process of the jugal are hard to determine with certainty due to breakage on either side of the specimen. However, on the right side, there are two main pieces of the maxilla preserved: a mediolaterally thin, posteriorly tapering and posterodorsally directed piece that overlaps the lateral surface of the anteroventral end of the lacrimal and contacts the dorsal margin of the jugal (Figure 1B, Figure 2A, Figure 6). This process is posteriorly bifurcated into two thin rami, which are visible in the fossil (see Sues et al., 2002: fig. 1B). The second main piece of posterior maxillary process is a posteriorly tapering process that aligns with the ventral skull margin, and articulates with the ventromedial surface of the jugal and possibly the ventral surface of the lacrimal (Figure 4B, Figure 6). This process extends to the position of the ectopterygoid, possibly contacting its anterior end. These two main pieces suggest that the posterior maxillary process was bifurcated into a dorsal ramus that framed the lacrimal-jugular area laterally, and a ventral ramus that framed this region

medially. As a consequence, the posteroventral process of the maxilla brackets the jugal and lacrimal in a paperclip-like fashion that is unknown in other theropods, with the possible exception of *Suchomimus*, which also seems to have a bifurcated posterior end of the maxilla (OR, SE, pers. obs., MNN GDF 501; Sereno et al., 1998).

Nasal

The nasals are nearly completely preserved (Figure 1, Figure 2, Figure 4A, Figure 7) with only slight breakage that has occurred on the anterior end of the bones, but much of their surface is somewhat abraded. The paired nasals are tightly fused with each other only on their posteriormost third, but a suture is traceable anteriorly (Figure 8). However, we segmented the nasals from the CT data as a single element, and the right and left nasals are described together in the following. The nasal contacts the premaxilla anteriorly, the maxilla and lacrimal ventrally and the prefrontal and frontal posteroventrally, forming the skull roof between the external nares and the orbit (Figure 2-4). The CT data suggest that there is an artificial insertion of a foreign body in the nasals, close to their mid-length, within a main fraction (Figure 1, Figure 7); thus, this part has not been considered in the description.

Whereas the posterior part of the nasal forms the dorsal skull roof, the bone flexes ventrally in its anterior part to form parts of the lateral wall of the snout in front of the ascending process of the maxilla. As preserved, right and left external nares are anteriorly confluent with one another, but we assume that this is due to breakage, and the premaxillae and nasals would have formed a midline contact that separates each narial opening from one another. Anteriorly, the dorsal and posterior margin of the external naris is formed by an oval notch produced by a dorsal premaxillary and a ventral maxillary process of the nasal. The premaxillary process is only preserved on

the right side, but its anterior end is missing. The process tapers anteriorly when seen in lateral view. The maxillary process of the nasal projects anteroventrally and overlies the maxilla laterally, forming an arced cap over the internal of the skull. The ventral margin of the nasal which meets the maxilla ascends from the maxillary process posteriorly along the anterodorsal margin of the ascending process of the maxilla. Here, the nasal slightly overlaps the maxilla dorsolaterally in its anterior portion, whereas the posterior end of the ascending process of the maxilla abuts the ventrolateral rim of the nasal laterally. Posteriorly, the nasals become dorsoventrally thicker and their ventral surface becomes less arched and nearly flat. On the dorsal surface, the remnant of a nasal crest is preserved and extends from shortly posterior to the external naris to nearly the posterior end of the bone. The nasal crest seems to have been dorsoventrally tall around the mid-length of the nasals, but becomes lower and transversely thin posteriorly before it disappears around 5 cm before the rounded posterior margin of the nasal is reached. Thus, the crest is not as pronounced in *Irritator* as it is in *Baryonyx* and *Suchomimus* where it extends to the posterior end of the nasal, forming a nasal cornet (Charig & Milner, 1997; MS, pers. obs. on cast, MNN GDF 214 referred to *Suchomimus*). A transverse posterior expansion of the crest at the level of the nasal-prefrontal contact, as it is present in *Baryonyx* and *Suchomimus* (Charig & Milner, 1997; MS, pers. obs. on cast, MNN GDF 214) is absent in *Irritator*, but the dorsal surface lateral and posterior to the crest is gently convex. However, it should be noted that the exact development of the crest is likely to have been affected by the abrasion of the dorsal surface of the nasals, especially in its anterior part, and it cannot be excluded that the crest above the mid-length of the nasal continued anteriorly. In contrast to a partial nasal referred to *Spinosaurus* (Dal Sasso et al., 2005), the crest is solid and not pneumatized in *Irritator*.

In contrast to various basal tetanurans (Rauhut, 2003), the nasal of *Irritator* does not contribute to the antorbital fossa. Instead, the joint nasals dorsally overlie the ascending process of the maxilla, the lacrimal and prefrontal. The nasals are mediolaterally broadest just posterior to the position of the small lacrimal boss. In this region, the nasal forms a posterior notch for the prefrontal, and the lateral margin of the nasal inserts between the lacrimal boss and the prefrontal (Figure 7A, C, Figure 8), resulting in an arrowhead-like shape of the posterior nasal, as in *Baryonyx* (Charig & Milner, 1997). This is better preserved on the right side. Posteromedial to the notch, Sues et al. (2002) inferred that a potential postnasal fenestra (named after the posterolateral notch in the nasal of *Baryonyx*; Charig & Milner, 1997) in *Irritator* has rather been produced by the “dorsal displacement” of the nasal from the prefrontal, lacrimal and frontal contact. Seemingly, this "fenestra" is rather a superficial depression between the prefrontal, frontal and nasal that is filled with sediment. The CT data suggest a tightly-fitting articulation of these bones here, with the nasal being considerably thickened in this region.

Based on our CT data, the nasals show an offset ventral platform (Figure 7C) that is wedged between the nasal processes of the frontals. The nasal processes of the frontal receive the nasals mainly anteromedially and the posterior surface of the platform abuts the anteromedial surface of the frontals. In lateral view, the posteriormost portion of the nasal overlies the frontals dorsally and the frontals dip beneath the nasal anteriorly. A ventral median ridge as present in *Baryonyx* (Charig & Milner, 1997) is absent in *Irritator*.

Lacrimal + Prefrontal

Both lacrimals and prefrontals are preserved (Figure 1, Figure 9). Although the

sutures between the lacrimal and the prefrontal are at least partially clearly visible on the fossil (Figure 10), both bones cannot be distinguished in the CT data, which might suggest a certain degree of fusion of the bones internally, as generally all other sutures are distinguishable in the specimen, including those of tightly aligned braincase bones. As a consequence, we segmented the lacrimal and prefrontal as a single model for each side. Both elements are described together in here, but lacrimal and prefrontal features are described separately as much as possible, starting with the lacrimal.

The lacrimal contacts the maxilla anteriorly, the nasal dorsally, the prefrontal posteromedially and the jugal ventrally (Figure 2-4). The right lacrimal is in a better condition than the left one, still showing a distinct lacrimal recess (Figure 11). As it is typical in non-avian theropods (Gauthier, 1986; Rauhut, 2003), the lacrimal has an inverted L-shape, but with an acute angle of c. 30-35° (as measured between the dorsal and posteroventral margins of the antorbital fenestra), rather than almost right-angled between the anterior end ventral processes, as in *Baryonyx* and *Suchomimus* (Charig & Milner, 1997; MS, pers. obs. on cast, MNN GDF 214). The anterior process is approximately 68% of the length of the ventral process (both measured from the posterodorsal edge of the lacrimal to the tip of the respective process), and due to the strong anteroventral inclination of the latter, its tip is placed anterior to the anterior end of the anterior process, a condition that seems to be unique in respect to all non-spinosaurid theropods. The posterodorsal part of the medial lacrimal surface articulates with the prefrontal. Anterodorsally, the lacrimal has an anterior process that forms the posterior part of the dorsal margin of the antorbital fenestra, and which is partially overlapped by the maxilla laterally and the nasal dorsally. This process is mediolaterally thin and dorsoventrally tall at its base while tapering anteriorly. Its

dorsal margin is slightly convex proximally and becomes straight distally, whereas the ventral margin is gently concave, forming the margin of the antorbital fenestra.

Posterior to the anterior process of the lacrimal, at the base of the ventral process, the posterior margin of the lacrimal which frames the anterior orbital margin is mediolaterally thickened. This thickened part of the lacrimal bears a dorsoventrally tall recess, which faces anteriorly and forms the posterior end of the antorbital fossa. The recess contains four dorsoventrally aligned main depressions that are separated from each other by mediolaterally oriented ridges. The second depression from dorsally is the smallest, but seems to represent a pneumatic foramen to a very small cavity network, stretching ventrally. CT data show that where the ridge that houses the lacrimal recess flattens laterally, some other small cavities are situated without any obvious connection to a pneumatic foramen. The lacrimal recess of *Baryonyx* is anteroposteriorly and dorsoventrally larger than in *Irritator* (Charig & Milner, 1997). Furthermore, the lamina that covers the recess laterally extends ventrally onto the ventral process of the lacrimal and marks the posterior border of the antorbital fossa in both taxa. The recess was originally covered by a very thin, bulbous bony lamina, which was apparently lost during preparation (OR, pers. obs.).

The ventral process of the lacrimal forms the articulation with the maxilla, jugal, and likely the palatine. The process is strongly anteroposteriorly expanded ventrally, making it roughly triangular in shape. The expansion is mainly anteroventrally, so that the lacrimal orbital margin is only about 72% of the length of the respective margin of the antorbital fenestra. As in other spinosaurids (Charig & Milner, 1997, Sereno et al., 1998), the anteroventral inclination of the anterior margin of the process results in an oval antorbital fenestra of which the lacrimal forms a substantial part of the posteroventral margin. Whereas the rim of the antorbital fenestra is very gently

concave, the orbital margin of the ventral process is slightly convex; a suborbital spur or process is absent. The orbital margin of the ventral process is mediolaterally notably convex and thickened dorsally in the area of the lacrimal recess, but becomes gradually thinner towards the jugal contact. The rim of the antorbital fenestra is also slightly thickened, but much less so than the orbital margin. The position of the lacrimal foramen and course of the lacrimal canal could not be established. Even more than in other basal tetanurans (Evers et al., 2020), the distal end of the ventral process articulates widely with the jugal ventrally and the maxilla anterolaterally. Unlike in most basal tetanurans, however, the lacrimal and maxilla exclude the jugal from participating in the margin of the antorbital fenestra (Evers et al., 2020). The ventral margin of the lacrimal articulates with the jugal along a relatively simple contact, with the suture being notably anteroventrally inclined. A broad overlap of the jugal over the ventral lamina of the lacrimal, as it is plesiomorphically present in saurischians (Sereno & Novas, 1993) does not seem to be present, although it cannot be completely excluded that this might be due to lack of resolution of the CT data, as this lamina is extremely thin in many non-avian theropods. Shortly before both bones form the anteroventral margin of the orbit, a notch is developed within the ventral margin of the lacrimal. A similar notch can also be discerned in *Allosaurus*, however without an anteroventrally inclined suture between the jugal and the lacrimal (Evers et al., 2020). The contact with the maxilla seems to be restricted to the anteroventral portion of the ventral process of the lacrimal, which is overlapped by the dorsal posterior process of the maxilla laterally (Figure 2A). This is in contrast to most non-avian theropods, in which the base of the lacrimal broadly contacts the dorsomedial surface of the maxilla medial to the jugal (Evers et al., 2020).

As with the antorbital fossa on the maxilla, a clearly defined antorbital fossa is only present in front of the lacrimal recess. The sharply defined rim of the fossa extending ventrally from the lacrimal recess ends at about the half-height of the posterior margin of the ventral process. Below this point, the lateral surface gradually deepens anteriorly, but a clearly rimmed antorbital fossa is absent. However, in contrast to most non-avian theropods, including *Baryonyx* (Charig & Milner, 1997), but with the exception of e.g., *Torvosaurus* (Britt, 1991), the dorsal and ventral parts of the lacrimal antorbital fossa on the ventral process are confluent, and not interrupted by an anterior expansion of the lateral lamina of the lacrimal. On the anterior process, there is also no defined rim of the antorbital fossa, but the lateral surface of the process is level with the lateral surface of the lacrimal anterior to the lacrimal recess, indicating that most of the process might have been occupied laterally by the antorbital fossa. The dorsal part of the anterior half of the process is very slightly depressed where it is overlain laterally by the posterior end of the ascending process of the maxilla.

Medially, the lacrimal shows two well developed ridges (Figure 9) that extend along the dorsal margin of the anterior process and the anterior margin of the ventral process and are aligned posterodorsally with the anterior and ventral processes of the prefrontal, respectively. The prominent orbitonasal ridge of the lacrimal and prefrontal thus extends from the posteromedial portion of the prefrontal to the anteroventral corner of the ventral process of the lacrimal. Here, the palatine possibly meets the lacrimal medially with a small lateral process. In *Baryonyx*, a very similar orbitonasal ridge is present (Charig & Milner, 1997). However, the ridge in *Baryonyx* is divided into a sharp anterior and a likewise sharp, parallel posterior crest by a longitudinal trough. Such a trough, but less deep and less clearly defined, might be present in the left lacrimal of *Irritator*, although this element is rather poorly

preserved. In the better preserved right lacrimal of *Irritator*, the orbitonasal ridge is broad and anteroposteriorly rounded below the prefrontal. In its ventral third, the posteroventral border of the ridge forms a sharp and very slightly overhanging crest. The medial surface of the ventral process posterior to the orbitonasal ridge is triangular in outline and gently concave between the ridge and the thickened orbital margin.

The ridge along the dorsal rim of the anterior process is slightly thinner than the orbitonasal ridge and disappears anteriorly at approximately the half length of the anterior process (as measured from the rim of the antorbital fenestra). In the proximal portion of the anterior process, this ridge is triangular in cross-section, with a flattened, dorsomedially facing surface and a mediolaterally shorter, also somewhat flattened, ventrally facing shelf. The surface between the two ridges, medial to the external lacrimal recess, is slightly concave and forms a deep recess anterior to the prefrontal.

The prefrontal is medially positioned with respect to the lacrimal, and its anterior and anteroventral processes contact the medial surface of the latter, whereas the short but stout posterior process extends posterior to the level of the lacrimal (Figure 9, Figure 10). As in most basal tetanuran theropods, the prefrontal is a roughly hook-shaped element, with distinct anterior and an anteroventral processes, which meet each other at an angle of 30-35°. Since the prefrontal seems to be at least partially fused with the lacrimal, the exact extent of the anterior and anteroventral processes cannot be discerned with certainty, but the morphology of the prefrontal-lacrimal complex and the sutures visible on the actual specimen give some indication of their morphology. The anteroventral process of the prefrontal contributes to the orbitonasal ridge and seems to extend to approximately one third of the height of the

orbit. Posterodorsally, the ridge is continuous with the crista cranii of the frontals, which separate the sulcus olfactorius medially from the lateral orbital facet. The anterior prefrontal process is shorter than the anteroventral process, but defines a dorsal margin to a posterodorsal recess of the internal antorbital space in the region where lacrimal, prefrontal and nasals contact each other. The posterior process of the prefrontal is visible in lateral view of the skull, and bridges the space between frontals and lacrimal. Thus, the prefronal forms a considerable part of the anterodorsal margin of the orbit and is visible in lateral view, in contrast to many other basal tetanurans.

Frontal

Both frontals are preserved (Figure 12). Although the interfrontal suture is discernible on the fossil (Figure 8), it was not possible to individually reconstruct them as they seem tightly fused with each other in the CT data, and thus are described in unison here. The frontal contacts the nasal anteriorly, the prefrontal anterolaterally, the parietal posteriorly, the postorbital posterolaterally and the orbitosphenoid and laterosphenoid posteroventrally (Figure 2-4). Dorsally, a low median ridge extends along the frontals, subdividing the otherwise nearly flat skull roof table formed by the frontals; this ridge is only preserved on the anterior half of the frontals, as the dorsal surface of the posterior half is largely abraded. In contrast to many other megalosauroids (e.g., Allain, 2002; Sadleir et al., 2008), the basal tetanuran *Piatnitzkysaurus* (Rauhut, 2004), and metriacanthosaurids (IVPP 10600; Currie & Zhao, 1993), but similar to the condition in *Acrocanthosaurus* (Eddy & Clarke, 2011) and other carcharodontosaurids (e.g., Coria & Currie, 2002), the frontals are rather short and broad, the articulated elements being slightly broader mediolaterally than

long anteroposteriorly. The frontals are mediolaterally widest on their posterior end and become narrower towards the nasals anteriorly. However, a marked postorbital process in the posterior part, as it is e.g., present in *Allosaurus* (Chure & Loewen, 2020), is absent, and the orbital margins are very slightly convex in dorsal view. The frontal is vaulted, so that the posterior part flexes downwards with regard to the anterior portion, which is aligned with the dorsal surface of the nasal (Figure 1, Figure 2, Figure 12). This contributes to the snout inclination that we have argued for on the grounds of horizontal semicircular canal orientation in a previous study (Schade et al., 2020).

In contrast to most non-avian theropods, the frontals become gradually thicker anteriorly. In general, the frontal is rather massive, with its maximal thickness (c. 18 mm) being more than 25% of its anteroposterior length. Anteriorly, the frontal articulates with the nasal in a complex suture. As noted above, dorsally, the low and rounded posteriormost portion of the nasals rests upon a roughened and semicircular medial surface of the frontals. This relatively short dorsal posterior process of the nasal is offset from the thickened main nasal body by a marked step, below which the nasal is slotted in between the lateral nasal processes and abuts the anterior end of the thickened frontals. In most basal tetanuran theropods, the frontals usually bear long, plate-like anterior projections that are extensively overlapped dorsally by the nasals (e.g., *Dubreuillosaurus*: Allain, 2002; *Sinraptor*: Currie & Zhao, 1993), which differs from the condition in *Irritator*. In addition, the anterior end of the frontal contacts the prefrontal anterolaterally. In contrast to the condition in the vast majority of non-avian theropods, the facet for the prefrontal is not developed as a deep socket, but has a rather flat to only slightly concave surface and faces more anteriorly than laterally.

In ventral view, the frontal of *Irritator* bears two small anterior processes that contact the nasals medially and the respective prefrontals anteriorly and laterally. While the right suture between frontal and prefrontal is rather straight in ventral view, the left frontal seems to bear a ventrolateral notch for the respective prefrontal (Figure 10; which might be a result of breakage). The medial orbitonasal ridge of the lacrimal and the prefrontal continues posteriorly to form paired ventral ridges of the frontal, the crista cranii, which confine the olfactory tract impression (sulcus olfactorius). Compared to other basal tetanuran theropods, the cristae cranii are pronounced, though not to the extent seen in troodontids (see Rauhut, 2003: fig. 11C). The olfactory tract is narrow posteriorly (c. 10 mm), but widens gradually anteriorly to a width of c. 15 mm. A large anterior expansion, as it is e.g., present in *Allosaurus*, is absent. The cristae cranii become slightly higher and more sharply defined anteriorly. The orbital facets are roughly trapezoidal in outline, being wider posteriorly than anteriorly, and are very gently concave anteroposteriorly but more or less straight mediolaterally, being inclined gently dorsolaterally. The frontal forms most of the dorsal border of the orbit, and the lateral margin of the bone forms a rather sharp lateral rim (Figure 1, Figure 2).

The supratemporal fossa on the posterodorsal surface of the frontal is a shallow but mediolaterally wide depression (Figure 12A). It is clearly delimited anteriorly and medially by low ridges and faces mainly posterodorsally, unlike the situation in many basal tetanurans, in which this fossa faces mainly dorsally, but comparable to the morphology seen in many non-avian coelurosaurs (Rauhut, 2003). However, the frontal is excluded from the supratemporal fenestra by the parietal, similar to e.g., *Allosaurus* (Chure & Loewen, 2020). In lateral view, the frontals show a slight arc on the dorsal margin of the orbit. The frontal articulates with the anterior process of the

postorbital via a shallow and anteroposteriorly short depression which is clearly visible on the left side.

At the posterior end, the frontals contact the anterior end of the parietals dorsally and the laterosphenoids ventrally. In ventral view, there is a notch on each side of the posterior end of the olfactory tract impression. Here, the articulation surface for the medial head of the laterosphenoid is discernible Figure 12B).

There are small cavities within the frontals that seem to be arranged in anteroposteriorly oriented, dashed rows. On either side of the dorsal median ridge, one such row is clearly discernable. The cavities are seldomly interconnected and are not associated with a pneumatic foramen.

Parietal

Both parietals are preserved but incomplete (Figure 13). The transverse nuchal crest is completely absent and the dorsal surfaces of both parietals are broken and eroded in most places, especially posteriorly (Figure 8, Figure 14). This is most obvious in comparison with a braincase that is probably referable to *Suchomimus*, where an anteroposteriorly and mediolaterally very prominent, mainly laterally pointing transverse nuchal crest is present (MS, pers. obs. on SMNS cast of MNN GDF 214). Additionally, the condition in *Suchomimus*, *Ceratosuchops* and *Riparovenator* suggest a relatively anteroposteriorly longer supratemporal fossa on the anterior lateral wing of the parietal in these taxa (MS, pers. obs. on cast, MNN GDF 214, Barker et al., 2021). The parietal contacts the frontal anteriorly, the postorbital anterolaterally, the laterosphenoid anteroventrally, the supraoccipital posteriorly and ventrally and the otoccipital and squamosal posteroventrally (Figure 2-4). In general,

the bone seems to be less massive than the frontal, although its thickness is certainly affected by the abrasion of its dorsal surface.

In dorsal view, the parietals form a straight and mediolaterally wide frontoparietal contact (Figure 3B, Figure 4A, Figure 8). Anterolaterally, the lateral tip of the parietal articulates with the postorbital, and, whereas the parietal articulates with the frontal on the skull roof, its anteroventral margin contacts the lateral process of the laterosphenoid. Anterolaterally, the parietal forms a dorsally facing shelf of the supratemporal fossa that is continuous with the portion of the fossa on the frontal and clearly delimited by a raised rim medially, placed c. 10 mm lateral to the midline of the joined parietals. The mid-section of the parietals is constricted to approximately one-third the width of the frontal suture. Whereas the anterior portion is flat and faces dorsally, in the mid-section, the sides flex downwards towards the contact with the lateral braincase wall, formed by the laterosphenoid, and, more posteriorly, the otoccipital. The lateral surface is deeply concave anteroposteriorly in dorsal view, forming the medial border of the supratemporal fossa. A median sagittal ridge, as that seen in *Suchomimus* and *Ceratosuchops* (MS, pers. obs. on cast, MNN GDF 214; Barker et al., 2021) might have been present but got eroded in *Irritator*. Posteriorly, the parietals of *Irritator* diverge laterally into two more vertically oriented, posterolateroventrally directed occipital wings, which articulate on the dorsal skull surface along the contact of the paraoccipital processes and the squamosal. As described by Sues et al. (2002), the distal ends of the wings taper and are slightly twisted (Figure 8, Figure 13, Figure 14). Posteromedially, the parietals receive a bifurcating process of the supraoccipital. Here, breakage creates a hole that penetrates through the skull roof and exposes parts of the interior of the braincase.

The parietals contact the laterosphenoids ventrally, with the laterosphenoid buttressing the parietal along nearly its entire length. Only in the posteriormost section, the parietals rest upon the supraoccipital and the otoccipital. There are very small, isolated cavities within the parietal. In dorsal view, these are situated posterolaterally to the hole that leads into the braincase.

Postorbital

Only the left postorbital is preserved (Figure 15). As noted by Sues et al. (2002), it has been disarticulated from its surrounding bones and turned around 45° so that the distal half of the descending jugal process is hidden by matrix and the lacrimal, and only the lateral side of the area where the three rami meet is exposed (Figure 1A). Our CT data made it possible to reconstruct the complete morphology of the postorbital. The element is T-shaped, anteroposteriorly short, mediolaterally thin and dorsoventrally tall, with the ventral process being about twice as long as the approximately equally long anterior and posterior processes. As is usual in basal tetanurans, both the anterior and posterior process are set at an angle of approximately 90° towards the ventral process, whereas the anterior process is directed anterodorsally in many non-avian coelurosaurs (e.g., Makovicky et al., 2004; Norell & Makovicky, 2004; Rauhut et al., 2018). The lateral and medial surfaces of the postorbital are generally smooth. The postorbital contacts the frontal, parietal and laterosphenoid anteromedially, the squamosal posteriorly and the jugal ventrally.

The anterior (frontal) process of the postorbital forms the posterodorsal margin of the orbit. The process articulates with the frontal, parietal and laterosphenoid medially, so that the frontal is more laterally positioned than other bones that are involved in contributing to the dorsal orbital margin (Figure 2-4). In anterior view, the broad

anterior surface of the postorbital, which forms the posterior wall of the orbital fossa, is entirely exposed. This indicates that the eyes may have faced at least partially forward, allowing for some stereoscopic vision. The anterior end of the frontal process of the postorbital is blunt and slightly downturned. A notable supraorbital rugosity is absent, in contrast to some large megalosaurids, such as *Torvosaurus* (Britt, 1991) and *Wiehenvenator* (Rauhut et al., 2016) and allosauroids, such as *Allosaurus* (Madsen, 1976), *Sinraptor* (Currie & Zhao, 1993), or *Acrocanthosaurus* (Eddy & Clarke, 2011). However, at the anterolateral end of the raised orbital margin, a small, anteroposteriorly elongate lateral tubercle is present.

On the medial surface of the anterior process, the postorbital forms an anteroposteriorly broad but mediolaterally short shelf, the medial surface of which bears the articulation facets for the medially adjacent bones (Figure 15C). A large anterior socket for the articulation with the frontal is subdivided by two anterodorsally inclined ridges into two, anterodorsally open slots that indicate the facets for the frontal anteriorly and the parietal posteriorly. A small, oval depression posteroventral to these facets receives the lateral laterosphenoid head. This socket for the laterosphenoid is thus relatively smaller than in most non-avian theropods and entirely placed on the anterior process of the postorbital, whereas it is usually found at the junction of the three postorbital processes (e.g., Madsen, 1976; Currie & Zhao, 1993). A thickened area just dorsal to this socket probably represents the contact with the lateralmost tip of the parietal. The morphology of the medial surface of the anterior process is very similarly developed in the megalosaur *Dubreuillosaurus* (Allain, 2002). In dorsal view, the posterior border of this medial shelf marks the anterior border of the supratemporal fenestra, and its dorsal surface flexes anterodorsally to form the postorbital portion of the supratemporal fossa, which is thus directed posterodorsally, as the frontal supratemporal fossa.

The anterior and posterior processes of the postorbital form a dorsal bar that contributes to the T-shape of the element. The dorsal margin of the postorbital that links these processes is straight and has a sharp edge along the lateral margin of the supratemporal fenestra, where the dorsomedially curving lateral side meets the vertical medial side in a sharp angle.

The short and straight posterior (squamosal) process of the postorbital fits into a deep notch, formed between two anterior processes of the squamosal. The posterior process of the postorbital tapers posteriorly and bears an anteroposteriorly elongated medial ridge that would have been wedged between the anterior processes of the squamosal, giving this process a twisted appearance, reminiscent of the ‚helical' articulation between the postorbital and squamosal seen in many carcharodontosaurids (Carrano et al., 2012). The squamosal process of the postorbital and the two anterior processes of the squamosal separate the supratemporal fenestra from the infratemporal fenestra.

The ventrally descending (jugal) process of the postorbital is broken in the center, but the distal third could be identified in the CT data, being in close association with the rest of the bone (Figure 15). The process tapers ventrally. Its anterior margin represents the posteroventral border of the orbit. The entire orbital margin is mediolaterally expanded to form the posterior orbital fossa, but the width of the fossa narrows ventrally (Figure 15B). As a consequence, both the lateral and the medial orbital margin stand out from the surface of the postorbital as slightly raised ridges (Figure 3A). At the level of the contact with the jugal, where the orbit becomes ventrally constricted between lacrimal, postorbital and jugal, the expanded anterior surface of the postorbital gives way to an anterior ridge with a sharp edge. The dorsal half of the posterior margin of the postorbital ventral process forms the anterodorsal

margin of the infratemporal fenestra and is gently convex in lateral view. Around its mid-length, the posterior margin of the jugal becomes straight to slightly concave and deeply recessed posteriorly, forming a U-shaped cross section that receives the posterodorsal process of the jugal, as in megalosaurids (Britt, 1991; Sereno et al., 1994; Allain, 2002; Sadleir et al., 2008; Rauhut et al., 2016). Concerning the two other postorbitals that have recently been assigned to spinosdaurids (*Ceratosuchops*, Barker et al., 2021; *Suchomimus*, Sereno et al., 2022), it might be worth mentioned that the postorbital of *Irritator* is a much more delicate bone (especially on its dorsal portion) in comparison to the others. Whereas the anterior process of the postorbital of *Irritator* is generally mediolaterally slender and lacks a prominent orbital boss or brow, a mediolaterally wide anterior process and a thickened brow are developed in material assigned to *Ceratosuchops* (Barker et al., 2021) and *Suchomimus* (Sereno et al., 2022), and even more so, in concert with clear rugosities, in carcharodontosaurids (e.g., Motta et al., 2016). Furthermore, the somewhat spoon-shaped posterodorsal articular facet for the squamosal seems mediolaterally much wider in *Ceratosuchops* (Barker et al., 2021), *Suchomimus* (Sereno et al., 2022) and carcharodontosaurids (Motta et al., 2016). Additionally, there is no infraorbital process in *Irritator* and the material assigned to *Suchomimus* (Sereno et al., 2022) which, on the other hand, is present in *Ceratosuchops* (Barker et al., 2021) and carcharodotosaurids (Motta et al., 2016).

Jugal

Both jugals are preserved (Figure 16), but the right jugal is better preserved than the left element (Figure 1). The jugal has three primary processes (maxillary, quadratojugal and postorbital process), which contact the maxilla anteriorly and

medially, the lacrimal anterodorsally, the postorbital posterodorsally, the quadratojugal posteriorly and the ectopterygoid medially. The jugal body is mediolaterally thin but notably thickened towards its ventral margin, forming a dorsoventrally broad longitudinal ridge on the lateral side just above the ventral margin, as it is present in many non-avian theropods, and a medially thickened ventral rim. The ventral margin of the jugal is very slightly concave, in contrast to the usually convex ventral margin of the jugal in most non-avian theropods (Sullivan & Xu, 2017).

The anterior process is triangular in front of the orbit in lateral outline, with the posterior part of the process being dorsoventrally expanded in comparison with the suborbital jugal body, while the anterior end tapers into an acute angle. The anterior process articulates with the maxilla, lacrimal, and probably the ectopterygoid medially (Figure 2-4). As described in the maxilla section, the maxilla has two posterior rami, the ventral of which contacts the ventromedial surface of the anterior process of the jugal, whereas the dorsal maxillary process contacts the dorsolateral margin of the jugal, thus tightly interlocking the cheek region. The jugal has a groove along its ventromedial surface for the posteroventral process of the maxilla. Just posterior to the contact with this maxillary process, the ectopterygoid contacts the medial surface of the jugal. However, the exact nature of this contact is unclear due to disarticulation of the ectopterygoid in the fossil and the lack of a clear ectopterygoid facet on the reconstructed medial jugal surface based on the CT data. The ventral process of the lacrimal contacts the mostly straight, anteroventrally inclined dorsal margin of the anterior process. The highest dorsoventral extent of the anterior process marks the transition point to the orbital margin of the jugal. Here, the dorsal margin of the jugal slopes down, forming a narrowly rounded anteroventral rim of the orbital opening.

The suborbital body of the jugal is notably high, being almost 2.5 times the height of the quadratojugal process.

The postorbital process of the jugal is elongate triangular in lateral outline and posterodorsally inclined, with a slightly convex anterior and a gently concave posterior margin. The process is not as steep as in other large-bodied theropods like e.g., *Majungasaurus* (Sampson & Witmer, 2007), *Acrocanthosaurus* (Eddy & Clarke, 2011) and *Alioramus* (Brusatte et al., 2012). The elongated process is slender and tapers into a rounded dorsal tip. A marked, rounded lateral ridge is present along the contact with the postorbital and the posteroventral margin of the orbit, as in some other non-avian theropods (e.g., *Acrocanthosaurus*; Eddy & Clarke, 2011). Posteriorly, a long and slender quadratojugal process of the jugal is developed. This process bifurcates into two rami, which receive the quadratojugal; this bifurcation extends anteriorly to the level of the posterior border of the postorbital process. The dorsal quadratojugal process of the jugal is dorsoventrally narrower and anteroposteriorly shorter than its ventral counterpart, which is more robust and embraces the ventral margin of the quadratojugal (Figure 2A, Figure 16). A longitudinal groove flanks the incision between the two processes along the ventral process on the medial side, and the distal end of the ventral process flexes medially in its ventral part. Together with the postorbital process, the quadratojugal process of the jugal forms the anteroventral border of the infratemporal fenestra (Figure 2A). Whereas the dorsal quadratojugal process of the jugal reaches only slightly posterior to the mid-length of this opening, the ventral process extends to the level of its posterior border.

In this context, it may be worth mentioned that the element that was identified as the jugal in the holotype of *Baryonyx* does not resemble the jugal of *Irritator*, since the supposed dorsal border that makes up the ventral margin of the orbit is much smaller

and there are medial articulation facets on this element which do not have an equivalent in *Irritator*. This bone of *Baryonyx* may rather represent a prearticular (as suggested by Sereno et al., 1998) with the putative quadratojugal contact rather being the contact for the surangular and articular and the ectopterygoid facet rather being the facet for the angular.

Quadratojugal

Only the right quadratojugal is preserved (Figure 1B, Figure 17). It is L-shaped, with a tall dorsal process, articulating with the quadrate medially and the squamosal dorsally, and a slightly shorter anterior process that meets the posterior process of the jugal (Figure 2-4). The two processes of the quadratojugal meet at an angle of approximately 90° and form the concave posteroventral margin of the infratemporal fenestra. It might be worth mentioning here that the bone figured as the quadrate of *Irritator* by Hendrickx et al. (2016: fig. 9M, N) actually represents a part of the quadratojugal, and the structure identified as the quadrate foramen by these authors is a break in this bone.

The jugal process of the quadratojugal gradually tapers anteriorly over its entire length. The margin of the quadratojugal that is exposed in the infraorbital fenestra is sharp-edged, whereas the anterior third of the anterior process that is wedged between the jugal is shaped to facilitate this articulation: the dorsal surface is slightly broadened, and a clear facet is developed on the ventrolateral surface of the anterior process. This facet is offset from the laterally exposed part of the process by a notable step and would have been covered laterally by the ventral posterior process of the jugal, fitting into the groove on the medial side along the dorsal rim of the latter described above (Figure 2, Figure 4B).

The posteroventral region of the quadratojugal has a roughened medial surface for the articulation with the quadrate. Along this articulation, the posterior margin of the quadratojugal is gently curved posteromedially towards the quadrate, wrapping around the posteroventral margin of the latter (Figure 1B, Figure 2A, Figure 3B, Figure 14), as it is the case in many non-avian theropods (Rauhut, 2003). Here, a small, tab-like posterior process possibly marks the posteriormost contact between the two bones (Figure 3B, Figure 17).

The dorsal squamosal process is an anteroposteriorly comparatively wide but mediolaterally thin plate of bone of the quadratojugal. At about its mid-height, a ridge appears towards its anterior margin that extends dorsally, forming a marked, anterolaterally directed edge. In the ventral part, where this edge is developed as a lateral ridge, a thin sheath of bone is present, facing somewhat anteromedially. The region posterior to the ridge and the emerging dorsal edge is inclined posteromedially, resulting in a slightly posteromedially twisted appearance of the process. The dorsal part of the squamosal process is damaged, but the contact area for the quadratojugal on the squamosal indicates that it was possibly tongue-shaped originally. The dorsal end of the quadratojugal was wedged between two slender processes of the squamosal, forming a large contact area with the latter bone (Figure 2A), while the medial sheath further contacts the lateral margin of the dorsal quadratojugal flange of the quadrate (Figure 3B).

Squamosal

The squamosal is solely represented by the left element, which is damaged by a mediolaterally oriented subvertical crack on its main body (Figure 18). It is preserved anterior to the basisphenoid (Figure 1A) and hence is situated far more

ventromedially and anteriorly in the fossil compared to its usual anatomic position. Our CT data reveal an almost completely preserved squamosal. The squamosal contacts the postorbital anteriorly, the parietal, otoccipital and possibly the supraoccipital posteriorly and medially, and the quadrate and quadratojugal ventrally (Figure 2-4). As it is usual in non-avian theropod squamosals, the bone is composed of four processes, an anterior postorbital process, a posterior process forming the roof of the cavity for the quadrate articulation, a ventral quadratojugal process, and a posteriorly placed medial process for the contact with the parietal.

The element has the greatest extend in its dorsoventral dimension, due to a long descending quadratojugal process, but has unusually short anterior and medial processes, although it cannot be excluded that the anterior end of the anterior process is missing. The bone forms the posterodorsal margin of the infratemporal fenestra and parts of the lateral and the posterior margin of the supratemporal fenestra.

The dorsal surface of the squamosal body bears a large, shallow depression, resulting in a markedly concave outline of the dorsal margin between the anterior and posterior processes in lateral view. In lateral view, the squamosal has a short, bifurcated anterior postorbital process (whereas the postorbital articulated mainly laterally with the squamosal in *Irritator*, material assigned to *Suchomimus* suggests a mediolaterally wide articulation on the ventral surface of the dorsal branch of the anterior process; Sereno et al., 2022). The dorsal branch of the process is slightly shorter than its ventral counterpart and has a blunt anterior end, although it cannot be excluded that a small portion of the bone might be missing here. This dorsal branch is considerably anterodorsally directed in comparison to the quadratojugal and posterior processes. The ventral branch is slightly flexed anteroventrally,

resulting in a continuously curved posterodorsal border of the infratemporal fenestra, in which the anterior part of the dorsal margin of this opening stands at an angle of c. 90° towards the posterior margin. The ventral branch of the anterior process has a shallow lateral ridge and a pointed tip. The lateral ridge is less pronounced than in many other non-avian theropods, such as *Allosaurus* (Gilmore, 1920; Chure & Loewen, 2020), and extends posteriorly to the level of about half the anteroposterior length of the ventral process. Where both branches of the anterior process meet, they form a distinct longitudinal lateral groove that receives the squamosal process of the postorbital. The groove becomes shallower posteriorly, extending onto the mid-length of the squamosal body. However, it is deeper than high over its entire length, in accordance with the transversely broadened posterior end of the postorbital.

The medial process is placed at about the anteroposterior mid-length of the squamosal. It is triangular in outline in dorsal view and anteromedially directed. The medial process is almost as long as the dorsal branch of the anterior process (in contrast to material assigned to *Suchomimus*, where the medial process is relatively much smaller and stronger medially directed; Sereno et al., 2022). In contrast to several non-avian theropods, including ceratosaurs (Gilmore, 1920; Madsen & Welles, 2000; Sampson & Witmer, 2007; Pol & Rauhut, 2012), allosauroids (e.g., Madsen, 1976; Currie & Zhao, 1993; Eddy & Clarke, 2011) and a few other taxa, the dorsal lamina between the anterior and medial process is emarginated by the supratemporal fenestra and thus concave to angled in dorsal view. The small lamina overhangs the cavity of the supratemporal fenesta, the posterolateral wall of which is formed by the main body of the squamosal. Three notable depressions are present in this wall, two are mainly posteriorly excavated. The dorsalmost depression is at the level of the base of the anterior and medial process. Ventroposteriorly, the second depression is situated at the base of the ventral process, and a third depression is

more laterally excavated further ventrally, at about the mid-height of the main body of the ventral process.

A large facet for the articulation of the quadrate head is formed by the posterior process and the descending quadratojugal process. The proximal part of the posterior process is perpendicular to the ventral process, but the posterior process is flexed strongly posteroventrally, resulting in a semicircular outline of the notch for the quadrate in lateral view. There is no anteroventrally pointing flange on the posterior part (Figure 18) that would cover the quadrate head laterally, as it is the case in metriacanthosaurids (e.g., Currie & Zhao, 1993) or *Acrocanthosaurus* (Eddy & Clarke, 2011), so the quadrate head is fully exposed in lateral view in the articulated skull (Figure 2A). In dorsal view, the posterior process forms a narrow triangle, with a pointed posterior tip laterally and a steeply anteromedially inclined medial edge, where the squamosal would have contacted the paroccipital process. This medial margin is rather sharp, while the lateral margin is rounded. The angle between the lateral and medial edge in dorsal view is slightly less than 45°. In ventral view, the process forms a triangular, anteroposteriorly strongly and mediolaterally weakly concave articulation facet for the quadrate head. The posteromedial side of the process that articulates with the paroccipital process bears a horizontal concavity. Anteriorly, between the base of the anteromedial process and the posterior process is a shallow medial depression. Furthermore, there is a marked medial ridge, extending from the anteromedial process to the posterior end of the posterior process, which forms the medial border of the quadrate head articulation surface.

The long quadratojugal process of the squamosal is straight and ventrally directed. It is anteroposteriorly wide and mediolaterally thin. The posterior margin of the process forms a vertical orientated, mediolaterally expanded and ventrally thinning articulation

facet for the quadrate head and shaft. The ventral end of the process has a concave margin between the thin but distinct anterior and posterior ventral processes. The anterior process is considerably longer than the posterior process; together, these two processes would have clasped the dorsal end of the quadratojugal (between these two processes, a thin lamina seems present in the squamosal assigned to *Suchomimus*; Sereno et al., 2022).

A network of different-sized cavities is present within the squamosal body, mainly behind the mentioned crack. Some further small cavities are scattered at the lateral base of the dorsal postorbital process. In a posterior direction, the cavities become bigger, interconnected and extend ventrally and medially. The posteriormost cavities are situated dorsally to the articulation surface for the quadrate head. No unequivocal connection of this network to a pneumatic foramen could be identified.

Quadrate

Only the left quadrate is preserved (Figure 1, Figure 19). Other than a mediolaterally oriented crack on the upper half of the quadrate foramen, the bone is complete. It is disarticulated from its original position. In the fossil, the quadrate head is visible through the right antorbital fenestra, while the left lateral aspect of the pterygoid flange is exposed below the left jugal. However, we were able to fully reconstruct the quadrate with the help of CT data. The quadrate contacts the pterygoid and, possibly, the epipterygoid anteriorly, the quadratojugal laterally, the squamosal and possibly the otoccipital dorsally and the surangular and articular ventrally (Figure 2-4).

The quadrate is dorsoventrally tall with the quadrate head forming the apex of the bone, and the contact to the squamosal. The quadrate shaft connects the quadrate head with the mediolaterally wide base where the quadrate articulates with the lower

jaw. Anteriorly, the quadrate forms an expanded semioval sheet of bone, the pterygoid wing.

The dorsal quadrate head is developed as a semicircular condyle in medial or lateral view, as in all non-avian theropods. In proximal outline, the head is subquadrangular in outline, as in *Baryonyx*, but unlike the more triangular shape seen in a quadrate referred to *Suchomimus* (Hendrickx et al., 2016). The quadrate head of *Irritator* is slightly wider mediolaterally than long anteroposteriorly, and its anterior side is slightly wider than the posterior one. Our skull reconstruction shows that the quadrate head was capped by the squamosal, and posteromedially additionally braced by the anterolateral surface of the paroccipital process of the otoccipital. The posterior margin of the quadrate shaft is distinctly concave between the quadrate head and ventral articulation surface for the jaw; however, both the dorsal and ventral half of the shaft are posteriorly rather straight, with a marked flexure at about mid-height of the bone. The quadrate shaft is slightly bent medially, mainly caused by the marked medial expansion of the ventral end and a medial expansion of the quadrate head, similar to the juvenile spinosaurid quadrate FSAC-KK-18120 (Lakin & Longrich, 2019). In contrast, the quadrates of *Baryonyx* and *Suchomimus* are rather laterally inclined, with a slightly convex medial margin of the shaft (Hendrickx et al., 2016). The quadratojugal flange is represented by an offset ridge, extending on the lateral side of the quadrate shaft. Its dorsal end is placed just below the quadrate head, at about the anteroposterior mid-width of the shaft, but it then extends posteroventrally and follows the posterolateral edge of the quadrate shaft. Ventrally, at about the half height of the quadrate, the ridge gives way to the quadrate foramen, which is proportionally larger than in material assigned to *Spinosaurus* (Hendrickx et al., 2016). The foramen in *Irritator* is elongate drop-shaped in outline, becoming wider ventrally. The medial margin of the foramen is formed by the lateral side of the

quadrate shaft, while the ventral margin is formed by a short but broad lateral process that forms the ventral quadratojugal contact. The foramen is laterally open, but would have been enclosed by the quadratojugal in the articulated skull. Only at the dorsal end of the foramen, a small ventral spur of the lateral edge of the quadratojugal forms a small part of its lateral border. The ventral quadratojugal contact is broad, and forms a posterodorsally open, cup-shaped articulation facet for the quadratojugal.

Ventrally, the quadrate is expanded to more than three times the minimal width of the quadrate shaft, with most of this expansion being accounted for by the medial side. It articulates with the lower jaw via two quadrate condyles. The slightly curved, laterally concave, lens-shaped and somewhat mediolaterally oriented ectocondyle lies lateral to the smaller and anteromedially-posterolaterally oriented entocondyle (Figure 19E). The medial half of the articular end with the entocondyle is approximately twice as deep anteroposteriorly than the lateral half. The condyles are separated by a broad, shallow intercondylar sulcus that is slightly anteromedially inclined. The intercondylar sulcus is more distinct than in other spinosaurids, e.g., FSAC-KK-18120, *Spinosaurus* and *Baryonyx* (Lakin & Longrich, 2019; Hendrickx et al., 2016).

Anteriorly, the quadrate forms a laminar process, the pterygoid wing, which extends almost over the entire height of the element from the quadrate head to the intercondylar sulcus at the base of the quadrate. The anterior margin of the pterygoid wing is convex, and the wing is anteroposteriorly deepest around its mid-height. This part of the wing overlies the quadrate ramus of the pterygoid laterally, and possibly is in contact with the epipterygoid at its anterior end (Figure 2A). The entire pterygoid wing is gently convex laterally. On the medial side, there is a large, oval fossa at the base of the pterygoid wing. This fossa houses a small pneumatic foramen in its

deepest part, leading to a small medial cavity at the base of the quadrate shaft. In contrast to other non-avian theropods (e.g., *Sinraptor*; Currie & Zhao, 1993), the ventral rim of the pterygoid wing does not seem to be flexed medially to form a medial shelf underneath the pterygoid (Figure 19A).

CT data reveal that there is a dorsoventrally tall network of irregularly-formed cavities, situated within the quadrate shaft. This network extends from the anterior margin of the quadrate head to the lower half of the quadrate foramen. This network of cavities does not seem to have a connection to an external pneumatic foramen.

Braincase

The braincase of *Irritator* is nearly completely preserved, with most bones in near-perfect articulation with one another (Figure 8, Figure 14, Figure 20-26). The general shape of the dorsoventrally high and anteroposteriorly short braincase has been described by Sues et al. (2002), as has the shape and size of the foramen magnum and many aspects of the directly visible morphology of the braincase elements and the openings for nerves and blood vessels.

The cavity for the vestibular apparatus is housed within the prootic (anterolaterally), otoccipital (posteroventrally) and the supraoccipital (posterodorsally). The cavity for the cochlea is formed by the prootic, otoccipital and basioccipital. The floccular fossa is contained within the prootic, supraoccipital and otoccipital (distally).

The following description of the braincase bones is based on the bone surfaces directly visible on the specimen and models that were segmented from the micro CT data. As the anterior end of the cultriform process is not included in the micro CT data, our braincase models are solely based on micro CT data (except for the

rearranged skull reconstructions, which source from the medical CT data only ; Figure 2-4).

Supraoccipital

The supraoccipital is present but lacks its dorsalmost portion (Figure 1, Figure 8, Figure 14). It is an unpaired bone, forming the dorsal part of the occipital complex (Figure 20-24). Our micro CT data suggest that an elongate and roughly rectangular portion of the supraoccipital is exposed on the lateral surface of the braincase, dorsal to the prootic and bordered posteriorly by the otoccipital, dorsally by the parietal and anteriorly by the laterosphenoid. Although the sutures are difficult to discern, this can be confirmed on both sides of the braincase directly on the fossil (Figure 1). This trait is unusual for non-avian theropods (see e.g., *Majungasaurus*; Sampson & Witmer, 2007; *Allosaurus*; Chure & Loewen, 2020; *Murusraptor*; Paulina-Carabajal & Currie, 2017; see also Paulina-Carabajal, 2015). However, the bone surface of this anterolateral exposure of the supraoccipital is markedly rugose, and thus it cannot be excluded that this area was originally covered by a lamina of the parietal. The supraoccipital contacts the parietal anteriorly, dorsally and laterally, the laterosphenoid and prootic anteriorly and the otoccipital posteroventrally.

In relation to the dorsal surface of the parietal and the posterior surfaces of the otoccipitals and basioccipital, the supraoccipital slopes anterodorsally at an angle of approximately 45°. It bears a centrally situated supraoccipital crest (nuchal crest of Sues et al., 2002 and Sampson & Witmer, 2007) on its posterodorsal surface. While most of the crest is broken off, a remnant of the base is still preserved. The crest becomes more prominent dorsally, but due to the inclination of the supraoccipital, its posterior margin remains vertical above the foramen magnum in lateral view. In

Baryonyx, Suchomimus and *Ceratosuchops* the crest is dorsoventrally tall (Charig & Milner, 1997; MS, pers. obs. on cast, MNN GDF 214; Barker et al., 2021), but due to the dorsal damage it cannot be said if this was also the case in *Irritator*. The supraoccipital crest is flanked by two funnel-like depressions, leading to the posterior openings for the vena cerebralis media (Figure 14, Figure 21A, B). The foramina for the vein are large and placed dorsal to the level of the dorsal rim of the paroccipital processes, being completely enclosed by the supraoccipital. In contrast to *Allosaurus* (Chure & Loewen, 2020) and *Asfaltovenator* (Rauhut & Pol, 2019), there is no curved groove on the posterior surface of the supraoccipital that connects the exit of the mid-cerebral vein with the posttemporal foramen. The latter opening is difficult to identify even with the aid of CT data, but it seems to be represented by a small foramen between the parietal and supraoccipital slightly ventrolateral to the posterior exits of the mid-cerebral vein, marked by a small notch on the dorsolateral suture with the parietal. The foramen is thus within the lateral rim of the funnel-like depression leading towards the opening of the vena cerebralis media, possibly indicating an occipital sinus in this area. On the medial surface of the supraoccipital, a large, but shallow depression is present anteroventral to the posterior opening for the mid-cerebral vein, representing the dorsal longitudinal sinus. However, a groove marking the course of the mid-cerebral vein from the sinus towards its anterolateral exit, as it is present in other dinosaurs (e.g., Janensch, 1936; Rauhut, 2004), seems to be absent both on the medial side of the supraoccipital and the laterosphenoid/prootic. The dorsal break of the nuchal crest reveals an anterior notch in dorsal view that leads into the brain cavity and separates the left and the right side of the supraoccipital. The notch continues ventrally as a narrow trough at the posterior end of the endocranial cavity towards the dorsal margin of the foramen magnum. Anteriorly, the lateral wall of the supraoccipital articulates with the laterosphenoid.

Laterododorsally and presumably dorsally, the bone articulates with the parietals, but due to the dorsal break it cannot be said if a posterior process of the parietal that capped the dorsal surface of the supraoccipital was present, as it occurs in many non-avian theropods. The ventral margin of the supraoccipital forms the entire dorsal roof of the foramen magnum. The ventrolateral suture with the otoccipital is complex (Figure 20C, D). Along the rim of the foramen magnum, each otoccipital sends a stout process dorsomedially, restricting the width of the ventral end of the supraoccipital, though not to the extent seen in some other basal tetanurans (e.g., *Allosaurus*, Chure & Loewen, 2020). Dorsolateral to this otoccipital process, the supraoccipital has a long and slender ventrolateral process, which reaches the level of the dorsal margin of the foramen magnum and slots into a notch in the otoccipital.

On each side, the bone has a ventrolateral bulbous projection that houses parts of the semicircular canals, with an anteroventral facet for the prootic and a posteroventral facet for the otoccipital. The supraoccipital has a distinct ventrolateral groove on the surface that articulates with the prootic, which invades the bone from the medial, endocranial side. Together with a corresponding dorsolateral groove on the articular facet of the prootic, this groove forms a prominent recess from the medial braincase surface for the flocculus, which is narrow, but very long, continuing posterolaterally into the otoccipital. While the opening for the anterior semicircular canal is situated dorsolateral to the channel, the opening for the posterior semicircular canal lies rather posteroventrally. The supraoccipital bears a large cavity posteriorly to the endosseous canal of the common crus; posteromedially followed by another, smaller one (Figure 26). Both cavities do not bear an obvious connection to a pneumatic foramen.

Otoccipital (Exoccipital-Opisthotic)

In most dinosaurs, including *Irritator*, the exoccipital is tightly fused with the opisthotic to form the otoccipital (Sues et al., 2002). Interestingly, this is not the case in the holotype of *Baryonyx* (Charig & Milner, 1997). Both otoccipitals are preserved in *Irritator* and form the lateral borders of the foramen magnum, as well as most of the paroccipital processes (Figure 14, Figure 20 C, D). The otoccipital contacts the basisphenoid anteroventrally, the prootic anterodorsally, the supraoccipital mediodorsally, the parietal laterodorsally, the squamosal and possibly the quadrate laterally, and the basioccipital ventrally (Figure 2-4).

While the left paroccipital process is almost complete, the right one misses its distalmost part. Both paroccipital processes are relatively short and project posteriorly and ventrolaterally. In contrast, the paroccipital processes of *Baryonyx*, *Ceratosuchops* and *Riparovenator* seem considerably longer (Charig & Milner, 1997; Barker et al., 2021); the paroccipital process of *Irritator* is c. 1.1 times longer than tall, whereas that of *Riparovenator* is 2.5 times longer (Barker et al., 2021). In *Irritator*, the dorsal and ventral margins of the paroccipital processes are almost straight and parallel to each other, but the processes are very slightly flexed ventrolaterally. The distal end that articulates with the squamosal is blunt and rounded. The ventral margin of the base of the paroccipital process is placed approximately at the level of the half-height of the occipital condyle, as in most non-avian averostrans, whereas it is placed relatively higher in non-averostran theropods (Rauhut, 2003). On the posterodorsal surface of the proximal part of the paroccipital process is a longitudinal groove that leads to the funnel-like dorsal depressions of the supraoccipital, which articulates with the anterodorsal surface of the otoccipital. The paroccipital process braces the prootic anteriorly, and the parietal and squamosal dorsally. In addition, the

distal end of the paroccipital process closes the quadrate facet of the squamosal posteromedially.

Ventral to the paroccipital process, the otoccipital articulates with the basioccipital along a long contact that consists of two processes of the otoccipital. One process is posteriorly directed, and forms the dorsolateral part of the occipital condyle on either side. These condylar processes of the left and right otoccipital remain separated from one another by a thin median crest of the basioccipital. The contact with the basioccipital continues anteriorly at the floor of the endocranial cavity to the level of the anterior rim of the crista interfenestralis. Within the foramen magnum, the left and right elements diverge anteriorly, making more room for the contribution of the basioccipital to the floor of the endocranial cavity. In ventral view, the broad articular facet for the basioccipital is elongate semioval in outline, being rounded posteriorly. The second process of the otoccipital that contacts the basioccipital forms the crista tuberalis [=crista metotica, metotic strut of other authors e.g., Gower & Weber, 1998; Rauhut, 2004)]. The crista tuberalis is developed as a robust, posterolaterally oriented ridge that is dorsally continuous with the ventral margin of the paroccipital process (Figure 23, Figure 25A). It separates the region of the inner ear, anteriorly, from the occipital region posteriorly. The crista tuberalis extends to the basioccipital/basisphenoid contact, and contacts the basisphenoid in the lateral braincase wall. The crista tuberalis and occipital process of the otoccipital define a posterior fossa, the paracondylar recess, ventrolateral to the occipital condyle. Within the paracondylar recess, there are three foramina: two smaller foramina penetrate the bone mediolaterally, and can be identified as two foramina for the CN XII (only one was found with the medical CT data in Schade et al. 2020). The third foramen ('posterior vagal foramen'; see below) penetrates the otoccipital anteroposteriorly,

and forms a short but broad canal that probably corresponds to the joint passage of CN IX–XI from the recessus scalae tympani to the occipital surface of the braincase.

On the anterior side of the crista tuberalis and below the proximal part of the paroccipital process, the columellar recess (sensu lato) is located. Two large, anteroposteriorly arranged openings are visible within the columellar recess, separated by a robust crista interfenestralis. The posterior aperture within the columellar recess was identified as the metotic foramen by Sues et al. (2002). However, a metotic foramen would only be present if the embryonic fissura metotica is not subdivied into a vagal foramen (=jugular foramen) and the fenestra pseudorotunda (=fenestra cochlea) during ossification of the chondrocranium (Gower & Weber, 1998; see also discussion in Bronzati & Rauhut, 2018). Whereas the posterior opening seems to be undivided in lateral view (thus justifying its identification as metotic foramen by Sues et al., 2002), the CT data reveal that a separate fenestra pseudorotunda is indeed present (Figure 23A-C), which functioned as a pressure-relief outlet for endolymphatic fluid flow within the inner ear (see Rieppel, 1985; Gower & Weber, 1998).The fenestra pseudorotunda is located medially to the crista interfenestralis and leads anteroposteriorly into the recessus scalae tympani. Although the medial wall of the fenestra pseudorotunda is ventrally broken on both sides of the braincase, it seems that this fenestra was largely or completely separated from the larger, more posteriorly situated opening, which would thus correspond to the vagal foramen. The latter thus represents the opening through which CN IX-XI and the jugular vein exited the endocranial cavity. The cranial nerves IX-XI probably occupied the dorsal part of the opening and diverged posteriorly, where a shallow groove on the otoccipital leads into the canal of the posterior foramen that opens into the paracondylar recess on the occiput, as described above. The jugular vein (posterior cephalic vein of Bronzati & Rauhut, 2018) thus left the

braincase through the ventral part of this opening, and might have diverged posteroventrally around the crista tuberalis of the otoccipital. As the posterior diversion of the vagal nerve group (CN X, and probably its accessories CN IX and XI) is thus a two-step procedure, in which the nerve first leaves the braincase into the recessus scalae tympani and then exits this cavity through a posteriorly directed foramen in the occiput, we suggest the terms 'medial vagal foramen' for the exit of the nerve from the braincase, and 'posterior vagal foramen' for its exit onto the occiput.

The anterior aperture within columellar recess is the fenestra ovalis (=fenestra vestibule), which was spanned by a membrane to receive the basal plate of the stapes, on the lateral aspect of the cochlea, and it is posteriorly bordered by the crista interfenestralis.

Posterolaterodorsal to the fenestra ovalis, the posterolaterally extending stapedial groove lies ventral to the sutural contact of the otoccipital and prootic on the anteroventral side of the paroccipital process, being bordered posteriorly by the otoccipital and anteriorly by the prootic.

In anterior view, there are three openings posterodorsally to the crista interfenestralis on the articular facet for the prootic of the otoccipital. Medially, a large opening for the posterior ampulla of the vestibular apparatus is situated. Dorsally to the posterior ampulla opening, a fossa for the distal portion of the flocculus invades the otoccipital from anteromedially and the opening for the horizontal semicircular canal can be found further laterally, slightly ventral to the floccular recess. In dorsal view, directly posteriorly to the floccular recess, there is a small and slit-like opening for the posterior semicircular canal in the broad contact area with the supraoccipital.
In medial view, the otoccipital forms the ventral part of the lateral wall of the

endocranial cavity anterior to the foramen magnum. In its ventral part, this wall is pierced by two anteroposteriorly separated foramina for the exit of branches of CN XII, the posterior of which is slightly larger than the anterior one. At the anterior end of the medial surface, the large and slightly more dorsally positioned vagal foramen pierces the lateral endocranial wall. Within the posterior portion of the otoccipital, an accumulation of partly webbed and interconnected cavities has been found with our micro CT data, however, without an obvious connection to a pneumatic foramen. Additionally, each otoccipital bears a smaller, anteroposteriorly elongated cavity on the distalmost portion of the paroccipital process (Figure 26).

Prootic

Both prootics are completely preserved (Figure 1, Figure 20-24), although each bears a dorsoventrally oriented crack posteriorly to the large CN V opening. The prootic contributes to the lateral wall of the braincase, and consists of a main body that is relatively short anteroposteriorly and high dorsoventrally, and a posterolateral, wing-like process that overlies the proximal part of the anterior surface of the paroccipital process of the otoccipital. The prootic contacts the laterosphenoid anterodorsally, the supraoccipital posterodorsally, the otoccipital posteriorly, the basioccipital posteroventrally, the basisphenoid anteroventrally, and the other prootic anteroventromedially. Due to the exposure of the supraoccipital on the lateral side of the braincase, there seems to be no prootic-parietal contact, which is, usually found in this area (e.g., Coria & Currie, 2016; Chure & Loewen, 2020). As mentioned above, it cannot be excluded that there might have been a thin lamina of the parietal extending ventrally over the supraoccipital here and thus contacting the prootic over a short distance.

In *Irritator*, the most distinctive feature of the prootic in lateral view is the large opening for CN V, which is developed as a roughly drop-shaped, anterodorsally open notch on the anterior part of the bone, extending over approximately half of the length of the prootic body, excluding the posterolateral process. Unlike in some other non-avian theropods (Bakker et al., 1988), the ophthalmic branch of the trigeminal nerve does not pass through a separate canal in the prootic and laterosphenoid; instead, there is a ventrally open groove under an overhanging ridge anterior to the trigeminal foramen on the laterosphenoid that provides evidence for the course of this nerve. As a consequence of the absence of an ophthalmic canal, a maxillomandibular foramen sensu Sampson & Witmer (2007) is not present, and the trigeminal ganglion was probably situated in a more extracranial position. Indeed, the opening for the trigeminal nerve in the rather thick prootic is slightly funnel-shaped, with a more marked depression ventral to the opening, as in *Eustreptospondylus* (Sadleir et al., 2008), probably indicating the position of the ganglion just outside the braincase and the ventral course of the mandibular branch of the nerve. Posterior to the trigeminal foramen, the orbitosphenoidal crest starts on the ventral side of the posterolateral wing that flanks the paroccipital process, where it forms the anterolateral border of the stapedial groove (Figure 20A, B, Figure 23A-C). Anterior to this wing, it curves sharply downward, but remains restricted to the posterior edge of the prootic. Thus, a well developed preotic pendant (ala basisphenoidalis of some authors; see Sampson & Witmer, 2007) is absent, in contrast to most non-avian theropods (Chure & Madsen, 1998; Rauhut, 2004). Posteroventral to CN V, the slit-like opening for CN VII leaves the braincase. In lateral view, only an incision in the orbitosphenoidal crest indicates the position of this foramen, as it extends from anteromedially towards posterolaterally and opens posteriorly below the orbitosphenoidal crest (Figure 23A-C, Figure 25). In contrast to some dinosaurs (e.g., *Efraasia*; Bronzati & Rauhut,

2018), there is only a single opening for the facial nerve, indicating that this nerve split into the hyomandibular and palatine rami outside the braincase, as it seems to be usual in non-avian theropods. Posterior to the foramen of the facialis nerve, a broad embayment in the posterior margin of the prootic below the paroccipital process forms the anterior margin of the fenestra ovalis.

Posterior and posteroventral to the CN V opening, the medial surface of the prootic bears several depressions and openings for the endosseous labyrinth, the flocculus and cranial nerves (Figure 24). Ventral and slightly posterior to the trigeminal foramen, the anteromedially opening entrance for the facial nerve lies within a marked depression. The posterolateroventrally oriented recess for the flocculus is developed as a narrow, but deep incision on the suture with the supraoccipital and otoccipital, posterior to the trigeminal foramen and approximately on the level of the half-height of the latter. Two openings for the anterior and horizontal semicircular canal are found on the medial side of the mediolaterally wide articular facet for the supraoccipital and in the ventral part of the articular facet for the otoccipital, respectively. Below the floccular recess, a large, anteriorly directed recess in the suture with the otoccipital that posteroventrally leads towards the fenestra pseudorotunda marks the anterior ampulla and the cochlear duct of the inner ear. The fenestra ovalis makes up a medioventral notch of the prootic. Both branches of CN VIII are situated within the prootic here, their foramina piercing the bone at the dorsal end of the cochlear duct within the osseous labyrinth. In most reptiles, including the megalosaur *Dubreuillosaurus*, a small opening posterodorsally to CN VII on the medial side of the prootic was identified as the foramen for CN VIII (Allain, 2002). This also seems to be the case in *Irritator*, where this area is damaged on the left side and a small overhanging crest in this position seems to hide the foramina for the acoustic nerve.

Anteriorly, both prootics flex medially and meet on their midline to form the central part of the robust dorsum sellae posterodorsal to the pituitary fossa, between the parabasisphenoid ventrally and the laterosphenoid dorsally. Here, they articulate via a mediolaterally wide surface with the laterosphenoid on the dorsal aspect and with the basisphenoid on the anterior and ventral aspect. The dorsum sellae of each prootic is anteroposteriorly pierced by a canal for the CN VI, which traverses the prootic and exits through a foramen at the basisphenoid-prootic suture from the braincase into the pituitary fossa. In posterior view, the canals are lateral to the anterior interprootic contact (Figure 21A, B). In contrast, in *Dubreuillosaurus*, an opening on the lateral aspect of the braincase, directly ventrally to CN V, has been identified as the exit of CN VI (Allain, 2002).

The posteromedial surface of the prootic meets the otoccipital and, more dorsally, the supraoccipital. The prootic of *Irritator*, and seemingly *Baryonyx* (Charig & Milner, 1997) and *Ceratosuchops* (Barker et al., 2021) makes up a substantial part of the anterolateral surface of the paroccipital process (Figure 20A, B, Figure 21, Figure 22). In *Piatnitzkysaurus* e.g., the contact of the prootic and the otoccipital ends shortly posterodorsal to the fenestra ovalis (Rauhut, 2004).

Our CT data reveal that ventral to CN V and anterior to CN VII, a very small and isolated cavity is present on both sides (not shown in Fig. 26, but within the 3D models of the sup. mat.). Further posteriorly, an isolated and complex network of different-shaped and different-sized cavities exists within the prootic portion of the paroccipital process (Fig. 26B,C). The right complex is more voluminous.

Basioccipital

The basioccipital is well preserved in *Irritator* (Figure 14). As in all theropods, it is a median unpaired bone that makes up the posterior floor of the endocranial cavity and the ventral part of the occiput (Figure 24). It forms a small median part of the ventral margin of the foramen magnum and the main portion of the occipital condyle. The basioccipital contacts the basisphenoid anteriorly and ventrally, the otoccipital laterally and the prootic anterodorsally (Figure 20-24).

The occipital condyle is ball-shaped, and has a slightly constricted neck. In relation to the skull roof, the hemispherical occipital articulation surface for the atlas projects posteroventrally in *Irritator*, *Baryonyx* (Charig & Milner, 1997) and *Suchomimus* (MS, pers. obs. on cast, MNN GDF 214), providing further evidence that the snout of spinosaurids was strongly ventrally inclined in a natural head posture (Schade et al., 2020).

In posterior view, a triangular, ventrally broadening basioccipital depression is present ventral to the occipital condyle, flanked by ventrolaterally directed ridges leading to the basal tubera. Lateral to these ridges, there is a shallow depression on the suture between the basioccipital and the ventral process of the otoccipital that extends ventrally from the paracondylar recess and becomes shallower ventrally. Thus, well developed subcondylar recesses, as they are present in *Dilophosaurus* and some other basal tetanurans (Witmer, 1997; Rauhut, 2004) are absent in *Irritator*.

Dorsolaterally, the basioccipital articulates with the otoccipital via a large, laterally placed articulation surface. The two otoccipital facets are separated from one another by a shallow median ridge of the basioccipital in the floor of the foramen magnum, which widens anteriorly towards the floor of the endocranial cavity. The facet for the otoccipital extends over nearly the entire anteroposterior length of the basioccipital.

Anterodorsally, the basioccipital bears a small dorsally directed facet for its anterodorsal contact with the prootic on either side. Lateral to the prootic contacts, the basioccipital forms a short surface that floors parts of the cavum labyrinthicum, has a contact with the crista interfenestralis of the otoccipital, and frames the fenestra pseudorotunda ventrally. Within the floor of the cavum labyrinthicum, the basioccipital and basisphenoid forms a narrow ventral cavity for the distalmost tip of the cochlea.

The short anterodorsal facet of the basioccipital for the prootic is posteriorly separated from the facet for the otoccipital by a dorsally open, U-shaped notch in the dorsolateral margin of the basioccipital. This notch forms the ventral margin of the medial vagal foramen, possibly for CN IX–XI and the jugular vein. The dorsal surface of the basioccipital is concave between the contacts to the bones forming the lateral wall of the braincase. This results in a cup-shaped, oval depression on the anterior part of the basioccipital, which continues anteriorly onto the dorsal surface of the basisphenoid, and holds the hindbrain.

Anteriorly, the basioccipital forms a dorsoventrally tall and slightly posteroventrally inclined surface that contacts the basisphenoid. Posteroventrally, two ventrolateral processes of the basioccipital brace the occipital condyle against the basisphenoid. These ventral processes represent the inconspicuous basal tubera, which are only formed by the basioccipital, and just slightly wider than the width of the occipital condyle. Although projecting tubera are thus absent, and the left side is damaged, the posterior surface of these processes is rugose (Figure 14), indicating the attachment of craniocervical musculature, as noted by Sues et al. (2002). In contrast to other non-avian theropods, in which the crista tuberalis of the otoccipital forms the lateral margin of the basal tubera (e.g., Sampson & Witmer, 2007), this structure ends above the base of these ventral processes of the basioccipital in *Irritator* (Figure

23). While *Baryonyx* (Charig & Milner, 1997), and possibly *Ceratosuchops* and *Riparovenator* (Barker et al., 2021) bear a posteriorly elevated sutural contact between the basioccipital and the basisphenoid, this is not the case in *Irritator* and *Suchomimus* (MS, pers. obs. on cast, MNN GDF 214). In *Baryonyx*, *Ceratosuchops* and *Riparovenator*, the posteriorly elevated sutural contact is roughly W-shaped and produces two dorsoventrally high depressions, flanking the ventral basisphenoid recess depression (Charig & Milner, 1997, Barker et al., 2021). Right and left tubera are separated by a deep, V-shaped incision that is spanned by a transverse lamina with a ventrally concave margin in *Irritator* (Figure 14, Figure 23E, F), *Ceratosuchops* and *Riparovenator* (Barker et al., 2021). This lamina forms the posterior wall of a dorsally deep cavity ('median opening' in Sues et al. 2002) that invades the basioccipital and basisphenoid at their contact in *Irritator* (Figure 24, Figure 26). The internal surface of the cavity is largely formed by bone of the basioccipital, whereas its ventral border is formed by the basisphenoid.

This opening leads to a partly webbed and irregular-shaped internal cavity network that extends dorsally below the floor of the braincase and to the base of the occipital condyle posteriorly. Sues et al. (2002) assigned the respective opening to the basisphenoid sinus and hence to the median pharyngeal system, a view that we concur with, as the bony relations of this opening - being bordered by the basisphenoid anteroventrally and the basioccipital posteriorly - correspond to the usual placement of this recess. As another part of the basisphenoid recess is placed below this recess in the basisphenoid (see below), this recess is thus subdivided (similar to the morphology observed in the Cleveland tyrannosaur CMNH 7541; Witmer & Ridgely, 2010).

Parabasisphenoid

As in all theropods, the basisphenoid is tightly fused with the parasphenoid, and we thus use the term ‘parabasisphenoid’ to refer to this compound bone within this section. Together, this unpaired element is well preserved and reversed L-shaped in lateral view (Figure 14, Figure 20-25). The parabasisphenoid includes a relatively robust cultriform process anteriorly. The cultriform process is largely embedded within the sediment but its morphology was uncovered with the CT data. The parabasisphenoid forms the anteroventral part of the braincase and contacts the pterygoid through the basipterygoid processes ventrally, the prootic dorsally and the basioccipital posterodorsally (Figure 1-4).

As in *Baryonyx* (Charig & Milner, 1997), *Ceratosuchops*, *Riparovenator* (Barker et al., 2021), a braincase referred to *Suchomimus* (MNN GDF 214), and caenagnathids (Sues, 1997), but in contrast to all other non-avian theropods, the basisphenoid is oriented vertically, so that the normally ventral surface is confluent with the occipital surface of the basioccipital and the basipterygoid processes are placed posteroventral to the basal tubera. This results in a dorsoventrally tall but anteroposteriorly short basisphenoid body in lateral view and a posteriorly opening basisphenoid recess. In *Irritator*, the basisphenoid body is notably longer than wide, with a maximal length of c. 4.5 cm from the basioccipital-basisphenoid suture to the basisphenoid web and a minimal transverse width of c. 3.5 cm (approximately at mid-length). The inconspicuous basal tubera are connected to the basipterygoid processes by stout, largely parallel and slightly lateroposteriorly directed lateral laminae, corresponding to the cristae ventrolateralis of other non-avian theropods (Sampson & Witmer 2007).

The posterior surface of the basisphenoid bears two prominent recesses, a smaller

dorsally situated one and a larger ventral one. Both recesses are placed in a marked longitudinal depression between the cristae ventrolateralis, which is bordered dorsally by the lamina of the basioccipital that spans between the basioccipital tubera. The normally anterior, now ventral border of this depression, formed by the basisphenoidal web (Bakker et al., 1988) is rather inconspicuous in *Irritator* so that the depression opens ventrally. This is due to the fact that the very stout basisphenoid web between the basipterygoid processes is ventrally rather than posteriorly directed. The dorsal recess within the depression is situated directly at the sutural contact between the basioccipital and parabasisphenoid. Our micro CT data reveal the complexity of this recess, dorsally leading over to the medial internal cavity below the condyle (already mentioned in the basioccipital section). Additionally, the recess leads to two cavities anteroventrally to the subcondylar cavity. These two cavities are dorsoventrally high, anteroposteriorly short and separated from each other by a mediolaterally oriented bony wall. The two cavities are flanked by two dorsoventrally tall and mediolaterally narrow cavity networks, invading the basipterygoid processes. The left network extends further ventrally than the right one. In the dorsal vicinity of the two aforementioned separated medial cavities, some minor channels and cavities are present, possibly connecting the medial cavities with the cavity networks of the basipterygoid processes. The ventralmost prominent recess in the posterior surface of the parabasisphenoid (‘basisphenoid recess’ in Sues et al., 2002) is a rather simple, dorsoventrally high and anteroposteriorly relatively shallow, cone-shaped depression. In its dorsal orientation, it is largely parallel to the more dorsal recess, from which it is separated by a bony lamina. As noted above in the description of the basioccipital, all of these posterior recesses, the one at the basioccipital-basisphenoid suture and the one only enclosed by the parabasisphenoid, are assigned to the basisphenoid recess. While *Irritator* thus

bears depressions, assigned to a transversally subdivided basisphenoid recess on the posterior surface of the parabasisphenoid, Baryonyx, *Suchomimus, Ceratosuchops and Riparovenator* do not seem to exhibit a subdivison of this recess (Charig & Milner, 1997; MS, pers. obs. on cast, MNN GDF 214; Barker et al., 2021).

In *Irritator*, the basipterygoid processes are very robust and short, the anteroposterior length of their articular surface being more than the distance that they protrude ventrally from the basisphenoid web. They project mainly ventrally and diverge only very little laterally, being separated by a broad, U-shaped gap in posterior view. The articular surface is almost parallelogram-shaped in ventral view, with a rounded posterior border and a pointed anteromedial corner. It has a rather complex morphology, being convex anteroposteriorly and mediolaterally in its posterior third, but rather flat to very slightly anteroposteriorly concave anteromedially, and rises slightly anterodorsally. Stout laminae extend anterodorsally from the basipterygoid processes towards the cultriform process and enclose a deep, cone-shaped subsellar recess, which is separated from the posterior depression on the parabasisphenoid by an anteroposteriorly broad, flat ventral surface of the basisphenoid web.

In lateral view, the basisphenoid bears a large, obliquely oval depression, the ‘lateral pneumatic recess’ of Sues et al. (2002), ventral to the articulation facets for the prootic. This depression corresponds to the anterior (=lateral) tympanic recess (Witmer, 1997b), which represents a theropodan or neotheropodan synapomorphy (Rauhut, 2003; see also Bronzati et al., 2018). The recess deepens dorsally and is markedly asymmetrical on the left and right side. Although it is subdivided into a larger anterior and smaller posterior depression within the recess on either side, the anterior depression is notably larger on the left than on the right side, while the

posterior depression is larger on the right side. Furthermore, the large anterior depression of the left side is divided by a thin bony lamina from another, smaller, triangular depression anterior to the anterior tympanic recess; this depression is absent on the right side. The large anterior depression within the anterior tympanic recess was identified as the entrance of the carotid canal for the cerebral carotid artery by Sues et al. (2002), but our CT data suggest that it is a blind ending pocket, extending anterodorsally. The actual openings of the vidian canal are small and inconspicuous, being placed in a narrow groove below this anterior pneumatic depression; while the entrance of the right vidian canal is placed within the anterior tympanic recess, the left one is placed just below this structure (Figure 22-25). There are minor internal channels in the vicinity of the anterior tympanic recess, partly leading over to the prootic and the basioccipital. Although the lateral sides of the parabasisphenoid body (between the cultriform process, anterior tympanic recess and the laminae leading towards the parabasisphenoid body from the basipterygoid processes) are slightly concave, there are no additional pneumatic recesses, such as the parasphenoid or basipterygoid recesses, which are present in some other non-avian theropods (Rauhut, 2004).

The cultriform process projects into the interorbital region. As also reported for *Majungsaurus* (Sampson & Witmer, 2007) and present in many other theropods, the 'cultriform process' of *Irritator* is strictly speaking not a singular medial structure, but composed of two parasagittal sheets of bone. These sheets arise from the anterior edges of the basipterygoid processes ventrally and converge dorsally, closer to the skull midline, thus confining a dorsally narrowing subsellar recess on the anteroventral surface of the parabasisphenoid, as described above. Left and right sheets are connected in the skull midline by a transverse bar of bone, which leaves deep dorsal and ventral longitudinal grooves between the sheeted parts of the

cultriform process (Figure 21). As a result, the cultriform process has an H-shaped cross section (Figure 20A, B), which, besides in *Majungsaurus* (Sampson & Witmer, 2007), has also been reported for the megalosaur *Dubreuillosaurus* (Allain, 2002). In *Irritator*, the cultriform process is flexed anteroventrally and anteriorly pointed, giving the cultriform process a hook-shaped appearance in lateral view (Figure 2B). The dorsal groove on the cultriform process leads posteriorly to a dorsoventrally deep depression, directly in front of a dorsal, plate-like projection (Figure 21A, B, Figure 22). The distal end of this projection is round and points posterodorsally. Such a projection is also present in e.g., *Allosaurus* (Chure and Loewen, 2020), the Cleveland tyrannosaur CMNH 7541 (holotype of *Nanotyrannus*; Witmer & Ridgely, 2010), *Suchomimus* (MS, pers. obs. on cast, MNN GDF 214) and *Ceratosuchops* (Barker et al., 2021). However, it is less prominent in these taxa, and seems to be absent in the megalosaur *Dubreuillosaurus* (Allain, 2002). This projection may have contacted the orbitosphenoid in *Irritator*, but incomplete preservation of the latter renders this detail unclear. The posterior margin of the dorsal projection is concave, forming a nearly round, window-like transverse opening between the plate itself and the posteriorly adjacent laterosphenoid and prootic. Sampson and Witmer (2007) describe an opening in a similar position in *Majungasaurus* as a fonticulus interorbitalis, and a dorsal plate connecting the cultriform process with the skull roof as a mineralized interobital septum, and furthermore report on the presence of similar mineralizations in several other ceratosaurs and at least one basal tetanuran, *Giganotosaurus*. Sampson and Witmer (2007) observe that the surfaces of these structures are usually striated and irregular, which supports their interpretations of the structure as calcified cartilage over the alternative that the structure is a proper ossification. However, in *Irritator*, the surface of the dorsal projection of the cultriform process is smooth, supporting the interpretation that the dorsal plate indeed is an

‘interorbital process’ of the cultriform process itself rather than a partially mineralized interorbital septum.

Directly anteroventral to the ‘interorbital process’, the cultriform process bears two small internal cavities, and posteroventral to the ‘interorbital process’ is a third, bigger, anterodorsally inclined and seemingly isolated cavity situated (Figure 26C). The three cavities cannot be assigned to a pneumatic sinus, since they seem to be unknown in other theropods. Behind the projection, a dorsal groove leads to the sella turcica (pituitary fossa) that housed the pituitary gland. The sella turcica is narrow, cone-shaped and dorsoventrally deep. Within the floor of this fossa, there is a singular opening for the cerebral carotid artery, representing the joint opening of the left and right vidian canals, which converge within the parabasisphenoid, as in other non-avian theropods. Posterior to the pituitary region, the parabasisphenoid transversely broadens towards its dorsal surface, which bears two large lateromedially oriented articulation facets for the prootics to form the dorsum sellae. As the prootics meet each other anteriorly and diverge posterolaterally, the prootics form parts of the dorsum sellae, and the parabasisphenoid only has a small dorsal exposure in the cup-shaped depression for the hindbrain, between the prootics anteriorly and the basioccipital posteriorly (Figure 21A, B).

Laterosphenoid

Both laterosphenoids are present. While the right laterosphenoid is largely intact, the left element bears a large hole in the center of the body (Figure 1, Figure 22). The element contacts the orbitosphenoid anteriorly, the frontal anterodorsally, the postorbital anterolaterally, the parietal dorsally, the supraoccipital posteriorly and the prootic ventrally (Figure 2-4).

The body of the laterosphenoid has a roughly trapezoidal shape, with the posterior and anterior margins paralleling each other. The posterior margin has a slight anterior inclination. It is perpendicular to the posteroventral margin in lateral view. In posterior view, the posteroventral portion of the laterosphenoid flares laterally. The posterior margin forms the contact with the supraoccipital. Here, the right element has a small rounded depression (Figure 25) which was identified as the opening for the vena cerebralis media by Sues et al. (2002). However, this opening would be in a much more posterior and dorsal position than in other non-avian theropods, and the micro CT data shows that it does not pierce the bone and may rather represent a damage; as noted below, the mid-cerebral vein probably exited the braincase through a foramen immediately dorsal to the trigeminal foramen (Figure 23A-C, Figure 25).

The dorsal margin is slightly anterodorsally inclined and articulates with the parietal over its full length. Anteriorly, there is a distinct process for the articulation with the orbitosphenoid, the posterior end of the frontal and a small anterior portion of the parietal. The process is anterodorsally and slightly medially directed and has a blunt anterior end that is anteroventrally directed, forming a small ventral hook (Figure 20A, B). Laterally, the process bears a longitudinal depression. The processes of the left and right side leave a median gap for the olfactory tract, which is ventrally bound by the orbitosphenoid. The ventrally recurved part of the process forms the dorsal and anterodorsal margin for a circular foramen for the passage of the CN IV, which is anteroventrally and ventrally bound by the orbitosphenoid. This foramen is distinctly large, although not as large as the trigeminal foramen. The anteromedial margin of the laterosphenoid ventral to the CN IV foramen is formed as a blunt ridge, against which the orbitosphenoid articulates. In this area (Figure 20, Figure 22, Figure 24, Figure 25), two more foramina are found between the laterosphenoid and the

orbitosphenoid, which are easier to see in the fossil than in the CT scans due to the delicate nature of the orbitosphenoid. In agreement with Sues et al. (2002), we identify the dorsal foramen as for the CN III. The more ventrally located foramen could be for the sphenoidal artery (see Sampson & Witmer, 2007), whereas the CN II is completely enclosed by the orbitosphenoid.

Posterior to the anterodorsal process, a second process is present at the dorsal part of the laterosphenoid, the capitate process, which is slightly shorter and projects mainly laterally and slightly anteriorly. The process contacts the frontal anterodorsally, the parietal dorsally and the postorbital laterally via a blunt head. Ventrally, the capitate process ascends directly from the lateral surface, and there is no expanded antotic crest that buttresses the process, as reported for *Majungasaurus* (Sampson & Witmer, 2007).

At its ventral base, the laterosphenoid bears a medial process that contacts its counterpart (Figure 21A, B). Together, they form a bridge-like contact in anterior view, forming the dorsal margin of the dorsum sellae. The base ends in an acute ventral tip that flanks the parabasisphenoid laterally and forms a small ventral process anterior to the trigeminal foramen. It is formed by the anterior and anteroventral margin of the laterosphenoid. The anterior margin is slightly inclined anterodorsally in lateral view and straight in anterior view. The ventral margin is slightly posterodorsally inclined. It contacts the prootic and forms the dorsal margin of the CN V opening, which is marked as a small, rounded rim in the anterior part of this margin.

The lateral surface of the laterosphenoid is almost flat, with the anterior portion curving slightly medially. Dorsal to the CN V opening there is a mediolaterally concave overhang of the bone, which houses the exit for the mid-cerebral vein (also

partly penetrating the prootic in *Irritator*), as in other non-avian theropods (e.g., Rauhut, 2004). Anterior to this overhang, an anterodorsally inclined depression for the ascending CN V1 ramus is present, which has about the same dorsoventral height as the respective opening and is bordered posteriorly by a steeply ascending, slightly anteroventrally overhanging step on the lateral surface of the laterosphenoid.

The medial surface of the laterosphenoid is concave (Figure 24), encapsulating the cerebral region of the braincase (the micro CT data allowed for a better separation of the orbitosphenoid, laterosphenoid and the sediment within the braincase indicating more voluminous cerebral hemispheres on the new endocast). In dorsal view, the dorsal margin is also medially concave, with the anteromedial process that forms the dorsum sellae being set at an angle of 90° towards the lateral part of the laterosphenoid.

Orbitosphenoid

Only the right orbitosphenoid is present, and it is unclear if the entire element is preserved (Figure 1, Figure 20, Figure 22, Figure 24, Figure 25). The bone is extremely thin, and many aspects of its morphology are easier conceivable in the fossil than in the (micro)CT data. The orbitosphenoid contacts the laterosphenoid posteriorly and possibly the frontal dorsally (Figure 2). Probably, the orbitosphenoid articulates dorsally with the ventral hook of the anterodorsal process of the laterosphenoid, hereby enclosing the foramen for the CN IV. However, it is not entirely clear if the orbitosphenoid contacts the frontal (as depicted by Sues et al., 2002), which may be suggested by the right element, or if the laterosphenoid actually borders the CN IV opening dorsally and anterodorsally, and thus separates the orbitosphenoid and the frontal, as our interpretation of the micro CT data shows. The

orbitosphenoid forms the anteroventral border for CN IV and the anteromedial border for CN III laterally, as well as the lateroventral margin for the olfactory tract and the lateral border for CN II medially. The orbitosphenoid is dorsoventrally tall and generally slender. Its dorsal portion is slightly expanded anteriorly to form a plate-like section that articulates with the anterior margin of the laterosphenoid posteriorly.

The CN III foramen is small and positioned in the sutural contact of laterosphenoid and orbitosphenoid. Ventrally to the CN III opening, an even smaller opening of unclear identity is present; it may belong to the sphenoidal artery, as noted above. Anteriorly, a large, semicircular medial concavity represents the CN II opening in the particularly thin central part of the orbitosphenoid. The left orbitosphenoid of *Suchomimus* possibly provides evidence for these assignments, as the foramina have a similar distribution (MS, pers. obs. on cast, MNN GDF 214).
Our micro CT data show that the interior of the orbitoshenoid of *Irritator* bears one big and one small cavity without an external connection in its dorsal portion, anteriorly to the opening for CN III (Figure 26). In non-avian theropods, no hollow orbitosphenoid has been reported by now, however, *Massospondylus carinatus* bears one cavity per orbitosphenoid (Chapelle & Choiniere, 2018).

Stapes

Concluding from its position on the fossil, only the right stapes is present (Figure 1B, Figure 27). It is preserved on the right basisphenoid and jugal.

The stapedial shaft is a straight and delicate rod. In articulation, the stapes lies within the stapedial groove, between the prootic and otoccipital, and extends between the fenestra ovalis anteriorly and the eardrum that would have been placed

posteroventral to the quadrate head-paroccipital process articulation posteriorly (Figure 2A, Figure 4B). Thus, the full length of the stapedial shaft seems preserved.

Vomer

In the specimen, only small parts of the posterior portion of the vomer are visible through the right antorbital fenestra (Figure 1B). The vomer is a fused, slender, elongate element and preserved in several pieces, as shown by the CT data (Figure 28). The vomer contacts the maxilla laterodorsally and the pterygoid and palatine posteriorly, and, possibly, the premaxilla anterodorsally (Figure 2, Figure 4B). As the premaxillae and anterior ends of the maxillae are missing in *Irritator*, the anterior end of the vomer is also not preserved, and thus its anterior extent cannot be established (Figure 2B). It is unclear if the vomer articulated with the premaxillae in spinosaurids, as it is the case in other non-avian theropods. The bone visible in ventral view between the premaxillae and identified as the vomer in *Baryonyx* by Charig & Milner (1997) represents the anteromedial processes of the maxillae and Rayfield et al. (2007) argued that the vomer did maybe not project as far anteriorly as previously thought. Despite the very long anterior ramus of the maxilla, the vomer reaches the level of the anterior part of the antorbital fenestra posteriorly, as in other non-avian theropods with relatively shorter snouts (e.g., Gilmore, 1920; Madsen, 1976; Rauhut et al., 2010).

Anteriorly, the preserved part of the vomer forms a thin rod-like process that is wedged ventrally between the median ridges of the maxillae. At the level where the maxillae diverge from the skull midline and lose their contact with one another, the vomer becomes a vertically sheeted plate, which almost immediately bifurcates dorsally into two laminae that bound a deep median, dorsally open trough (Figure

28C, E). This posterior portion of the vomer becomes dorsoventrally taller and the lateral sheets of the vomer are almost parallel to one another, only slightly diverging dorsally, resulting in a deep, narrow U-shaped cross-section of the bone. In dorsal view, the two lateral sheets diverge very slightly posteriorly. At the posteriomost end of the vomer, the two lateral vomerine sheets are ventrally not floored by bone, but form short posterior processes for the articulation with the palatine and pterygoid. These vomerine processes are sandwiched between the pterygoids medially and the palatine laterally, which each have short plated processes for the vomer articulation.

Palatine

Both palatines are preserved (Figure 1, Figure 29), having the typical tetraradiate shape found in most non-avian theropods (Rauhut, 2003). The right element lacks the anterior maxillary process (Figure 28A, C, D), which is present in the left element (Figure 28E, F). On the other hand, the right palatine bears a better preserved posteroventral aspect than its left counterpart (Figure 28B). The palatine contacts the vomer anterodorsally, the maxilla anteroventrally, the jugal and possibly the lacrimal posterolaterally and the pterygoid posteromedially (Figure 2, Figure 4). Solely the dorsal portions of the palatines are exposed in the antorbital fenestrae (Figure 1), but their whole morphology is revealed by our CT data. Whereas we were able to segment the maxillary process of the left palatine from the maxilla, this is not the case on the right.

The maxillary process is wide at its base but narrows anteriorly to an elongate rod. This rod tapers anteriorly and represents by far the longest process of the palatine. There is a shallow anteroposteriorly oriented depression on the anteriormost third of

the process, which faces ventrolaterally towards the maxilla. With this facet, the palatine articulates with the dorsal surface of the median ridge of the maxilla.

Dorsally, the vomeropterygoid process borders the internal choana anteriorly and the pterygopalatine fenestra posteriorly (Figure 4B). The process has a transversely broad ventral base, the posterior surface of which is excavated by a deep fossa between the posterior processes of the palatine. The vomeropterygoid process ascends dorsomedially, and twists from a posterolaterally-anteromedially oriented base into an anteroposteriorly expanded, vertical, wing-shaped bony plate. This plate is more anteriorly expanded and tapers to a point anteriorly. However, a dorsoventrally high, but short and rounded posterior expansion is also present, as in most basal tetanurans (e.g., Madsen, 1976; Currie & Zhao, 1993; Eddy & Clarke, 2011), but in contrast to most non-avian coelurosaurs (e.g., Barsbold & Osmolska, 1999; Rauhut et al., 2010). The medial surface of the plate is parallel with the sagittal skull axis, and principally contacts the lateral surface of the vomeropalatine process of the pterygoid. However, anteriorly, the short articular process of the vomer becomes wedged between palatine and pterygoid (Figure 2, Figure 4).

Posteroventral to the vomeropterygoid process, there is a medial process for the pterygoid and a lateral one for the jugal contact, which diverge posteriorly at an acute angle, framing the anteriorly narrow pterygopalatine/suborbital fenestra. The jugal process forms a vertically oriented plate that lies against the medial surface of the jugal. Its dorsal margin is continuous with the posteroventral margin of the vomeropterygoid process, forming a semicircular margin. The ventral margin of the jugal process is offset from the ventral margin of the maxillary process by a small concavity, but otherwise the process is posteriorly continuous with the maxillary process. As in most non-avian averostrans (see Carrano & Sampson, 2008), the

jugal process is dorsolaterally more expanded than the maxillary process. At its posterior end, the jugal process bears a notch, possibly separating the process in a dorsal lacrimal process and a ventral jugal process, although it cannot be excluded that this notch might be an artifact of preservation, as this part of the palatine is only preserved on the right side and no contact with the lacrimal is obvious. The pterygoid process of the palatine is anteroposteriorly longer than the jugal process (as preserved). It is dorsoventrally high and lateromedially thin, with its distal end tapering. Its dorsal surface is markedly concave between the more vertical medial side and the lateroventrally flexed ventral margin. The medial margin of the pterygoid process of the palatine extends onto the medial surface of the vomeropterygoid process, and forms the medial margin of the posterior fossa on the base of the vomeropterygoid process.

Pterygoid

Both pterygoids are nearly completely preserved, but disarticulated from their life positions (Figure 1, Figure 30). The left pterygoid is rotated clockwise out of its former position, and large parts of it are exposed in the fossil above the left surangular. The posterior portion of the right pterygoid lies ventrolateral to the basisphenoid. Our CT data reveal that both elongated pterygoids are largely intact, except for minor parts of their vomeropalatine processes and the posteriormost portion of the left quadrate wing (Figure 31). The pterygoid forms a connection of the anterior palate with the basicranial region. In contrast to other non-avian theropods, it is composed of only two main structures: an anteriorly directed palatine process, which contacts the ectopterygoid centrally and laterally, and the vomer and palatine at its anterior end, and the posterior quadrate wing, which forms articulation surfaces

for the epipterygoid and quadrate (Figure 2-4). In between the two main parts lies the articular facet for the basipterygoid processes of the basisphenoid.

The vomeropalatine process is elongated and mediolaterally thin. It is slightly bowed anterodorsally where it ascends towards the vomeropterygoid process of the palatine. As in most non-avian theropods (e.g., Madsen, 1976; Ostrom, 1969; Currie & Zhao, 1993), the vomeropalatine process is approximately L-shaped in cross-section, with a more vertical medial and a more horizontal lateral part. Both rami are of subequal width and gently curve into each other, rather than meeting at a pronounced 90° angle, as it is the case in some non-avian theropods. From the basipterygoid processes posteriorly, the right and left anterior processes approach one another medially, thus constricting the interpterygoid vacuity. The surface of the anterior process is dorsolaterally concave and ventromedially convex. Around the mid-length of the process, the ectopterygoid articulates laterally on an unremarkable surface of the margin of the vomeropalatine process. This ectopterygoid-pterygoid contact is unusual, both in terms of its position and morphology: usually, the ectopterygoid contacts the pterygoid at the posterior end of the latter along a lateroventral ectopterygoid ramus, which projects of the contact point between vomeropalatine process and quadrate wing of the pterygoid (Madsen, 1976, Eddy & Clarke, 2011, Brusatte et al., 2012, Chure & Loewen, 2020). However, an ectopterygoid ramus of the pterygoid is entirely absent in both pterygoids of *Irritator*. In order to close the pterygoplatine fenestra/suborbital fenestra transversely, the ectopterygoid position is inferred relatively far anteriorly in comparison to other non-avian theropods; this also coincides with the position that both ectopterygoids are preserved in relation to their respective pterygoids in the specimen (see ectopterygoid section for additional details). Furthermore, both pterygoids show a slight lateral thickening at the approximate site of the ectopterygoid contact, with a

small, semicircular ventral expansion of a very thin bony lamina on the left element, being visible on the fossil (Figure 1A, Figure 30, Figure 31A, D). Anterior to the ectopterygoid contact, the anterior third of the vomeroplatine process underlies the ventromedial surface of the palatine in our articulated skull reconstruction. At its anterior tip, the vomeropalatine process bears a short, plate-like process, which is slightly turned downwards with regard to the main axis of the vomeropalatine process. This plate-like process articulates with the vomer anteriorly and with the palatine medially (Figure 2, Figure 4B).

Posteriorly, the pterygoid forms a large, more laterally positioned quadrate wing and short posteromedial process; the right wing is posterodorsally more complete and exhibits a small area medially to the right jugal-quadratojugal contact (Figure 1B). The quadrate wing is a posteriorly and slightly laterally directed, transversely thin sheet of bone that is considerably higher dorsoventrally than long anteroposteriorly. The anterior margin of the wing is ventrally slightly thickened, and ascends almost perpendicularly from the dorsal margin of the vomeropalatine process. The posterior margin is concave, and the pointed ventral part extends as wide posteriorly as the dorsal part. The anterior and posteroventral margins are flexed inwards, so that the medial surface of the quadrate wing is concave, whereas the lateral surface is convex. The lateral surface articulates with the pterygoid flange of the quadrate (Figure 2, Figure 3B, Figure 4). Ventrally, at the base of the quadrate wing, the pterygoid has a short posteromedial process, which is separated from the quadrate wing by a broad shallow groove. The process is posteriorly directed and receives the basipterygoid process of the parabasisphenoid dorsomedially. Above the basipterygoid articulation, the parabasisphenoid and pterygoid leave a dorsoventrally tall anteroposterior passage, the cranioquadrate space. A distinct notch is present

between the basipterygoid process and the ventral portion of the quadrate wing (Figure 31C).

Ectopterygoid

The CT data reveal that both ectopterygoids are well preserved (Figure 32) but not in articulation with their neighboring bones anymore. Solely a small portion of the posteromedial process of the left ecotpterygoid is visible on the fossil below the left pterygoid (Figure 1A, Figure 30). Both elements bear a transverse crack in a very similar manner on the jugal process. The ectopterygoid of *Irritator* is conspicuously small and slender and lacks the typical medial expansion seen in basically all non-avian theropods (Rauhut, 2003). The ectopterygoid likely contacted the jugal laterally and the pterygoid medially and formed the anterior margin of a large, elongate oval subtemporal fenestra of the articulated skull reconstruction in ventral view (Figure 2-4).

As is typical for non-avian theropods, the lateral jugal process is hook-shaped, being flexed posterolaterally so that the jugal facet is almost parallel to the pterygoid contact. The medial ectopterygoid body is anteroposteriorly long and dorsoventrally slim. The jugal contact is flexed posteriorly at a perpendicular angle. The lateral facing contact area is elongated and pointed posteriorly; it misses the anteroventral process present in, e.g., *Dubreuillosaurus* (Allain, 2002) and *Asfaltovenator* (Rauhut & Pol, 2019). The ectopterygoid articulates with the jugal at about the mid-length of the latter which is similar to other non-avian theropods (Sampson & Witmer, 2007, Brusatte et al., 2012).

The medial ectopterygoid body is angled posteroventrally at an angle of approximately 45° towards the jugal articulation. The pterygoid contact is formed by a short and broad, wing-shaped bony lamina anteriorly and a long, slender, but dorsoventrally more massive posterior process. The articulation surface for the pterygoid is only slightly longer than the articulation surface for the jugal. A marked, posteriorly deepening longitudinal step separates the anterior sheet from the posterior process, thus defining a posteriorly deepening ventral depression on the medial side of the ectopterygoid body (Figure 32D). This depression corresponds to the ventral ectopterygoid fossa that is present in all non-avian neotheropods, with the exception of ceratosaurs (Rauhut 2003). However, this fossa does not invade the lateral part of the ectopterygoid body, as it is the case in most other basal tetanurans (e.g., Madsen, 1976; Currie & Zhao, 1993; Eddy & Clarke, 2011).

The combined pterygoid-ectopterygoid morphology of *Irritator* suggests that these elements had a mode of articulation that is unusual for non-avian theropods. Usually, the strongly expanded medial surface of the ectopterygoid contacts both the lateral margin of the base of the vomeropalatine process of the pterygoid and a posteroventrally directed ectopterygoid ramus of the pterygoid, thus accounting for the notable twist between the jugal articulation and the pterygoid contact (Madsen, 1976, Sampson & Witmer, 2007, Eddy & Clarke, 2011, Brusatte et al., 2012, Chure & Loewen, 2020). In *Irritator*, the ectopterygoid ramus of the pterygoid is entirely absent, but the general morphology of the contact between the pterygoid and ectopterygoid is the same as in other non-avian theropods (Sampson & Witmer, 2007), with the thin anterior lamina of the ectopterygoid body overlapping the pterygoid dorsally, whereas the latter overlaps the thickened ectopterygoid body posteriorly (Figure 2B, Figure 4B). Furthermore, the twist between the articular surfaces is still present, as noted above. As noted in the description of the pterygoid,

the narrow mediolateral width of the ectopterygoid in *Irritator* suggests that this bone had a relatively far-forward position in the skull: the ectopterygoid is mediolaterally not wide enough to reach the pterygoid and the jugal simultaneously on the posterior portion of the pterygoid. In this area, the slightly anterodorsally flexed vomeropalatine process of the pterygoid is steeply anterodorsally inclined in the articulated skull, probably explaining why the twist between the articular ends of the ectopterygoid is present despite of the absence of an ectopterygoid wing of the pterygoid. In our articulated skull reconstruction, the ectopterygoid thus contacts the jugal immediately posterior to the posterior end of the paperclip-like maxilla-jugal contact, in a position between the orbit and antorbital fenestra (Figure 4B). Usually, the ectopterygoid articulates with the jugal around its mid-length and below the orbit in non-avian theropods (Sampson & Witmer, 2007, Brusatte et al., 2012, Evers et al., 2020).

Close to the articulation surface for the pterygoid, there are small, discreet cavities within the ectopterygoid body, without a clear connection to a pneumatic foramen.

Epipterygoid

The epipterygoid contacts the pterygoid ventromedially. In our CT data, we found two exceptionally thin elements (Figure 33) that are, partly visible in the fossil, wedged between the posterior portion of the right surangular and articular and the quadratojugal and jugal, and thus not preserved in their original position (Figure 1B). However, comparison with described epipterygoids of other non-avian theropods (Eddy & Clarke, 2011, Brusatte et al., 2012) allows unambiguous identification of the thin elements as epipterygoids. The left epipterygoid is slightly better preserved than the right element, but both agree in general morphology.

The epipterygoid of *Irritator* is a dorsoventrally tall plate with an anteroposteriorly wide base and tapering dorsal end. The anterior margin of the epipterygoid is somewhat thickened with regard to the thin blade of the remainder of the bone. Furthermore, its medial surface that would lie against the quadrate wing of the pterygoid is gently concave. Anteroventrally, there is a small, posteriorly recurved flange on the medial surface, which appears to have received the anterior margin of the quadrate wing of the pterygoid, similar to the condition described in *Alioramus* (Brusatte et al., 2012). *Acrocanthosaurus* and *Alioramus* bear a distinct articulation surface for the epipterygoid on their dorsolateral quadrate process of the pterygoid (Eddy & Clarke, 2011, Brusatte et al., 2012). This is not the case in *Irritator*, which makes it difficult to determine its exact position. However, based on the aforementioned flange for the anterior quadrate wing margin, we placed the epipterygoid along the anterior margin, at a mid-height level of the quadrate wing of the pterygoid (Figure 2A).

Mandible

As noted by Sues et al. (2002), the mandible is incompletely preserved on both sides, with only the surangular and articular being preserved for both mandibular rami, plus the almost complete prearticular and parts of the angular on the left side (Figure 1). In contrast to most non-avian theropods, the jaw articulation is anteroventrally inclined, so that the posterior end of the mandible is approximately level with the posterior end of the skull (Figure 2). A relatively large mandibular fenestra is present and largely preserved (Figure 1A, Figure 2A, Figure 34A), being bordered dorsally and posterodorsally by the surangular and anteroventrally, ventrally and posteroventrally by the angular; the fenestra is unusual in shape in that

the ventral margin is strongly concave, whereas the dorsal rim is rather straight. The fenestra is ventrally placed in the mandible so that the surangular accounts for approximately half the height of the mandible in this area.

Surangular + Articular

Both surangulars are largely complete (Figure 34, Figure 35), but the right element misses its anterior end. Additionally, both retroarticular processes are damaged and the ventral margins of the surangulars near the contact with the respective angular are unclear, as the morphology differs slightly between the right and left element. In the fossil, the left surangular is largely exposed in lateral view close to its original position in the articulated skull, whereas the right surangular is rotated approximately 180° along its anteroposterior axis with regard to its original position, which results in its medial surface being exposed on the right side of the specimen (Figure 1). As preserved, the surangular of *Irritator* contacts the dentary anteriorly, the prearticular medially, the angular ventrally and the articular posterodorsally (Figure 2).

The surangular and articular seem to be fused in both mandibular rami. There is no unequivocal external sutural contact between both bones, and our CT data fail to completely follow sutures internally. Thus, the surangular and articular were segmented in single models, and their morphology is described together here.

The surangular is anteroposteriorly elongated. The anterior portion of the bone is mediolaterally thin. The dorsal margin of this anterior part of the bone is straight. The ventral margin parallels the dorsal margin in the area where it forms the dorsal margin of the mandibular fenestra, but expands ventrally at the level of the posterior end of this opening. On the better preserved right side, there is a small, anteriorly

opening notch at the dorsal end of this expansion, marking the narrowly rounded, dorsally placed posterior end of the mandibular fenestra. However, the exact position, size and shape of the fenestra can only be estimated based on the angular, as the ventral margin of the anterior surangular ramus itself shows no notch or curvature that would allow identification of the anteroposterior length of the fenestra just based on surangular morphology. Anterior to the mandibular fenestra, the ventral margin of the surangular very slightly converges with the dorsal margin, and the blunt anterior end of the surangular was overlapped laterally by the dentary, of which a small fragment is preserved in this position on the left side, as shown by Sues et al. (2002). In cross-section, this anterior part of the surangular is slightly convex laterally and concave medially. On approximately one-fifth of the length of the surangular posterior to its anterior end, the dorsal margin of the anterior surangular ramus becomes gradually thicker until it forms a robust, medially infolding shelf for the articulation with the coronoid. The shelf becomes wider and more robust posteriorly, until it turns into a dorsomedially opening groove above the posterior end of the mandibular fenestra, where the dorsal margin of the surangular is strongly thickened and approximately triangular in cross-section. The groove ends at approximately the level of the posterior end of the mandibular fenestra, posterior to which the dorsal margin of the surangular becomes gradually thinner again towards the jaw articulation. The facet for the obviously anteroposteriorly elongate coronoid thus forms a dorsally facing medial shelf anteriorly and a dorsomedially facing groove posteriorly, in contrast to the simple medially facing facet in other non-avian theropods (e.g., Madsen, 1976; Currie & Zhao, 1993). There is no sign of an anterior surangular foramen and an anteriorly extending groove from that foramen on the lateral side, as it is present in many other non-avian theropods (e.g., Madsen, 1976; Currie & Zhao, 1993; Currie, 2003; Sampson & Witmer, 2007; Rauhut et al., 2010).

The laterally rugose coronoid eminence at the level of the posterior end of the mandibular fenestra marks the transition to the posterior portion of the surangular, forming a distinct kink in lateral view so that the straight dorsal margin of the posterior portion slopes ventrally at an angle of approximately 35° with respect to the anterior portion. The dorsal margin is maximally mediolaterally thickened in this area, so that the medial surface of the surangular keeps the concavity seen in the anterior portion.

The lateral surface of the posterior portion bears a prominent surangular shelf, which projects lateroventrally. The shelf starts anteriorly with a marked lateral thickening dorsal and slightly posterior to the posterior margin of the external mandibular fenestra, and stretches posteroventrally to below approximately the half-length of the glenoid fossa of the articular. In the left element, the shelf is not completely preserved. Based on the CT data of the right surangular, the shelf is posteriorly rounded and expands far lateroventrally. Dorsal to the shelf, a marked, anteroposteriorly long, oval adductor fossa is present, being placed somewhat anterolateral to the jaw articulation and directed dorsolaterally and very slightly posteriorly. The shelf seems to be similar in *Baryonyx* (Charig & Milner, 1997), but different in other non-avian theropods, where it is less prominent and projects laterally without a ventral deflection (e.g., Madsen, 1976, Sampson & Witmer, 2007, Eddy & Clarke, 2011, Brusatte et al., 2012). Posteriorly and very slightly dorsal to the shelf, a marked, rounded lateral tubercle is present at the posterior end of the glenoid fossa. Anterodorsal to this tubercle and thus dorsal to the posterior end of the lateral surangular shelf, the anterolateral margin of the glenoid is marked by a raised, slightly laterally overhanging ridge.

Below the lateral surangular shelf, the left side shows two foramina, leading to the medial side of the surangular. The anterior foramen is placed slightly more ventrally,

approximately 1 cm anterior to the anterior rim of the glenoid and seems to pierce the surangular more or less straight mediolaterally, whereas the second foramen is placed slightly more dorsolaterally in the lateral shelf, just below the anterior rim of the glenoid, and opens posterolaterally. Two posterior surangular foramina are also present in some other non-avian theropods, such as *Sinraptor* (Currie & Zhao, 1993), *Proceratosaurus* (Rauhut et al., 2010) and *Allosaurus* (Benson, 2010).

Both articulars are present but not complete. The articular surface for the quadrate is formed between the articular and surangular, and exact contributions cannot be discerned due to the fusion of the latter two elements. The entire articular region is mediolaterally wide and medially expanded with regard to the vertical plate formed by the anterior parts of the surangular. The articular surface shows two distinct facets that subdivide the glenoid; a mediolaterally smaller but anteroposteriorly slightly longer medial one for the entocondyle and a lateral one for the ectocondyle. The posterior margin of the lateral facet of the glenoid is strongly dorsally elevated to form a high, transversely oriented projection that is tongue-shaped in posterior view. This projection is separated from the also slightly elevated posteromedial edge of the medial condyle by a wide, incision that forms an obtuse angle in posterior view. The anterior margin of the glenoid is bound by a low ridge on its lateral half. At the anteromedial end of the glenoid fossa, a slightly anteriorly recurved ridge descends along the margin of the articular (‘medial hook process’ of *Alioramus*; Brusatte et al., 2012).

The left surangular bears a medial anteroventrally facing spur for articulation with the prearticular that seems to be absent in other non-avian theropods (e.g., Madsen, 1976; Brusatte et al., 2012). The left articular is still in original contact with the prearticular and this area appears to be intact in medioventral view, with the

entocondyle of the quadrate exactly fitting into the respective glenoid (in the articulated skull reconstruction).

The retroarticular process is unusual in *Irritator*. In lateral view, it is strongly offset ventrally from the glenoid portion of the surangular/articular, being placed entirely below the level of the lateral surangular shelf, and forming an almost right angle with the subvertical posterior wall of the glenoid. Some aspects of the retroarticular process are better preserved on the right side (Figure 35) and some are better preserved on the left side (Figure 34). The left retroarticular process is lobe-shaped in medioventral view and rather thin dorsoventrally, being somewhat inclined mediodorsally. In contrast to most other non-avian averostrans (e.g., Madsen, 1976; Sampson & Witmer, 2007), the articular surface for the m. depressor mandibulae is not developed as a concavity, but the dorsal surface of the process is gently convex mediolaterally. The posteriormost portion of the left process is missing. In contrast, the right retroarticular process is anteroposteriorly longer than its left counterpart, indicating that the process was originally about twice the anteroposterior length of the glenoid fossa. The medial side of the right glenoid region and retroarticular process is largely eroded, but the left side shows that a ridge extended from the dorsomedial side of the process to the posteromedial edge of the glenoid. A marked, ventrally overhanging angular medial process, as it is present in some non-avian theropods in this region (e.g., Yates, 2005) is absent. The chorda tympani foramen could not be identified in the CT images.

There is a diffuse cavity network present ventrally to the glenoid fossa, close to the surangular and articular articulation surface, comprised by many different-sized cavities which are not always interconnected. The cavities of the right network are usually bigger. The anteriormost of those are situated anteroventral to the articular surface for the quadrate and seem to bear foramina on the anteromedial articular

surface for the prearticular. Posteriorly, cavities of this network extend to the retroarticular process base. Posteroventrally to the glenoid fossa for the ectocondyle, the right surangular bears a comparatively large cavity. Such a cavity is more ventrally situated and smaller in the left surangular.

Angular

Only the left angular is preserved, being in its presumed original position with regard to the left surangular, but only a portion of its anterior part is present (Figure 1, Figure 34). Thus, little can be said with certainty about the angular morphology in *Irritator*. As preserved, the dorsal margin of the angular is deeply convex and borders the external mandibular fenestra ventrally. This margin seems to be original and thus indicates the shape of the mandibular fenestra. The dorsal concavity of the bone is more marked than in most other non-avian theropods, with the dorsal margin of the anterior prong being set at an angle of c. 70° in respect to the dorsal margin at the posteroventral part of the mandibular fenestra, similar to the condition in *Acrocanthosaurus* (Eddy & Clarke, 2011). However, this angle is about 30° in *Majungasaurus* (Sampson & Witmer, 2007), 40° in *Allosaurus* (Madsen, 1976) and *Sinraptor* (Currie & Zhao, 1993), and 50° in *Alioramus* (Brusatte et al., 2012). Consequently, the anterior prong of the angular is strongly anterodorsally directed and reaches the level of the ventral margin of the surangular dorsally, as in *Herrerasaurus* (Sereno & Novas, 1993). The anterior end of the anterior prong is pointed. Anterodorsally, a small, laterally facing shelf is developed, which might indicate a contact with the surangular. Here, the medial side is markedly flattened, probably for the contact with the prearticular. At the ventral end of the anterior prong, a small, anteriorly projecting process is present. Whereas the anterior prong of the

angular is thickened, as it is usual in non-avian theropods, the posterior half of the preserved portion is just represented by a thin and dorsally bent bridge. Posterior to the preserved part, the angular most probably broadly overlapped the ventral lamina of the surangular laterally, but there does not seem to be a marked facet for the angular at the level of the retroarticular process, indicating that the angular did not reach the posterior end of the mandible. Between the posterior bridge of the preserved part of the angular and the surangular, a foreign body has been added to the fossil, which can clearly be discerned with the CT data (Figure 1, Figure 34).

Prearticular

Only the left prearticular of *Irritator* is preserved, but the element is nearly complete except for a central piece that is entirely missing, and possibly a part of the ventral margin in the posterior half of the element (Figure 1, Figure 34). The left prearticular is preserved in articulation with the left surangular/articular, which it contacts posterolaterally. The other bone contacts are not preserved, but based on lower jaw morphology of other non-avian theropods, it probably contacted the splenial anteriorly, the coronoid posterodorsally, the angular anteroventromedially, and possibly the dentary anterodorsally (Figure 2-3; see e.g., Zhao & Currie, 1993). As preserved, the prearticular is a mediolaterally thin and anteroposteriorly long element. It is ventrally bowed along its mid-length, forming a distinctly concave dorsal and convex ventral margin. The ventral margin in the anterior portion parallels the dorsal margin, although it cannot be completely excluded that minor portions of the very thin ventral bony lamina are broken away here. The anterior part of the prearticular is dorsoventrally expanded with regard to central portion of the bone. The latter seems to have been very slender, although it possibly misses minor parts of the

ventral lamina and only the dorsal margin is still intact. There is no incision in the anteroventral margin of the anterior part, as it is present in *Allosaurus* (Madsen, 1976) and *Acrocanthosaurus* (Eddy & Clarke, 2011). Posteriorly, the bone ends with a dorsoventrally expanded, triangular surface that lies medially against the surangular and the articular at the level of the glenoid fossa (Figure 1B, Figure 34). Although this expansion seems to taper posteriorly in its ventral part, the prearticular of *Irritator* does not seem to form a thin process that underlies the retroarticular process, a condition seen in many other non-avian theropods, including *Majungasaurus* (Sampson & Witmer, 2007) and *Acrocanthosaurus* (Eddy & Clarke, 2011). Anterior to this posterior expansion, the ventral margin of the prearticular becomes slightly thickened mediolaterally.

Dentition

The only tooth-bearing bone preserved in *Irritator* is the maxilla (Figure 1). One unusual character of *Irritator*, also in comparison to other spinosaurids for which maxillae are known (Charig & Milner, 1997; Sereno et al., 1998; Taquet & Russell, 1998; Dal Sasso et al., 2005), is the extremely wide spacing of the anterior maxillary teeth (Figure 1, Figure 2, Figure 4-6). The teeth are wider-spaced in the maxilla anteriorly than posteriorly in *Irritator*. From the first to the seventh preserved alveoli of the left maxilla, the distance between the alveoli is larger than the mesiodistal length of the alveoli. In the last six preserved tooth positions in the detached fragment of the right maxilla (Figure 6), this spacing rather abruptly becomes less than the mesiodistal length of the teeth; this seems also to be the case on the left side. This is opposite to the condition found in a snout referred to *Spinosaurus*, in which the spacing of the teeth increases in more distal teeth (Dal Sasso et al., 2005). This was

apparently also the situation in the maxilla fragment of the holotype of *Spinosaurus* (Stromer, 1915).

The number of teeth in the maxilla of *Irritator*, as well as the identification of the preserved teeth (and thus the total number of teeth originally present in the maxilla) have been contentious. Martill et al. (1996) stated in the diagnosis of the taxon that more than 11 teeth were present in the maxilla, and later mentioned that the snout "bears at least 16 large teeth" (Martill et al., 1996: 6), though they did not clarify if this was the total number of preserved teeth or supposedly the number of teeth in one maxilla. Sues et al. (2002) identified nine teeth in the left and ten tooth positions in the right maxilla, and suggested that the total number of maxillary teeth was at least eleven. In comparison with other known spinosaurid maxillae, Sales & Schultz (2017) suggested that the first preserved maxillary alveolus of *Irritator* is the third one and identified eight additional tooth positions in the left maxilla, resulting in a total number of nine preserved maxillary teeth; their counting suggested the positions three to 11 to be present. However, our results show that ten tooth positions are preserved in the left maxilla (Figure 4B, Figure 5). Sues et al. (2002) and Sales & Schultz (2017) were only able to identify 9 tooth positions in this element, because the crown of the 8th preserved tooth position is lost and the respective alveolus is covered by sediment. Furthermore, this is exactly the position in which the tooth spacing switches from widely to closely spaced, resulting in the impression that the 7th and 9th preserved tooth positions might be as widely spaced as more anterior teeth. However, an additional alveolus between these positions is clearly visible in the CT data.

In the right maxilla, two tooth positions are preserved in the main body and still articulated with the rest of the skull (contra to Sales & Schultz, 2017, who identified the first preserved tooth in the detached fragment as the second preserved tooth

position in total), whereas the detached toothed fragment includes preserved teeth or fragments of ten tooth positions, resulting in a total number of 12 preserved tooth positions on this side (Figure 6). Mirroring the detached fragment of the right maxilla onto the left maxilla, the last two tooth positions would be placed in a short section of the left maxillary body that is broken away posterior to the tenthpreserved tooth, so that twelve tooth positions might also have originally been present in the left element. The number of preserved tooth positions in the holotype of *Irritator* can now be established as 12.

Concerning the question, which tooth positions are preserved and thus how many teeth were originally present in the maxilla of *Irritator*, this is more complicated to answer. As noted above, Sales & Schultz (2017) identified the first preserved tooth position as the 3rd maxillary tooth, arguing that the fourth maxillary tooth is the largest in all known spinosaurid maxillae, which would coincide with the second tooth preserved in the left maxilla of *Irritator*. However, although the second preserved tooth on the left side is indeed larger than the first, the CT data show that the first and second preserved alveoli in *Irritator* are of subequal size. Furthermore, the condition in other spinosaurids is less clear than argued by Sales & Schultz (2017). Although the fourth alveolus is clearly the largest in the snout referred to *Spinosaurus* by Dal Sasso et al. (2005) and apparently also in the spinosaurid snout MNHN SAM 124 (Taquet & Russell, 1998), it is the third alveolus in *Baryonyx* (NHMUK R 9951; Charig & Milner, 1986, 1997), whereas alevoli three to six are largest and of subequal size in *Suchomimus* (MNN GAD 501). Thus, given the subequal size of the first two alveoli, the first alveolus preserved in *Irritator* might well be tooth position three, four or five, resulting in a total tooth count of fourteen to sixteen teeth, which would be more than in the snout referred to *Spinosaurus* (12 maxillary teeth; Dal Sasso et al., 2005), but considerably less than in *Suchomimus* (22 maxillary teeth; Sereno et al., 1998). On

the other hand, in all known spinosaur snouts (Charig & Milner, 1997; Sereno et al., 1998; Taquet & Russell, 1998; Dal Sasso et al., 2005), the snout starts to flex upwards approximately at the level of the fourth tooth position, and the alveolar border is already markedly flexed anterodorsally at the level of the third alveolus. This does not seem to be the case in the first preserved alveolus in *Irritator*, indicating that this might represent a tooth position posterior to the third. Given the uncertainty in the tooth count, tooth positions given in the following always refer to preserved positions.

The 3rd preserved alveolus of the right maxilla houses a replacement tooth while the remnants of the respective functional tooth are preserved in the detached maxilla fragment (Figure 6). It is unclear if the 4th preserved position holds the original functional crown which is anteriorly and posteriorly surrounded by splinters of this same crown, or if three discreet teeth are situated here which could be interpreted from the CT data. Potentially, this situation is pathologic; the carniae of the anterior 'splinter' are somewhat obliquely oriented in comparison to the definite functional tooth in this position. However, because of this uncertain situation and the fact that the crown of the 4th tooth position is labiolingually thin, more labially situated in comparison to other crowns, and seems – in respect to the 3rd and 5th tooth position – distally shifted, we consider it as artificially glued there. The 5th tooth position is devoid of a functional crown, but bears one relatively large and one small replacement tooth. Furthermore, in some tooth positions, e.g. breakages may obscure exact conditions: the left 6th tooth is completely split. Additionally, in the left maxilla, mesially to the 5th root, a splinter-like body is positioned and since the root seems complete there, it is not entirely clear what it represents; a similar condition can be found in the left 7th and right 9th position. Most of the tooth positions are represented by at least partially erupted and thus functional teeth and/or the

respective roots on the left side: 1-7 and 9-10 (the 8th alveolus seems to be empty). The right side preserves functional teeth and/or the respective roots in the following alveoli: 1-2 and, within the tooth-bearing fragment, 3-4, 6-11 (the 11th was just about to erupt). Relatively large replacement teeth can be found in the left maxilla in positions 1-2 and 4-9 (Figure 5D). The right side preserves comparable replacement teeth in the positions 1-3 and 5-9 and 12 (Figure 6D). Relatively younger replacement teeth seem to be preserved within the second left alveolus and within the first, second and fifth right alveolus. These interpretations base on relative size and position of individual teeth. The CT data reveal that the replacement teeth in the maxillae of *Irritator* tend to be positioned lingually and slightly distal to the roots of the respective predecessors. Additionally, very small replacement teeth seem to start their growth relatively high up the root base of functional teeth. Normally, the maxillary replacement teeth of non-avian theropods grew in a ventral direction and migrated labially during growth (Hanai & Tsuihiji, 2019). However, the conditions in *Oxalaia* (Kellner et al., 2010) and *Irritator* seem to suggest that spinosaurid (pre)maxillary replacement teeth additionally moved slightly mesially during growth; possibly a result of the narrowness of spinosaurid snouts. Furthermore, the fragmentary distal dentary of *Iberospinus* also shows two generations of replacement teeth with a similar pattern of eruption (Mateus & Estraviz-López 2022).

The teeth of *Irritator* have been described in some detail by Sues et al. (2002), with additional details being mentioned by Sales & Schultz (2017) and Hendrickx et al. (2019). The teeth have long roots, which are usually longer than the respective crowns. All roots have their bases on the same level within the maxilla, which is different from e.g., *Tarbosaurus* (Hanai & Tsuihiji, 2019). As noted by Sues et al. (2002), the teeth of *Irritator* are conical and weakly recurved. However, whereas Sues et al. (2002: 539) state that the teeth are round in cross-section, the CT data

shows that they are quite notable compressed labiolingually, with the ratio between mesiodistal length and labiolingual width at their bases varying between 1.3 and 1.7, whereas most other spinosaurids have considerably more rounded teeth, with ratios between 1.1 and 1.5 (Stromer, 1915; Richter et al., 2013; Hendrickx et al., 2015). The crowns of *Irritator* bear carinae along their full length on the mesial and distal aspect but are devoid of serrations. Both Sues et al. (2002) and Hendrickx et al. (2019) noted that the carinae in *Irritator* have a 'beaded' appearance, mainly referring to the sixth and seventh tooth position preserved in the detached maxillary fragment (8^{th} and 9^{th} preserved tooth position in total). However, the carinae of these teeth are damaged by numerous cracks traversing the teeth, and the anteriormost teeth in the left maxilla show completely smooth mesial and distal carinae. As noted and illustrated by Sues et al. (2002), Sales & Schultz (2017) and Hendrickx et al. (2019), small, weakly developed undulations are present along the distal carina in several teeth. In agreement with Hendrickx et al. (2019), we cannot confirm the presence of a granulated enamel surface, as it is present in *Baryonyx* (Charig & Milner, 1997; Hendrickx et al., 2019) and was said to be present in *Irritator* by Sues et al. (2002). In contrast, the enamel is completely smooth; only under highest magnification and in oblique light, can a very fine pitting be noticed, which might, however, be diagenetic.

RESULTS

Phylogenetic analyses

The phylogenetic analysis of the complete data set resulted in 8184 equally parsimonious trees (most parsimonious tree, MPT) with a length of 1515 steps (Supplementary Data 4). The strict consensus tree of these trees is rather well-resolved, with the exception of a major polytomy within spinosaurids and another one

within Allosauroidea (Figure 36A). Our primary aim is not to present a new phylogeny of basal (non-coelurosaurian) tetanurans, but to evaluate the morphological distinctiveness of spinosaurids. However, we still briefly comment on similarities and differences to the results of other recent phylogenetic analyses, at least as far as the relationships of megalosauroids are concerned, and on the characters supporting these results. Our results support the monophyly of Carnosauria, as found by Rauhut & Pol (2019). However, within this clade, we found a more traditional arrangement of a monophyletic Megalosauroidea (including Spinosauridae) and Allosauroidea (Figure 36, Figure 37). Nevertheless, the Piatnitzkysauridae were found as an early branching clade within Allosauroidea, again, as in Rauhut & Pol (2019).

In contrast to most analyses, which usually found Megalosauroidea to be comprised (among others) of a sister-taxon arrangement of a monophyletic Megalosauridae and a monophyletic Spinosauridae (e.g., Allain, 2002; Benson, 2010; Carrano et al., 2012; Rauhut et al., 2016), the taxa classically grouped as megalosaurids are here found as a grade to Spinosauridae (Figure 36, Figure 37) . According to our analysis, the immediate sister taxon to Spinosauridae is the late Middle Jurassic *Monolophosaurus*, which was found in different phylogenetic positions in previous analyses (e.g., Allain, 2002; Benson, 2010; Carrano et al., 2012; Rauhut et al., 2016). The sister taxon to the *Monolophosaurus*-Spinosauridae clade are the Megalosaurines, a clade composed by the genera *Torvosaurus*, *Megalosaurus* and *Wiehenvenator*. The genus *Afrovenator* is placed one step further outside this clade, followed by a clade including the genera *Eustreptospondylus*, *Dubreuillosaurus*, *Magnosaurus* and *Piveteausaurus*. Finally, the genera *Streptospondylus* and *Duriavenator* are found in a polytomy as the earliest branching members of Megalosauroidea.

Support for the inclusion of spinosaurids in the Megalosauroidea is high; an arrangement similar to that was found by Rauhut & Pol (2019). Forcing spinosaurids outside of a megalosaurid-allosauroid clade requires at least 11 additional steps in our current analysis. Uniting the megalosaurids of other analyses in a monophyletic clade is also considerably less parsimonious, requiring at least five additional steps. Creating a monophyletic Avetheropoda (Allosauroidea + Coelurosauria) to the exclusion of megalosauroids needs at least an additional 12 steps.

The position of *Monolophosaurus* as sister taxon to spinosaurids is supported by relatively few unambiguous synapomorphies. These characters include the relatively low placement of the dorsal quadrate condyle (below two-thirds of the height of the orbit; also present in *Asfaltovenator*, *Allosaurus*, coelurosaurs and some other theropods), the presence of a quadrate foramen (reversal to the plesiomorphic carnosaur condition), dentary teeth that are considerably smaller and more numerous than the maxillary teeth, and an unexpanded ischial symphysis (reversed in *Ichthyovenator* and a probable reversal to the plesiomorphic carnosaurian condition). Moving *Monolophosaurus* to the basis of Megalosauroidea or outside the megalosauroid-allosauroid clade requires only two additional steps. Moreover, a position of *Monolophosaurus* as the earliest branching member of Megalosauroidea was found in the analysis using implied weights (Supplementary Data 5); in this case, the megalosaurines (*Megalosaurus*, *Torvosaurus* and *Wiehenvenator*) are found as sister taxon to Spinosauridae (Figure 36B).

Within Spinosauridae, the strict consensus tree shows rather poor resolution (Figure 36A), with a basal polytomy and only two monophyletic groups. One of these clades includes the Asian spinosaurid *Ichthyovenator* and the specimen FSAC KK 11888 (the proposed neotype of *Spinosaurus aegyptiacus*; Ibrahim et al., 2014), whereas the other represents the Baryonychinae, with the genera *Sigilmassasaurus*,

Baryonyx, *Riparovenator*, *Suchomimus* and *Ceratosuchops*. Reduced consensus methods remove the Spanish spinosaurid *Vallibonavenatrix*, as this taxon can appear in multiple positions within this clade. After removal of *Vallibonavenatrix*, three clades are found within Spinosauridae (Figure 37). The earliest branching clade includes *Ichthyovenator* and FSAC KK 11888. This clade forms the sister group to a Spinosaurinae-Baryonychinae dichotomy, with the Spinosaurinae showing a polytomy including the OTUs *Angaturama*, *Irritator*, MSNM V 4047, and *Spinosaurus* (Figure 37). Some runs of the pcrprune algorithm also removed *Angaturama* from the reduced consensus tree; in this case, the snout MSNM V 4047 was found as sister taxon to *Spinosaurus aegyptiacus* (see below). Within the Baryonychinae, *Sigilmassasaurus* was found as the earliest branching taxon, followed by a pectinate arrangement of *Baryonyx*, *Riparovenator*, *Suchomimus* and *Ceratosuchops*, as in the strict consensus tree (Figure 36A, Figure 37).

The placement of FSAC KK 11888 depends on a number of shared postcranial characters with *Ichthyovenator* and several quadrate characters that are different from the condition seen in *Irritator*, *Baryonyx* and *Suchomimus*. Apomorphic characters shared between *Ichthyovenator* and FSAC KK 11888 are the absence of L-shaped neural spines in the mid-caudals (a reversal to the non-carnosaurian condition, within higher spinosaurids only known in *Riparovenator*; Barker et al., 2021), the presence of a spinodiapophyseal ridge or lamina on the caudal neural spines, a straight dorsal margin of the ilium, and a heart-shaped cross-section of the articulated ischia. The quadrate characters excluding FSAC KK 11888 from the Spinosaurinae-Baryonychinae clade include the medially flexed ventral margin of the pterygoid wing (the normal theropod condition, whereas *Baryonyx* and *Irritator* apomorphically show a sharp-edged ventral margin), the lack of a mediolateral expansion of the quadrate head (apomorphically present in *Irritator*, *Baryonyx* and

Suchomimus), and the presence of a foramen on the medial side of the ventral quadrate body (a character shared with *Afrovenator* and *Torvosaurus* and interpreted as a synapomorphy of the *Afrovenator*-Megalosaurinae-Spinosauridae clade that is reversed in higher spinosaurids). Moving FSAC KK 11888 into Spinosaurinae or as sister taxon to *Spinosaurus* requires six additional steps. It might be worth noting, however, that several characters that might unite this specimen with spinosaurines (mainly dental and postcranial characters) could either not be evaluated or have not been included in this analysis, so our results should not be seen as a test of the proposed spinosaurine affinities of this specimen, or its proposed referral to *Spinosaurus*.

The analysis of cranial characters (i.e., removing all non-cranial characters, see methods) resulted in 153 equally parsimonious trees with a length of 778 steps (Supplementary Data 7). The strict consensus largely conforms to the results of the analysis of the entire data set (Figure 38A), especially in respect to showing a monophyletic Carnosauria within Tetanurae, although with relatively poor resolution within this clade. Clades found in the strict consensus tree include Spinosauridae (with the same basic topology as in the entire dataset, see below), a *Sinraptor*-*Yangchuanosaurus* clade, and Carcharodontosauria (Figure 38A). In the reduced consensus tree, monophyletic Megalosauroidea and Allosauroidea are found, with very similar taxonomic compositions as those in the analysis of the entire dataset (Figure 38B). One notable exception is *Megalosaurus*, which is recovered as a basal member of Allosauria in the cranial dataset analysis. Strictly speaking (i.e. adhering to phylogenetic nomenclature), this means that the megalosaur-spinosaurid clade should not be called Megalosauroidea under the current hypothesis; however, for the sake of comparison of the results, we nevertheless retain this name here. Within Megalosauroidea, *Afrovenator* is found as an early branching taxon, followed by a

clade composed of *Torvosaurus*, *Wiehenvenator* and *Leshansaurus*, and the monophyletic Spinosauridae (Figure 38B). Within spinosaurids, FSAC KK 11888 forms the sister taxon to a Baryonichinae-Spinosaurinae clade (Figure 38), which shows the same taxonomic composition and interrelationships as in the analysis of the complete data set (with the exception of the taxa *Sigilmassasaurus* and *Ichthyovenator*, for which no cranial material is known).

Reduced consensus methods also show that *Monolophosaurus*, *Dubreuillosaurus* and *Eustreptospondylus* can take variable positions within Megalosauroidea (Figure 38B). *Monolophosaurus* is either found as the earliest branching taxon within this clade (as in the implied weights analysis of the entire dataset), or as sister taxon to Spinosauridae, as in the equal weights analysis of the entire dataset. Likewise, and depending on the position of *Monolophosaurus*, *Eustreptospondylus* and *Dubreuillosaurus* are either found as early branching megalosauroids (if *Monolophosauruus* forms the sister taxon to spinosaurids), or as closely related to spinosaurids (if *Monolophosaurus* is placed at the base of Megalosauroidea). Cranial characters shared between *Dubreuillosaurus* and/or *Eustreptospondylus* and spinosaurids include the anteroventrally angled anteriormost maxillary teeth (in *Eustreptospondylus*; Sadleir et al., 2008), the absence of a pneumatic recess on the medial side of the maxilla posterior to the maxillary fenestra (in *Eustreptospondylus*, but not in *Dubreuillosaurus*; within carnosaurs, this recess is also absent in the megalosaurines *Torvosaurus* and *Wiehenvenator* and in the allosauroid *Asfaltovenator*), the presence of a lateral ridge along the postorbital facet on the jugal (only known in *Dubreuillosaurus* and convergently also present in allosauroids), the straight or slighly concave dorsal margin of the postorbital (in both *Dubreuillosaurus* and *Eustreptospondylus*; reversal to the non-carnosaurian condition, convergently also in carcharodontosaurs and again reversed in *Ceratosuchops*), the reduced and

anteriorly placed laterosphenoid facet on the medial side of the postorbital (in both *Dubreuillosaurus* and *Eustreptospondylus*; again reversed in *Ceratosuchops*), absence of a supraorbital brow in the postorbital (in both *Dubreuillosaurus* and *Eustreptospondylus*; reversal to the non-carnosaurian condition, and again reversed in *Ceratosuchops*), possibly the absence of a constriction of the infratemporal fenestra through the ventral process of the squamosal (under DELTRAN; unknown in most megalosauroids), possibly a relatively elongate posterior process of the squamosal (under DELTRAN; in *Dubreuillosaurus* and spinosaurids; unknown in megalosaurines and *Eustreptospondylus*), a broad exposure of the supraoccipital on the margin of the foramen magnum, a dorsoventrally expanded anterior end of the dentary (convergently present in *Monolophosaurus*, *Marshosaurus*, *Asfaltovenator* and some other allosauroids within carnosaurs), and the presence of a pronounced lateral groove on the dentary, housing the neurovascular foramina (convergently present in many allosauroids).

Another interesting result of the reduced consensus tree of the cranial character matrix is that, within spinosaurines, the exclusion of *Angaturama* results in the snout MSNM V4047 from Morocco being clustered with *Spinosaurus aegyptiacus* (Figure 38B), lending support to the interpretation of Dal Sasso et al. (2005) that this specimen represents the genus *Spinosaurus*. This relationship is based on a single character, an increase of tooth spacing in the posterior part of the maxilla (see Stromer, 1915; Dal Sasso et al., 2005), whereas other spinosaurids, such as *Suchomimus* and *Irritator*, show more widely spaced teeth in the mid-section of the maxilla, but a decrease of spacing posteriorly.

Rates of character evolution

Optimization of cranial character states on the reduced consensus tree pruned to taxa that preserve cranial material (see methods for details) resulted in 209 character state transitions (ACCTRAN, including unambiguous transition) for Megalosauroidea (including spinosaurids). Of those, 88 were accountable to the Spinosauridae, and 119 to the paraphyletic grade of megalosauroids that are not spinosaurids. Two character state transitions can additionally be attributed to either spinosaurids (DELTRAN) or the megalosauroid grade (ACCTRAN), and we used the former interpretation for rate calculations. Allosauroidea experienced 219 character state transitions according to our optimization. These numbers resulted in the following per-Ma rates of character change: Megalosauroidea = 0.7 (character state changes per Ma); Spinosauridae = 0.4 (character state changes per Ma); Megalosauroid grade = 1.3 (character state changes per Ma); Allosauroidea = 0.6 (character state changes per Ma). However, the sampling of cranial characters varies among these groups, with Megalosauroidea as a whole having 37.4% of all possible characters scored. The proportion of scored characters is 32.3% for spinosaurids, 42.5% for megalosauroids excluding spinosaurids, and 48.6% for allosauroids. When the character evolution rates are corrected for these sampling proportions, megalosauroids experienced 1.9 character state transitions per million year per sampled character. The respective rate values are 1.3 (character state transitions per million year per sampled character) for spinosaurids, 3.1 (character state transitions per million year per sampled character) for megalosauroids excluding spinosaurids, and 1.2 (character state transitions per million year per sampled character) for Allosauroidea.

Both the ‘raw’ and the sampling-corrected per-group character state transition rates indicate that magalosauroids have higher rates of morphological evolution than allosauroids. However, the absolute number of character changes and relative rate

differences increase strongly when sampling is accounted for, with megalosauroids having a rate that is more than 1.5-times as high as that of allosauroids (1.9 vs. 1.2 character state transitions per million year per sampled character). The high rate of megalosauroids is caused by its non-spinosaurid members, which have elevated rates in comparison to spinosaurids in both rate metrics. Using 'raw' rates, the difference is roughly threefold, whereas the difference is only about twofold when sampling is accounted for (3.1 vs. 1.3 character state transitions per million year per sampled character). According to the sampling-corrected rates, spinosaurids have slightly higher rates of evolution than allosauroids (1.3 vs. 1.2 character state transitions per million year per sampled character), whereas the opposite is true when 'raw' rates are used (0.4 vs. 0.6 character state changes per Ma).

DISCUSSION

Phylogeny and the evolutionary history of spinosaurids

As noted in the results section, the primary aim of our phylogenetic analyses was not to present a novel hypothesis of theropod or carnosaur interrelationships. Instead, we evaluate the morphological disparity of spinosaurid skulls and the influence of spinosaurid cranial characters on the phylogeny of carnosaurs and especially megalosauroids, based on the new anatomical information presented herein. Reasons why our phylogenetic results should be seen with caution with respect to new hypotheses of theropod interrelationships more widely include the limited taxon sampling (especially for non-carnosaurian theropods) and the uneven treatment of cranial and postcranial characters. Whereas we revised the character definitions and codings of Rauhut & Pol (2019) for cranial characters rather thoroughly and added a number of new characters, we did not do the same for the postcranial characters, for which *Irritator* provides no novel information. For postcranial characters, we mainly

used the character definitions and codings presented by Rauhut & Pol (2019) (which, in turn, were largely based on definitions and codings of Carrano et al., 2012). Nevertheless, we will offer a short discussion on some aspects of our phylogenetic analysis.

As several recent analyses (e.g., Cau, 2018; Rauhut & Pol, 2019), our current phylogeny supports the inclusion of most large-bodied basal tetanurans in a monophyletic clade, the Carnosauria. However, in contrast to the results of Rauhut & Pol (2019), who found three major clades, the Spinosauridae, Megalosauroidea, and Allosauroidea, in a pectinate arrangement within Carnosauria, we found a more conventional arrangement of a monophyletic Megalosauroidea that includes Spinosauridae. Moreover, in contrast to most previous analyses that found spinosaurids within Megalosauroidea (e.g., Benson et al., 2010; Carrano et al., 2012; Rauhut et al., 2016), the remaining megalosaurs were not found to form a monophyletic Megalosauridae as sister taxon to the Spinosauridae, but rather to represent different grades on the evolutionary lineage towards spinosaurids. In comparison with previous hypotheses, this reduces the ghost lineage for spinosaurids by approximately 5 Ma; however, from the appearance of the possible sister taxon *Monolophosaurus* in the probable Late Callovian (c. 164 Ma) to the first occurrence of spinosaurids in the Early Barremian (c. 129 Ma), a vast ghost lineage of some 35 Ma remains. This ghost lineage is reflected in the acquisition of numerous craniodental modifications in spinosaurids if compared to other megalosaurids. Thus, a total of 44 character transitions of craniodental characters were recovered under ACCTRAN at the node of Spinosauridae in our analysis (based on character transformations evaluated in Mesquite), and 39 transformation were found by DELTRAN at one node higher (given that the earliest branching spinosaurid OTUs in our analysis, *Ichthyovenator* and FSAC KK 11888, have no or

only very limited cranial material preserved). These were by far the highest numbers of transformations recorded at any internal node within Megalosauroidea. Interestingly, our analysis of evolutionary rates did not find elevated rates of transformations at the base of or within spinosaurids, but instead indicates that cranial character evolution rates are twice (sampling-corrected rates) or thrice ('raw' rates) as high for non-spinosaurid megalosauroids than for spinosaurids. Thus, the disparate cranial morphology of spinosaurids, if compared to other basal tetanurans, might rather reflect an accumulation of modifications over the long ghost lineage than a sudden acquisition of a unique cranial morphology. It might thus be expected to find stem-lineage spinosaurids with intermediate cranial morphologies in the future. As to why we see this long ghost lineage and still lack intermediate morphologies on the lineage to spinosaurids can currently only be speculated on. One possibility might be that spinosaurids originated in the southern hemisphere and are thus missing from the fossil record because of the generally abysmal Gondwanan theropod fossil record from the Middle Jurassic to the late Early Cretaceous (see Rauhut & López-Arbarello, 2008; Rauhut & Pol, 2021). Arguments in favour of this explanation might be the presence of possible spinosaurid teeth in the probably Middle Jurassic of the Tiourarén Formation of Niger (Serrano-Martínez et al., 2015, 2016) and the Late Jurassic Tendaguru Formation of Tanzania (Buffetaut 2011). However, the spinosaurid identity of both of these occurrences has been questioned (Rauhut, 2011; Hendrickx et al., 2019). Furthermore, based on our phylogenetic results, the closest known relative of spinosaurids either occurred in eastern Asia (*Monolophosaurus*, under unweighted parsimony of the entire data matrix) or Europe (Megalosaurinae under weighted parsimony of the entire data matrix or *Eustreptospondylus* and *Dubreuillosaurus*, if only cranial characters are considered), all options indicating a non-Gondwanan origin of the group. A European origin might

be in line with the hypothesis that Europe was a center of megalosauroid evolution in the Middle Jurassic (Rauhut et al., 2020). However, due to the extremely poor Jurassic theropod record of Africa and other Gondwanan continents, it also cannot be ruled out that this impression represents an artefact of the fossil record.
Another aspect worth mentioning is our generally poor knowledge of megalosauroid skulls. In the matrix including cranial characters only, megalosauroids in general could be scored for only 44.5% of cranial characters, (whereas, as mentioned in the materials and methods section, the average of coded characters for all included OTUs was 49%), and this proportion is not evenly distributed among all relevant taxa (those with cranial remains preserved). Only two taxa (*Monolophosaurus* and *Irritator*) have more than 75% of the cranial characters coded, while eight out of the 18 included megalosauroid have less than 25% of the data. Indeed, the second highest number of transformations under DELTRAN (26) was found for *Irritator*, one of the few taxa for which an almost complete skull is known. Assuming that the cranial anatomy of this taxon is not unusually strongly modified, this most probably reflects our still very poor knowledge of the cranial anatomy of spinosaurids, especially spinosaurines. This is reflected by the amount of missing data, which is 58% for non-spinosaurid megalosauroids, but 68.5% for spinosaurids.

Head posture

Based on the orientation of the lateral semicircular canal (LSC) in the endosseous labyrinth and the orientation of the occipital condyle, we have recently proposed a strongly ventrally inclined habitual head posture (c. 45°) for *Irritator* (Schade et al., 2020). Although the orientation of the LSC is no exact predictor of habitual head orientation (Marugán-Lobón et al., 2013, Benoit et al., 2020), a significant correlation

between LSC orientation and head orientation still exists (Benoit et al., 2020). The latter study found statistical evidence that ‘bottom feeding’ ungulates, such as grazers, have stronger ventral head inclinations than ‘top feeders’, such as browsers, based both on observed head postures and angles inferred from LSC orientation. Furthermore, absolute angle deviations between head posture and LSC plane in extant mammals and birds never achieve values that would suggest that the snout of *Irritator* could have been held horizontally (Marugán-Lobón et al., 2013, Benoit et al., 2020). This provides tentative support for the hypothesis of Schade et al., (2020) that ventral head orientation in *Irritator* can be explained by the primary prey target of *Irritator* being small animals on the ground or submerged in water. Regardless, we can here present novel anatomical observations that independently provide evidence for a strongly ventrally inclined head posture of *Irritator* (Figure 1, Figure 2).

The new reconstruction of the *Irritator* skull shows a distinct angle between the rostrum and the postrostral skull region, while the orientation of the occipital condyle indicates a horizontally orientated braincase, as is typical for non-avian theropods. This ventral angulation of the rostrum is caused by a posteroventral rotation of the orbital and postorbital regions of the skull against the snout, evidenced by the different lengths of the jugal and ascending rami of the maxilla, the marked acute angle between the ventral and anterior processes of the lacrimal, the ventrally concave margin of the jugal, the slightly vaulted frontal and anteroventrally directed jugal process of the postorbital, and the placement of the infratemporal fenestra posteroventral to the orbit. Interestingly, the same angulation is also evident in the mandible, with the distinct ventral kink of the anterior portion of the surangular and the more anterior elements in respect to the region of the jaw articulation and insertion area of main jaw muscles. In other words: if the foramen magnum faces in a straight posterior direction, the snout shows a strong ventral inclination of around 45°,

confirming previous assessments based on the LSC plane (Schade et al., 2020). The morphological similarities of the lacrimal and occipital region to other spinosaurids, including material assigned to *Suchomimus* (MS, pers. obs. on cast, MNN GDF 214), *Baryonyx* (Charig & Milner, 1997), *Ceratosuchops* and *Riparovenator* (Barker et al., 2021), indicate that these theropods probably had a similar head posture as *Irritator*.

Arden et al. (2019) considered *Irritator* as spending most of the time in the water, based on a proposed elevation of the orbits evidenced by the vaulted frontal. The new reconstruction of *Irritator* indicates that, due to the inclination of the rostrum and the more laterally placed postorbital compared with the preorbital bones, *Irritator* was most likely to have binocular vision (see Stevens, 2005; Schade et al., 2020). This is generally advantageous for predatory animals, but especially if rapid and precise head movements are used to fixate small and elusive prey items underwater, as well as on or close to the ground. This would be in line with the apparent dorsal displacement of the orbits noted by Arden et al (2019). As the preorbital and orbital region in *Suchomimus* is closely comparable to that of *Irritator* (MS, pers. obs. on cast, MNN GDF 214), a similar vision is indicated.

Functional anatomy of the jaws

Further evidence on the ecology of *Irritator* (and, by inference, other spinosaurids) comes from the biomechanics of its skull. Vertebrate mandibles can biomechanically be understood as third-order levers, as the adductor muscles insert on the lower jaw between the potential load anteriorly and the jaw joint, serving as the fulcrum, posteriorly (Figure 39; e.g., Barel, 1983; Westneat, 1994, 2003). In a third-order lever, the mechanical advantage is defined as the input moment arm (distance between fulcrum and adductor muscles; i.e., jaw joint–coronoid eminence, as the

most anterior insertion point of the adductor muscles; Holliday & Witmer, 2007; Holliday, 2009) divided by the output moment arm (distance between fulcrum and load, e.g., anteriormost tooth position for anterior mechanical advantage). Lower mechanical advantage values indicate speedy but low forced bites and vice versa. Thus, the ratio between pre- and postcoronoid lengths determine the relative speed and force of bites in vertebrate mandibles. One crucial feature for the functional anatomy is thus the configuration of the articulation of the skull with the lower jaw. There are three main types of the squamosal-quadrate-articular setup in non-avian theropods. First, the squamosal-quadrate articulation being more or less in a straight vertical line with the quadrate-articular articulation. This seems to be the most widespread condition in in non-avian theropods (Rauhut, 2003). In the second setup, the dorsal contact of the quadrate is slightly to considerably more anteriorly situated in comparison to its ventral articulation with the lower jaw, as can be seen in many ceratosaurs (e.g., Gilmore, 1920, Sampson & Witmer, 2007, Zaher et al., 2020). In contrast, *Irritator* shows the third setup in which the dorsal contact of the quadrate is positioned more posteriorly than the ventral one (in relation to the long axis of the mandible, the downward orientation of the snout in general mentioned above notwithstanding), as can be seen in some maniraptoriformes, e.g., *Archaeopteryx* (Rauhut, 2014) and Ornithomimosauria (Makovicky et al., 2004). Assuming a comparable relative position of the coronoid eminence and thus the insertions of the jaw muscles, this third arrangement of bones results in different jaw mechanisms, which likely produced a weak bite (lower mechanical advantage) in comparison to other large-bodied theropods (see Henderson, 2002; Therrien et al., 2005). This is partially due to the fact that, in comparison to theropods with posteroventrally inclined or straight quadrates, the leverage for the jaw closing muscles (the input moment arm) is shortened in taxa with an anteroventrally inclined quadrate, such as

spinosaurids, as the jaw joint moves closer to the insertion areas of the main jaw closing muscles. This is exemplified by the insertion areas of the m. adductor mandibulae externus group (see Holliday & Witmer, 2007; Holliday, 2009). The insertion of the m. adductor mandibulae externus profundus, the most anterior of the m. adductor mandibulae externus group (on the lower jaw), is marked as a slightly elevated, laterally placed and rugose patch at the point where the dorsal margin of the surangular flexes ventrally in *Irritator*. This patch is posterior to the mid-length between the jaw articulation and the surangular-dentary suture in *Irritator*, whereas it is at approximately two-thirds of that length in taxa with a posteroventrally inclined quadrate, such as *Majungasaurus* (Holliday, 2009: fig. 8C) and in a similar position also in animals with a more vertical quadrate, such as *Tyrannosaurus* (Gignac & Erickson 2017). Likewise in *Majungasaurus*, the large insertion area for m. adductor mandibulae externus superficialis is anteriorly offset from the jaw articulation and extends anteriorly to the middle of the anterior half of the surangular (Holliday, 2009). In most large-bodied theropods, an anteroposteriorly elongate, flattened or slightly depressed facet for the attachment of this muscle is present on the dorsal surface of the surangular anterior to the jaw joint. In *Irritator*, we interpret the well-marked depression on the surangular shelf as the insertion facet for this muscle, which is thus restricted to the posterior half of this bone and partially overlaps the mandibular articulation laterally at its posterior end. Thus, the reconstruction of the adductor muscles in *Irritator* indicate a shortening of the input moment arm not only by the anterior rotation of the jaw joint, but also a relatively more posterior placement of the main jaw closing muscles on the mandible. Apart from reducing the input moment arm, this reduction in distance between the jaw joint and the closing muscle insertions also increases the angular momentum of the lower jaw: the jaws close more rapidly, as less muscle contraction (in terms of distance) is needed to adduct

the mandible. A second, and likely even stronger effect on mechanical advantage comes from elongation of the out-lever, i.e. the part of the jaw anterior to the anteriormost insertion point of the adductor muscles, which clearly is elongated in *Irritator* and other spinosaurids with known mandibles. Low mechanical advantage and bite forces in *Irritator* and other spinosaurids are in line with the rather slender snouts and lower jaws of these animals, which are less resistant to bending stresses resulting from biting than those of high-snouted oreinorostral theropods (see Rayfield 2011).

The lower jaw of *Irritator* bears an enlarged retroarticular process in comparison to most other non-avian averostran theropods. This structure forms the attachment site for the *m. depressor mandibulae*, which must have been rather strongly developed in *Irritator* (see Holliday & Witmer, 2007; Snively & Russell, 2007, Holliday, 2009). The m. depressor mandibulae stretched between the posterolateral surface of the paroccipital process and the posterodorsal surface of the retroarticular process (Holliday 2009), allowing a powered and fast opening movement (Holliday & Witmer 2007) in *Irritator*.

In addition, the quadrate-jaw articulation in *Irritator* supports potential lateral mandibular spreading, as proposed by Hendrickx et al. (2016). These authors suggested that the lower jaws of spinosaurids had kinetic mandibular rami which displaced laterally when being depressed, based on the lateromedial orientation of the intercondylar sulcus of the quadrate. The sulcus orientation and lateromedially wide ectocondyle, which morphologically differs strongly from most other non-avian theropods, forced the articular and surangular laterally during jaw opening. Indeed, our reconstruction of *Irritator* suggests that the entocondyle of the quadrate intersects with the mandibular articular facet and the posterior edge of the articular fossa cuts

into the quadrate when the lower jaw gets depressed, unless compensatory lateral movement of the mandibular rami is introduced (Figure 40; Supplementary Data 18,19). To keep a tight but non-intersecting articulation between quadrate and articular, a maximal range of jaw opening of approximately 40° is expected for *Irritator* (with the jaw joint covered by cartilage, there might be slightly higher ranges of motion possible). As the mandibular symphyses of spinosaurids are unfused and show the typical rather unspecialized morphology of most theropods (Stromer, 1915; Charig & Milner, 1997), indicating that the jaws were held together anteriorly by soft tissues (Holliday & Nesbitt, 2013), a certain lateral expansion of the jaws with lateral stretching of the connective tissue situated in the symphyses might have been possible (see Charig & Milner, 1997; Sereno et al. 1998; Holliday & Nesbitt, 2013; Hendrickx et al., 2016). However, this setting would need considerable muscle effort of the abductor muscles, including m. depressor mandibulae (see above). This is because the lateral expansion of the lower jaw would create additional tension on the bone and the adductor muscles, including the m. pterygoideus ventralis (inserting on the ventral surface of the prominent lateral surangular shelf) of the internal adductor musculature. Reaching the point of maximal tension, the relaxation of the abductor muscles would reinforce the contraction speed of the adductor muscles, further supporting the hypothesis of a very rapid jaw closure. In summary, the skull morphology of *Irritator* indicates fast, rather than strong biting, supporting previous studies on skull strength and bite force in non-avian theropods (Henderson 2002; Therrien et al. 2005; Rayfield 2011).

Further evidence on feeding ecology of spinosaurids comes from the anterior jaw morphology and dentition. The articulated premaxillae and maxillae of these animals are narrow, but rather robust and closely appressed, mainly due to the medially swollen and ventrally expanded paradental lamina that covers the (apparently fused)

paradental plates medially (see description above; Charig & Milner, 1997; Sereno et al., 1998; Dal Sasso et al., 2005). Together with the – in relation to the tooth bearing bones - deep roots of the teeth, this results in a rather rigid implantation of the teeth in the jaws of spinosaurids. The more rounded cross section of the teeth and presence of longitudinal flutes further increase their robustness. The long and slender snouts of spinosaurids were certainly less suited to withstand the high impact forces created by other large theropod skulls upon impact on large prey animals (Rayfield et al., 2001; Henderson, 2002; Rayfield, 2004, 2011; Cuff & Rayfield, 2013). However, the elongate snouts and mandibles, the high angular momentum created by the jaw muscles and the resulting rapid closing of the jaws, together with the enlarged teeth in the anterior part of the maxilla and dentary, are ideally suited to capture and secure small and elusive prey, including fish, but also other smaller vertebrates, such as pterosaurs (Buffetaut et al., 2004) or juvenile dinosaurs (Charig & Milner, 1997). During snapping, the large and conical teeth would puncture the prey item at high speed, leading to severe injuries. The prey can then be lifted off the ground or from the water, with the deep implantation and rigid medial anchoring of the teeth by the expanded paradental lamina, the more rounded cross section and longitudinal flutings all helping to prevent tooth loss or breakage caused by the struggling prey. The unusually high tooth replacement rates in spinosaurids (Heckeberg & Rauhut, 2020) might be a further indication that tooth loss by struggling prey and the need for rapid replacement was an issue during feeding in spinosaurids.

Ecology

Hypotheses on the appearance and ecology of spinosaurids, and in particular *Spinosaurus*, have changed over the last decades. The earliest reconstructions depicted *Spinosaurus* as a tyrannosaur-like creature with an erect posture and a sail on its back (Stromer, 1936). Following the initial suggestion of a piscivorous diet for spinosaurids by Taquet (1984), based on fragmentary remains from the late Early Cretaceous of Niger, the discovery of *Baryonyx* in the Barremian Wessex Formation of England half a century after the first reconstruction by Stromer shaped the picture of spinosaurids to be long-snouted piscivorous predators with a terrestrial lifestyle and facultative quadrupedality (Charig & Milner, 1986). Later, Charig and Milner (1997) reconstructed *Baryonyx* as a piscivorous predator with a typical theropod-like bipedal posture. The same general body plan was found in the closely related *Suchomimus* from the Aptian Elrhaz Formation of Niger (Sereno et al., 1998).

It is by now generally accepted that spinosaurids were probably largely - but not exclusively - piscivorous predators (as mainly indicated by tooth and jaw morphology and gut contents; e.g., Charig & Milner, 1997), and likely possessed a greater affinity to water bodies than other large-bodied theropods (Amiot et al., 2010 a, b; Ibrahim et al., 2014, 2020; Sales et al., 2016; Hassler et al., 2018; Fabbri et al., 2022). Rauhut et al. (2016) found statistical evidence that megalosaurs in general preferred nearshore over inland environments, and it seems likely that the ancestors of spinosaurids, which represent derived megalosaurs, developed a certain affinity for shallow waters somewhen in the Jurassic (Hone & Holtz, 2017, 2021; Malafaia et al., 2020). Later, the respective resources were exploited more efficiently by this group, due to adaptations in the skull, neck and manus (e.g., Charig & Milner, 1986; Sereno et al., 1998; Evers et al., 2015; Schade et al., 2020).

More recent life reconstructions of *Spinosaurus*, which are based on cranial and postcranial material of multiple individuals, draw this theropod as a highly specialized aquatic pursuit predator with a crocodylian-like swimming/diving lifestyle, which would likely rely on quadrupedal locomotion on land when transferring between water bodies (Ibrahim et al., 2014, 2020, Arden et al., 2019; Fabbri et al., 2022). However, this scenario has been questioned on various anatomical and ecological considerations by Hone & Holtz (2021), who argue that *Spinosaurus* and other spinosaurids were possible generalists, mainly bipedal predators preying along shorelines (see also Henderson, 2018). Based on differences in the bone compactness between *Baryonyx*, *Suchomimus* and FSACK-KK 11888 (proposed neotype of *Spinosaurus aegyptiacus*, but see Evers et al., 2015) and a large comparative dataset of extant and fossil tetrapods, Fabbri et al. (2022a,b) proposed that *Spinosaurus* and *Baryonyx* are subaqueous foragers (though see Myhrvhold et al. 2022). However, spinosaurids seem to have a certain degree of ecological disparity regarding their adaptation to the aquatic milieu, as bone compactness for *Suchomimus* indicates non-diving foraging behaviour (Fabbri et al. 2022a,b). In the context of bone compactness, our re-examination of the cranial material of *Irritator*, provides no new insights into the paleoecology of spinosaurids. However, given that *Irritator* represents the most complete cranial material that also includes mandibular remains, anatomical and functional considerations may help to further specify the feeding style of this taxon, which is related to its foraging, and thus, ecology. Based on our findings, we propose *Irritator* as being an agile predator (indicated by the endosseous labyrinth morphology and large flocculus; Schade et al., 2020, and binocular vision; Schade et al., 2020; this work), with its snout held habitually inclined (indicated by the horizontal semicircular canals, orientation of foramen magnum, occipital condyle), and a long, strong, but flexible neck (indicated by long cervicals in

other spinosaurids, ventral rugosities on cervicals of *Sigilmassasaurus*; Charig & Milner, 1997; Ibrahim et al., 2020 b; Evers et al., 2015). As outlined above, the rather weak bite force, in combination with a rapid jaw closure and robust dentition indicate that the animal hunted rather small prey, probably small enough to be lifted before killing and swallowing it. Possibly, *Irritator* patrolled the shores of water bodies, snatching small prey items opportunistically with rapid neck and head movements. It might also at least partially have been an ambush predator, with its snout partially submerged (posteriorly placed external nares) and using its rapidly closing lower jaws to catch and swallow aquatic prey. Thus, this would render at least *Irritator* ecologically more similar to giant storks or herons - with grappling hands and potentially spreading jaws when gulping - than to crocodiles, as recently suggested by Hone & Holtz (2021).

Data availability

The CT slice data and 3D files of SMNS 58022, are published online, in the repository MorphoSource, projects ‘Schade et al. 2020. Irritator challengeri SMNS 58022 neuroanatomy’ (https://www.morphosource.org/Detail/ProjectDetail/Show/project_id/951) and

‘Schade et al. 2022. Irritator challengeri SMNS 58022 osteology’ (https://www.morphosource.org/projects/000372273?locale=en).

The phylogenetic data matrices can be found on Morphobank (morphobank.com) under project 3955 (https://morphobank.org/index.php/MyProjects/List/select/project_id/3955).

ACKNOWLEDGMENT

We are deeply grateful to Rainer Schoch for access to SMNS 58022 and permission to loan the specimen in order to conduct CT examinations. We thank Nicole Kreuzer and Stephan Tomaschko (Zeiss in Essingen) as well as Jacqueline Jendick and Cornelia Pankalla (Deutsches Herzzentrum in Munich) for the CT examinations of the skull of *Irritator.* We are very thankful for the support of Martin Nose (Freunde der Bayerischen Staatssammlung für Paläontologie und Geologie München e.V. for financial support), Tanja Schulz-Mirbach (Lehre@LMU for financial support), Nils Knötschke, Benjamin Englich, Brian Bernecker and Jens Kosch (Dinosaurier-Park Münchehagen for casts) and Heinrich Mallison (Palaeo3D for 3D prints). Susannah Maidment took photographs and provided access to material of *Baryonyx.* Additionally, we thank Ingelore Hinz-Schallreuter, Stefan Meng, Marie Hörnig, Jakob Krieger, Georg Brenneis, Steffen Harzsch, Gertrud Rößner, Christoph Kettler and Chris Barker. MS is supported by the Bogislaw PhD scholarship of the University of Greifswald.

Ethics statement

As the specimen described here originates from Brazil, and there currently is a debate about the legality and ethics of dealing with Brazilian specimens deposited outside of this country (Cisneros et al. 2021, 2022), we acknowledge the possibly problematic status of SMNS 58022. Thus, we want to present some background and considerations on this matter.

The type specimen of *Irritator* was purchased by the Staatliches Museum für Naturkunde Stuttgart from a German fossil dealer in 1991. The specimen was imported to Germany prior to 1990 when the decree on the export of fossils and the handling of type specimens from Brazil was passed (Cisneros et al. 2022); the previous legislation in Brazil (Decreto-Lei 4.146 from March 1942) governs the need of permits for the collection of specimens, but not their export (see Cisneros et al. 2022). Most fossils from the Araripe Basin are collected and sold by local collectors (Vila Nova et al. 2011; Vilas Boas et al. 2013; Cisneros et al. 2022). D. Martill (in Sues et al. 2002) mentioned that local collectors recalled seeing the specimen (later becoming the holotype of *Irritator*), so that it is likely that it was purchased from such collectors prior to its export. Currently, as part of the collection of the Staatliches Museum für Naturkunde Stuttgart, the specimen is property of the German Bundesland (province) of Baden-Württemberg, and a clarification of its legal status lies neither within our nor the local curator's power.

Since the acquisition of the specimen by the Staatliches Museum für Naturkunde Stuttgart, it has been studied repeatedly. The new taxon *Irritator challengeri* was established and initially described by Martill et al. (1996), with additional information having been provided by Sues et al. (2002), Hendrickx et al. (2016, 2019), Sales & Schultz (2017) and Schade et al. (2020). As the specimen is part of a public

collection and thus available for additional study for anybody with a scientific interest in it, we provide new information here.

In order to make our data available to the broader scientific community, we already deposited the available neuroanatomical models and CT data (a medical CT of the entire skull and a microCT of the braincase) in the online repository MorphoSource (Schade et al. 2020. Irritator challengeri SMNS 58022 neuroanatomy // MorphoSource) in the framework of our previous publication on the endocranial anatomy of *Irritator* (Schade et al. 2020). These CT data, which also formed the basis for the current work, are freely available for download from that platform. All new 3D models created from that data, in addition to photogrammetric models of the fossil, are also deposited on MorphoSource (Schade et al. 2022. Irritator challengeri SMNS 58022 osteology // MorphoSource).

Author contributions

MS and OWMR designed the project. MS organized CT scans. MS segmented the medical and micro CT data. OM segmented the medical CT data and produced the cranial rearrangement and videos. MS, OM, CF, SWE and OWMR coded and scored phylogenetic characters, and OWMR performed the cladistic analyses. SWE performed the character optimization. CF and SWE calibrated the time-tree and performed character rate analyses. MS, OM, CF, SWE and OWMR interpreted the data, prepared the figures, discussed the phylogeny and wrote the manuscript.

Competing interests

The authors declare no competing interests.

Additional information

Correspondence and request for material should be addressed to MS.

REFERENCES

Allain, R. and Chure, D.J. 2002. *Poekilopleuron* bucklandii, the theropod dinosaur from the Middle Jurassic (Bathonian) of Normandy. Palaeontology, 45:1107–1121.

Allain, R. 2002. Discovery of a megalosaur (Dinosauria, Theropoda) in the Middle Bathonian of Normandy (France) and its implications for the phylogeny of basal Tetanurae. Journal of Vertebrate Paleontology, 22: 548–563. doi:10.1671/0272-4634(2002)022[0548:domdti]2.0.co;2

Amiot, R., Buffetaut, E., Lécuyer, C., Wang, X., Boudad, L., Ding, Z., Fourel, F., Hutt, S., Martineau, F., Medeiros, M.A., Mo, J., Simon, L., Suteethorn, V., Sweetman, S., Tong, H., Zhang, F., and Zhou, Z. 2010a. Oxygen isotope evidence for semi-aquatic habits among spinosaurid theropods. Geology, 38:139–142. doi:10.1130/G30402.1

Amiot, R., Wang, X., Lécuyer, C., Buffetaut, E., Boudad, L., Cavin, L., Ding, Z., Fluteau, F., Kellner, A.W.A., Tong, H., and Zhang, F. 2010b. Oxygen and carbon isotope compositions of Middle Cretaceous vertebrates from north africa and brazil: ecological and environmental significance. Palaeogeography, Palaeoclimatology, Palaeoecology, 297:439–451. doi:10.1016/j.palaeo.2010.08.027

Arden, T.M., Klein, C.G., Zouhri, S., and Longrich, N.R. 2019. Aquatic adaptation in the skull of carnivorous dinosaurs (Theropoda: Spinosauridae) and the evolution of aquatic habits in spinosaurids. Cretaceous Research, 93:275-284. https://doi.org/10.1016/j.cretres.2018.06.013

Bakker, R.T., Williams, M., and Currie, P.J.. 1988. *Nanotyrannus,* a new genus of pygmy tyrannosaur, from the latest Cretaceous of Montana. Hunteria, 1:1–30.

Bapst, D.W. 2012. Paleotree: an R package for paleontological and phylogenetic analyses of evolution. Methods in Ecology and Evolution, 3:803-807. https://doi.org/10.1111/j.2041-210X.2012.00223.x

Bapst, D.W. 2013. A stochastic rate-calibrated method for time-scaling phylogenies of fossil taxa. Methods in Ecology and Evolution, 4:724-733. https://doi.org/10.1111/2041-210X.12081

Barel, C.D.N. 1983. Toward a constructional morphology of cichlid fishes (Teleostei, Perciformes). Netherlands Journal of Zoology, 33:357-424.

Barker, C.T., Naish, D., Newham, E., Katsamenis, O.L., and Dyke, G. 2017. Complex neuroanatomy in the rostrum of the Isle of Wight theropod *Neovenator salerii*. Scientific Reports, 7,1:3749. doi:10.1038/s41598-017-03671-3

Barker, C.T., Hone, D.W.E., Naish, D., Cau, A., Lockwood, J.A.F., Foster, B., Clarkin, C.E., Schneider, P., and Gostling, N.J. 2021. New spinosaurids from the Wessex formation (Early Cretaceous, UK) and the European origins of Spinosauridae. Scientific Reports, 11:19340. doi:10.1038/s41598-021-97870-8

Barsbold, R. and Osmólska, H. 1999. The skull of *Velociraptor* (Theropoda) from the Late Cretaceous of Mongolia. *Acta Palaeontologica* Polonica, 44:189–219.

Bell, M.A. and Lloyd, G.T. 2015. Strap: an R package for plotting phylogenies against stratigraphy and assessing their stratigraphic congruence. Palaeontology, 58:379-389. https://doi.org/10.1111/pala.12142

Benoit, J., Legendre, L., Farke, A., Neenan, J., Mennecart, B., Costeur, L., Mérigeaud, S., and Manger, P. 2020. A test of the lateral semicircular canal

correlation to head posture, diet and other biological traits in “ungulate” mammals. Scientific Reports, 10. 10.1038/s41598-020-76757-0

Benson, R.B.J. 2008b. A redescription of *‘Megalosaurus’ hesperis* (Dinosauria, Theropoda) from the Inferior Oolite (Bajocian, Middle Jurassic) of Dorset, United Kingdom. Zootaxa, 1931:57–67.

Benson, R.B.J. 2010. A description of *Megalosaurus bucklandii* (Dinosauria: Theropoda) from the Bathonian of the UK and the relationships of Middle Jurassic theropods. Zoological Journal of the Linnean Society, 158:882–935. doi:10.1111/j.1096-3642.2009.00569.x

Britt, B. B. 1991. Theropods of Dry Mesa Quarry (Morrison Formation, Late Jurassic), Colorado, with emphasis on the osteology of *Torvosaurus tanneri*. BYU Geology Studies, 37:1–72.

Brusatte, S., Benson, R.B.J., Zhao, X.-J., and Currie, P. J. 2010a. The skull of *Monolophosaurus jiangi* (Dinosauria: Theropoda) and its implications for early theropod phylogeny and evolution. Zoological Journal of the Linnean Society, 158:573–607.

Brusatte, S.L., Carr, T.D., and Norell, M.A. 2012. The osteology of *Alioramus*, a gracile and long-snouted tyrannosaurid (Dinosauria: Theropoda) from the Late Cretaceous of Mongolia. Bulletin of the American Museum of Natural History, 366:1–197. doi:10.1206/770.1

Bronzati, M. and Rauhut, O.W.M. 2018. Braincase redescription of *Efraasia minor* Huene, 1908 (Dinosauria: Sauropodomorpha) from the Late Triassic of Germany, with comments on the evolution of the sauropodomorph braincase.

Zoological Journal of the Linnean Society, 182:173–224. doi:10.1093/zoolinnean/zlx029

Bronzati, M., Langer, M.C., and Rauhut, O.W.M. 2018. Braincase anatomy of the early Sauropodomorph *Saturnalia tupiniquim* (Late Triassic, Brazil). Journal of Vertebrate Paleontology, 38:e1551973. DOI: 10.1080/02724634.2018.1559173

Buffetaut, E. 1989. New remains of the enigmatic dinosaur *Spinosaurus* from the Cretaceous of Morocco and the affinities between *Spinosaurus* and *Baryonyx*. Neues Jahrbuch für Geologie und Paläontologie, Monatshefte, Stuttgart, 2:79-87.

Buffetaut, E. 1992. Remarks on the Cretaceous theropod dinosaurs *Spinosaurus* and *Baryonyx*. Neues Jahrbuch für Geologie und Paläontologie, Monatshefte, Stuttgart, 2:88-96.

Buffetaut, E., Martill, D., and Escuillie, F. 2004. Pterosaurs as part of a spinosaur diet. Nature, 430:33. https://doi.org/10.1038/430033a

Carrano, M.T. and Sampson, S.D. 2008. The phylogeny of Ceratosauria (Dinosauria: Theropoda). Journal of Systematic Palaeontology, 6:182–236.

Carrano, M.T., Benson, R.B.J., and Sampson, S.D. 2012. The phylogeny of Tetanurae (Dinosauria: Theropoda). Journal of Systematic Palaeontology, 10:211–300. doi:10.1080/14772019.2011.630927

Chapelle, K.E.J. and Choiniere, J.N. 2018. A revised cranial description of *Massospondylus carinatus* Owen (Dinosauria: Sauropodomorpha) based on computed tomographic scans and a review of cranial characters for basal Sauropodomorpha. PeerJ, 6:e4224. doi:10.7717/peerj.4224

Charig, A.J. and Milner, A.C. 1986. *Baryonyx*, a remarkable new theropod dinosaur. Nature, 324:359-361.

Charig, A.J. and Milner, A.C. 1997. *Baryonyx walkeri*, a fish-eating dinosaur from the Wealden of Surrey. Journal of Systematic Palaeontology, 53:11–70.

Chure, D.J. and Madsen, J.H. 1998. An unusual braincase (?*Stokesosaurus clevelandi*) from the Cleveland-Lloyd dinosaur quarry, Utah (Morrison formation; Late Jurassic). Journal of Vertebrate Paleontology, 18:115–125. doi:10.1080/02724634.1998.10011038

Chure, D.J. and Loewen, M.A. 2020. Cranial anatomy of *Allosaurus jimmadseni*, a new species from the lower part of the Morrison Formation (Upper Jurassic) of Western North America. PeerJ, 8:e7803. doi:10.7717/peerj.7803

Cisneros, J.C., Raja, N.B, Stewens, P., and Ghilardi, A.M. 2021. The moral and legal imperative to return illegally exported fossils. Nature Ecology & Evolution. 10.1038/s41559-021-01588-9.

Cisneros, J.C., Raja, N.B., Ghilardi, A.M., Dunne, E.M., Pinheiro, F.L., Fernández, O.R.R., Sales, M.A.F., Rodríguez-de la Rosa, R.A., Miranda-Martínez, A.Y., González-Mora, S., Bantim, R.A.M, de Lima, F.J., and Pardo, J.D. 2022. Digging deeper into colonial palaeontological practices in modern day Mexico and Brazil. Royal Society Open Science, 9:210898. https://doi.org/10.1098/rsos.210898

Coria, R.A. and Currie, P.J. 2002. The braincase of *Giganotosaurus carolinii* (Dinosauria, Theropoda) from the Upper Cretaceous of Argentina. Journal of Vertebrate Paleontology, 22:802–811.

Coria, R.A. and Currie, P.J. 2016. A new megaraptoran dinosaur (Dinosauria, Theropoda, Megaraptoridae) from the Late Cretaceous of Patagonia. PLoS ONE, 11:e0157973. doi:10.1371/journal.pone.0157973

Cuff, A.R. and Rayfield, E.J. 2013. Feeding mechanics in spinosaurid theropods and extant crocodilians. PLoS ONE, 8:e65295. https://doi.org/10.1371/journal.pone.0065295

Currie P.J. and Zhao, X.-J. 1993. A new carnosaur (Dinosauria, Theropoda) from the Jurassic of Xinjiang, People's Republic of China. Canadian Journal of Earth Sciences, 30:2037–2081. DOI 10.1139/e93-179

Currie, P.J. 2003. Cranial anatomy of tyrannosaurid dinosaurs from the Late Cretaceous of Alberta, Canada. Acta Palaeontologica Polonica, 48:191-226. 10.1017/CBO9780511608377.023

Dal Sasso, C., Maganuco, S., Buffetaut, E., and Mendez, M.A. 2005. New information on the skull of the enigmatic theropod *Spinosaurus*, with remarks on its size and affinities. Journal of Vertebrate Paleontology, 25:888–896. doi:10.1671/0272-4634(2005)025[0888:NIOTSO]2.0.CO;2

Pol, D. and Rauhut, O.W.M. 2012. A Middle Jurassic abelisaurid from Patagonia and the early diversification of theropod dinosaurs. Proceedings of the Royal Society B, 279:3170–3175. http://doi.org/10.1098/rspb.2012.0660

Eddy, D.R. and Clarke, J.A. 2011. New information on the cranial anatomy of *Acrocanthosaurus atokensis* and its implications for the phylogeny of Allosauroidea (Dinosauria: Theropoda). PLoS ONE, 6,3:e17932. doi:10.1371/journal.pone.0017932

Evers, S.W., Foth, C., and Rauhut, O.W.M. 2020. Notes on the cheek region of the Late Jurassic theropod dinosaur *Allosaurus*. *PeerJ*, 8:e8493. doi:10.7717/peerj.8493

Fabbri, M., Navalón, G., Benson, R.B.J., Pol, D., O'Connor, J.K., Bhullar, B.-A.S., Erickson, G.M., Norell, M.A., Orkney, A., Lamanna, M.C., Zouhri, S., Becker, J., Emke, A., Dal Sasso, C., Bindellini, G., Maganuco, S., Auditore, M. and Ibrahim, N. 2022. Subaqueous foraging among carnivorous dinosaurs. *Nature* 603:852–857.

Gauthier, J.A. 1986. Saurischian monophyly and the origin of birds, p. 1–47. In Padian, K. (ed.), The Origin of Birds and the Evolution of Flight. Memoirs of the California Academy of Sciences, 8.

Gilmore, C.W. 1920. Osteology of the carnivorous Dinosauria in the United States National Museum, with special reference to the genera *Antrodemus (Allosaurus) and Ceratosaurus*. Bulletin of the United States National Museum, 110:1–154.

Gignac, P. and Erickson, G. 2017. The Biomechanics behind extreme osteophagy in *Tyrannosaurus rex*. Scientific Reports, 7:12. 10.1038/s41598-017-02161-w

Goloboff, P.A. and Catalano, S.A. 2016. TNT version 1.5, including a full implementation of phylogenetic morphometrics. Cladistics, 32:221-238. https://doi.org/10.1111/cla.12160

Gower, D.J. and Weber, E. 1998. The braincase of *Euparkeria*, and the evolutionary relationships of birds and crocodilians. Biological Reviews, 73:367-411. https://doi.org/10.1111/j.1469-185X.1998.tb00177.x

Hanai, T. and Tsuihiji, T. 2019. Description of tooth ontogeny and replacement patterns in a juvenile *Tarbosaurus bataar* (Dinosauria: Theropoda) using CT-scan data. The Anatomical Record, 302:1210–1225. doi:10.1002/ar.24014

Hassler, A., Martin, J.E., Amiot, R., Tacail, T., Arnaud Godet, F., Allain, R. and Balter, V. 2018. Calcium isotopes offer clues on resource partitioning among Cretaceous predatory dinosaurs. Proceedings of the Royal Society B 285:20180197.

Heckeberg, N. and Rauhut, O.W.M. 2020. Histology of spinosaurid dinosaur teeth from the Albian-Cenomanian of Morocco: implications for tooth replacement and ecology. Palaeontologia Electronica, 23:a48. doi:10.26879/1041

Henderson, D.M. 2003. The eyes have it: the sizes, shapes, and orientations of theropod orbits as indicators of skull strength and bite force. Journal of Vertebrate Paleontology, 22:766–778. doi:10.1671/0272-4634(2002)022[0766:TEHITS]2.0.CO;2

Hendrickx, C. and Mateus, O. 2014. *Torvosaurus gurneyi* n. sp., the largest terrestrial predator from Europe, and a proposed terminology of the maxilla anatomy in nonavian theropods. PLoS ONE, 9:e88905. doi:10.1371/journal.pone.0088905

Hendrickx, C., Mateus, O., and Buffetaut, E. 2016. Morphofunctional analysis of the quadrate of Spinosauridae (Dinosauria: Theropoda) and the presence of *Spinosaurus* and a second spinosaurine taxon in the Cenomanian of North Africa. PLoS ONE, 11:e0144695. doi:10.1371/journal.pone.0144695

Hendrickx, C., Mateus, O., Araújo, R., and Choiniere, J. 2019. The distribution of dental features in non-avian theropod dinosaurs: Taxonomic potential, degree

of homoplasy, and major evolutionary trends. Palaeontologica Electronica. 22:1–110.

Henderson, D.M. 2018. A buoyancy, balance and stability challenge to the hypothesis of a semi-aquatic *Spinosaurus* Stromer, 1915 (Dinosauria: Theropoda). PeerJ, 6:e5409. https://doi.org/10.7717/peerj.5409

Holliday, C.M. 2009. New insights into dinosaur jaw muscle anatomy. The Anatomical Record, 292:1246–1265. doi:10.1002/ar.20982

Holliday, C.M. and Witmer, L.M. 2007. Archosaur adductor chamber evolution: integration of musculoskeletal and topological criteria in jaw muscle homology. Journal of Morphology, 268:457–484. doi:10.1002/jmor.10524

Holliday, C. and Nesbitt, S. 2013. Morphology and diversity of the mandibular symphysis of archosauriforms. Geological Society of London Special Publications, 379:555-571. 10.1144/SP379.2.

Hone, D.W.E. and Holtz, T.R., Jr. 2017. A century of spinosaurs - a review and revision of the Spinosauridae with comments on their ecology. Acta Geologica Sinica-English Edition, 93:1120-1132. https://doi.org/10.1111/1755-6724.13328

Hone, D.W.E. and Holtz, T.R., Jr. 2021. Evaluating the ecology of *Spinosaurus*: Shoreline generalist or aquatic pursuit specialist? Palaeontologia Electronica, 24:a03. https://doi.org/10.26879/1110

Ibrahim, N., Sereno, P.C., Dal Sasso, C., Maganuco, S., Fabbri, M., Martill, D.M., Zouhri, S., Myhrvold, N., and Iurino, D.A. 2014. Semiaquatic adaptations in a giant predatory dinosaur. Science, 345:1613-1616. https://doi.org/10.1126/science.1258750

Ibrahim, N., Maganuco, S., Dal Sasso, C., Fabbri, M., Auditore, M., Bindellini, G., Martill, D.M., Zouhri, S., Mattarelli, D.A., Unwin, D.M., and Wiemann, J. 2020a. Tail-propelled aquatic locomotion in a theropod dinosaur. Nature, 581:67-70. https://doi.org/10.1038/s41586-020-2190-3

Isasmendi, E., Navarro-Lorbés, P., Sáez-Benito, P., Viera, L.I., Torices, A., and Pereda-Suberbiola, X. 2022 New contributions to the skull anatomy of spinosaurid theropods: Baryonychinae maxilla from the Early Cretaceous of Igea (La Rioja, Spain). Historical Biology. DOI:10.1080/08912963.2022.2069019

Janensch, W. 1936. Über Bahnen von Hirnvenen bei Saurischiern und Ornithischiern, sowie einigen anderen fossilen und rezenten Reptilien. Paläontologische Zeitschrift, 18:181-198.

Kellermann, M. 2021. New data on dinosaur diversity in the “middle“ Cretaceous (Albian, Cenomanian) of North Africa. Unpublished Master’s thesis, Ludwig-Maximilians-Universität Munich, 106 pp.

Kellner, A.W.A. and Campos, D. 1996. First Early Cretaceous theropod dinosaur from Brazil with comments on Spinosauridae. Neues Jahrbuch Geologie und Paläontologie Abhandlungen, 199:151–166.

Kellner, A.W.A., Azevedo, S.A.K., Machado, E.B., Carvalho, L.B. de, and Henriques, D.D.R. 2011. A new dinosaur (Theropoda, Spinosauridae) from the Cretaceous (Cenomanian) Alcântara Formation, Cajual Island, Brazil. Anais de Academia Brasileira de Ciências, 83:99–108.

Lloyd, G. T. 2016. Estimating morphological diversity and tempo with discrete character-taxon matrices: implementation, challenges, progress, and future

directions. Biological Journal of the Linnean Society, *118*:131-151. https://doi.org/10.1111/bij.12746

Lacerda, M.B.S., Grillo, O.N., and Romano, P.S.R. 2021. Rostral morphology of Spinosauridae (Theropoda, Megalosauroidea): premaxilla shape variation and a new phylogenetic inference. Historical Biology. DOI: 10.1080/08912963.2021.2000974

Lakin, R. and Longrich, N. 2018. Juvenile spinosaurs (Theropoda: Spinosauridae) from the middle Cretaceous of Morocco and implications for spinosaur ecology. Cretaceous Research, 93:129–142. 10.1016/j.cretres.2018.09.012.

Maddison, W.P. and Maddison, D.R. 2009. Mesquite: a modular system for evolutionary analysis. Version 2.6.

Madsen, J.H., Jr. 1976a. *Allosaurus fragilis*: a revised osteology. Utah Geological and Mineral Survey Bulletin, 109:1–163.

Madsen, J.H., Jr. and Welles, S.P. 2000. *Ceratosaurus* (Dinosauria, Theropoda): a revised osteology. Utah Geological Survey, Miscellaneous Publications*,* 2:1–80.

Malafaia, E., Gasulla, J.M., Escaso, F., Narváez, I., Sanz, J.L., and Ortega, F. 2020. A new spinosaurid theropod (Dinosauria: Megalosauroidea) from the Upper Barremian of Vallibona, Spain: implications for spinosaurid diversity in the Early Cretaceous of the Iberian peninsula. Cretaceous Research, 106:104221. doi:10.1016/j.cretres.2019.104221

Makovicky, P. J., KobayashiI, Y., and Currie, P. J. 2004. Ornithomimosauria. In Weishampel, D.B., Dodson, P., and Osmólska, H. (eds.), The Dinosauria (2nd ed., pp. 137–150). University of California Press. http://www.jstor.org/stable/10.1525/j.ctt1pn61w.12

Martill, D.M., Cruickshank, A.R.I., and Frey, E. 1996. A new crested maniraptoran dinosaur from the Santana Formation (Lower Cretaceous) of Brazil. Journal of the Geological Society, 153:5–8.

Marugan-Lobon, J., Chiappe, L.M., and Farke, A.A. 2013. The variability of inner ear orientation in saurischian dinosaurs: Testing the use of semicircular canals as a reference system for comparative anatomy. PeerJ, 1:e124.

Mateus, O. and Estraviz-López, D. 2022. A new theropod dinosaur from the early cretaceous (Barremian) of Cabo Espichel, Portugal: Implications for spinosaurid evolution, PLoS ONE, 17: e0262614. https://doi.org/10.1371/journal.pone.0262614

Molnar, R.E. and Farlow, J.O. 1990. Carnosaur paleobiology. In: Weishampel, D.B, Dodson, P, Osmolska, H, eds. *The Dinosauria.* Berkeley: University ofCalifornia Press, 210–224.

Motta, M., Aranciaga Rolando, A., Rozadilla, S., Agnolin, F., Chimento, N., Brissón, E.F., and Novas, F. 2016. New theropod fauna from the Upper Cretaceous (Huincul Formation) of northwestern Patagonia, Argentina. New Mexico Museum of Natural History and Science Bulletin.

Munt, M., Blackwell, G., Clark, J., Foster, B., Gostling, N., Lockwood, J., Murray, K., Peaker, A., Rankin, K., and Sweetman, S. 2017. New spinosaurid dinosaur finds from the Wessex Formation (Wealden Group, Early Cretaceous) of the Isle of Wight. Poster.

Myhrvold, N., Sereno, P.C., Baumgart, S.L., Formoso, K.K., Vidal, D., Fish, F.E., and Henderson, D.M. 2022. Spinosaurids as ‘subaqueous foragers’ undermined by selective sampling and problematic statistical inference. Nature. https: 764

//www.biorxiv.org/content/10.1101/2022.04.13.487781v1, doi:https://doi.org/10.1101/2022.04.13.487781.

Ostrom, J.H. 1969. Osteology of *Deinonychus antirrhopus*, an unusual theropod dinosaur from the Lower Cretaceous of Montana. Peabody Museum of Natural History, Bulletin, 30:1–165.

Paradis, E. and Schliep, K. 2019. Ape 5.0: an environment for modern phylogenetics and evolutionary analyses. R. Bioinformatics, 35:526-528. doi: 10.1093/bioinformatics/bty633. PMID: 30016406

Paulina-Carabajal, A. and Canale, J.I. 2010. Cranial endocast of the carcharodontosaurid theropod *Giganotosaurus carolinii* Coria & Salgado, 1995. Neues Jahrbuch für Geologie und Paläontologie - Abhandlungen, 258:249–256. doi:10.1127/0077-7749/2010/0104

Paulina-Carabajal, A. 2015. Guía para el studio de la neuroanatomía de dinosaurios saurischia, con énfasis en formas sudamericanas. Publicación Electrónica de la Asociación Paleontológica Argentina, 15:108-142. 10.5710/PEAPA.15.06.2015.102

Paulina-Carabajal, A. and Currie, P.J. 2017. The braincase of the theropod dinosaur *Murusraptor*: osteology, neuroanatomy and comments on the paleobiological implications of certain endocranial features. Ameghiniana, 54:617. doi:10.5710/AMGH.25.03.2017.3062

Pol, D. and Escapa, I. 2009. Unstable taxa in cladistic analysis: Identification and the assessment of relevant characters. Cladistics, 25:515-527. 10.1111/j.1096-0031.2009.00258.x

Porfiri, J., Novas, F., Calvo, J., Agnolin, F., Ezcurra, M., and Cerda, I. 2014. Juvenile specimen of *Megaraptor* (Dinosauria, Theropoda) sheds light about tyrannosauroid radiation. Cretaceous Research, 51:35–55. 10.1016/j.cretres.2014.04.007

Raath, M.A. 1977. The anatomy of the Triassic theropod *Syntarsus rhodesiensis* (Saurischia: Podokesauridae) and a consideration of its biology. Unpublished PhD thesis, Rhodes University, 233 pp.

Rauhut, O.W.M. 2001. Morphology and mechanics of the jaws of spinosaurid theropods (Dinosauria): implications for predation. Ameghiana, Suplemento-Resumenes, 38,4.

Rauhut, O.W.M. 2003. The interrelationships and evolution of basal theropod dinosaurs. Special Papers in Palaeontology, 69:1–213.

Rauhut, O.W.M. 2004. Braincase structure of the Middle Jurassic theropod dinosaur *Piatnitzkysaurus*. Canadian Journal of Earth Sciences, 41:1109–1122.

Rauhut, O.W.M., Milner, A.C., and Moore-Fay, S. 2010. Cranial osteology and phylogenetic position of the theropod dinosaur *Proceratosaurus bradleyi* (Woodward, 1910) from the Middle Jurassic of England. Zoological Journal of the Linnean Society, 158:155–195. doi:10.1111/j.1096-3642.2009.00591.x

Rauhut, O.W.M., Hübner, T.R., and Lanser, K.-P. 2016. A new megalosaurid theropod dinosaur from the late Middle Jurassic (Callovian) of north-western Germany: Implications for theropod evolution and faunal turnover in the Jurassic. Palaeontologia Electronica, 19:26A. https://doi.org/10.26879/654

Rauhut, O.W.M. and Carrano, M.T. 2016. The theropod dinosaur *Elaphrosaurus bambergi* Janensch, 1920, from the Late Jurassic of Tendaguru, Tanzania. Zoological Journal of the Linnean Society, 178:546-610.

Rauhut, O.W.M., Foth, C., and Tischlinger, H. 2018. The oldest *Archaeopteryx* (Theropoda: Avialiae): a new specimen from the Kimmeridgian/Tithonian boundary of Schamhaupten, Bavaria. PeerJ, 6:e4191. https://doi.org/10.7717/peerj.4191

Rauhut, O.W.M. and Pol, D. 2019. Probable basal allosauroid from the early Middle Jurassic Cañadón Asfalto Formation of Argentina highlights phylogenetic uncertainty in tetanuran theropod dinosaurs. Scientific Reports, 9:18826. doi:10.1038/s41598-019-53672-7

Rauhut, O.W.M., Schwermann, A.H., Hübner, T.R., and Lanser, K.-P. 2020. The oldest record of the genus *Torvosaurus* (Theropoda: Megalosauridae) from the Callovian Ornatenton Formation of north-western Germany. Geologie und Paläontologie in Westfalen, 93:31–43.

Revell, L.J. 2012. Phytools: an R package for phylogenetic comparative biology (and other things). Methods in Ecology and Evolution, 3:217-223. https://doi.org/10.1111/j.2041-210X.2011.00169.x

Rayfield, E.J., Norman, D., Horner, C., Horner, J., Smith, P., Thomason, J., and Upchurch, P. 2001. Cranial form and function in a larger theropod dinosaur. Nature, 409:1033-1037. 10.1038/35059070

Rayfield, E.J., Milner, A.C., Xuan, V.B., and Young, P.G. 2007. Functional morphology of spinosaur 'crocodile-mimic' dinosaurs. Journal of Vertebrate

Paleontology, 27:892–901. doi:10.1671/0272-4634(2007)27[892:FMOSCD]2.0.CO;2

Rayfield, E.J. 2004. Cranial mechanics and feeding in *Tyrannosaurus rex*. Proceedings of the Royal Society of London B, 271:1451-1459.

Rayfield, E.J. 2011. Structural performance of tetanuran theropod skulls, with emphasis on the Megalosauridae, Spinosauridae and Carcharodontosauridae. *Special Papers in Palaeontology*, 86:241-253.

Richter, U., Mudroch, A., and Buckley, L.G. 2013. Isolated theropod teeth from the Kem Kem Beds (Early Cenomanian) near Taouz, Morocco. Paläontologische Zeitschrift, 87:291–309. doi:10.1007/s12542-012-0153-1

Rieppel, O. 1985. The recessus scalae tympani and its bearing on the classification of reptiles. Journal of Herpetology, 19:373-384.

Sadleir, R., Barrett, P.M., and Powell, H.P. 2008. The anatomy and systematics of *Eustreptospondylus oxoniensis,* a theropod dinosaur from the Middle Jurassic of Oxfordshire, England. Monograph of the Palaeontographical Society, London, 160:1–82.

Sales, M.A.F., Lacerda, M.B., Horn, B.L.D., Oliveira, I.A.P. de, and Schultz, C.L. 2016. The "χ" of the matter: testing the relationship between paleoenvironments and three theropod clades. PLoS ONE, 11:e0147031. doi:10.1371/journal.pone.0147031

Sales, M.A.F. and Schultz, C.L. 2017. Spinosaur taxonomy and evolution of craniodental features: evidence from Brazil. PLoS ONE, 12:e0187070. doi:10.1371/journal.pone.0187070

Sampson, S.D. and Witmer, L.M. 2007. Craniofacial anatomy of *Majungasaurus crenatissimus* (Theropoda: Abelisauridae) from the Late Cretaceous of Madagascar. Society of Vertebrate Paleontology Memoir, 8:32–102.

Schade, M., Rauhut, O.W.M., and Evers, S.W. 2020. Neuroanatomy of the spinosaurid *Irritator challengeri* (Dinosauria: Theropoda) indicates potential adaptations for piscivory. Scientific Reports, 10:211. doi:10.1038/s41598-020-66261-w

Sereno, P.C. and Novas, F. 1994. The skull and neck of the basal theropod *Herrerasaurus ischigualastensis*. Journal of Vertebrate Paleontology, 13:451-476.

Sereno, P.C., Forster, C.A., Larsson, H.C.E., Dutheil, D.B., and Sues, H.-D. 1994. Early Cretaceous dinosaurs from the Sahara. Science, 266:267–271.

Sereno, P.C., Beck, A.L., Dutheil, D.B., Gado, B., Larsson, H.C.E., Rauhut, O.W.M., Sadleir, R.W., Sidor, C.A., Varricchio, D.J., Wilson, G.P., and Wilson, J.A. 1998. A long-snouted predatory dinosaur from Africa and the evolution of spinosaurids. Science*,* 282:1298-1302.

Sereno, P.C., Myhrvold, N., Henderson, D.M., Fish, F.E., Vidal, D., Baumgart, S.L., Keillor, T.M., Formoso, K.K., and Conroy, L.L. 2022. *Spinosaurus* is not an aquatic dinosaur. bioRxiv.

Smith, J.B., Lamanna, M.C., Mayr, H., and Lacovara, K.J. 2006. New information regarding the holotype of *Spinosaurus aegyptiacus* Stromer, 1915. Journal of Paleontology, 80:400–406. doi:10.1666/0022-3360(2006)080[0400:NIRTHO]2.0.CO;2

Smith, J. 2007. Dental morphology and variation in *Majungasaurus crenatissimus* (Theropoda: Abelisauridae) from the Late Cretaceous of Madagascar. Journal of Vertebrate Paleontology, 27:103-126.

Smyth, R.S.H., Ibrahim, N., and Martill, D.M. 2020. *Sigilmassasaurus* is *Spinosaurus*: a reappraisal of African spinosaurines. Cretaceous Research, 114:104520. doi:10.1016/j.cretres.2020.104520

Snively, E. and Russell, A.P. 2007. Functional morphology of neck musculature in the Tyrannosauridae (Dinosauria, Theropoda) as determined via a hierarchical inferential approach. Zoological Journal of the Linnean Society, 151:759–808. doi:10.1111/j.1096-3642.2007.00334.x

Sues, H.D. 1997. On *Chirostenotes*, a Late Cretaceous oviraptorosaur (Dinosauria: Theropoda) from Western North America. Journal of Vertebrate Paleontology, 17:698–716. doi:10.1080/02724634.1997.10011018

Sues, H.-D., Frey, E., Martill, D.M., and Scott, D.M. 2002. *Irritator challengeri*, a spinosaurid (Dinosauria: Theropoda) from the Lower Cretaceous of Brazil. Journal of Vertebrate Paleontology, 22:535–547. doi:10.1671/0272-4634

Stevens, K.A. 2006. Binocular vision in theropod dinosaurs. Journal of Vertebrate Paleontology, 26:321–330. doi:10.1671/0272-4634(2006)26[321:BVITD]2.0.CO;2

Stromer, E. 1915. Ergebnisse der Forschungsreisen Prof. E. Stromers in den Wüsten Ägyptens. II. Wirbeltier-Reste der Baharîje -Stufe (unterstes Cenoman). 3. Das Original des Theropoden *Spinosaurus aegyptiacus* nov. gen., nov. spec. Abhandlungen der Königlichen Bayerischen Akademie der Wissenschaften. Mathematisch-Physikalische Klasse, 28:1–28.

Stromer, E. 1936. Ergebnisse der Forschungsreisen Prof. E. Stromers in den Wüsten Ägyptens. VII. Baharije-Kessel und -Stufe mit deren Fauna und Flora. Eine ergänzende Zusammenfassung. Abhandlungen der Bayerischen Akademie der Wissenschaften, Mathematisch-naturwissenschaftliche Abteilung, 33:1–102.

Taquet, P. 1984. Une curieuse spécialisation du crâne de certains Dinosaures carnivores du Crétacé: Le museau long et étroit des Spinosauridés. Comptes Rendus de l'Académie des Sciences, Paris, série II, 299:217–222.

Taquet, P. and Russel, D.A. 1998. New data on spinosaurid dinosaurs from the Early Cretaceous of the Sahara. Comptes Rendus de l'Académie des Sciences, Paris, série II, 327:347–353.

Therrien, F., Henderson, D.M., and Ruff, C.B. 2005. Bite me: biomechanical models of theropod mandibles and implications for feeding behavior. In Carpenter, K. (ed.), The Carnivorous Dinosaurs: Indiana University Press, Bloomington and Indianapolis, p. 179- 237.

Therrien, F. and Henderson, D.M. 2007. My theropod is bigger than yours … or not: estimating body size from skull length in theropods. Journal of Vertebrate Paleontology, 27:108–115. doi:10.1671/0272-4634(2007)27[108:MTIBTY]2.0.CO;2

Vilas Boas, M., Brilha, J.B.R. and De Lima, F.F. 2013. Conservação do patrimônio paleontológico do Geopark Araripe (Brasil): enquadramento, estratégias e condicionantes. Boletim Paranaense de Geociências, 70:156-165. doi: 10.5380/geo.v70i0.31418

Vila Nova, B.C., Saraiva A.A., Moreira J.K., Sayão, J.M. 2011. Controlled excavations in the Romualdo formation lagerstatte (Araripe Basin, Brazil) and

pterosaur diversity: remarks based on new findings. Palaios, 26:173-179. doi:20110310091832

Westneat, M.W. 1994. Transmission of force and velocity in the feeding mechanisms of labrid fishes (Teleostei, Perciformes). Zoomorphology, 114:103-118.

Weastneat, M.W. 2003. A biomechanical model for analysis of muscle force, power output and lower jaw motion in fishes. Journal of Theoretical Biology, 223:269–281.

Witmer, L.M. 1997. The evolution of the antorbital cavity of archosaurs: a study in soft-tissue reconstruction in the fossil record with an analysis of the function of pneumaticity. *Society of Vertebrate Paleontology, Memoir, 3*:1–76. doi:10.1080/02724634.1997.10011027

Wilkinson, M. 1995. Coping with abundant missing entries in phylogenetic inference using parsimony. Systematic Biology, 44:501–514. https://doi.org/10.2307/2413657

Witmer, L. M. 1997b. Craniofacial air sinus systems. In Currie, P.J. and Padian, K. (eds.), Encyclopedia of Dinosaurs. Academic Press, New York, p. 151–159.

Witmer, L.M. and Ridgely, R.C. 2010. The Cleveland tyrannosaur skull (*Nanotyrannus* or *Tyrannosaurus*): New findings based on CT scanning, with special reference to the braincase. Kirtlandia, 57:61–81.

Yates, A. 2005. A new theropod dinosaur from the Early Jurassic of South Africa and its implication for the early evolution of theropods. Palaeontologia Africana, 41:105–122.

Zaher, H., Pol, D., Navarro, B.A., Delcourt, R., and Carvalho, A.B. 2020. An Early Cretaceous theropod dinosaur from Brazil sheds light on the cranial evolution of the Abelisauridae. Comptes Rendus Palevol, 19:101–115. doi:10.5852/cr-palevol2020v19a6

Zhao, X.-J. and Currie, P.J. 1994. A large crested theropod from the Jurassic of Xinjiang, People's Republic of China. Canadian Journal of Earth Sciences, 30:2027–2036.

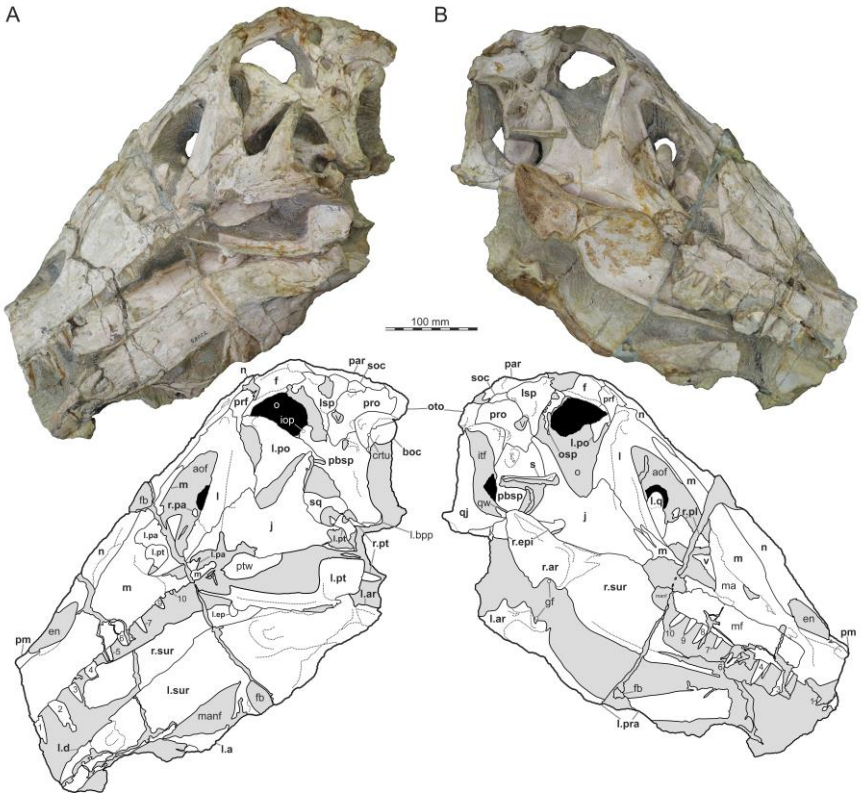

Figure 1. Photographs (top) and interpretative line drawings (bottom) of *Irritator challengeri* (SMNS 58022). A, left lateral view; B, right lateral view. Note that bones are labelled in bold, and other anatomical structures in regular font. Also note that tooth positions are numerically labelled but refer to preserved tooth position from anterior to posterior, not to anatomical tooth positions, which are unknown (see main text). Abbreviations: an, angular; aof, antorbital fenestra; ar, articular; boc, basioccipital; d, dentary; manf, mandibular fenestra; en, external naris; f, frontal; fb, foreign body; gf, glenoid fossa; iop, interorbital process of parabasisphenoid; itf, infratemporal fenestra; j, jugal; l, lacrimal; l.ar; left articular; l.d, left dentary; l.ep, left ectopterygoid; l.bpp, left basipterygoid process of the parabasisphenoid; l.sur, left surangular; l.sq, left squamosal; l.pa, left palatine; l.pra, left prearticular; l.pt, left pterygoid; l.q, left quadrate; m, maxilla; n, nasal; ma, maxillary antrum; mf, maxillary fragment; r.ar, right articular; r.epi, epipterygoid; r.pa, right palatine; r.sur, right surangular; lsp, laterosphenoid; m, maxilla; n, nasal; o, orbita; osp, orbitosphenoid; oto, otoccipital; pa, palatine; par, parietal; pbsp, parabasisphenoid; pm, premaxilla; po, postorbital; pro, prootic; prf, prefrontal; pt, pterygoid; ptw, pterygoid wing of left quadrate; qw, quadrate wing of right pterygoid; qj, quadratojugal; s, stapes; soc, supraoccipital; sq, squamosal; v, vomer; V, trigeminal nerve foramen (CN V); 1-10 mark preserved tooth positions of the maxillae (because of their size, position 11 and 12 of the maxillary fragment are not perceivable in this depiction).

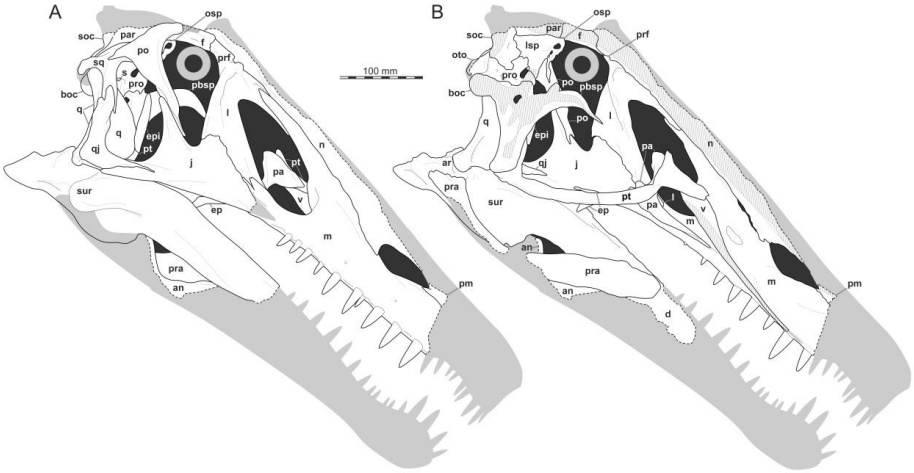

Figure 2. Interpretative line drawings of the re-arranged and articulated skull of *Irritator challengeri* (SMNS 58022). A, right lateral view; B, sagittal cut with removed right skull half, revealing medial aspects of the left skull half. Speculatively, grey silhouettes add unknown parts to the skull known from other spinosaurids. Abbreviations: an, angular; ar, articular; boc, basioccipital; d, dentary; ep, ectopterygoid; epi, epipterygoid; f, frontal; j, jugal; l, lacrimal; ls; laterosphenoid; m, maxilla; n, nasal; osp, orbitosphenoid; oto, otoccipital; pa, palatine; par, parietal; pbsp, parabasisphenoid; pm, premaxilla; po, postorbital; pro, prootic; pra, prearticular; prf, prefrontal; pt, pterygoid; q, quadrate; qj, quadratojugal; s, stapes; sur, surangular; soc, supraoccipital; sq, squamosal; v, vomer.

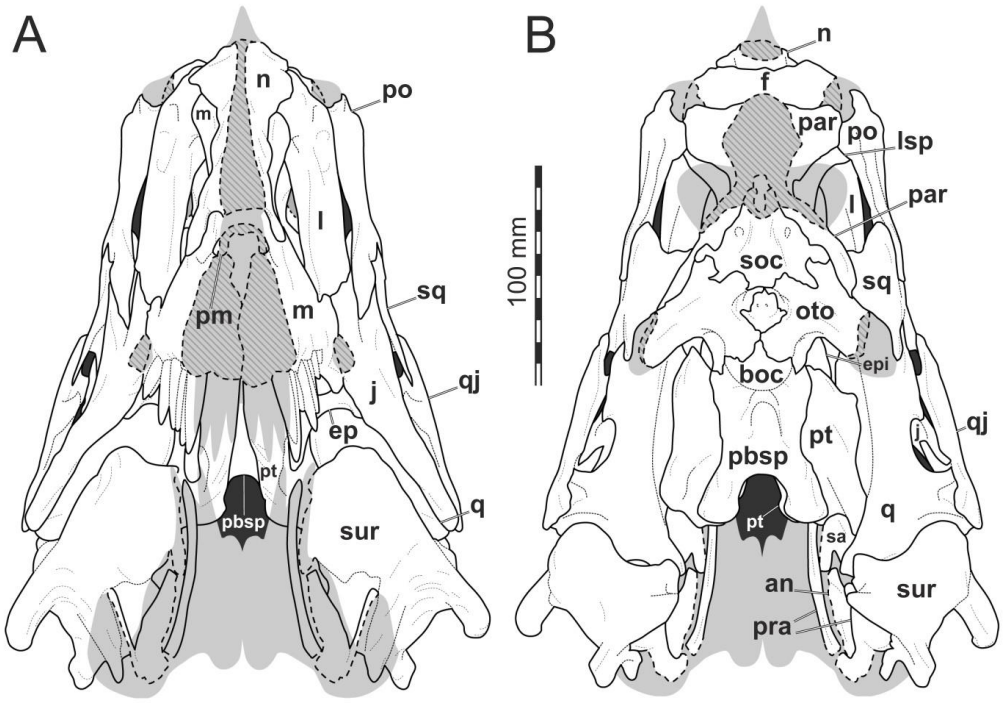

Figure 3. Interpretative line drawings of the re-arranged and articulated skull of *Irritator challengeri* (SMNS 58022). A, anterior view; B, posterior view. Speculatively, grey silhouettes add unknown parts to the skull known from other spinosaurids. Abbreviations: an, angular; boc, basioccipital; ep, ectopterygoid; epi, epipterygoid; f, frontal; j, jugal; l, lacrimal; lsp, laterosphenoid; m, maxilla; n, nasal; oto, otoccipital; par, parietal; pbsp, parabasisphenoid; pm, premaxilla; po, postorbital; pro, prootic; pra, prearticular; prf, prefrontal; pt, pterygoid; q, quadrate; qj, quadratojugal; sur, surangular; soc, supraoccipital; sq, squamosal.

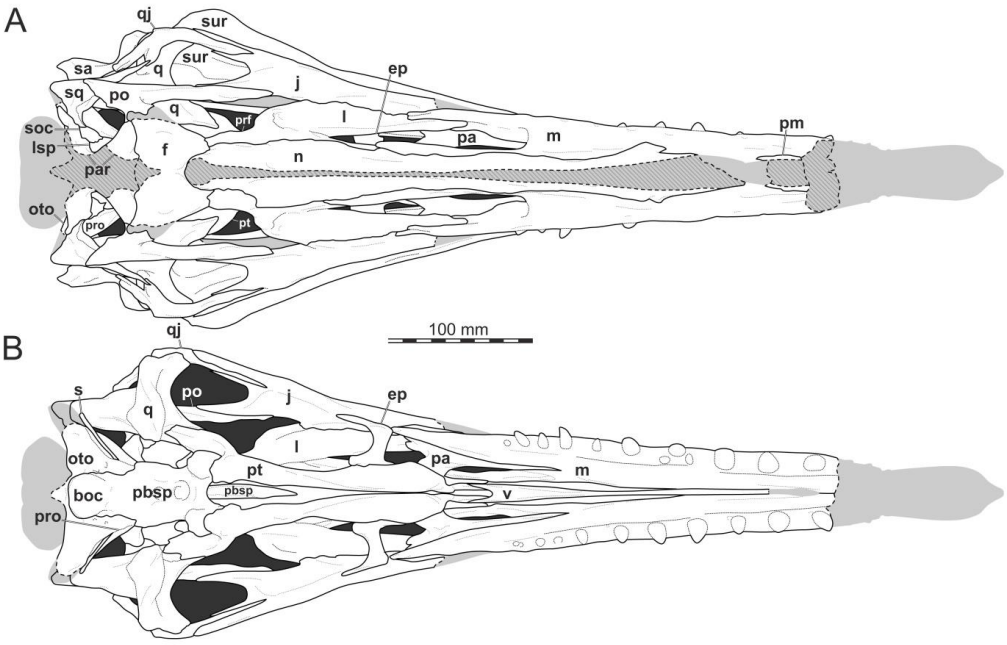

Figure 4. Interpretative line drawings of the re-arranged and articulated skull of *Irritator challengeri* (SMNS 58022). A, dorsal view; B, ventral view without the lower jaw. Speculatively, grey silhouettes add unknown parts to the skull known from other spinosaurids. Abbreviations: boc, basioccipital; ep, ectopterygoid; f, frontal; j, jugal; l, lacrimal; lsp, laterosphenoid; m, maxilla; n, nasal; oto, otoccipital; par, parietal; pbsp, parabasisphenoid; pm, premaxilla; po, postorbital; pro, prootic; prf, prefrontal; pt, pterygoid; q, quadrate; qj, quadratojugal; sur, surangular; soc, supraoccipital; sq, squamosal.

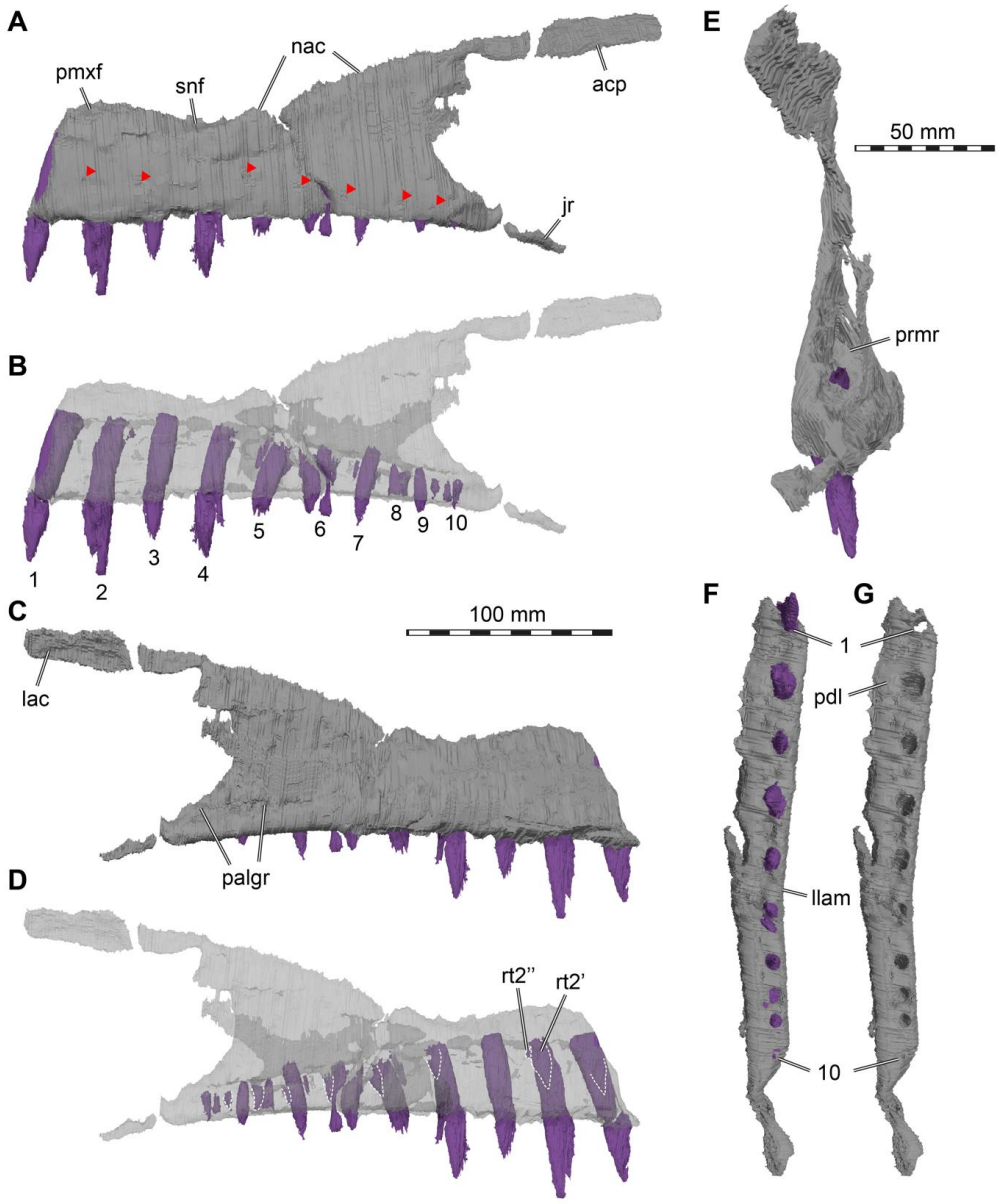

Figure 5. 3D renderings of the left maxilla of *Irritator challengeri* (SMNS 58022). A, lateral view; B, lateral view with maxilla bone rendered transparent; C, medial view; D, medial view with maxilla bone rendered transparent; E, posterior view; F, ventral view (anterior to top); G, ventral view without teeth, showing alveoli. Note different scale for E. Also note that tooth positions are numerically labelled but refer to preserved tooth position from anterior to posterior, not to anatomical tooth positions, which are unknown (see main text). Replacement teeth are highlighted with dashed lines in D, and different generations are indicated with prime (‘) or double prime (‘’). Red arrow heads point to neurovascular foramina. Abbreviations: acp, ascending process; jr, jugal ramus; lac, lacrimal contact; llam, lateral lamina; nac, nasal contact; palgr, palatine groove; pdl, paradental lamina; pmxf, premaxillary facet; prmr, promaxillary recess; rt, replacement tooth; snf, subnarial fossa.

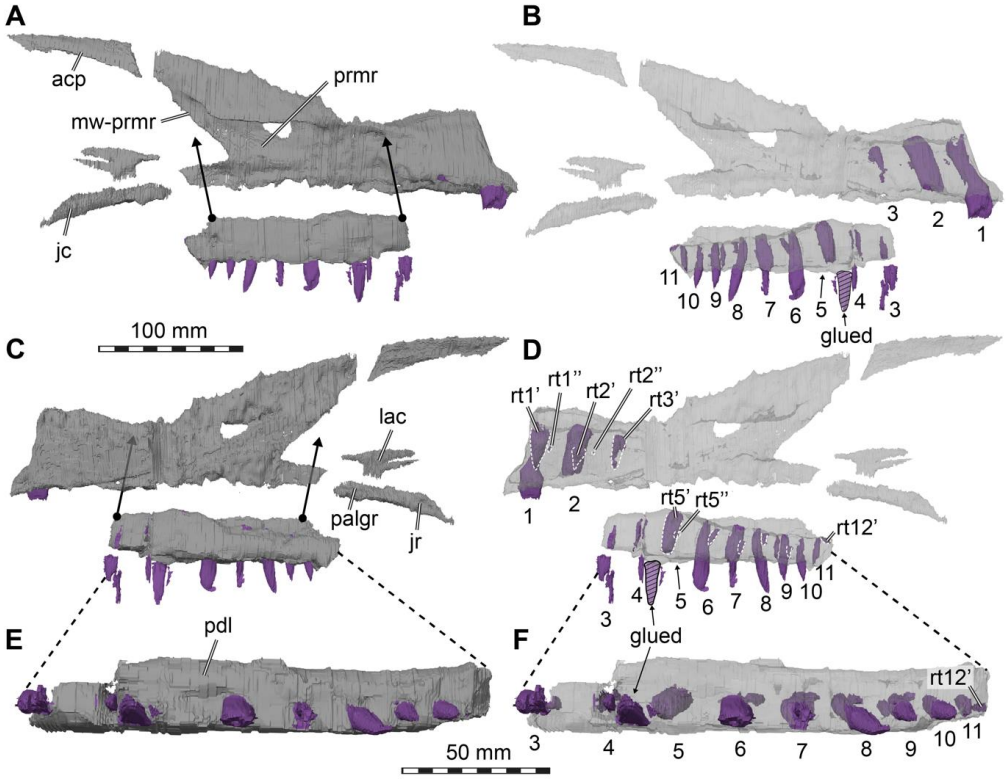

Figure 6. 3D renderings of the right maxilla of *Irritator challengeri* (SMNS 58022). A, lateral view; B, lateral view with maxilla bone rendered transparent; C, medial view; D, medial view with maxilla bone rendered transparent; E, ventral view of tooth row fragment; F, ventral view rendered transparent. Note different scale for E–F. Also note that tooth positions are numerically labelled but refer to preserved tooth position from anterior to posterior, not to anatomical tooth positions, which are unknown (see main text). Replacement teeth are highlighted with dashed lines in D, and different generations are indicated with prime (‘) or double prime (‘’). Arrows in A & C indicate approximate original position of tooth-bearing fragment. Abbreviations: acp, ascending process; jr, jugal ramus; lac, lacrimal contact; mw-prmr, medial wall of promaxillary recess; palgr, palatine groove; pdl, paradental lamina; prmr, promaxillary recess; rt, replacement tooth.

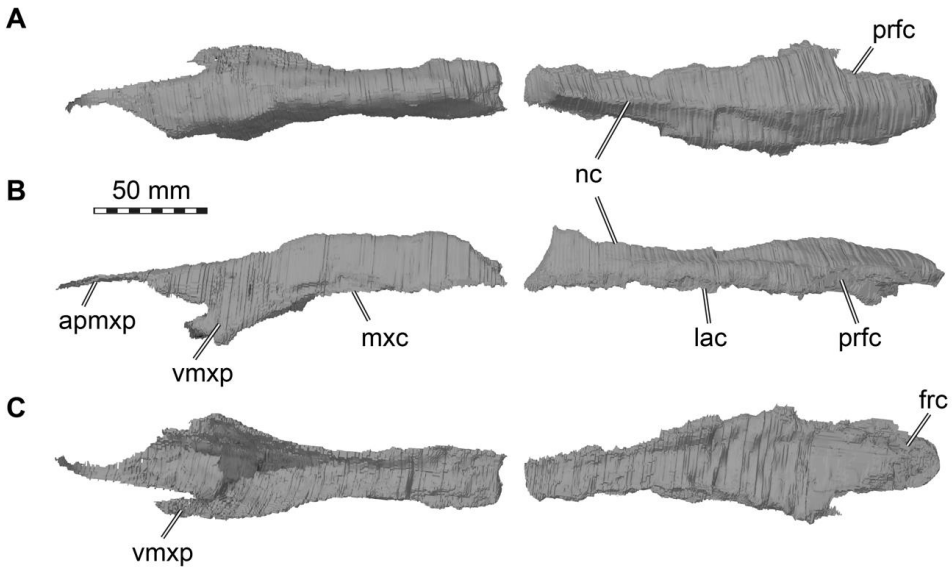

Figure 7. 3D renderings of the fused nasals of *Irritator challengeri* (SMNS 58022). A, dorsal view; B, left lateral view; C, ventral view. Abbreviations: apmxp, anterior premaxillary process; frc, frontal contact; lac, lacrimal contact; mxc, maxillary contact; nc, nasal crest; prfc, prefrontal contact; vmxp, ventral maxillary process.

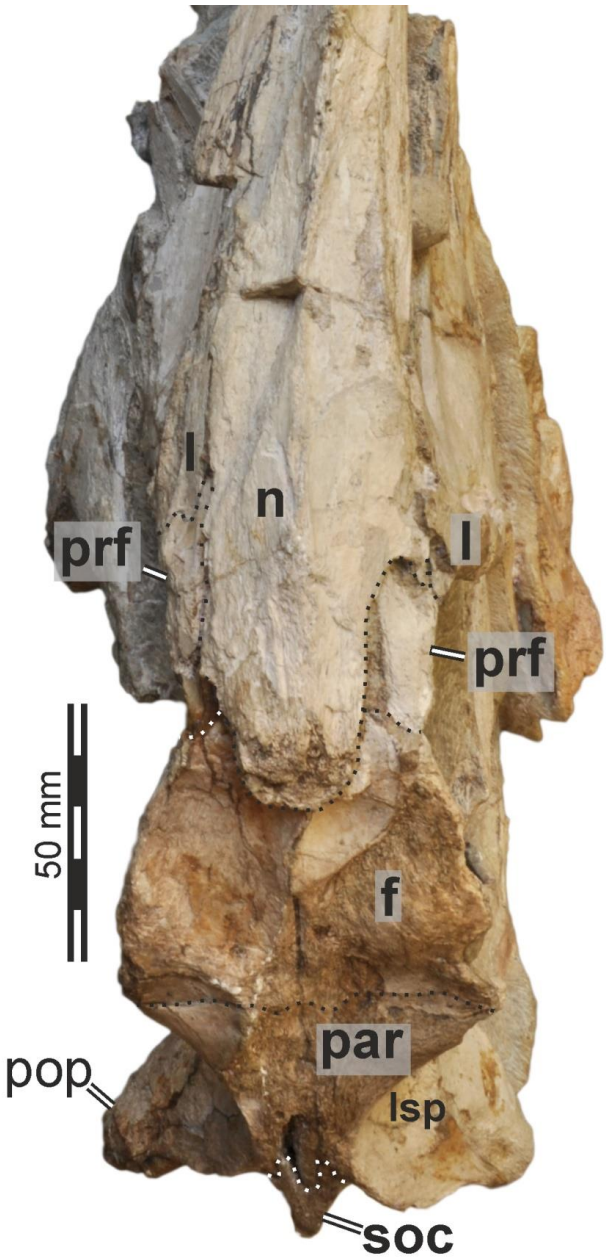

Figure 8. Photograph of posterior skull roof of *Irritator challengeri* (SMNS 58022) in dorsal view. Note that bones are labelled in bold, and other anatomical structures in regular font. Dashed lines mark sutures. Abbreviations: f, frontal; l, lacrimal; lsp, laterosphenoid; n, nasal; par, parietal; pop, paroccipital process; prf, prefrontal; soc, supraoccipital.

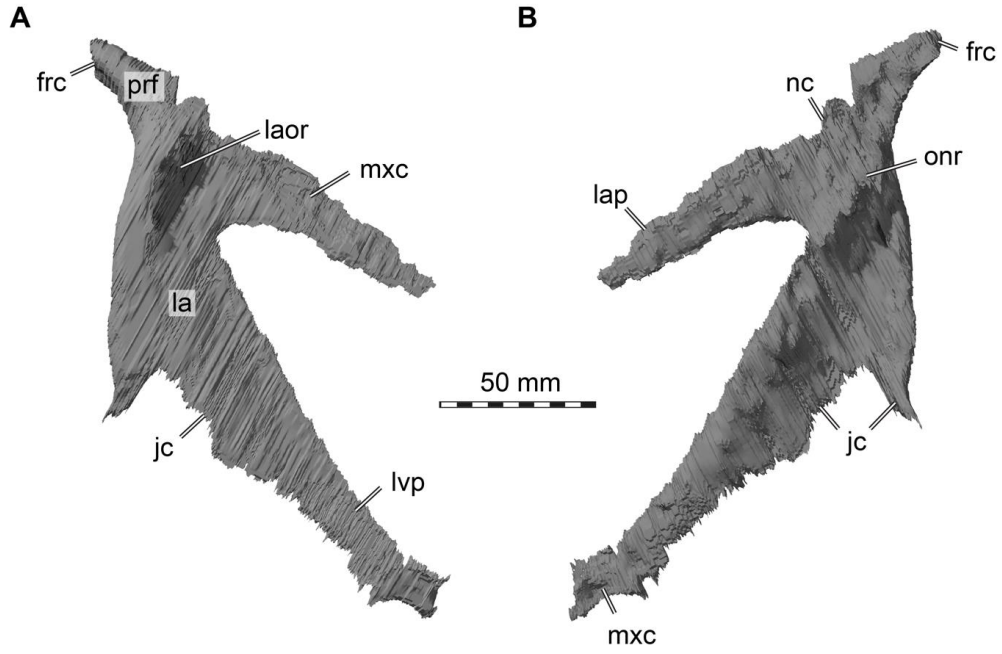

Figure 9. 3D renderings of the right lacrimal and prefrontal of *Irritator challengeri* (SMNS 58022). Note that sutures between these two bones could not be identified in the CT data, but externally visible sutures on the specimen show that these bones are only partially fused (see Figure 10). A, lateral view; B, medial view. Abbreviations: frc, frontal contact; jc, jugal contact; la, lacrimal; laor, lacrimal antorbital recess; lap, lacrimal anterior process; lvp, lacrimal ventral process; mxc, maxillary contact, nc, nasal contact; onr, orbitonasal ridge; prf, prefrontal.

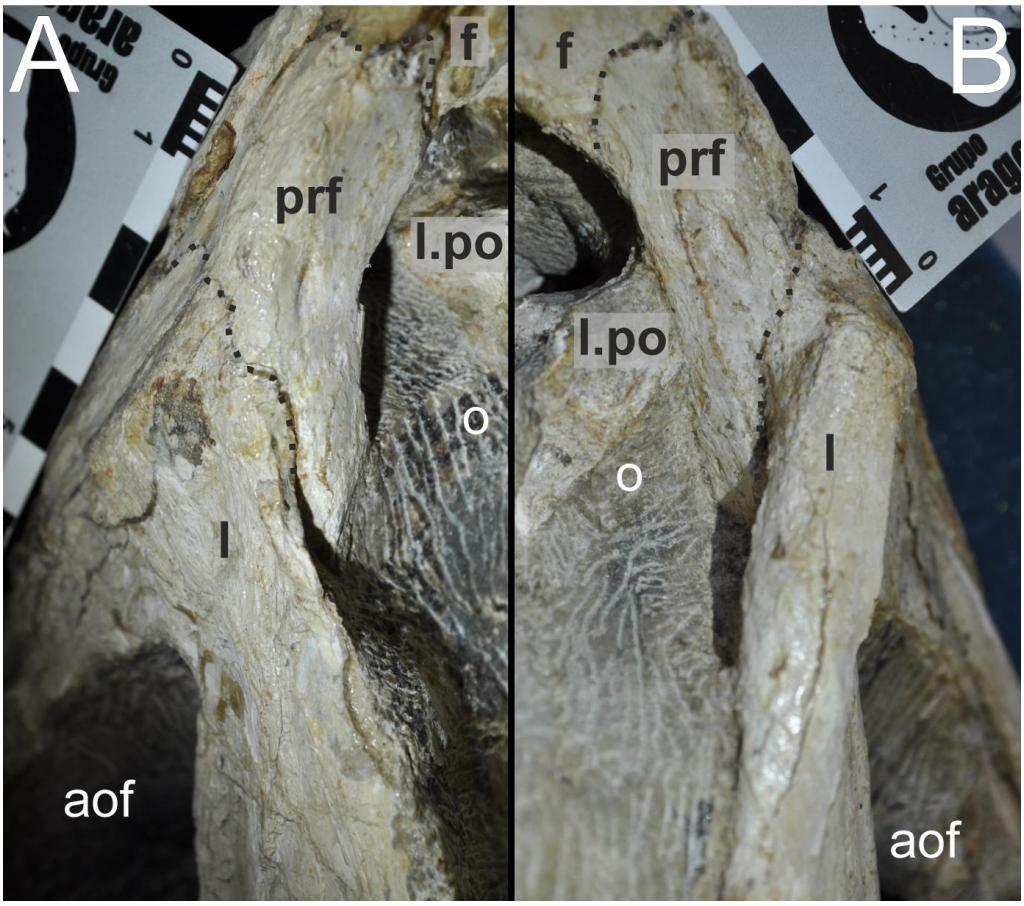

Figure 10. Close-up photographs of the lacrimal/prefrontal region of *Irritator challengeri* (SMNS 58022). A, left posterolateral view; B, right posteroventral view. Note that bones are labelled in bold, and other anatomical structures in regular font. Dashed lines mark sutures. Abbreviations: aof, antorbital fenestra; f, frontal; l, lacrimal; l.po, left postorbital; o, orbita; prf, prefrontal.

Figure 11. Olli's Dia.

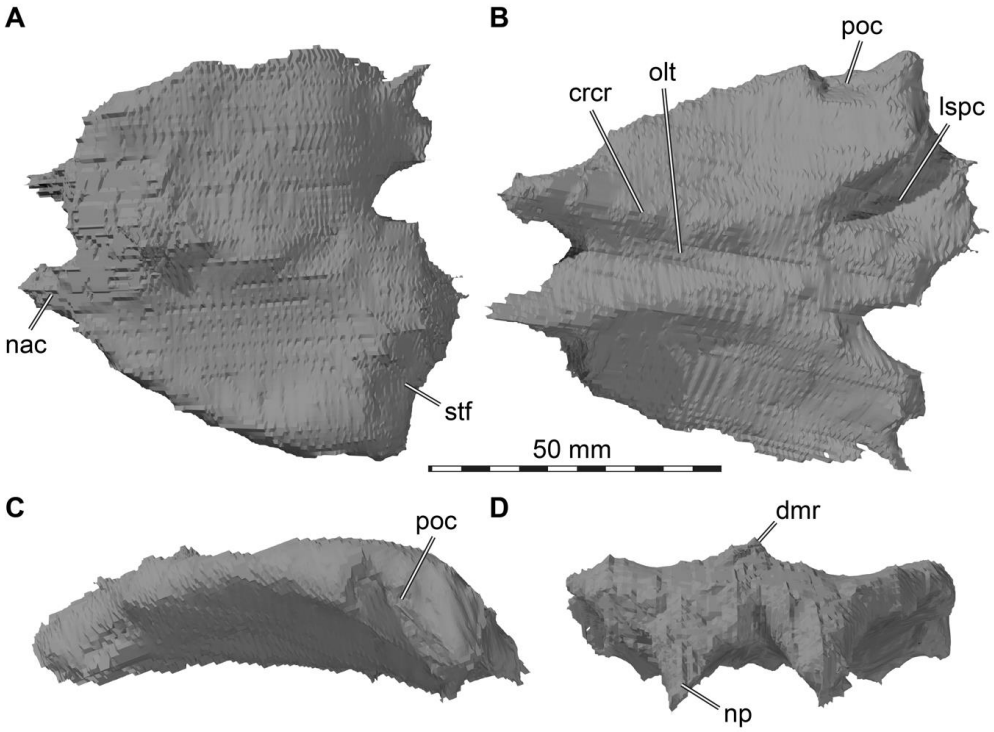

Figure 12. 3D renderings of the right and left frontals of *Irritator challengeri* (SMNS 58022). Note that the interfrontal contact could not be identified in the CT data, but externally visible sutures on the specimen show that these bones are only partially fused (see Figure 8). A, dorsal view; B, ventral view; C, left lateral view; D, anterior view. Abbreviations: crcr, crista cranii; dmr, dorsal median ridge; lspc, laterosphenoid contact; nac, nasal contact; np, nasal process; olt, olfactory tract, poc, postorbital contact, stf, supratemporal fossa.

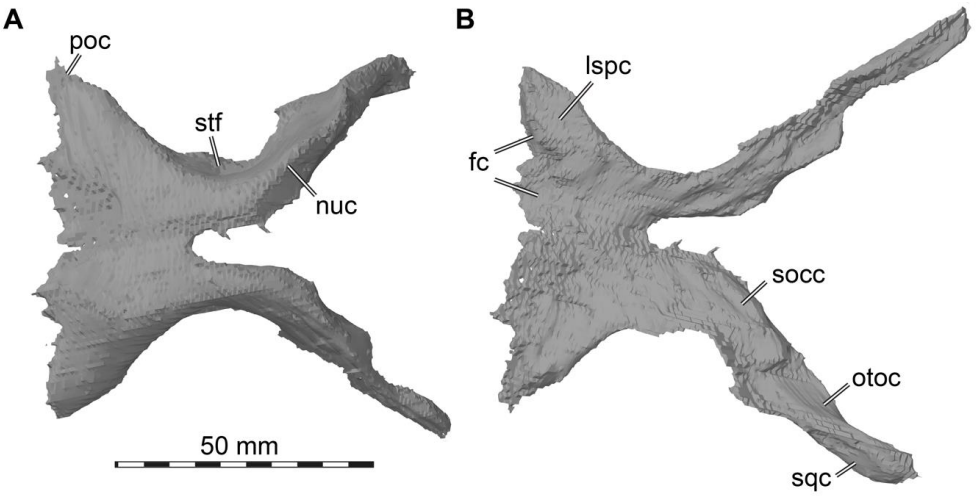

Figure 13. 3D renderings of the right and left parietals of *Irritator challengeri* (SMNS 58022). A, dorsal view; B, ventral view. Abbreviations: fc, frontal contact; lsp c, laterosphenoid contact; nuc, nuchal crest base; oto, otoccipital contact; poc, postorbital contact, socc, supraoccipital contact; stf, supratemporal fossa; sqc, squamosal contact.

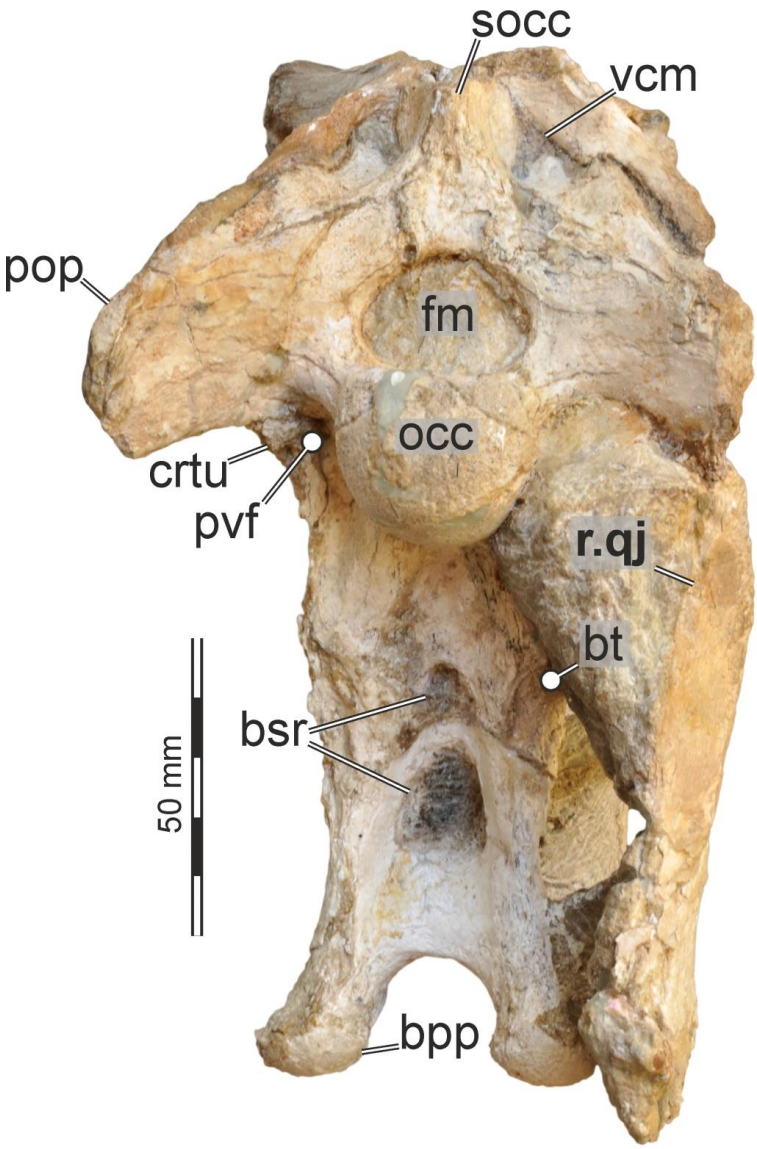

Figure 14. Photograph of the braincase of *Irritator challengeri* (SMNS 58022) in posterior view. Note that the bone is labelled in bold, and other anatomical structures in regular font. Abbreviations: bpp, basipterygoid process of parabasisphenoid; bsr, basisphenoid recess; bt, basal tubera; crtu, crista tuberalis; fm, foramen magnum; occ, occipital condyle; pop, paroccipital process; pvf, posterior vagal foramen; r.qj, right quadratojugal; socc, supraoccipital crest; vcm, vena capitis media foramen.

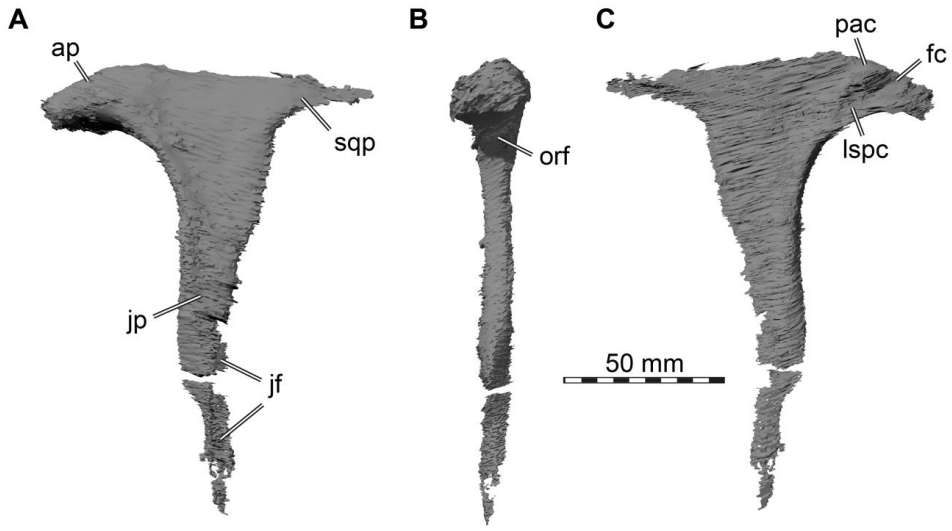

Figure 15. 3D renderings of the left postorbital of *Irritator challengeri* (SMNS 58022). A, lateral view; B, anterior view; C, medial view. Abbreviations: ap, anterior process; fc, frontal contact; jf, jugal facte; jp, postorbital jugal process; lspc, laterosphenoid contact; orf, orbital fossa; pac, parietal contact; sqp, squamosal process.

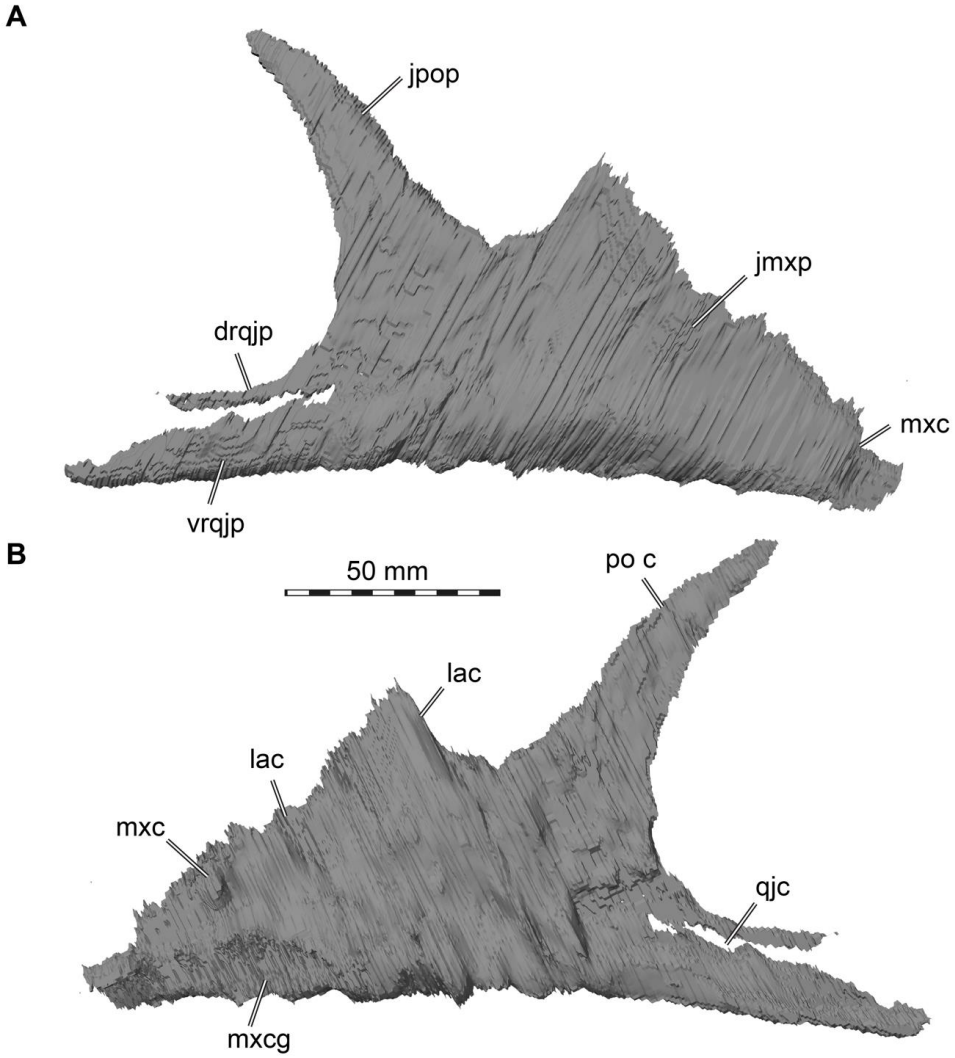

Figure 16. 3D renderings of the right jugal of *Irritator challengeri* (SMNS 58022). A, lateral view; B, medial view. Abbreviations: drqjp, dorsal ramus of quadratojugal process; jmxp, maxillary process; jpop, postorbital process; lac, lacrimal contact; mxc, maxillary contact; mxcg, maxillary contact groove; poc, postorbital contact; qjc, quadratojugal contact; vrqjp, ventral ramus of quadratojugal process.

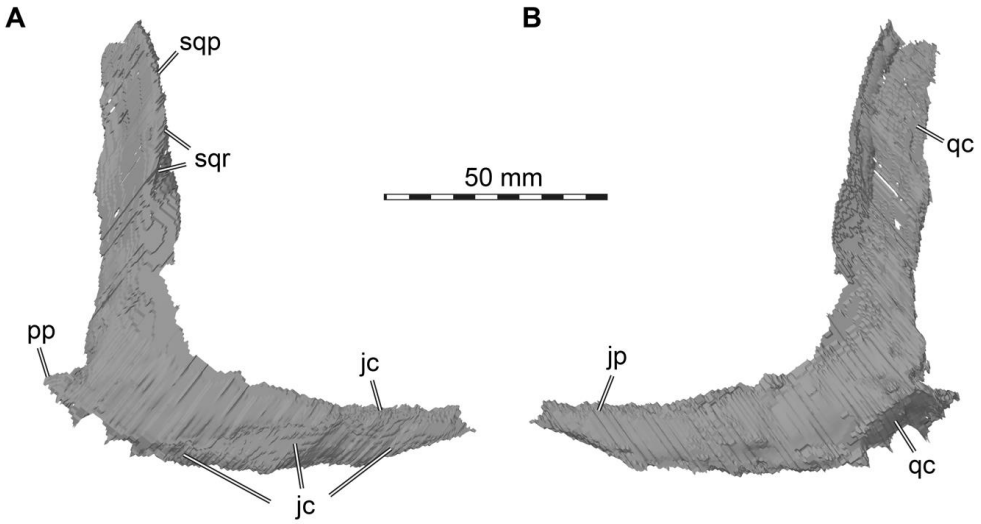

Figure 17. 3D renderings of the right quadratojugal of *Irritator challengeri* (SMNS 58022). A, lateral view; B, medial view. Abbreviations: jc, jugal contact; jp, jugal process; pp, posterior process; qc, quadrate contact; sqp, squamosal process; sqr, squamosal ridge.

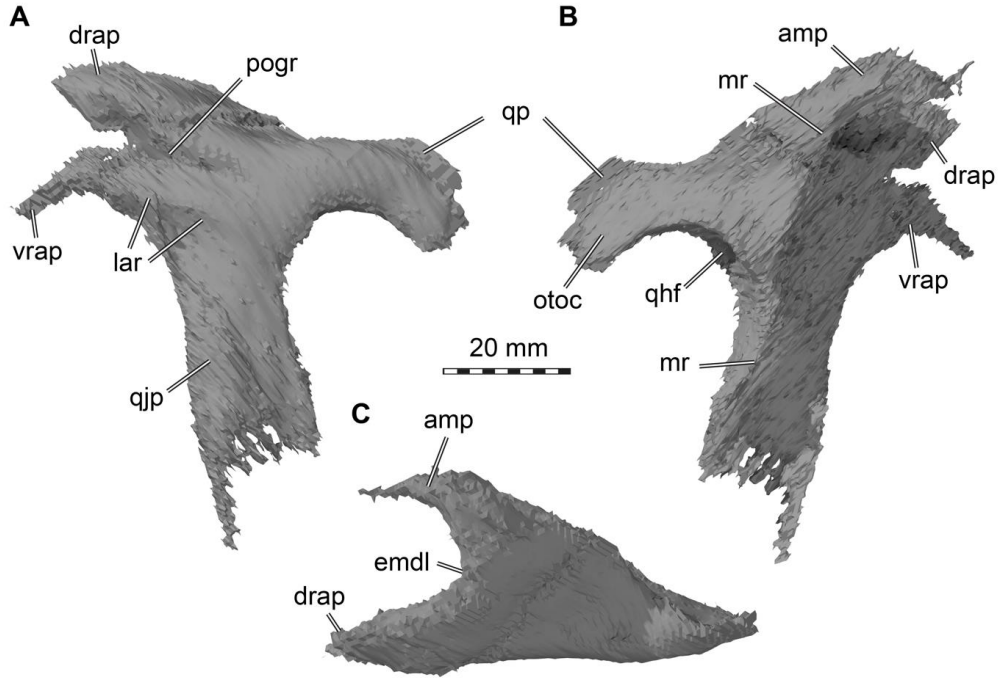

Figure 18. 3D renderings of the left squamosal of *Irritator challengeri* (SMNS 58022). A, lateral view; B, medial view; C, dorsal view. Abbreviations: amp, anteromedial process; drap, dorsal ramus of anterior process; emdl, emarginated dorsal lamina; lar, lateral ridge; mr, medial ridge; pogr, postorbital groove; qhf, quadrate head facet;

qjp, quadratojugal process; qp, quadrate process; vrap, ventral ramus of anterior process.

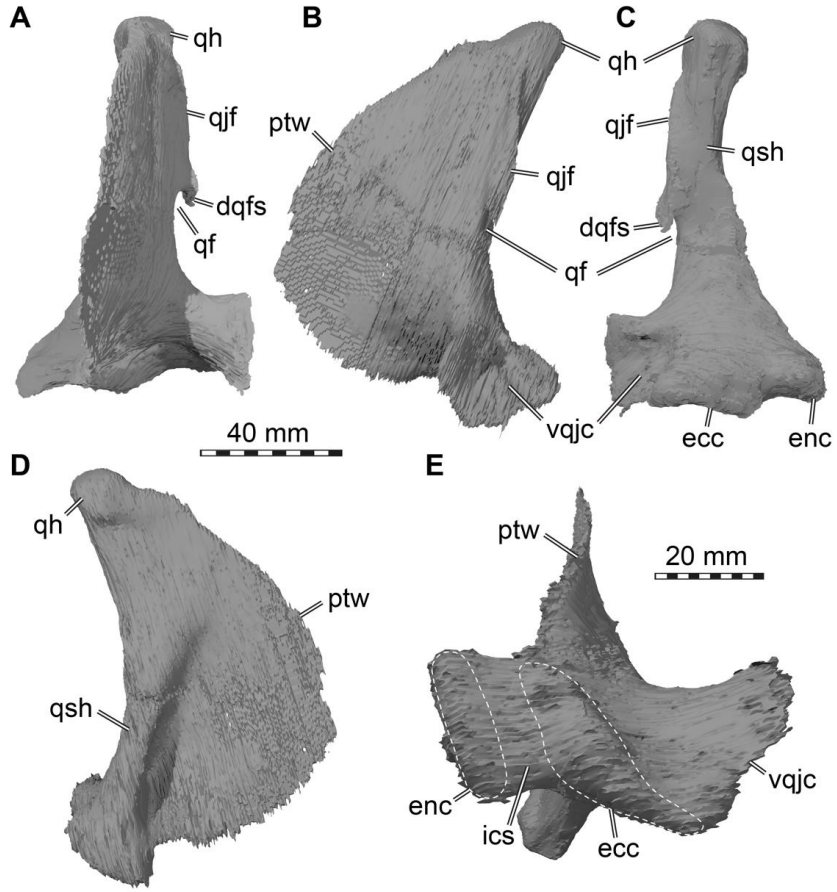

Figure 19. 3D renderings of the left quadrate of *Irritator challengeri* (SMNS 58022). A, anterior view; B, lateral view; C, posterior view; D, medial view; E, ventral view (anterior to top). Note that A–D are to same scale, E with separate scale bar. Dashed lines in D are approximate shapes of quadrate articulation condyles. Abbreviations: dqjf, dorsal quadratojugal flange; ecc, ectocondyle; enc, entocondyle; ics, intercondylar sulcus; ptw, pterygoid wing; qh, quadrate head; qf, quadrate foramen; qfs, quadrate foamen spur; qsh, quadrate shaft; vqjc, ventral quadratojugal contact.

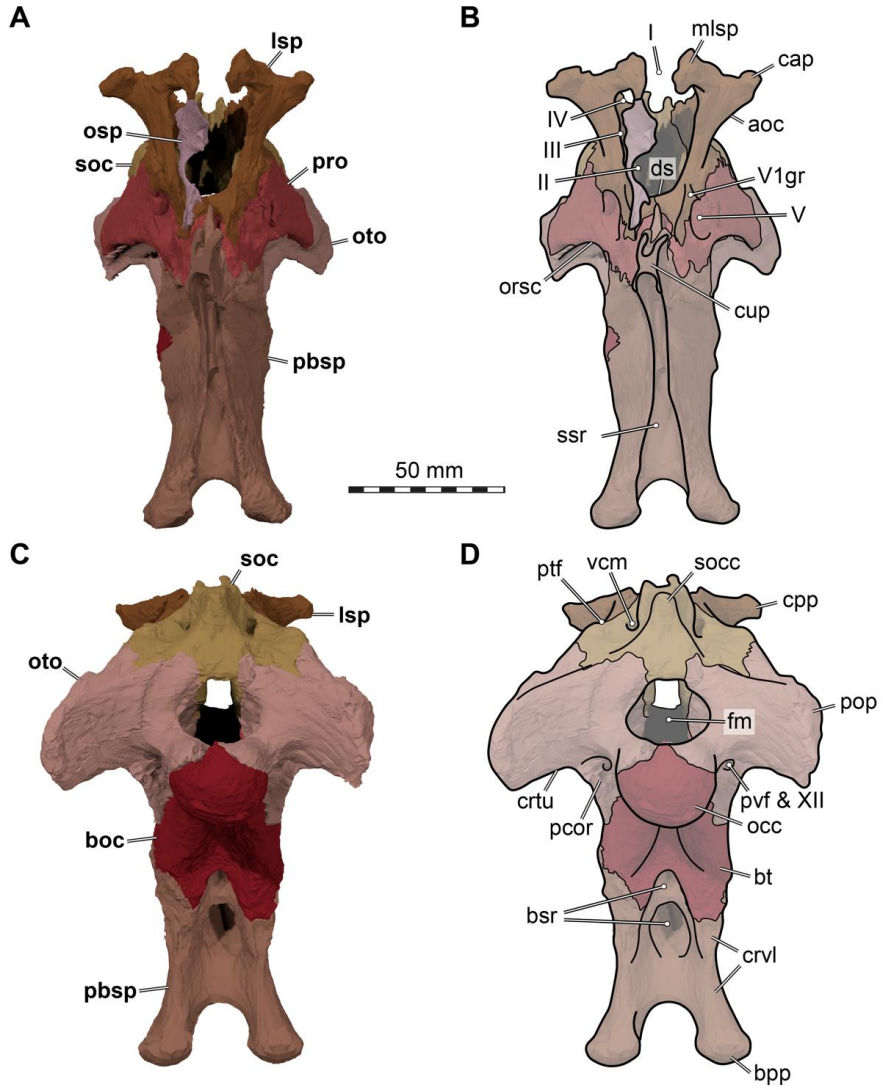

Figure 20. 3D renderings of the articulated braincase elements of *Irritator challengeri* (SMNS 58022). A, anterior view; B, anterior view with interpretative line drawings; C, posterior view; D, posterior view with interpretative line drawings. Note that bones are labelled in bold, and other anatomical structures in regular font. Abbreviations: aoc, antotic crest; boc, basioccipital; bpp, basipterygoid process; bsr, basisphenoid recess; bt, basal tuber; cap, capitate process; crtu, crista tuberalis; crvl, crista ventrolateralis; cup, cultriform process; ds, dorsum sellae; fm, foramen magnum; lsp, laterosphenoid; mlsp, medial laterosphenoid process; occ, occipital condyle; osp, orbitosphenoid; oto, otoccipital; orsc, orbitosphenoidal crest; pbsp, parabasisphenoid; pcor, paracondylar recess; pop, paroccipital process; pro, prootic; ptf, posttemporal fenestra; pvf & XII, are for posterior vagal foramen and hypoglossal nerves (CN XII), see Figure 23 for details of this region; soc, supraoccipital; socc, supraoccipital crest; ssr, subsellar recess; vcm, vena capitis media foramen; I, olfactory nerve foramen (CN I); II, optic nerve foramen (CN II); IV, trochlear nerve foramen (CN IV); V, trigeminal nerve foramen (CN V); V_1gr, ophthalmic groove for V_1 branch.

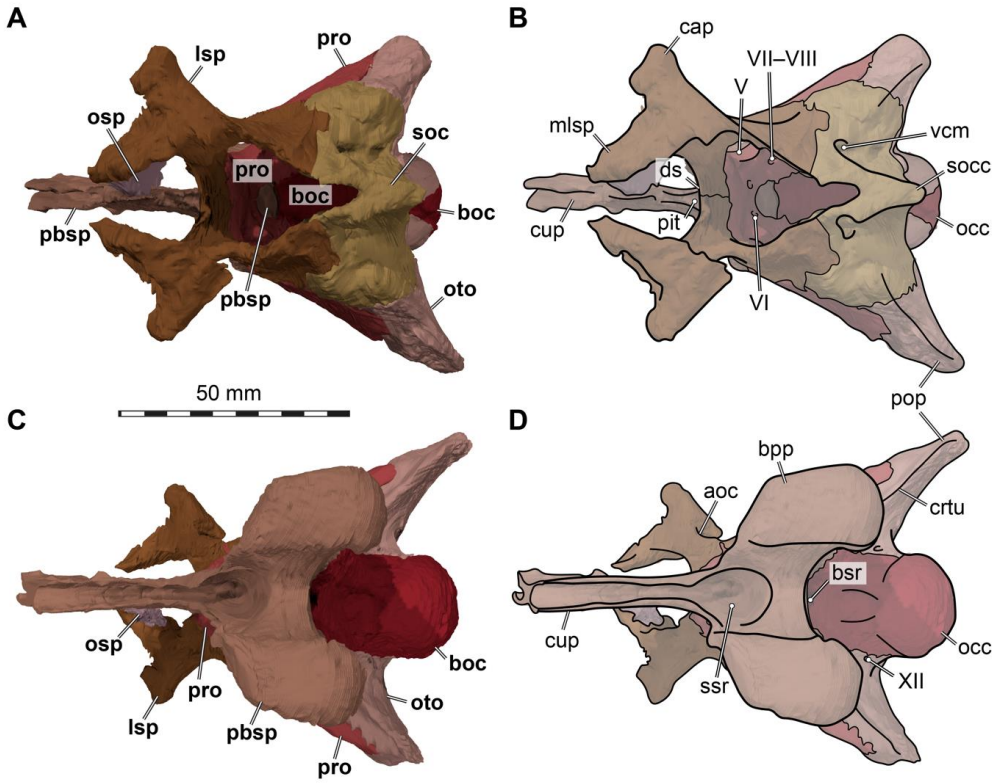

Figure 21. 3D renderings of the articulated braincase elements of *Irritator challengeri* (SMNS 58022). A, dorsal view; B, dorsal view with interpretative line drawings; C, ventral view; D, ventral view with interpretative line drawings. Note that bones are labelled in bold, and other anatomical structures in regular font. Abbreviations: aoc, antotic crest; boc, basioccipital; bpp, basipterygoid process; bsr, basisphenoid recess; cap, capitate process; crtu, crista tuberalis; cup, cultriform process; ds, dorsum sellae; lsp, laterosphenoid; mlsp, medial laterosphenoid process; occ, occipital condyle; osp, orbitosphenoid; oto, otoccipital; pbsp, parabasisphenoid; pit, pituitary fossa (sella turcica); pop, paroccipital process; pro, prootic; soc, supraoccipital; socc, supraoccipital crest; ssr, subsellar recess; vcm, vena capitis media foramen; V, trigeminal nerve (CN V) foramen; VI, (posterior) foramen for abducens nerve (CN VI); VII–VIII, medial fossa for entry of facial nerve (CN VII) and optic nerve (CN VIII) into prootic; XII, foramen for the hypoglossal nerve (CN XII).

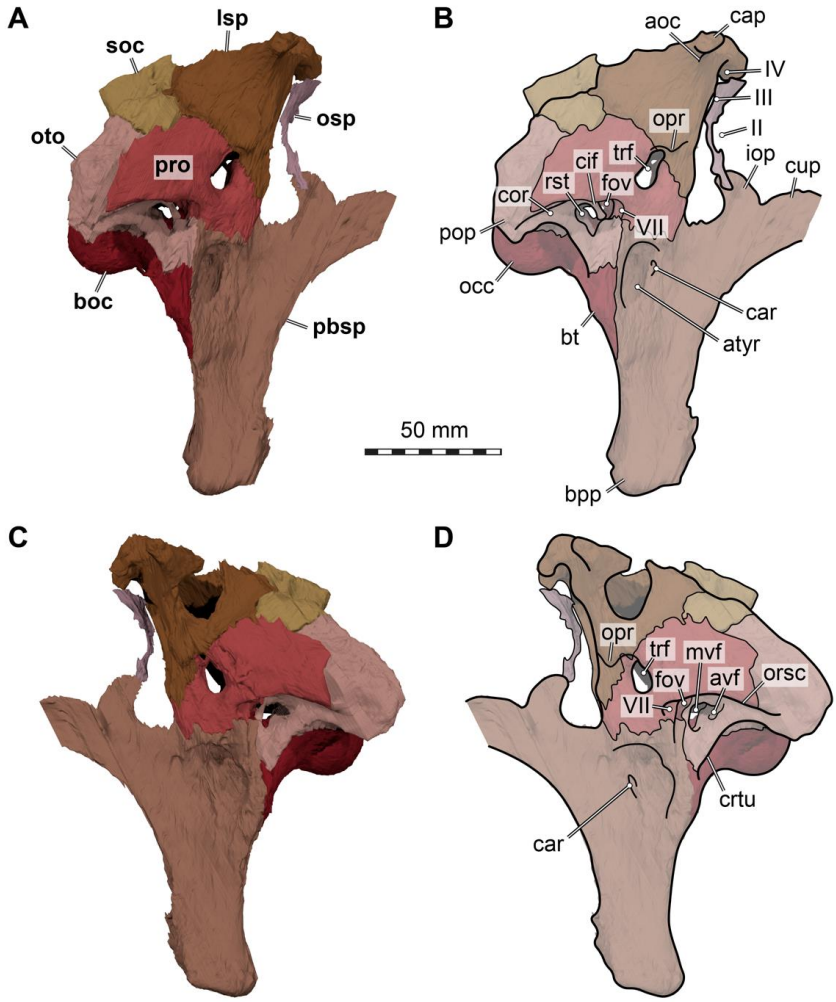

Figure 22. 3D renderings of the articulated braincase elements of *Irritator challengeri* (SMNS 58022). A, right lateral view; B, right lateral view with interpretative line drawings; C, left lateral view; D, left lateral view with interpretative line drawings. Note that bones are labelled in bold, and other anatomical structures in regular font. Abbreviations: aoc, antotic crest; atyr, anterior tympanic recess; avf, (anterior) vagal foramen (connecting recessus scalae tympani region with paracondylar recess via a vagal canal); boc, basioccipital; bt, basal tuber; cap, capitate process; car, external foramen for the internal carotid artery (=vidian) canal; cor, columella recess; cif, crista interfenestralis; crtu, crista tuberalis; cup, cultriform process; fov, fenestra ovalis;; iop, interorbital process of the parabasisphenoid; lsp, laterosphenoid; mvf, medial vagal foramen (connecting brain cavity with recessus scalae tympani); occ, occipital condyle; opr, ophthalmic ridge defining groove for ophthalmic branch (CN V_1); oto, otoccipital; orsc, orbitosphenoidal crest; pbsp, parabasisphenoid; pop, paroccipital process; pro, prootic; rst, recessus scalae tympani/tympanic region of middle ear; soc, supraoccipital; II, medially open foramen for optic nerve (CN II); III, foramen for oculomotor nerve (CN III); IV, foramen for trochlear nerve (CN IV); V, trigeminal nerve foramen (CN V); VII, foramen for the facial nerve (CN VII).

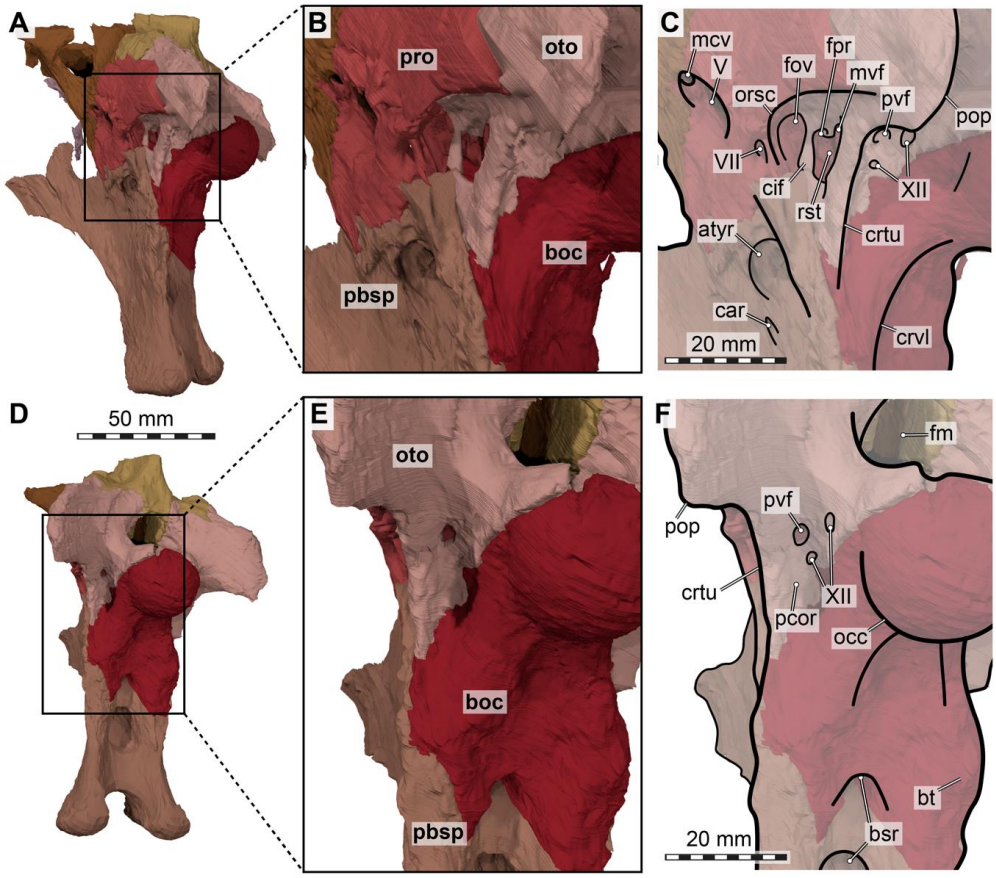

Figure 23. 3D renderings of the articulated braincase elements of *Irritator challengeri* (SMNS 58022). A, slightly posteriorly rotated view of left side; B, detailed view on tympanic region; C, as B, with interpretative line drawings; D, strongly posteriorly rotated view of left side; E, detailed view on paracondylar region; F, as E, with interpretative line drawings. Note that bones are labelled in bold, and other anatomical structures in regular font. Abbreviations: atyr, anterior tympanic recess; boc, basioccipital; bsr, basisphenoid recess; bt, basal tuber; car, external foramen for the internal carotid artery (=vidian) canal; cif, crista interfenestralis; crtu, crista tuberalis; crvl, crista ventrolateralis; fm, foramen magnum; fov, fenestra ovalis; fpr, fenestra pseudorotunda (anteroposterior opening between labyrinth cavity and recessus scalae tympani); lsp, laterosphenoid; mcv, mid cerebral vein foramen; mvf, medial vagal foramen (connecting brain cavity with recessus scalae tympani); occ, occipital condyle; oto, otoccipital; orsc, orbitosphenoidal crest; pbsp, parabasisphenoid; pcor, paracondylar recess; pop, paroccipital process; pro, prootic; pvf, posterior vagal foramen; rst, recessus scalae tympani/tympanic region of middle ear; socc, supraoccipital crest; V, trigeminal nerve foramen (CN V); VII, foramen for the facial nerve (CN VII); XII, foramina for the hypoglossal nerves (CN XII).

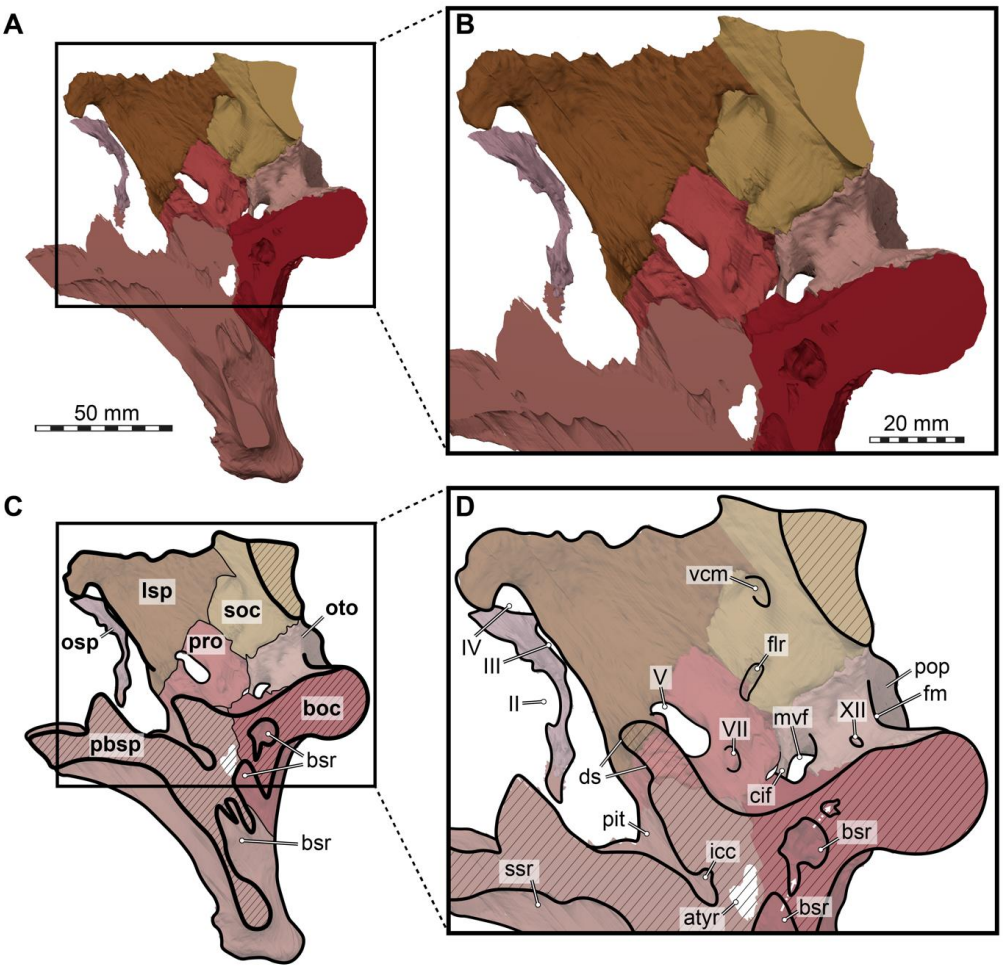

Figure 24. 3D renderings of the sagitally sectioned articulated braincase elements of the right side of *Irritator challengeri* (SMNS 58022) in medial view. A, complete rendering of right side; B, detailed view endocranial cavity; C, as A, with interpretative line drawings; D, as B, with interpretative line drawings. Note that bones are labelled in bold, and other anatomical structures in regular font. White arrows indicate internal connections of basisphenoid recess not covered in section. Abbreviations: atyr, anterior tympanic recess; boc, basioccipital; bsr, basisphenoid recess; cif, crista interfenestralis; ds, dorsum sellae; flr, floccular recess opening; fm, foramen magnum; icc, internal carotid artery (=vidian) canal;; lsp, laterosphenoid; mvf, medial vagal foramen (connecting brain cavity with recessus scalae tympani); oto, otoccipital; pbsp, parabasisphenoid; pit, pituitary fossa; pop, paroccipital process; pro, prootic; soc, supraoccipital; ssr, subsellar recess; vcm, vena capitis media foramen; II, medially open foramen for optic nerve (CN II); III, foramen for oculomotor nerve (CN III); IV, foramen for trochlear nerve (CN IV); V, trigeminal nerve foramen (CN V); VII, foramen for the facial nerve (CN VII); XII, foramina for the hypoglossal nerves (CN XII).

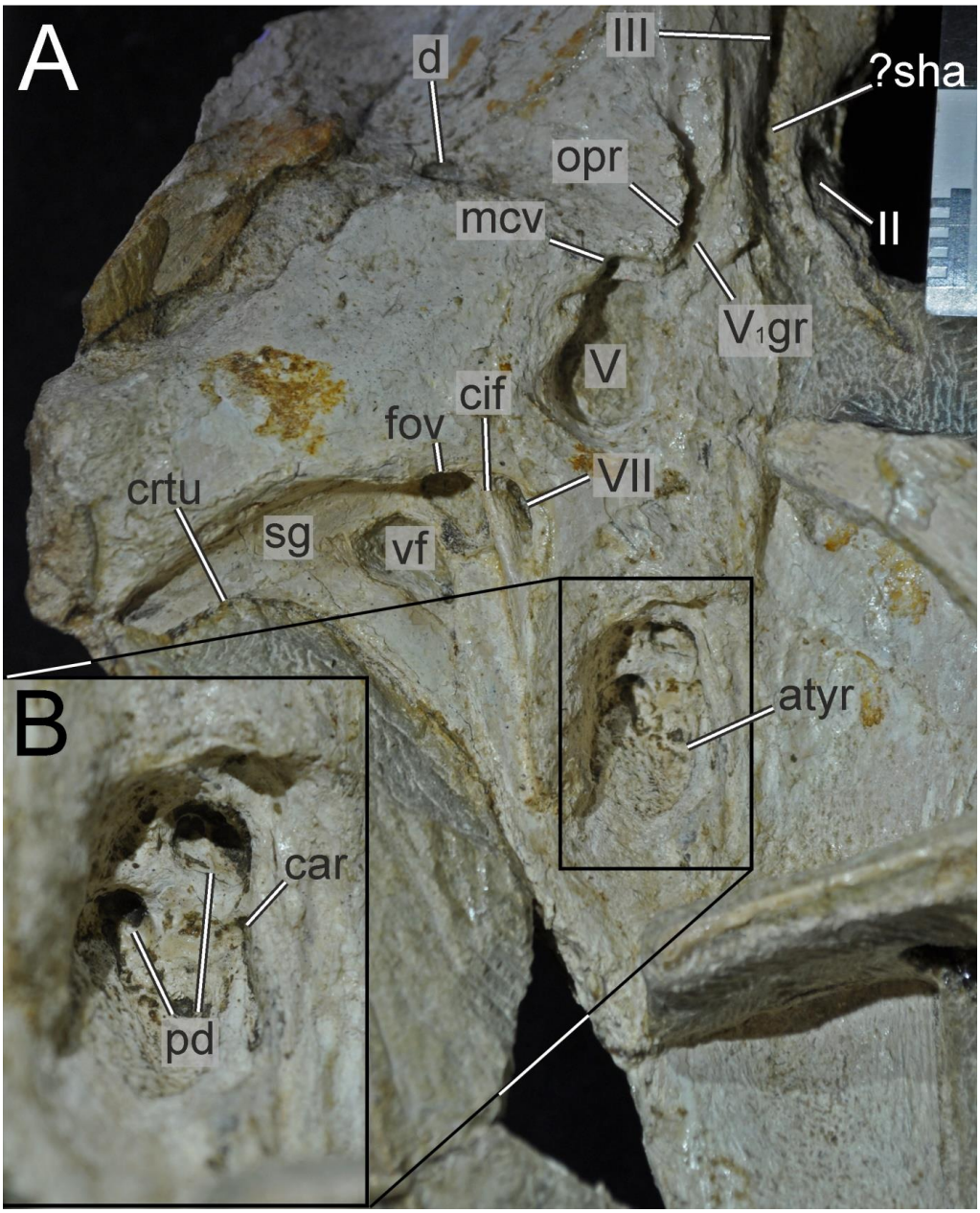

Figure 25. Close-up photographs of right lateral braincase of *Irritator challengeri* (SMNS 58022). A, right lateral view; B, magnified anterior tympanic recess. Note that bones are labelled in bold, and other anatomical structures in regular font. Abbreviations: atyr, anterior tympanic recess; car, external foramen for the internal carotid artery (=vidian) canal; cif, crista interfenestralis; crtu, crista tuberalis; d, damage; fov, fenestra ovalis; mcv, mid cerebral vein foramen; opr, ophthalmic ridge defining groove for ophthalmic branch (CN V_1); pd, (blind) pneumatic depression; sg, stapedial groove; vf, (lateral) vagal foramen; ?sha, potential sphenoidal artery opening; II, medially open foramen for optic nerve (CN II); III, foramen for oculomotor nerve (CN III); V, trigeminal nerve foramen (CN V); V_1gr, ophthalmic groove for V_1 branch; VII, foramen for the facial nerve (CN VII).

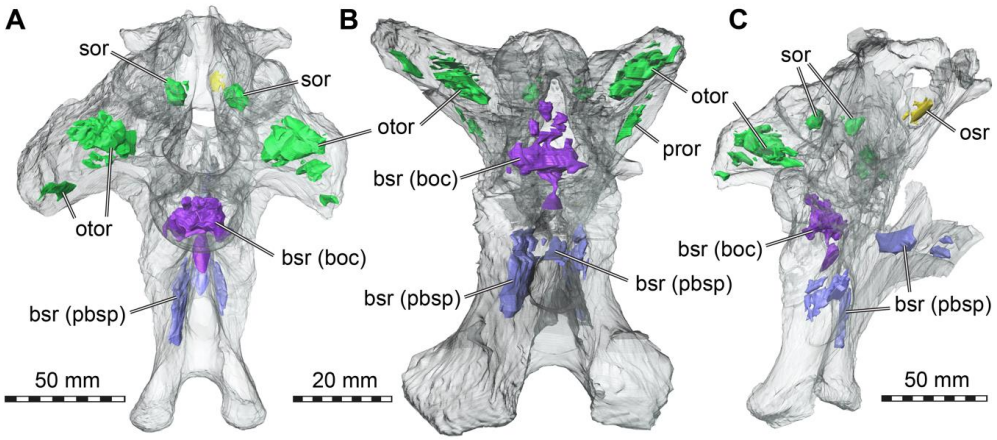

Figure 26. 3D renderings of the intracranial cavities within the articulated braincase of *Irritator challengeri* (SMNS 58022). A, posterior view; B, ventral view; C, right anterolateral view. Colours reflect cavity identity, whereas green cavities are within the otic bones, purple cavities are within the basioccipital, blue cavities are within the parabasisphenoid, and yellow recesses are within the orbitosphenoid. Abbreviations: bsr, basisphenoid recess; osr, orbitosphenoid recess; otot, otoccipitical recess; pror, prootic recess; sor, supraoccipital recess.

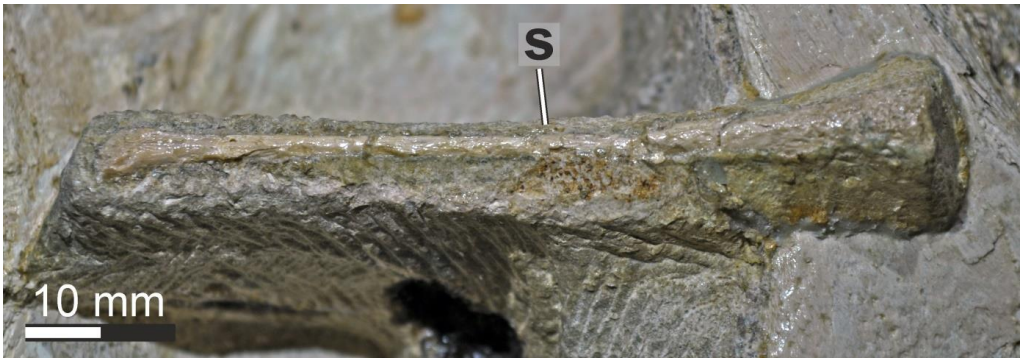

Figure 27. Close-up photograph of the stapes of *Irritator challengeri* (SMNS 58022). Abbreviation: s, stapes.

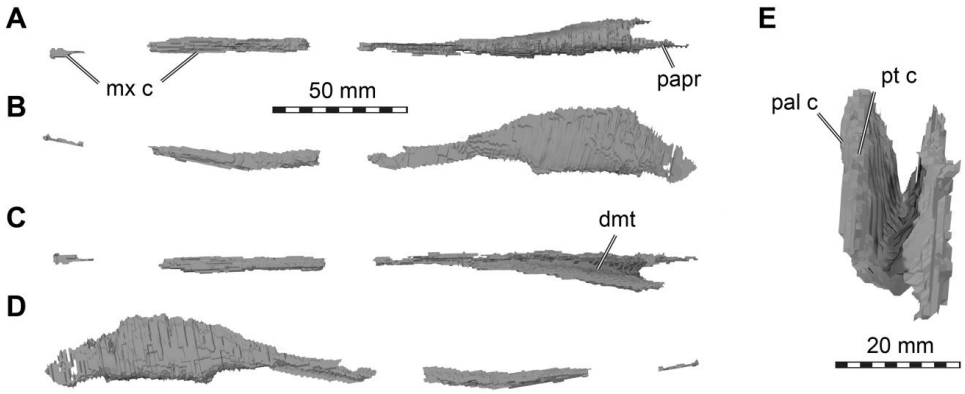

Figure 28. 3D renderings of the vomer of *Irritator challengeri* (SMNS 58022). A, ventral view (anterior to left); B, left lateral view; C, dorsal view (anterior to left); D, right lateral view; E, posterior view. Note different scale in E. Abbreviations: dmt, dorsomedian trough of vomer; mxc, maxillary contact, palc, palatine contact; papr, posterior articular process of vomer; ptc, pterygoid contact.

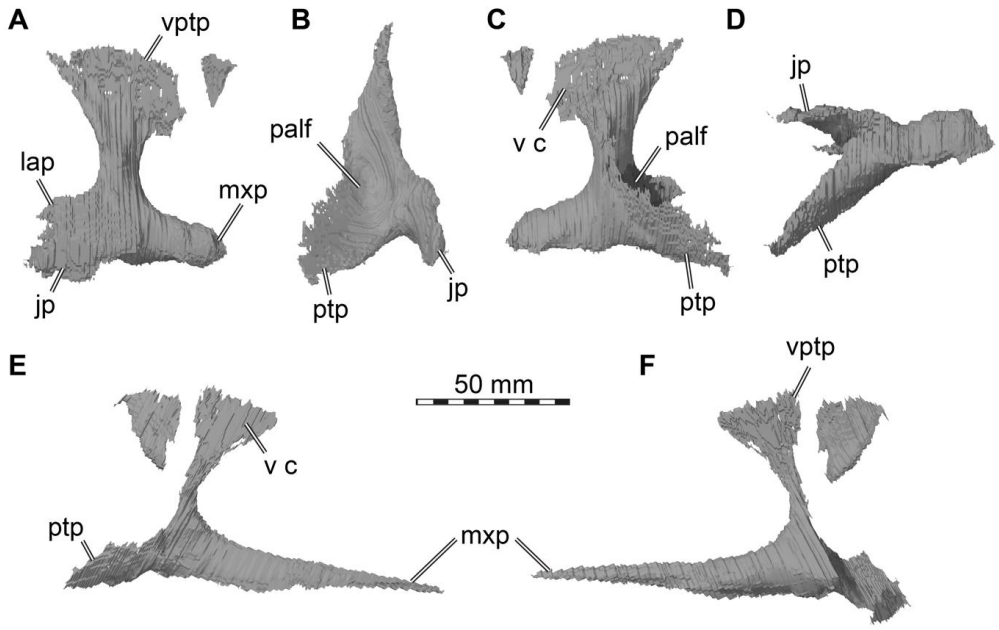

Figure 29. 3D renderings of the palatines of *Irritator challengeri* (SMNS 58022). A–D, right palatine in A, lateral view; B, posterior view; C, medial view; D, ventral view (anterior direction to the right). E–F. left palatine in E, medial view; F, lateral view. Abbreviations: jp, jugal process; lap, lacrimal process; mxp, maxillary process; palf, posterior palatine fossa; ptp, pterygoid process; vc, surface for contact with vomer; vptp, vomeropterygoid process.

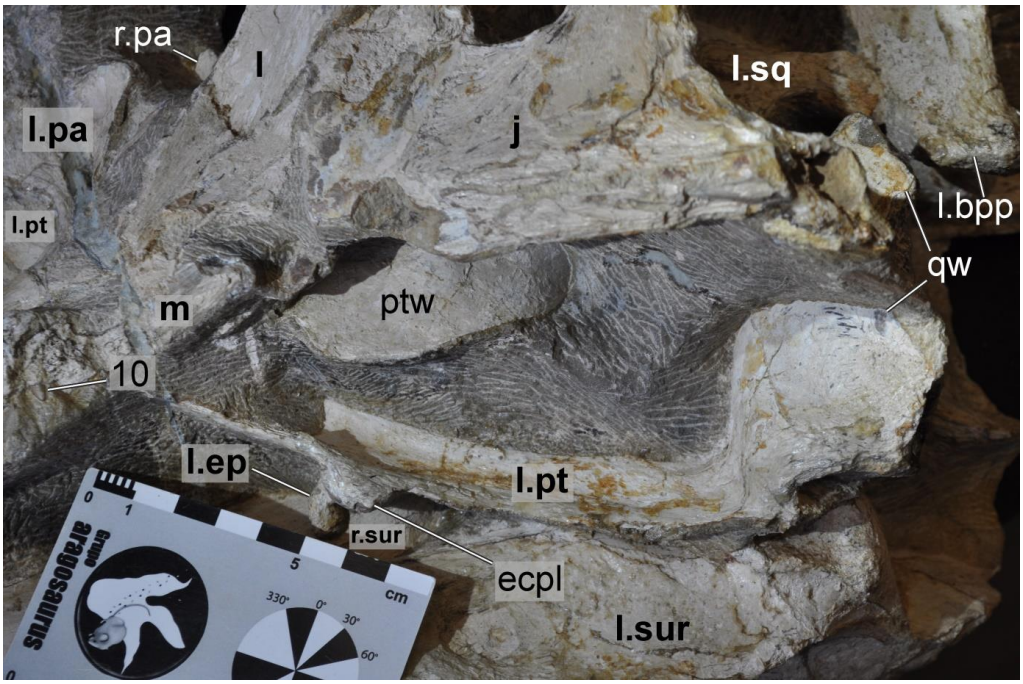

Figure 30. Close-up photograph of the left cheek region of *Irritator challengeri* (SMNS 58022). Note that bones are labelled in bold, and other anatomical structures in regular font. Abbreviations: j, jugal; l, lacrimal; l.ep, left ectopterygoid; ecpl, ectopterygoid lamina of the left pterygoid; l.bpp, left basipterygoid process of the parabasisphenoid; l.sur, left surangular; l.sq, left squamosal; l.pa, left palatine; l.pt, left pterygoid; m, maxilla; n, nasal; ptw, pterygoid wing of left quadrate; qw, quadrate wing of left pterygoid; r.pa, right palatine; r.sur, right surangular; 10, tenth preserved tooth position of the left maxilla.

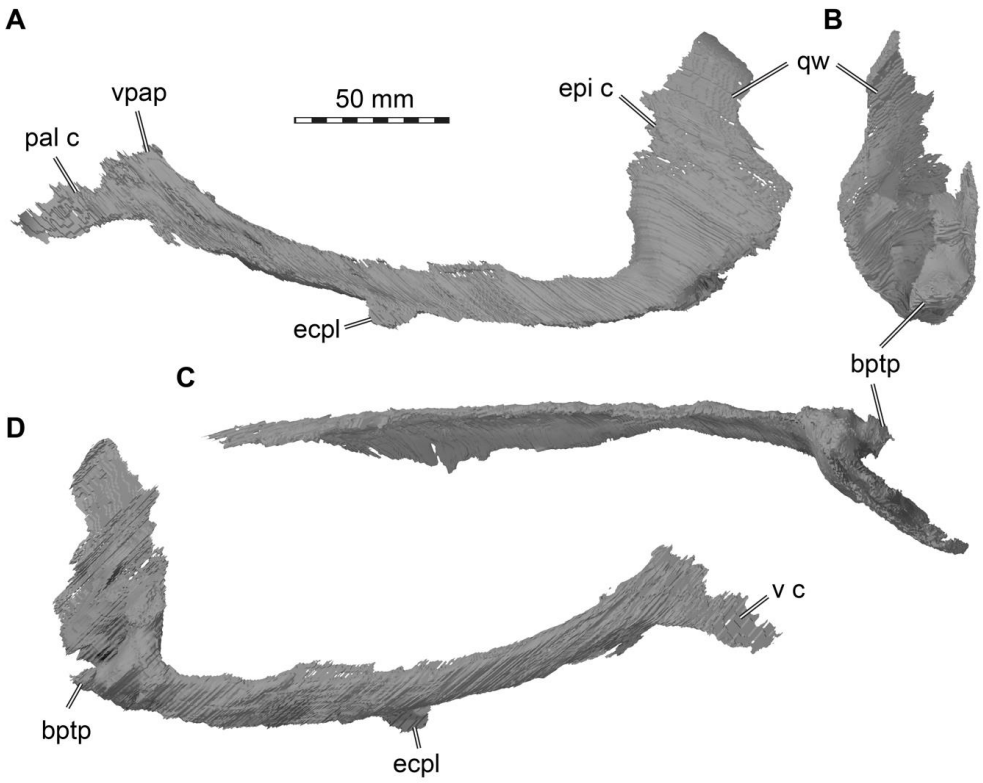

Figure 31. 3D renderings of the left pterygoid of *Irritator challengeri* (SMNS 58022). A, lateral view; B, posterior view; C, dorsal view; D, medial view. Abbreviations: bptp, basipterygoid process; ecpl, ectopterygoid lamina; epic, epipterygoid contact; palc, palatine contact; qw, quadrate wing; vc, vomer contact; vpap, vomeropalatine process.

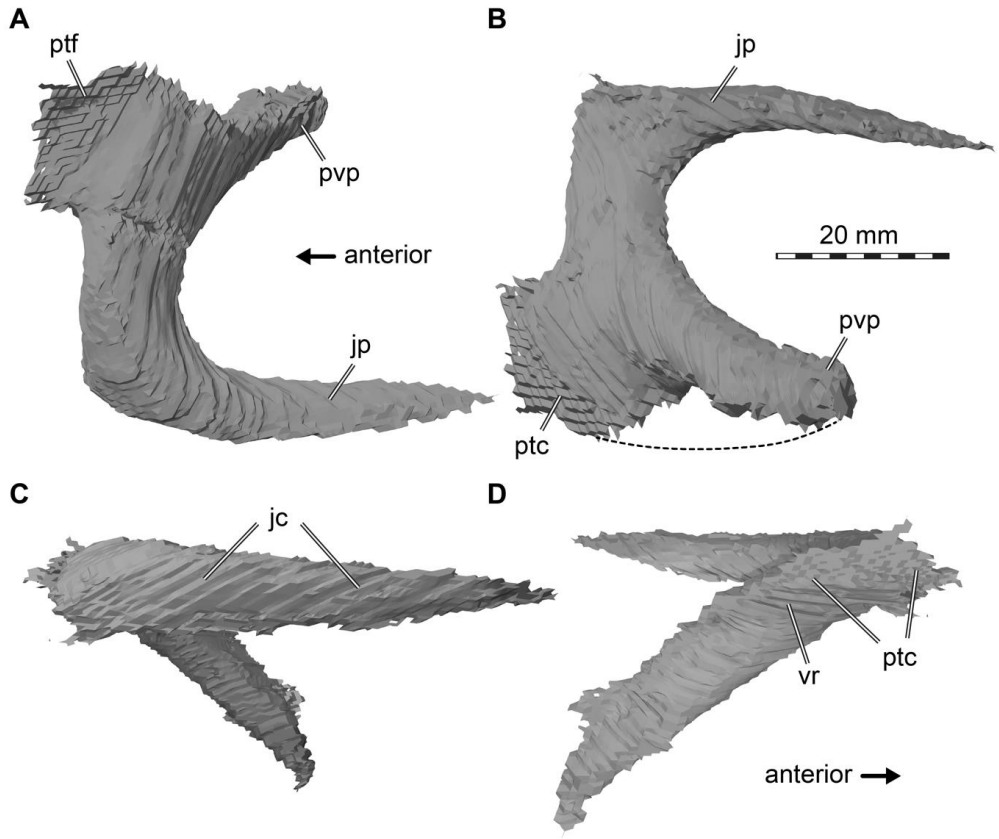

Figure 32. 3D renderings of the left ectopterygoid of *Irritator challengeri* (SMNS 58022). A, dorsal view; B, ventral view; C, lateral view; D, medial view. Arrow in A valid for A-C. Note that dashed line indicates approximate former extent of bone. Abbreviations: jc, jugal contact; jp, jugal process; ptc, pterygoid contact; ptf, pterygoid flange; pvp, posteroventral process; vr, ventral recess.

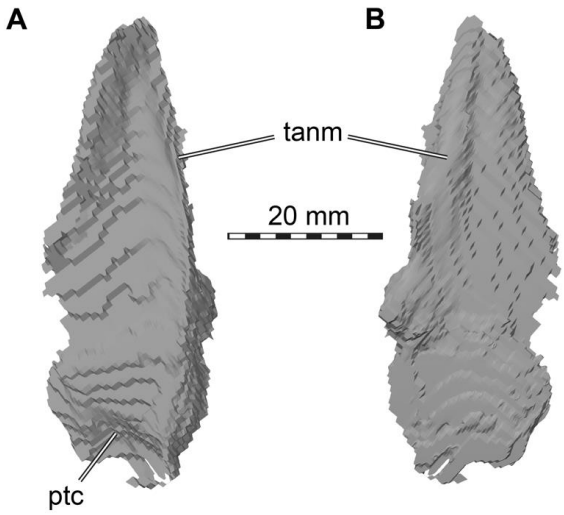

Figure 33. 3D renderings of the left epipterygoid of *Irritator challengeri* (SMNS 58022). A, medial view; B, lateral view. Abbreviations: tanm, thickenend anterior margin; ptc, pterygoid contact.

view. Abbreviations: tanm, thickenend anterior margin; ptc, pterygoid contact.

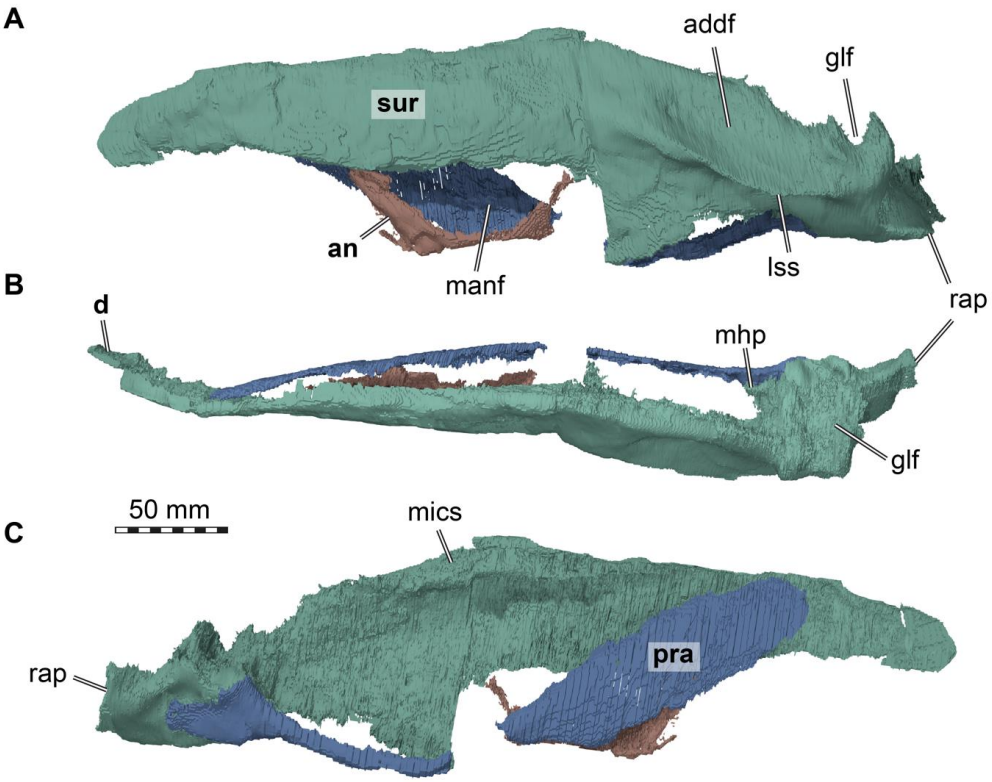

Figure 34. 3D renderings of left mandibular elements of *Irritator challengeri* (SMNS 58022). A, lateral view; B, dorsal view; C, medial view. Abbreviations: addf, adductor fossa; an, angular; d, dentale; glf, glenoid fossa; lss, lateral surangular shelf; manf, mandibular fenestra; mhp, medial hook process; mics, medially inclined coronoid shelf; pra, prearticular; rap, retroarticular process; sur, surangular. Note that different bones are rendered in different colours, and that bone labels are in bold. Also note that the articular is fused with the surangular and thus segmented in a joint model with that bone.

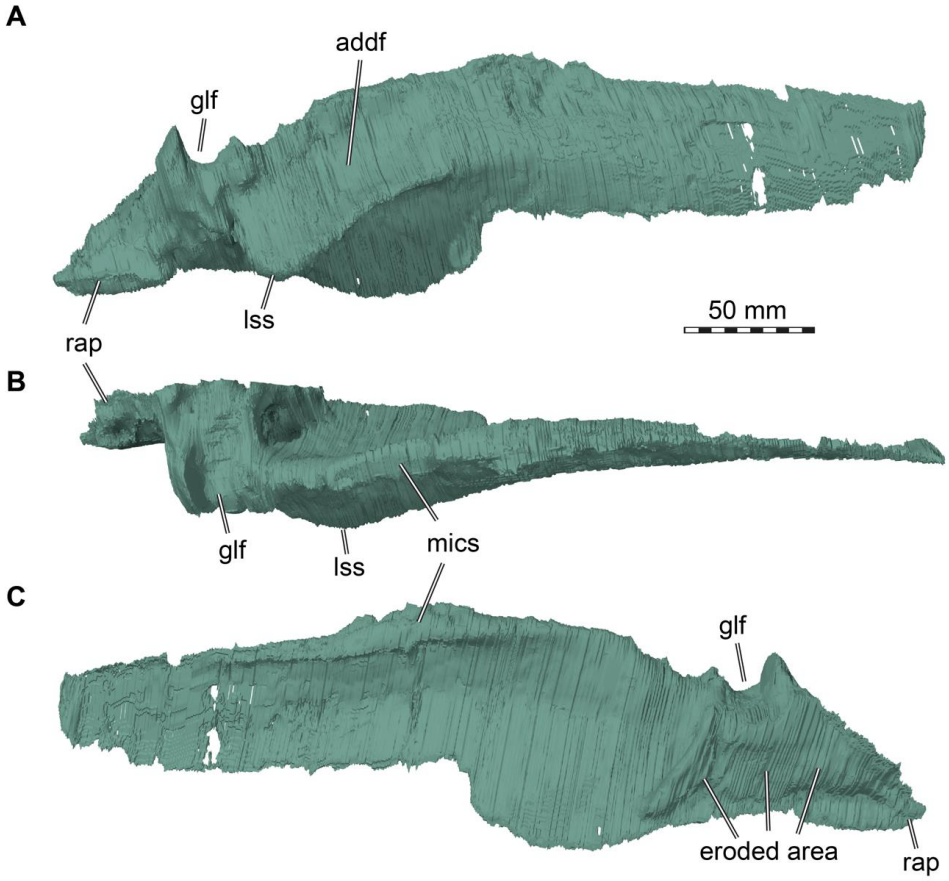

Figure 35. 3D renderings of right surangular of *Irritator challengeri* (SMNS 58022). A, lateral view; B, dorsal view; C, medial view. Abbreviations: addf, adductor fossa; glf, glenoid fossa; lss, lateral surangular shelf; mics, medially inclined coronoid shelf; rap, retroarticular process. Note that the articular is fused with the surangular and thus segmented in a joint model with that bone.

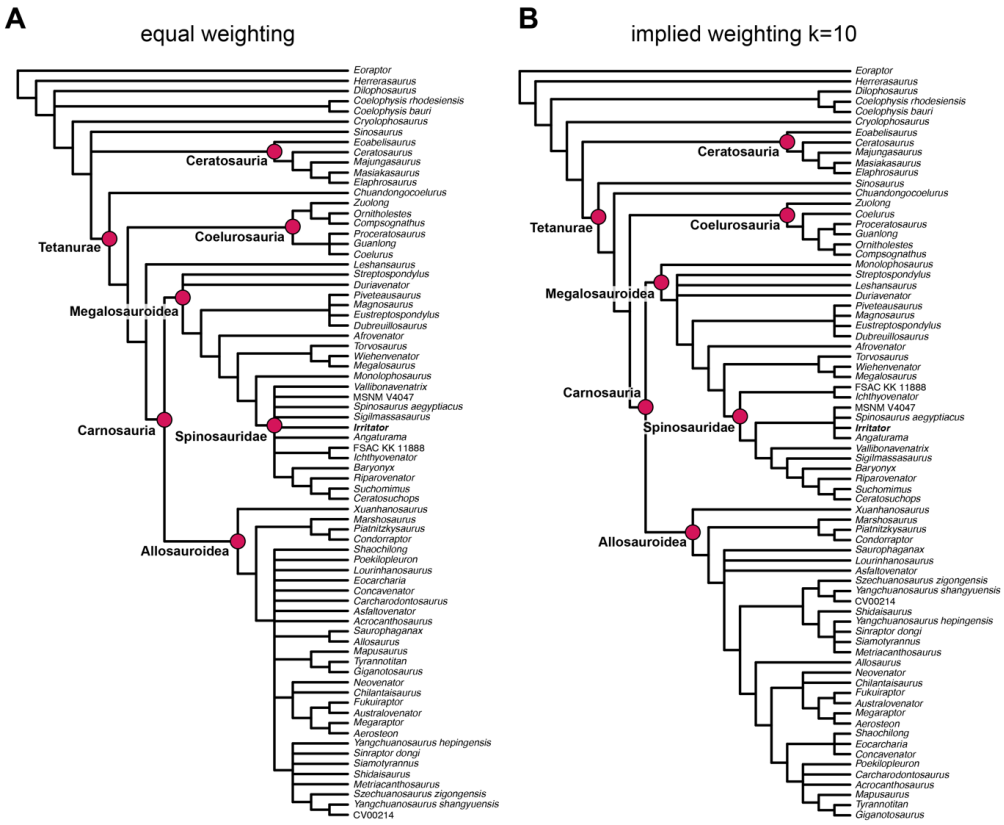

Figure 36. Phylogenetic results from parsimony analysis using the full dataset. A, strict consensus tree of 8184 MPTs retained from an equal weighting analysis (see methods for details); B, strict consensus tree of 406 MPTs retained from an implied weighting analysis using a concavity constant of k=10 (see methods for details). Important clades are labelled. *Irritator* as the main focus of our study is highlighted in bold face among the clade Spinosauridae.

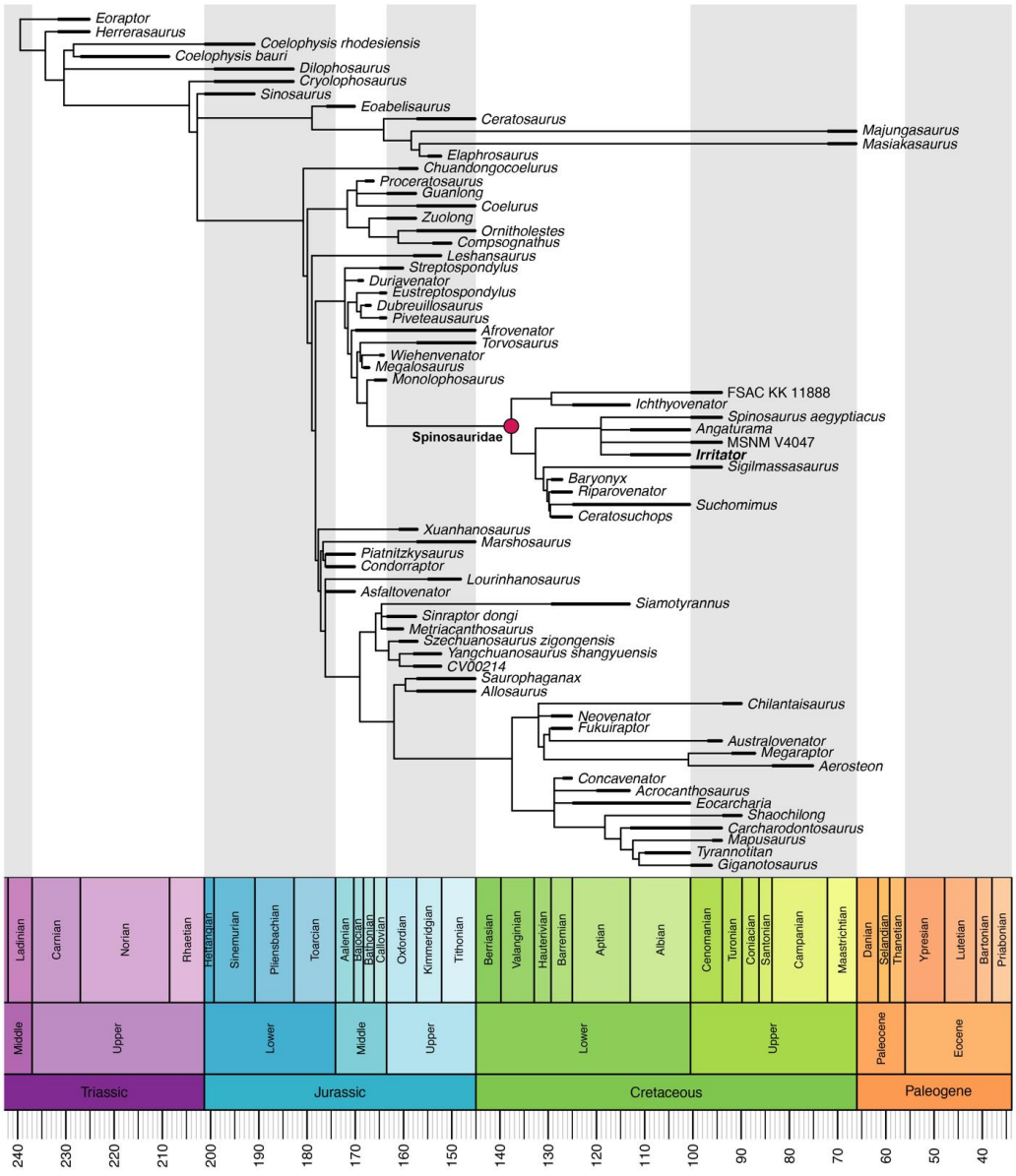

Figure 37. Reduced consensus tree for the full dataset, scaled to geologic time (see methods for details). *Irritator* as the main focus of our study is highlighted in bold face among the clade Spinosauridae.

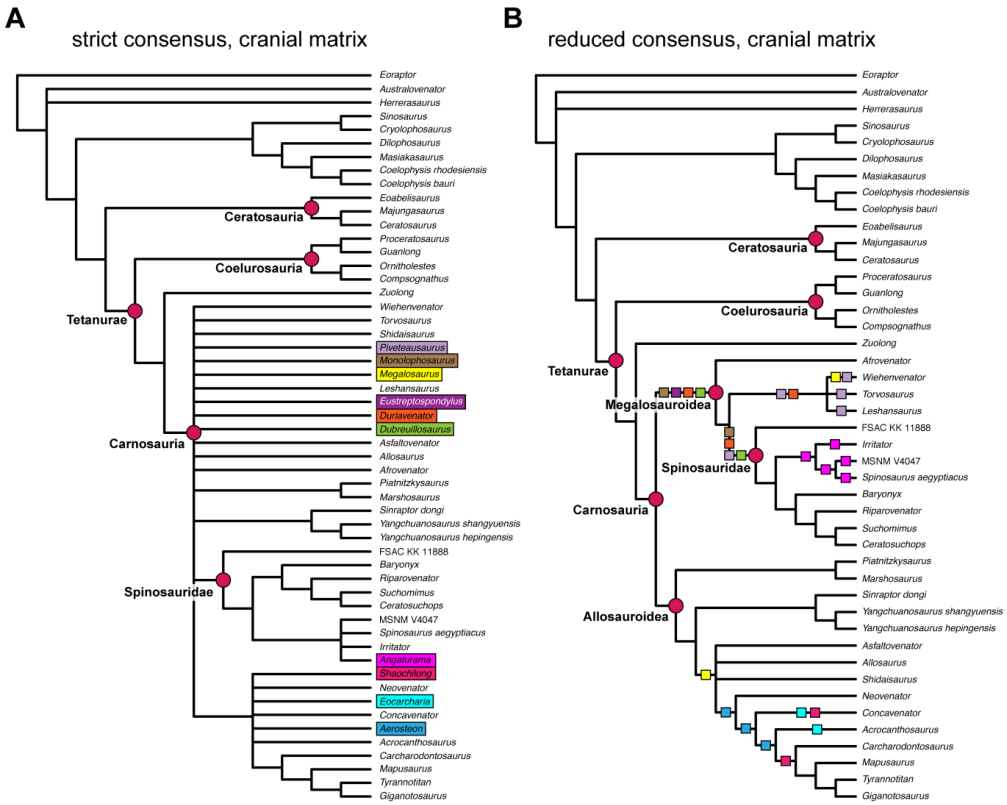

Figure 38. Phylogenetic results from parsimony analysis using the cranial dataset. A, strict consensus tree of 153 MPTs retained from an equal weighting analysis (see methods for details); B, reduced consensus tree, pruning wild card taxa from the strict consensus. Wild card taxa are highlighted with coloured boxes in A, and their possible topological positions are shown with same coloured squares in B. Important clades are labelled.

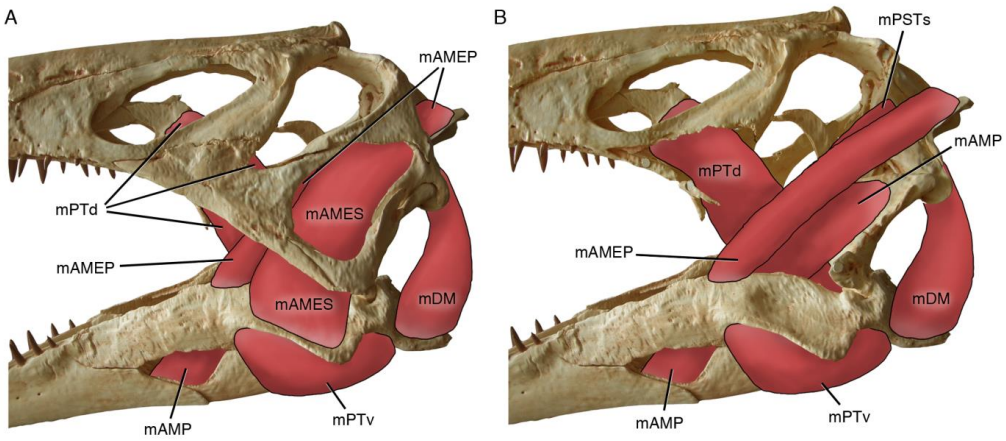

Figure 39. Medical CT data-based 3D print of *Irritator challengeri* (SMNS 58022) with jaw muscle anatomy in left lateral view. A, with superficial muscles; B, with removed cheek bones, revealing deeper muscles. mAMEP, m. adductor mandibulae externus profundus; mAMES, m. adductor mandibulae externus superficialis; mAMP, m. adductor mandibulae posterior; mDM, m. depressor mandibulae; mPSTs, m. pseudotemporalis superficialis; mPTd, m. pterygoideus dorsalis; mPTv, m. pterygoideus ventralis.

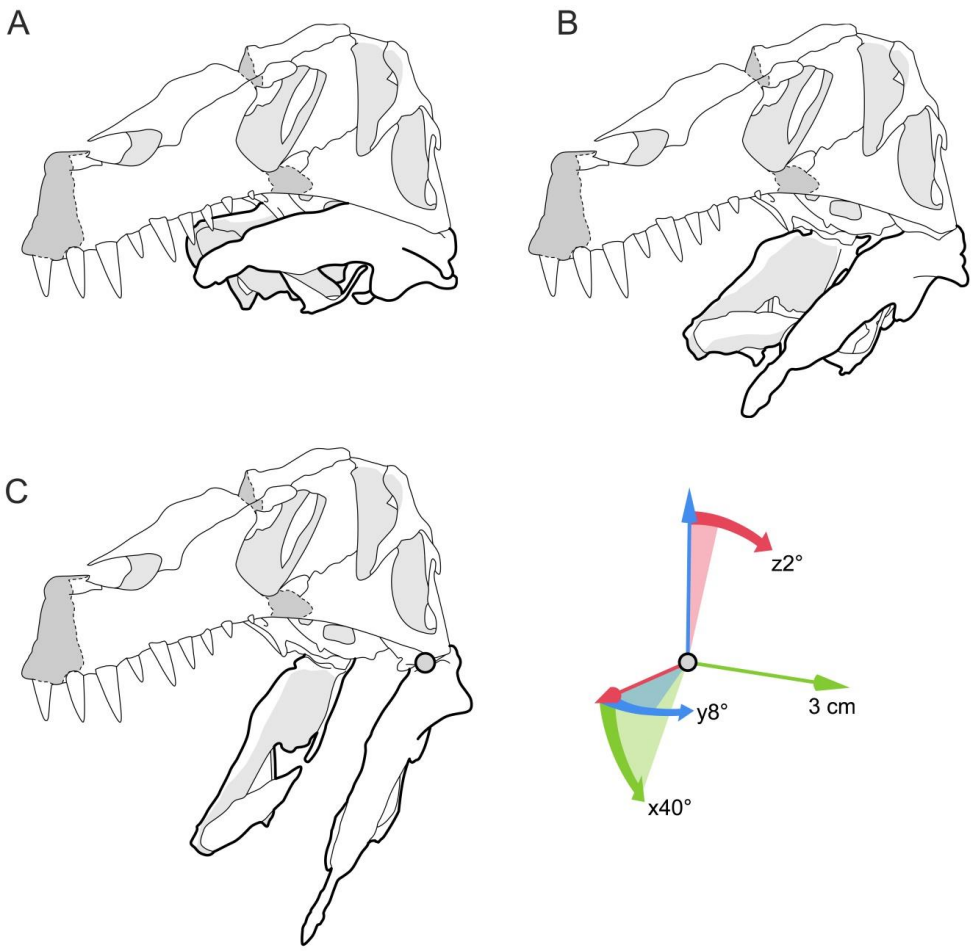

Figure 40. Line drawings of the re-arranged and articulated skull of *Irritator challengeri* (SMNS 58022). A, completely closed lower jaw; B, laterally spreading and rotating lower jaw rami during depression; C, the maximum opening angle of around 40° (in wider angles, the raised posterolateral margin of the glenoid fossa hits the quadrate) with a pharynx mediolaterally widened of around 3cm per side.

9. Acknowledgement

This thesis was supported by the Bogislaw scholarship,
financed by the University of Greifswald (April 2020 - March 2023).

The following entities provided support, trust and kindness on several occasions which enabled me to go on.

Anna, Nanna, Ragnar, Sabine, Ingrid and Eberhard Schade,
Dirk Gundlach, Martin Gothe

Christian Vogt
Julia Wirkus
Christian Reiske
Nils Knötschke
Benjamin Englich
Elsa Girard
Anna Gehrmann
Ingelore Hinz-Schallreuter
Serjoscha Evers
Christian Foth
Oliver Rauhut
Steffen Harzsch
Katrin Purps
Jürgen Kriwet

Michael ‘Ede‘ Kenzler
Marie Hörnig
Sebastian ‘Lote‘ Stumpf
Jakob Krieger
Georg ‘Brenner‘ Brenneis
Gertrud Rößner
Mike Reich
André Deutschman
Julian Neuschild
Jennifer Legat
Carina Paetzel
Jörg Ansorge
Rainer Schoch